

POLITECNICO
MILANO 1863

MASTER THESIS

**First Order Analytical Solution for
Distant Retrograde Orbits in the
Circular Restricted Three-Body
Problem**

Author:
Matteo NICOLI

Supervisor:
Dr. Camilla COLOMBO
Co-Supervisor:
Dr. Elisa Maria ALESSI
Dr. Martin LARA

*A thesis submitted in fulfillment of the requirements
for the Master of Science in Space Engineering*

in the

School of Industrial and Information Engineering
Department of Aerospace Sciences and Technologies

Academic Year 2017-2018

Copyright © April 2019 by Matteo NICOLI.
All rights reserved.

This content is original, written by the Author, Matteo NICOLI. All the non-originals information, taken from previous works, are specified and recorded in the Bibliography.

When referring to this work, full bibliographic details must be given, i.e. Matteo NICOLI, “First Order Analytical Solution for Distant Retrograde Orbits in the Circular Restricted Three-Body Problem”.

2019, Politecnico di Milano, School of Industrial and Information Engineering, Department of Aerospace Sciences and Technologies, Master of Science in Space Engineering, Supervisor: Dr. Camilla COLOMBO, Co-Supervisor: Dr. Elisa Maria ALESSI and Dr. Martin LARA

Printed in Italy

*Dedicato alla persona che ha cambiata per sempre la mia vita, a
te che sei la mia rosa su un asteroide, unica
Arianna*

Acknowledgements

Dopo 12 lunghi e intensi mesi, finalmente il giorno è arrivato: scrivere queste frasi di ringraziamento è il tocco finale della mia tesi. È stato un periodo di profondo apprendimento, non solo a livello scientifico, ma anche personale. Scrivere questa tesi ha avuto un forte impatto sulla mia personalità. Vorrei spendere due parole di ringraziamento nei confronti di tutte le persone che mi hanno sostenuto e aiutato durante questo periodo.

Prima di tutto, vorrei ringraziare i colleghi che ho incontrato durante il mio corso di studio e per la loro fantastica collaborazione, in particolare Filippo e Giovanni.

Un ringraziamento particolare va alla mia relatrice, la Dr. Camilla COLOMBO per i suoi preziosi consigli, al Dr. Elisa Maria ALESSI e al Dr. Martin LARA per l'aiuto e il supporto durante la fase di ricerca. Essi mi hanno fornito tutti gli strumenti di cui avevo bisogno per intraprendere la strada giusta e portare a compimento il lavoro di tesi.

Vorrei ringraziare i miei genitori le mie sorelle i mie zii, cugine e nonni, per i loro saggi consigli e la loro capacità di ascoltarmi e aiutarmi anche quando il lavoro era noioso. Siete sempre stati al mio fianco.

Per ultimi ma non meno importanti, i miei amici che mi hanno supportato e spronato a dare il meglio in tutti questi anni di università, vorrei in particolare ricordare Jo, Angelo, Sheila e Cioce, che non hanno mai smesso di incoraggiarmi nelle mie aspirazioni e li considero come i mie migliori amici.

Un sentito grazie a tutti!

Matteo NICOLI
Milano, 16 April 2019

Declaration of Authorship

I, Matteo NICOLI, declare that this thesis titled, “First Order Analytical Solution for Distant Retrograde Orbits in the Circular Restricted Three-Body Problem” and the work presented in it are my own. I confirm that:

- This work was done wholly or mainly while in candidature for a research master at this University.
- Where any part of this thesis has previously been submitted for a master or any other qualification at this University or any other institution, this has been clearly stated.
- Where I have consulted the published work of others, this is always clearly attributed.
- Where I have quoted from the work of others, the source is always given. With the exception of such quotations, this thesis is entirely my own work.
- I have acknowledged all main sources of help.
- Where the thesis is based on work done by myself jointly with others, I have made clear exactly what was done by others and what I have contributed myself.

Signed:

Date:

“La Terra è la culla dell’umanità, ma non si può vivere per sempre in una culla.”

Konstantin Èduardovič Ciolkovskij

“Trovo difficile capire uno scienziato che non riconosca la presenza di una razionalità superiore dietro l’esistenza dell’universo, così come il comprendere un teologo che voglia negare i progressi della scienza.”

Wernher von Braun

“La vita vola via come un sogno e spesso non riesci a far nulla prima che ti sfugga l’istante della sua pienezza. Per questo è fondamentale apprendere l’arte del vivere, tra tutte la più ardua ed essenziale: colmare ogni istante di un contenuto sostanziale, nella consapevolezza che esso non si ripeterà mai più come tale.”

Pavel Aleksandrovič Florenskij

Abstract

School of Industrial and Information Engineering
Department of Aerospace Sciences and Technologies

Master of Science in Space Engineering

**First Order Analytical Solution for Distant Retrograde Orbits in the
Circular Restricted Three-Body Problem**

by Matteo NICOLI

The work carried out in this thesis uses the Circular Restricted Three Body Problem (CR3BP model). The CR3BP attracted the attention of many researchers and mathematicians since it was considered for the first time three centuries ago. The main reason for this continuous interest is that this mathematical model represents a good first approximation in a series of real scenarios in orbital mechanics. In the framework of the planar CR3BP this thesis focuses on the study of distant retrograde orbits and in particular aims at *finding an approximate analytical solution for this type of orbit*. The periodic distant retrograde orbit derives from the work of Hénon who developed a systematic theory for the study of periodic orbits in the CR3BP. The work of Hénon is limited to the problem of Hill, which is a special case of the CR3BP in which the mass parameter of the system tends to zero. Hénon calculated periodic and non-periodic orbits; in the present work, we limit our attention only to periodic orbits. In particular, only the family f is taken into consideration and analysed. Starting from valid initial conditions given by Hénon for the model of Hill, we reproduced the evolution of these families in the CR3BP (that is, where the gravitational parameter is a finite and constant value). A differential correction method, together with a continuation method, has been exploited to find the initial conditions for each orbit in the CR3BP obtaining the complete continuation of these periodic orbits. The most interesting feature of the DROs is the great distance they reach from the secondary attractor, remaining, however, to orbit around it. The problem was written with a Lagrangian approach and then, using the variational principles, in the Hamiltonian form. This latter form is convenient because it allows to reduce the problem to a series of differential equations of the first order. Before applying the perturbation theory, a Taylor series expansion, respect mass ratio, on CR3BP was done in order to obtain a model that is a intermediate step between that of Hill and the CR3BP that we will call CR3BP-1. Since this latter model is still complex, the less relevant terms, in mass, have been neglected, this model will be called CR3BP-1₁₃. Subsequently, the classical perturbation theory was applied, applying a canonical transformation to the non-perturbed part of Hamiltonian (quadratic form of the Hamiltonian) and subsequently applying the Lie transform. This leads to a series of differential equations of more immediate analytical solution. This procedure was created for the Hill model and then for the CR3BP-1₁₃. These solution was then compared with the numerical solution for DROs, both in terms of maximum error and in terms of computational speed, resulting very reliable and computationally fast compared to the numerical model. However, the solution found does not have a noticeable improvement over that of Hill unless we take very low mass relations into consideration. This is due to the fact that the potential of the

primary is considered, in part, as a disturbance and the closer we get to the primary, the less this assumption is valid.

Keywords: Circular Restricted Three-Body Problem, CR3BP, Distant Retrograde Orbits, DRO, Hill, Deprit, Canonical Transformation, Lie, Lie Transformation

POLITECNICO DI MILANO

Sommario

Scuola di Ingegneria Industriale e dell'Informazione
Dipartimento di Scienze e Tecnologie Aerospaziali

Dottore in Ingegneria Spaziale

First Order Analytical Solution for Distant Retrograde Orbits in the Circular Restricted Three-Body Problem

di Matteo NICOLI

Il lavoro svolto in questa tesi riguarda prevalentemente il Circular Restricted Three Body Problem (modello CR3BP). Il CR3BP ha attirato l'attenzione di molti ricercatori e matematici da quando è stato preso in considerazione per la prima volta tre secoli fa. La ragione principale di questo continuo interesse è che questo modello matematico rappresenta una buona prima approssimazione in una serie di scenari reali in meccanica orbitale. Nel quadro del planar CR3BP questa tesi si concentra sullo studio di orbite retrograde distanti e in particolare per cercare di trovare una *prima soluzione analitica approssimata per questo tipo di orbite*. Le orbite retrograde distanti periodiche derivano dal lavoro di Hénon che ha sviluppato una teoria sistematica per lo studio delle orbite periodiche nel CR3BP. Il lavoro di Hénon è limitato al problema di Hill, il quale rappresenta un caso particolare del CR3BP in cui il parametro di massa del sistema tende a zero. Hénon ha calcolato orbite periodiche e non periodiche; nel presente lavoro, limitiamo la nostra attenzione solo alle orbite periodiche. In particolare è stata presa in considerazione e analizzata solo la famiglia f . Partendo dalle condizioni iniziali di Hénon valide per il modello di Hill abbiamo riprodotto l'evoluzione di queste famiglie di orbite periodiche nel CR3BP (cioè, dove il parametro gravitazionale risulta essere un valore finito e costante). Un metodo di correzione differenziale, insieme a un metodo di continuazione, è stato applicato per trovare le condizioni iniziali per ciascuna orbita nel CR3BP ottenendo la continuazione completa di queste orbite periodiche. La caratteristica più interessante dei DRO è la grande distanza che raggiungono dall'attrattore secondario, rimanendo comunque in orbita attorno ad esso. Il problema è stato scritto con un approccio lagrangiano e poi, usando i principi variazionali, nella forma hamiltoniana. Quest'ultima forma risulta comoda in quanto permette di ridurre il problema ad una serie di equazioni differenziali del primo ordine. Prima di applicare la teoria perturbativa è stato fatto un'espansione in serie di Taylor, surapparto di massa del CR3BP in modo da ottenere un modello che risulta essere una via di mezzo tra quello di Hill e il CR3BP che chiameremo CR3BP-1. Dato che quest'ultimo modello risulta essere ancora complesso, sono stati trascurati i termini, in massa, meno rilevanti questo modello verrà chiamato CR3BP-1₁₃. Successivamente, è stata applicata la teoria classica delle perturbazioni, applicando una trasformata canonica alla parte di Hamiltoniano non perturbato (forma quadratica dell'Hamiltoniano) e successivamente applicando la trasformata di Lie. Questo porta a una serie di equazioni differenziali di più immediata soluzione analitica. Tale procedimento è stato realizzato prima per il modello di Hill e poi per il CR3BP-1₁₃. Queste soluzioni sono state poi confrontate con la soluzione numerica, sia in termini di errore massimo sia in termini di velocità computazionale, risultando molto affidabile e computazionalmente veloce. Tuttavia, la soluzione trovata non ha un miglioramento notevole rispetto a quella di Hill a meno

di prendere in considerazione rapporti di massa molto bassi. Ciò è dovuto al fatto che il potenziale del primario viene considerato, in parte, come una perturbazione e più ci si avvicina al primario meno questa assunzione è valida.

Keywords: Circular Restricted Three-Body Problem, CR3BP, Distant Retrograde Orbits, DRO, Hill, Deprit, Canonical Transformation, Lie, Lie Transformation

Contents

Acknowledgements	v
Abstract	xi
Sommario	xiii
Contents	xv
List of Figures	xix
List of Tables	xxiii
List of Abbreviations	xxv
List of Symbols	xxvii
Physical Constants	xxxix
1 Introduction	1
1.1 State of the art	2
1.1.1 Three body interaction models and dynamics	2
1.1.2 Missions examples	3
1.1.3 Solution attempt	4
1.2 Thesis aim	5
1.2.1 Thesis objective	5
1.3 Organization of the work	6
1.3.1 Dynamic models by newtonian's approach	6
1.3.2 Lagrange's approach and Hamiltonian mechanics	6
1.3.3 Perturbation approach to the Hill model	6
1.3.4 Perturbation approach applied to the first term of the circular restricted three-body problem	7
1.3.5 Model comparison	7
1.3.6 conclusion	7
2 Dynamic models by newtonian's approach	9
2.1 Assumptions	9
2.2 Geometry	10
2.3 Circular restricted three-body problem	11
2.3.1 Existence and location of the libration points	14
2.3.2 The Jacobi constant	15
2.3.3 Zero velocity surfaces and curves	16
2.4 Simplification	20
2.4.1 Restricted two-body problem in synodic system	20
2.4.2 Hill's model	20

	Hill's reference frame	22
	Hill's Jacobi constant and zero velocity curves	23
2.4.3	First term of the circular restricted three-body problem	25
3	Lagrange's approach and Hamiltonian mechanics	27
3.1	CR3BP model	28
3.1.1	Inertial reference frame	28
3.1.2	Rotating reference frame	29
3.1.3	Rotating reference frame centred in the second attractor	31
3.2	Hill's model	32
3.3	First order term of the circular restricted three-body problem model	33
3.3.1	First term of the circular restricted three-body problem model	35
4	Perturbation approach applied to the Hill model	37
4.1	Canonical transformation	38
4.1.1	Hamilton-Jacobi equation	39
4.2	Unperturbed solution	42
4.3	Perturbed solution	45
4.4	Lie transform perturbation theory	46
4.4.1	Deprit's method to the Hamiltonian system	46
4.4.2	Lie transformation applied to the Hill problem	47
4.5	Motion described by analytical solution	50
4.5.1	Solution of the 7 th order	50
4.5.2	Solution of the 9 th order	52
4.6	Short-periodic correction	57
4.6.1	Short-periodic correction until 7 th order	58
4.6.2	Short-periodic correction of the 8 th -9 th orders	60
5	Perturbation approach applied to the first term of the circular re- stricted three-body problem	65
5.1	Canonical Hamiltonian	65
5.2	Lie transformation applied on the CR3BP-1 ₁₃	66
5.3	Motion by full normalised Hamiltonian in canonical form (8 th order)	70
5.4	Short-periodic correction	73
5.4.1	Short-periodic correction 7 th order	73
5.4.2	Short-periodic correction 8 th order	78
6	Model comparison	79
6.1	Jacobi constant	79
6.2	Numerical comparison CR3BP vs. CR3BP-1, CR3BP-1 ₁₃ and Hill	79
6.2.1	Error comparison	79
6.3	Comparison CR3BP vs. Hill	83
6.3.1	Run time comparison	87
6.4	Comparison CR3BP vs. analytical CR3BP-1 ₁₃ and Hill	87
6.4.1	Results for the model with assumption $\mathcal{O}[\chi^5]$	90
6.4.2	Results for the model with assumption $\mathcal{O}[\chi^3]$	95
6.4.3	Results for the model with assumption $\mathcal{O}[\chi^2]$	100
6.4.4	Results for the model with assumption $\mathcal{O}[\chi^1]$	105
7	Conclusion	111
7.1	Prospective works and improvements	112

A	Coordinate frame transformations	113
A.1	Rotating to inertial transformation	113
A.2	Inertial to rotating transformation	113
B	Differential corrections and family continuation	115
B.1	Dynamical sensitivities	115
B.1.1	Obtaining a baseline solution	115
B.1.2	State transition matrix	116
	Monodromy matrix	117
B.2	Single shooting differential corrector	117
B.3	Family continuation	118
	References Cited	121
	References No Cited	127
	Index	131

List of Figures

2.1	Geometry of the General Three-Body Problem.	10
2.2	Geometry of the Circular Restricted Three-Body Problem.	11
2.3	Representation of the configuration that the five Libration points have compared to the 2 main attractors.	16
2.4	CR3BP's Forbidden regions	17
2.5	Zero Velocity Curve (black line) and and motion regions not allowed (green surface): $J=J_1$ with $\mu=0.1$	18
2.6	Zero Velocity Curve (black line) and and motion regions not allowed (green surface): $J=J_2$ with $\mu=0.1$	18
2.7	Zero Velocity Curve (black line) and and motion regions not allowed (green surface): $J=J_3$ with $\mu=0.1$	19
2.8	Zero Velocity Curve (black line) and and motion regions not allowed (green surface): $J=J_4$ and $J=J_5$ with $\mu=0.1$	19
2.9	Hill's Reference System.	23
2.10	Hill's Zero Velocity Curve with $\mu=0.1$ and $n=1$	24
2.11	Hill's Zero Velocity Surface with $\mu=0.1$ and $n=1$	24
2.12	Zero Velocity Curve (black line) and and motion regions not allowed (green surface), with $\mu=0.1$ and $n=1$	25
4.1	Generic configuration and features of DRO.	37
4.2	Geometric meaning of the auxiliary variables.	43
4.3	Comparison between the numerical Hill model and the analytical solution of the unperturbed part of Equation (4.40) with IC of Equation (4.42).	44
4.4	Trend of the maximum in absolute value of the terms of Equations (4.67a) to (4.67k) in MD.	49
4.5	Comparison between the numerical Hill model and the analytical 7 th order solution with IC of Equation (4.43).	52
4.6	Comparison between the numerical Hill model and the analytical 7 th order solution with IC of Equation (4.42).	52
4.7	Comparison between the numerical Hill's model and the analytical 7 th and 9 th order solution with IC of Equation (4.43).	57
4.8	Comparison between the numerical Hill's model and the analytical 7 th and 9 th order solution with IC of Equation (4.42).	57
4.9	Comparison between the numerical Hill's model and the analytical 7 th order solution with and without SPC with IC of Equation (4.43). . . .	60
4.10	Comparison between the numerical Hill's model and the analytical 7 th order solution with and without SPC with IC of Equation (4.42). . . .	60
4.11	Comparison between the numerical Hill's model and the analytical 9 th order solution with and without SPC with IC of Equation (4.43). . . .	63
4.12	Comparison between the numerical Hill's model and the analytical 7 th order solution with and without SPC with IC of Equation (4.42). . . .	64

5.1	Trend of the maximum in absolute value of the terms of Equation (5.5) in MD.	67
6.1	Jacobi constant trend vs. initial condition along x direction with varying mass ratio.	80
6.2	Comparison for DROs in rotating reference frame in SEM with $A_x=1.4311$ between CR3BP, CR3BP-1, CR3BP-1 ₁₃ and Hill's model.	81
6.3	Comparison for DROs in rotating reference frame in SEM with $A_x=2.8593$ between CR3BP, CR3BP-1, CR3BP-1 ₁₃ and Hill's model.	81
6.4	Comparison for DROs in rotating reference frame in SEM with $A_x=5.7129$ between CR3BP, CR3BP-1, CR3BP-1 ₁₃ and Hill's model.	81
6.5	Comparison for DROs in rotating reference frame in SEM with $A_x=11.4146$ between CR3BP, CR3BP-1, CR3BP-1 ₁₃ and Hill's model.	82
6.6	Comparison for DROs in rotating reference frame in SEM with $A_x=22.8066$ between CR3BP, CR3BP-1, CR3BP-1 ₁₃ and Hill's model.	82
6.7	Maximum error trend between Hill, CR3BP-1 ₁₃ and CR3BP-1 models compared to CR3BP with increasing orbit dimensions in the SEM. . .	83
6.8	Comparison for DROs in rotating reference frame with $A_x=1.4311$ between numerical Hill model's and analytical one.	84
6.9	Comparison for DROs in rotating reference frame with $A_x=2.8593$ between numerical Hill's model and analytical one.	84
6.10	Comparison for DROs in rotating reference frame with $A_x=5.7129$ between numerical Hill's model and analytical one.	85
6.11	Comparison for DROs in rotating reference frame with $A_x=11.4146$ between numerical Hill's model and analytical one.	85
6.12	Comparison for DROs in rotating reference frame with $A_x=22.8066$ between numerical Hill's model and analytical one.	85
6.13	Maximum error trend of analytical Hill's model and numerical.	86
6.14	Maximum error trend of the numerical/analytical Hill's model vs. CR3BP.	86
6.15	"Run Time" numerical/analytical vs x amplitude	87
6.16	Trend of the assumption $b/p = \mathcal{O}[\chi^j]$ for Sun-(Earth-Moon) system as the size of the orbit increases (A_x).	88
6.17	Trend of the assumption $b/p = \mathcal{O}[\chi^j]$ for Mars-Deimos system as the size of the orbit increases (A_x).	89
6.18	Trend of the assumption $b/p = \mathcal{O}[\chi^j]$ for Sun-Alauda system as the size of the orbit (A_x) increases.	89
6.19	Trend of the maximum error as the size of the orbit in the Sun-(Earth-Moon) system increases with the assumption $b/p = \mathcal{O}[\chi^5]$	90
6.20	Trend of the maximum error as the size of the orbit in the Mars-Deimos system increases with the assumption $b/p = \mathcal{O}[\chi^5]$	91
6.21	Trend of the maximum error as the size of the orbit for Sun-Alauda system increases with the assumption $b/p = \mathcal{O}[\chi^5]$	91
6.22	Behaviour of the various numerical and analytical models to vary the size of the orbit for Sun-Alauda system, with analytical model under the hypothesis $b/p = \mathcal{O}[\chi^5]$	92
6.23	Behaviour of the various numerical and analytical models to vary the size of the orbit for a Mars-Deimos system, with analytical model under the hypothesis $b/p = \mathcal{O}[\chi^5]$	93
6.24	Behaviour of the various numerical and analytical models to vary the size of the orbit for a Sun-(Earth-Moon) system, with analytical model under the hypothesis $b/p = \mathcal{O}[\chi^5]$	94

6.25	Trend of the maximum error as the size of the orbit in the Sun-(Earth-Moon) system increases with the assumption $b/p = \mathcal{O}[\chi^3]$	96
6.26	Trend of the maximum error as the size of the orbit in the Mars-Deimos system increases with the assumption $b/p = \mathcal{O}[\chi^3]$	96
6.27	Trend of the maximum error as the size of the orbit for Sun-Alauda system increases with the assumption $b/p = \mathcal{O}[\chi^3]$	96
6.28	Behaviour of the various numerical and analytical models to vary the size of the orbit for Sun-Alauda system, with analytical model under the hypothesis $b/p = \mathcal{O}[\chi^3]$	97
6.29	Behaviour of the various numerical and analytical models to vary the size of the orbit for a Mars-Deimos system, with analytical model under the hypothesis $b/p = \mathcal{O}[\chi^3]$	98
6.30	Behaviour of the various numerical and analytical models to vary the size of the orbit for a Sun-(Earth-Moon) system, with analytical model under the hypothesis $b/p = \mathcal{O}[\chi^3]$	99
6.31	Trend of the maximum error as the size of the orbit in the Sun-(Earth-Moon) system increases with the assumption $b/p = \mathcal{O}[\chi^2]$	101
6.32	Trend of the maximum error as the size of the orbit in the Mars-Deimos system increases with the assumption $b/p = \mathcal{O}[\chi^2]$	101
6.33	Trend of the maximum error as the size of the orbit for Sun-Alauda system increases with the assumption $b/p = \mathcal{O}[\chi^2]$	101
6.34	Behaviour of the various numerical and analytical models to vary the size of the orbit for Sun-Alauda system, with analytical model under the hypothesis $b/p = \mathcal{O}[\chi^2]$	102
6.35	Behaviour of the various numerical and analytical models to vary the size of the orbit for a Mars-Deimos system, with analytical model under the hypothesis $b/p = \mathcal{O}[\chi^2]$	103
6.36	Behaviour of the various numerical and analytical models to vary the size of the orbit for a Sun-(Earth-Moon) system, with analytical model under the hypothesis $b/p = \mathcal{O}[\chi^2]$	104
6.37	Trend of the maximum error as the size of the orbit in the Sun-(Earth-Moon) system increases with the assumption $b/p = \mathcal{O}[\chi^1]$	106
6.38	Trend of the maximum error as the size of the orbit in the Earth-Moon system increases with the assumption $b/p = \mathcal{O}[\chi^1]$	106
6.39	Trend of the maximum error as the size of the orbit for Sun-Alauda system increases with the assumption $b/p = \mathcal{O}[\chi^1]$	106
6.40	Behaviour of the various numerical and analytical models to vary the size of the orbit for Sun-Alauda system, with analytical model under the hypothesis $b/p = \mathcal{O}[\chi^1]$	107
6.41	Behaviour of the various numerical and analytical models to vary the size of the orbit for a Mars-Deimos system, with analytical model under the hypothesis $b/p = \mathcal{O}[\chi^1]$	108
6.42	Behaviour of the various numerical and analytical models to vary the size of the orbit for a Sun-(Earth-Moon) system, with analytical model under the hypothesis $b/p = \mathcal{O}[\chi^1]$	109
B.1	Baseline Arch.	115
B.2	Variable-Time Single Shooting Differential Corrector.	118
B.3	Hénon family- f orbit continuation in Sun-(Earth-Moon) synodic system.	119

List of Tables

4.1 Canonical transformation in the Phase Space.	39
--	----

List of Abbreviations

Abbreviation	Description
ARM	Asteroid Redirect Mission
CR3BP	Circular Restricted Three-Body Problem
CR3BP-1	Circular Restricted Three-Body Problem 1th order TSE
CR3BP-1₁₃	Circular Restricted Three-Body Problem 1th order TSE and μ simplification
CWE	Clohessy-Wiltshire Equations
DRO	Distant Retrograde Orbit
EM	Earth Moon system
EOL	End Of Life
IC	Initial Condition
JE	Jupiter Europa system
JI	Jupiter Io
LEO	Low Earth Orbit
MD	Mars Deimos system
MP	Mars Phobos system
NEO	Near Earth Objects
ODE	Ordinary Differential Equations
PDE	Partial Differential Equations
QED	Quod Erat Demonstrandum
RE3BP	Restricted Elliptical Three-Body Problem
R2BP	Restricted Two-Body Problem
R3BP	Restricted Three-Body Problem
SA	Sun Alauda system
SE	Saturn Enceladus system
SEM	Sun(Earth-Moon) system
S/C	SpaceCraft
SJ	Sun Jupiter system
SM	Sun Mars system
SPA	Solar Phase Angle
SPC	Short-Period Correction
STM	State Transition Matrix
TSE	Taylor Series Expansion

List of Symbols

Latin Capitals	Description	SI unit	SI unit before normalization
A_x	x -Amplitude	[-]	[m]
\underline{A}	Jacobian Matrix	[-]	[-]
\underline{E}	Energy of the System	[-]	[J]
G	Universal Gravitational Parameter	[m ³ /(kg s ²)]	[-]
\tilde{G}	Non-dimensional Universal Gravitational Parameter	[-]	[m ³ /(kg s ²)]
\underline{G}_R	Partial Derivative Matrix with respect to the Position Vector	[-]	[-]
\underline{G}_V	Partial Derivative Matrix with respect to the Velocity Vector	[-]	[-]
\mathcal{H}	Hamiltonian function	[-]	[J]
J	Jacobi Constant	[-]	[J]
\mathcal{K}	Canonical Hamiltonian function	[-]	[-]
$\bar{\mathcal{K}}$	Mean Canonical Hamiltonian function	[-]	[-]
\mathcal{K}_L	Lie Canonical Hamiltonian function	[-]	[-]
\mathcal{L}	Lagrangian function	[-]	[J]
\underline{M}	Monodromy Matrix	[-]	[-]
\underline{N}	Mean Motion	[rad/s]	[-]
\underline{P}	Canonical Conjugate Momenta	[-]	[-]
Q	Second Canonical Conjugate Momenta	[-]	[rad]
\underline{Q}	Canonical Coordinate	[-]	[-]
\underline{R}_{R2I}	Rotating Matrix from Inertial to Rotating Frame	[-]	[-]
\underline{R}_{I2R}	Rotating Matrix from Rotating to Inertial Frame	[-]	[-]
\underline{R}_R^I	Position Rotating Matrix from Rotating to Inertial Frame	[-]	[-]
$\dot{\underline{R}}_R^I$	Time Derivative Position Rotating Matrix from Rotating to Inertial Frame	[-]	[-]
\underline{R}_I^R	Position Rotating Matrix from Inertial to Rotating Frame	[-]	[-]
$\dot{\underline{R}}_I^R$	Time Derivative Position Rotating Matrix from Inertial to Rotating Frame	[-]	[-]
S	General Generating Function	[-]	[-]
T	Kinetic Energy	[-]	[J]
\mathcal{T}	Canonical Trasformation	[-]	[-]
\mathcal{U}	Potential Energy	[-]	[J]
V	Potential Function	[-]	[J]
W	Generating Function	[-]	[-]

Latin Capitals	Description	SI unit	SI unit before normalization
X, Y, Z	Non-dimensional Coordinate of Inertial Reference System	[-]	[m]
\underline{X}	State Vector	[-]	[m,m/s]
Latin Lowercase	Description	SI unit	SI unit before normalization
a	Semi-major Axis	[-]	[m]
b	Semi-minor Axis	[-]	[m]
k	Scaling Canonical Factor	[-]	[-]
l^*	Characteristic Length	[m]	[-]
m^*	Characteristic Mass	[kg]	
m_1	Main Attractor	[kg]	
m_2	Second Attractor	[kg]	
n	Non-dimensional Mean Motion	[-]	[rad/s]
p	Non-dimensional Distance between primary and secondary attractor	[-]	[m]
\underline{p}	Generalized Conjugate Momenta	[-]	[-]
q	Second Canonical Coordinate	[-]	[rad]
\underline{q}	Generalized Coordinate	[-]	[-]
\underline{r}	Non-dimensional Position Vector	[-]	[m]
t	Time	[-]	[s]
$t_{2\pi}$	Non-dimensional Orbit Period	[-]	[s]
x, y, z	Non-dimensional Coordinate of Rotating Reference System	[-]	[m,m/s]
Greek Capitals	Description	SI unit	SI unit before normalization
Λ	Pulsation of Hill Canonical Solution	[-]	[-]
$\bar{\Lambda}$	High order Pulsation of Hill Canonical Solution	[-]	[-]
Φ	First Canonical Conjugate Momenta	[-]	[-]
$\underline{\Psi}$	State Transition Matrix	[-]	[-]
$\bar{\Omega}$	Centrifugal Potential function	[-]	[J]
Greek Lowercase	Description	SI unit	SI unit before normalization
γ	Perturbed Coefficient	[-]	[-]
ε	Error	[-]	[-]
μ	Mass Parameter	[-]	[-]
ξ, η, ζ	Hill Coordinates in the Rotating Reference System	[-]	[m]
ρ	Position Vector	[m]	[-]
σ	Normalised Semi-minor Axis	[-]	[m]
τ^*	Characteristic Time	[-]	[s]
τ	Non-dimensional Time	[-]	[s]
ϕ	First Canonical Coordinate	[-]	[rad]
χ	Normalised Semi-major Axis	[-]	[m]

Greek Lowercase	Description	SI unit	SI unit before normalization
I_{ω^R}	Angular Velocity from Inertial to Rotating Reference Frame	[-]	[rad/s]

Nota Bene: In this work most of the variables have been normalized, removing the dimension, as is common in the CR3BP, to facilitate the dimensional analysis a column with the measurement units is reported before normalization.

Physical Constants

Latin	Description	Mantissa	Base/Exp	SI unit
l_{EM}^*	Characteristic Length Earth-Moon	3.85	10^5	[km]
l_{JE}^*	Characteristic Length Jupiter-Europa	6.70900	10^5	[km]
l_{JI}^*	Characteristic Length Jupiter-Io	4.217	10^5	[km]
l_{MD}^*	Characteristic Length Mars-Deimos	2.34632	10^4	[km]
l_{MP}^*	Characteristic Length Mars-Phobos	9.376	10^3	[km]
l_{SE}^*	Characteristic Length Saturn-Enceladus	2.37948	10^5	[km]
l_{SEM}^*	Characteristic Length Sun-(Earth-Moon)	1.496	10^8	[km]
l_{SJ}^*	Characteristic Length Sun-Jupiter	7.784	10^8	[km]
l_{SM}^*	Characteristic Length Sun-Mars	2.279	10^8	[km]

Greek	Description	Mantissa	Base/Exp	SI unit
μ_{EM}	Mass Ratio Earth-Moon	1.20047157410116	10^{-2}	[-]
μ_{JE}	Mass Ratio Jupiter-Europa	2.52663615948415	10^{-5}	[-]
μ_{JI}	Mass Ratio Jupiter-Io	4.70507861193606	10^{-5}	[-]
μ_{MD}	Mass Ratio Mars-Deimos	2.79999999216	10^{-9}	[-]
μ_{MP}	Mass Ratio Mars-Phobos	1.989999960399	10^{-8}	[-]
μ_{SA}	Mass Ratio Sun-Alauda	1	10^{-12}	[-]
μ_{SE}	Mass Ratio Saturn-Enceladus	2.09999955900009	10^{-7}	[-]
μ_{SEM}	Mass Ratio Sun-(Earth-Moon)	3.04042340206594	10^{-6}	[-]
μ_{SJ}	Mass Ratio Sun-Jupiter	9.53683903339555	10^{-4}	[-]
μ_{SM}	Mass Ratio Sun-Mars	3.22715033002455	10^{-7}	[-]
τ_{EM}^*	Characteristic Time Earth-Moon	3.75764820639965	10^5	[s]
τ_{JE}^*	Characteristic Time Jupiter-Europa	4.88322440608913	10^4	[s]
τ_{MD}^*	Characteristic Time Mars-Deimos	1.73666230713636	10^4	[s]
τ_{MP}^*	Characteristic Time Mars-Phobos	4.38693210031263	10^3	[s]
τ_{SE}^*	Characteristic Time Saturn-Enceladus	1.88462335994808	10^4	[s]
τ_{SEM}^*	Characteristic Time Sun-(Earth-Moon)	5.00860605910195	10^6	[s]

Chapter 1

Introduction

This dissertation was conducted under the supervision of Professor Dr. Camilla COLOMBO and assisted by Dr. Elisa Maria ALESSI and Dr. Martin LARA at the Politecnico di Milano.

The aim of this thesis is to find a first approximate analytical solution for Distant Retrograde Orbit (DRO) for a model closer to the Circular Restricted Three-Body Problem (CR3BP) than the Hill's model. An analytical solution becomes very important in the preliminary design phases as it allows to reduce the computational simulation times due to the numerical integration. This is advantageous in the optimization processes, used to guarantee the requirements of the mission.

In the orbital dynamics the effect of the third body of the body is very important, in fact, it produces an attraction that modifies the dynamics of a body of negligible mass. Hence, it allows us to understand how a body of negligible mass moves in the presence of two masses that attract it, for example a satellite that is affected by the effect of the Earth and the Moon.

The Restricted Three-Body Problem (R3BP) is a well known problem in multi-body dynamics. This model consists in considering the orbital dynamics due to three attracting bodies of which one is sufficiently small to consider its gravitational contribution negligible. In this thesis work the CR3BP was considered, it consists in simplifying the R3BP, considering the dynamics of the second attractor as circulating around the primary and the secondary orbit on circular orbit around their centre of mass. In its best known form, it has been extensively studied for two classical systems, the Sun-(Earth-Moon) system and the Earth-Moon system.

Some important studies in this field have been carried out by Poincaré and Hill ([35, 36]). Hill, in 1887, obtained this model considering the motion in the vicinity of the secondary attractor and treating the primary attractor as if it were at an infinite distance. The Hill's model, which is valid starting from the assumption that the mass parameter of R3BP tends to zero, has the advantage of not being dependent on any mass parameter and has some symmetries that in R3BP do not exist. This model has become so important that it commonly takes its name from the one who first treated it, precisely Hill.

Subsequently, other works of considerable importance were drawn. To be remembered are those of Hénon [27–34] who took advantage of the Hill planar model to obtain analytical approximations and study the various families of orbits that the model of Hill produces. These families are well listed in [30].

Szebehely [56], who once again developed Hill's model formally from the R3BP and at the same time studied it, through the variational principles, deriving various mathematical forms of CR3BP. Even the Russian school, which until recently was very little known, has produced several studies and research on R3BP and the most common CR3BP model. Among the most important for the purposes of this thesis is the Arnold [3], who has produced interesting treaties that concern the application of

the classical perturbation theory and the study of the integrability of the system by exploiting the variational principles. Extremely important in this thesis work is the work done by Boccaletti [10, 11], as it defines well the canonical perturbation theory and in particular the method of Deprit [21, 22], which allows to obtain an analytical solution of the problem and which is the purpose of this thesis.

In this thesis we will deal in particular with the planar CR3BP which makes it easier to apply the canonical perturbation theory, allowing us to solve some integrals. Through the study and data provided by [30] and based on well-known differential correction algorithms, we obtain the orbits of the Hénon family-f, which are in fact the DRO. Successively with analogous numerical algorithms we define this family for various orbital systems, i.e. with finite mass parameters. This initial work serves as a yardstick for verifying and validating the analytical model obtained. The first one, who treated this for Hill's model, was Lara in [39]. Subsequently introducing a finite mass parameter, leading us to to a more accurate model and going to the first order analytical solution of the CR3BP for the DRO.

1.1 State of the art

The effort of many researchers in the field of astrodynamics in recent decades is to study those orbital trajectories generated by the interaction between three bodies of which one has a negligible mass compared to the first two.

Below, follows a brief description of the most important achievements that led to the development of this thesis.

1.1.1 Three body interaction models and dynamics

In particular, some studies focused on Restricted Elliptical Three-Body Problem RE3BP, where the dynamics of the secondary attractor is elliptical around the primary and no longer circular, and the interactions between bodies produce trajectories that are stable in the long period. Some of the most important studies were produced by Lidov, [42–44]. He was one of the first to exploit the variational principles to study and compare an analytical approach with a numerical one. Already in [42], Lidov performs an analysis on the evolution of quasi-satellite orbits; they are a special class of periodic orbits, taking advantage of the model produced by Hill [35, 36] which represents a simplification of the CR3BP. Subsequently, He produced, in [42–44], interesting analytical results for quasi-satellite orbits comparing them with numerical results. Lidov is perhaps the first to exploit the canonical transformations to simplify the mathematical problem trying to solve it.

Retrograde orbits are found in great amount of literature and have high number of applications, especially under Hill's model. In this filed an important study is the work of Namouni, [48]; he exploited semi-analytical approaches to study the families of retrograde orbits formed by the third-body effect. These families of orbits have been treated and studied, even if only numerically, by Hénon in [29, 30].

In addition, many researches start from the Hill model, which is simpler as it allows to obtain very promising and realistic results on the dynamics in R3BP in the vicinity of the secondary attractor. In this sense, the variational approach and the classical perturbation theories provide very convincing results. In this regard, Lara, [40], represents a first step as it uses the Hill model to study a mission near Enceladus; in fact, systems of celestial bodies like Jovian or Saturn and their moons, are very interesting as the effect of the third body cannot be neglected.

The same author, in [38], obtained an analytical solution for the Hill problem in the

vicinity of the libration points by means of perturbation techniques. There he manages to calculate the higher orders of the perturbed solution, which are necessary to describe all relevant periodic orbits. The validity of the solution extends to energy values very distant from those of the libration points and, therefore, can be used to compute e.g. Halo orbits and for DROs as an alternative to the classic Lindstedt-Poincaré approach.

Other studies have focused the search for stability regions in particularly mass-rich systems such as the Jovian or Saturn ones. Lara tried to classify these regions in the vicinity of Europe, in [41].

DROs, that are part of the Hénon family-f [30], in recent years, have been re-discovered and are subject to a more in-depth analysis for different types of missions. The general stability of this particular family of orbits has been studied in [8, 9, 13].

Outside orbital mechanics field, the Hill's model, in recent years, has been very interesting also in astrophysics, as it models well the dynamics of a star with respect to the centre of the galaxy and the exoplanets that revolve around it, as can be seen in study [25].

1.1.2 Missions examples

Among all the proposed missions that have been taken into consideration in recent years, those about Near Earth Objects (NEO) are those of greatest interest. In particular is worth mentioning the Asteroid Redirect Mission, ARM, [12, 51], which consists in a robotic mission on asteroids (particularly near the Moon) to obtain surface samples. The ARM mission is presented in [53], where the stability of DRO (for example near the Moon for over 100 years) is related to the fragments that are generated during robotic interaction with asteroids. The fragments would accumulate in these regions which have a very low escape rate (< 1 m/s).

Another example is the study [52], where the DRO are exploited for their stability around the secondary attractor and in particular for those small objects like NEO or small moons like Phobos. The solar system exploration missions make full use the dynamics of the DRO due to the stability property, especially when the payload must be pointing to small and irregularly shaped bodies. By modifying the eccentricity of the orbit, it is possible to approach the body or stay in a relatively distant parking orbit for a long time.

Other studies are aimed at creating a constellation of satellites able to monitoring and providing detection warning for the NEO incoming to an impact to Earth, especially those coming from the direction of the Sun, which are not visible using Earth-based monitoring systems. Stramacchia and Colombo, [17, 55], tried to analyse the feasibility of a constellation around the Earth, as a means of monitoring asteroids that come from behind the Sun and are difficult to monitor, as the sunlight prevents us to detect them. There the use of DROs can lead to a decrease in the reaction time to detect potential objects that could impact with the Earth, decrease the costs of entry from Low Earth Orbit (LEO) and, thanks to their stability, significantly reduce propellant consumption for station maintenance.

Other studies focused on missions on the Moon or in its vicinity, exploiting the DRO. Murakami, in [47], proposed rendez-vous mission on lunar orbits for future space outposts or supply stations. The DRO is the object of that study for achieving a low cost transfer from LEO and reasonable flight time. Similar studies, [14, 45, 46], exploit the DRO as low energy transfer orbits; in fact, as those orbits are obtained in the CR3BP, it is possible to exploit the manifolds to reach or to leave them with a much

lower cost compared to traditional manoeuvres in the Keplerian model. Similarly, missions can be designed in very perturbed systems, such as the Jovian system. Studies such as [37, 41], actually exploit DROs for long-term parking missions or End of Life (EOL) strategies. These orbits, as already mentioned, prove to have considerable long-term stability and are therefore convenient to avoid the impact of the S/C with the body surface after the end of the mission, as the spacecrafts remain in a state of equilibrium between the attraction of the primary and the secondary. In the Jovian system the dimensions of Europe allows to place the S/C at a safe distance, moreover the whole Hénon family-f allows to widen or reduce the orbit with dramatically reduced costs; this is potentially interesting for developing low-cost EOL strategies.

Another approach is to use the DROs as a support orbits for long-term missions to Mars, exploiting Phobos and Deimos. Among the various missions we can mention DePhine [49], scheduled for 2030, that will use an orbiter to collect physical data from the moons of Mars. For this type of mission the DROs were chosen mainly for their stability. However, due to the small size of those celestial objects, the sphere of influence is smaller than the dimensions of the objects their-self. Thus, the DROs are quite close to the surface of the object itself. All this, combined with the fact that they have a low speed and a long time near the surface, improves the resolution of the instruments. In [57], Wallace aimed at performing hovering manoeuvres in the vicinity of Phobos and Deimos. In this perspective, the study divides the orbits between the flat and the non-flat trajectories, to see which ones are best suited for the study of the poles.

Conte, [18, 19], instead, exploited the DROs as support trajectories for refuelling. Indeed, exploiting the low gravity of Phobos and Deimos, the stability of these trajectories and the low cost of entry. It is possible to leave a S/C on DRO to constitute a refuelling station for missions on Mars or in deep space. Regarding Phobos, Gil, in [23], performs an analysis on the stability of DRO and their impact on the mission objectives, exploiting the phase space like the Delaunay variables.

Bezrouk, proposed a study [7], in which he takes advantage of the ballistic entry trajectories, around Phobos. This capture occurs almost naturally with small correction manoeuvres that give time to ground operators to correct any errors without losing the general trajectory. Although the study was developed for Phobos, the problem has its own intrinsic generality that allows it to be extended to other systems.

Despite the previously indicated studies refer for the most part to end-of-life, captures strategies are equally important; as for example [59], which proposes an analysis for the construction and insertion on DRO in ARM.

Oki in [50] aims to exploit a gravity assist to leave the DRO. Earth gravity assist is very efficient in terms of Δv and time of flight. Similarly Demeyer in [20], analyses the entry on DRO starting from LEO.

1.1.3 Solution attempt

All the approaches described in the previous section require the use of numerical simulations, highly expensive in terms of computational time. This preclude the implementation of optimisation strategies, especially in phase A design. For this purpose an analytical solution, although approximate, would be extremely advantageous. From all the previous works and the experiments derived from them, Lara has reached an analytical solution for the DRO in the case of Hill's problem. In [39], he exploited the classical theory of the perturbation of the variational principles to obtain an analytical

solution. it is obtained by considering the effect due to the secondary attractor as a perturbation, deriving an average Hamiltonian from Lie transform, which is analytically solvable.

1.2 Thesis aim

This thesis has as its ultimate goal to produce a first analytical approximation of the DRO, a special solution of the CR3BP. This will be done starting from the work proposed by Lara [39] in which, as already mentioned in the previous paragraphs, he produced an approximate analytical solution of the DRO in the Hill model. Starting from this solution we will reformulate the Hill's problem by introducing into the potential, higher order terms, which depend directly on the mass ratio. These terms mean that the primary attractor is no longer at an infinite distance from the secondary as foreseen by the Hill model. These terms are, therefore, the first terms necessary to get to the solution of CR3BP. An analytical solution is extremely versatile in the preliminary design phases. In fact, in the initial stages it is necessary to analyze different orbits to find the best compromise that meets the requirements of the mission. To do this, optimization algorithms are normally used today. However, they are computationally long and heavy. This is due to the fact that the dynamic is numerically integrated into them. The use of an analytical solution allows to obtain the state vector at a given instant of time without the need to calculate all the previous dynamics. This entails considerable computational advantages, making the preliminary design times considerably lower.

1.2.1 Thesis objective

To achieve the aim described above, there are several intermediate objectives that must be achieved. An analysis of the literature, in particular in paper [39], shows how the classical theory of perturbation plays a decisive role in the approach to the problem.

First of all, we need to reformulate the CR3BP model, in particular to obtain the formulation of the potential function, especially in the case where the rotating reference system is centred in the secondary attraction and not in the barycentre, as re-proposed by Hill.

Secondly, it is necessary to impose the same assumptions adopted in the Hill model for the simplification of the potential, to obtain the Hill model itself and then to derive a more accurate model.

Successively, by exploiting the variational principles and its peculiarities, the model is rewritten in the form of a Hamiltonian. Thanks to this particular change of notation one of the most interesting approaches can be applied, namely the canonical transformation. By satisfying some mathematical properties, it allows to further simplify the formulation of the problem with variables called action/angle. However, we are constraint to have a canonical transformation that is also reversible and this is only possible if the Hamiltonian has a quadratic form.

Because of this restriction, we must exploit the classical theory of canonical perturbation. This theory, although decisively old, is still valid today and has never fallen short, even when hundreds of variables were used.

It consists in generating the so-called Lie series that provides, based on the degree to which we want to approximate our new Hamiltonian, a new approximation of the Hamiltonian and of the generating function of the canonical transformation. The most important aspect is undoubtedly the averaging process on the angular part of

the canonical transformation. This process makes it possible to further simplify the problem and thus generate differential equations of the first order, solved by known techniques. We must also dedicate some words to methods for solving non-linear differential equations. When the classical approaches do not allow to find a solution, perturbed techniques, such as the Lindstedt-Poincaré technique, offer an excellent tool.

Finally, all the numerical models obtained will be subjected to a verification, with the numerical model CR3BP, which in this work is considered the reference model. The goal is to improve the solution with respect to the model proposed by Lara in [38, 39] and to understand under what limits of validity it can be used.

All these aspects, so far mentioned, are essential and must be adequately understood to approach and solve the problem.

1.3 Organization of the work

The thesis work is organised as follows.

1.3.1 Dynamic models by newtonian's approach

In the first part, Chapter 2, of the thesis the model CR3BP is derived. In this part of the work we start from the Newtonian formulation of the orbital problem identifying the correct assumptions that lead to the definition of the problem itself. The reference system that will be used to derive the equations of motion is identified. Then we get the equations of the non dimensional problem. Once the equations have been identified, a brief description of the model is given, showing the Lagrangian points, the Jacobi constant and the zero velocity curves.

Subsequently, the simplifications of greater interest are presented. The first is called R2BP in a rotating system, where the mass parameter is set to zero. The second is the Hill model, which consists in making the mass parameter to tend to zero, which produces an implicit assumption that ideally brings the primary attractor to an infinite distance from the secondary. This model and its derivation involve the fulcrum of the solution seen hereafter. Finally, we derive the model CR3BP-1 which corresponds to a middle ground between the CR3BP and the Hill model.

1.3.2 Lagrange's approach and Hamiltonian mechanics

In this part of the work, Chapter 3, the model CR3BP is used with the Lagrangian approach. It consists in starting from the energies involved, obtaining the Lagrangian function of the model. This work is done for all the models obtained in the previous chapter. At this point there is a brief but nevertheless complete definition of the variational principles and of the Hamiltonian approach. Subsequently, using the definitions, we derive the Hamiltonian formulation of all the models. This is done because the perturbation approach that is exploited starts from the Hamiltonian formulation and therefore a description of it turns out to be important in order to adequately understand the starting points of the thesis.

1.3.3 Perturbation approach to the Hill model

At this point of the thesis, Chapter 4, we proceed with obtaining the analytical solution of the Hill problem by exploiting the classical canonical perturbation theory. We start using the Lagrangian approach to obtain the Hill model from which, taking

advantage of what has been said in the previous chapters, we obtain the Hamiltonian formulation. At this point, using the variational principles and the properties of canonicity, the generating function of the canonical transformation is obtained, which is produced only for the quadratic part of the Hamiltonian. Thanks to the canonical transformation just found, a perturbation approach is applied to the complete Hamiltonian from which a Lie transformation is performed, obtaining the mean term which allow to solve the problem analytically.

1.3.4 Perturbation approach applied to the first term of the circular restricted three-body problem

In this part of the thesis, Chapter 5, starting from the simplified CR3BP model, we follow the same steps seen in the previous chapter, keeping the same canonical transformation obtained for the model of Hill, arriving at a similar solution but for a more complex model.

1.3.5 Model comparison

At this point, Chapter 6, a comparison is made of the analytical and numerical models obtained in the previous chapters. The comparison is made both at the computational timing and for the errors produced by the analytical model with respect to the numerical one.

1.3.6 conclusion

At the end, a conclusion is proposed with the work limitations and some ideas about possible future developments.

Chapter 2

Dynamic models by newtonian's approach

In this chapter we will obtain the CR3BP model using the classic approach defining the assumptions and the geometry that characterizes it. We will identify some of the most important features, such as the Lagrangian points. Then we will identify the main simplifications to the CR3BP, which are the subject of this thesis, in particular the Hill's model and the CR3BP-1.

2.1 Assumptions

The problem formulation is based on a set of assumptions that are critical in gaining insight but retain the most significant dynamical features of the model. Initially, assume that all bodies are modeled as point masses. From Newton's Second Law, the motion of a particle P_i under the influence of $N - 1$ gravitating bodies, P_j , is described by the following differential equation:

$$m_i \ddot{\underline{r}}_i = -G \sum_{j=1, j \neq i}^n \frac{m_i m_j}{\|\underline{r}_{ji}\|^3} \underline{r}_{ji} \quad (2.1)$$

in which m_i represents the mass of the particle of interest and m_j identifies the other bodies that gravitationally influence its motion and vice versa. The symbol G is the gravitational constant expressed in dimensional units. The vectors \underline{r}_i and \underline{r}_j describe the position of these particles relative to an inertially fixed base point and $\underline{r}_{ji} = \underline{r}_j - \underline{r}_i$, and dot denotes differentiation with respect to dimensional time. The N-body model is simplified considerably by incorporating only three bodies ($N = 3$) and reduces Equation (2.1) to the form:

$$m_3 \ddot{\underline{r}}_3 = -\frac{Gm_3m_1}{\|\underline{r}_{13}\|^3} \underline{r}_{13} - \frac{Gm_3m_2}{\|\underline{r}_{23}\|^3} \underline{r}_{23} \quad (2.2)$$

where the particle of interest is arbitrarily selected to be P_3 . A complete, closed form solution to the three-body problem requires 18 integrals of the motion. Since there are only 10 known constants, an analytical solution is not currently known. The geometry representing the general three-body problem appears in Figure 2.1. After reducing the N-body problem to three bodies, the problem is further simplified by assuming that the mass of the smallest body, m_3 , is negligible in comparison to the masses of P_1 and P_2 , that is, $m_3 \ll m_2 < m_1$. Consequently, the motion of P_3 does not influence the motion of either P_1 or P_2 . As a result, the orbits of P_1 and P_2 are represented by conics in an isolated two-body system, this is called the Restricted

Three-Body Problem (R3BP). In addition, we add the assumption that P_2 move in circular orbits around P_1 , this is called CR3BP.

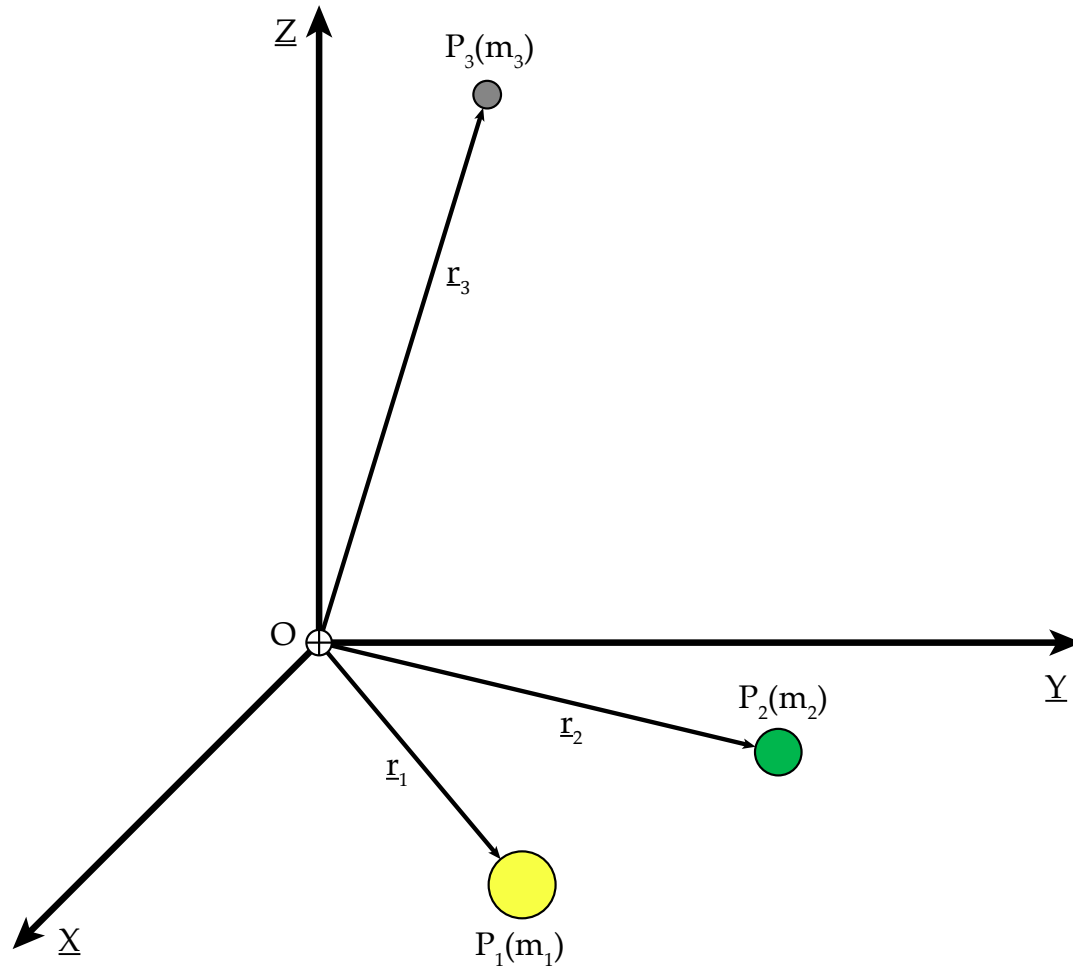


Figure 2.1: Geometry of the General Three-Body Problem.

2.2 Geometry

Two coordinate frames are particularly significant in the formulation of the CR3BP. An inertial reference frame, I , is centred at the barycentre, B , and is defined in terms of the unit vectors $\hat{X} - \hat{Y} - \hat{Z}$ where \hat{Z} is aligned with the angular momentum vector of the orbits of P_1 and P_2 .

Since it is assumed that the primaries move in conic orbits, their motion is restricted to the $\hat{X} - \hat{Y}$ plane. However, P_3 is not constrained to a plane and is free to move in any spatial direction. A rotating reference frame, R , also centred at B , is defined via unit vectors $\hat{x} - \hat{y} - \hat{z}$. The \hat{z} axis, like \hat{Z} , is also aligned with the angular momentum vector of the main and second attractors. The unit vector \hat{x} is directed from the main attractor, P_1 , toward the secondary attractor, P_2 , and \hat{y} completes the right-handed triad. The angle ϑ orients the rotating reference frame R relative to the inertial frame I . The geometry is illustrated in Figure 2.2. The positions of the first 2 attractors relative to the barycentre, B , are described by the vectors, \underline{D}_1 and \underline{D}_2 . The relative position vectors, \underline{D} and \underline{R} , define the position of the third body with respect to P_1

and P_2 , respectively. The vector $\underline{\rho}$ denotes the location of P_3 with respect to the barycentre.

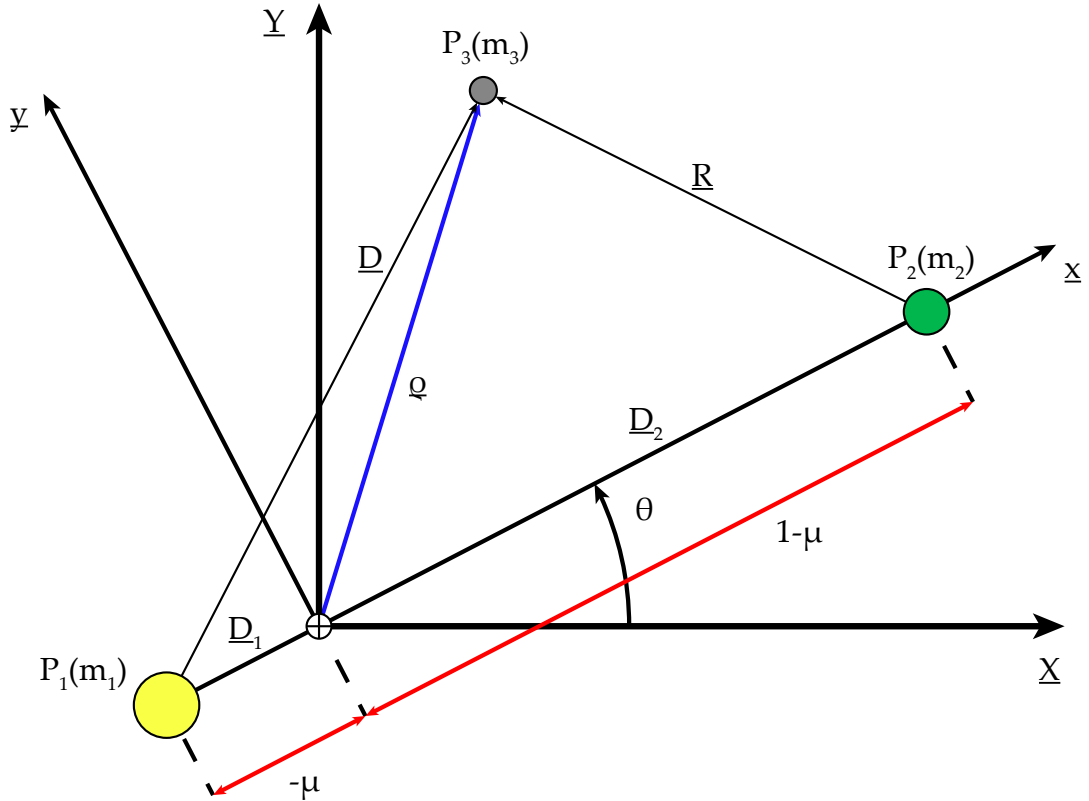


Figure 2.2: Geometry of the Circular Restricted Three-Body Problem.

2.3 Circular restricted three-body problem

To compute trajectories in the CR3BP, it is first necessary to derive the appropriate equations of motion. Given the geometry of the CR3BP (Figure 2.2), Equation (2.2) yields the following differential equation:

$$m_3 \ddot{\underline{\rho}} = -\frac{Gm_3m_1}{\|\underline{D}\|^3} \underline{D} - \frac{Gm_3m_2}{\|\underline{R}\|^3} \underline{R} \quad (2.3)$$

Despite the simplifying assumptions, the problem, Equation (2.3), is still not available to solve analytically; numerical solutions are required to gain some understanding of the behaviour.

The non-dimensional characteristic quantities associated with length, mass, and time are introduced. The characteristic length, l^* , is defined to be the distance between the main and second attractor, that is:

$$l^* = \|\underline{D}_1 + \underline{D}_2\| \quad (2.4)$$

and the characteristic mass, m^* , is evaluated as the sum of the masses of the two primaries:

$$m^* = m_1 + m_2 \quad (2.5)$$

The characteristic time, τ^* , is deduced from Kepler's third law, assuming that the orbital period associated with the motion of the first two attractors about their common barycentre is 2π in non-dimensional time, i.e.:

$$\tau^* = \sqrt{\frac{l^{*3}}{\tilde{G}m^*}} \quad (2.6)$$

this leads to define the non-dimensional gravitational constant, $\tilde{G} = 1$. A Kepler definition of the dimensional mean motion, N , corresponding to the behaviour of the first 2 attractors is given by Restricted Two-Body Problem (R2BP):

$$N = \sqrt{\frac{\tilde{G}m^*}{l^{*3}}} \quad (2.7)$$

It follows that the non-dimensional mean motion, n , is then written as:

$$n = N\tau^* = \sqrt{\frac{l^{*3}}{\tilde{G}m^*}} \sqrt{\frac{\tilde{G}m^*}{l^{*3}}} = 1 \quad (2.8)$$

Note that the non-dimensional mean motion, n , is unity in the traditional formulation of the CR3BP.

Incorporating the characteristic quantities, the non-dimensional position vectors, \underline{r}_1 and \underline{r}_2 , mass parameter, μ , and non-dimensional time parameter, τ , are defined as follows:

$$\underline{r}_2 = \frac{\underline{R}}{l^*} \quad (2.9a)$$

$$\underline{r}_1 = \frac{\underline{D}}{l^*} \quad (2.9b)$$

$$\mu = \mu_2 = \frac{m_2}{m^*} \quad (2.9c)$$

$$\tau = \frac{t}{\tau^*} \quad (2.9d)$$

As a consequence, the mass of the first attractor is represented as:

$$\mu_1 = \frac{m_1}{m^*} = 1 - \mu \quad (2.10)$$

The non-dimensional position vector, \underline{r} , representing the position of P_3 with respect to the barycentre. it is obtained by non-dimensionalizing the position vector, $\underline{\rho}$, so the relationship:

$$\underline{r} = \frac{\underline{\rho}}{l^*} = x\hat{x} + y\hat{y} + z\hat{z} \quad (2.11)$$

The governing differential equation for the motion of P_3 , that is, Equation (2.3), is also non-dimensionalized using the characteristic quantities. These non-dimensional quantities are now substituted into Equation (2.3) to obtain the non-dimensional differential equation governing the motion of P_3 , that is:

$$\ddot{\underline{r}} = -\frac{(1-\mu)}{\|\underline{r}_1\|^3}\underline{r}_1 - \frac{\mu}{\|\underline{r}_2\|^3}\underline{r}_2 \quad (2.12)$$

From the geometry in Figure 2.2 and the definition of the centre of mass, it is apparent that the non-dimensional relative position vectors, \underline{r}_1 and \underline{r}_2 , are determined

respectively, as:

$$r_1 = (x + \mu) \hat{x} + y \hat{y} + z \hat{z} \quad (2.13a)$$

$$r_2 = (x - (1 - \mu)) \hat{x} + y \hat{y} + z \hat{z} \quad (2.13b)$$

Much insight into the motion of P_3 is available through Equation (2.12) from a kinet-ics perspective, but a kinematic relationship is also necessary to produce the scalar equations of motion. The derivative of \underline{r} with respect to time, as viewed by an inertial reference frame and expressed in terms of rotating reference frame is determined via the appropriate transformation relationship:

$$\frac{{}^I d\underline{r}}{dt} = \frac{{}^R d\underline{r}}{dt} + {}^I \underline{\omega}^R \wedge \underline{r} \quad (2.14a)$$

$$\frac{{}^I d^2 \underline{r}}{dt^2} = \frac{{}^R d^2 \underline{r}}{dt^2} + 2 {}^I \underline{\omega}^R \wedge \frac{{}^R d\underline{r}}{dt} + {}^I \underline{\omega}^R \wedge ({}^I \underline{\omega}^R \wedge \underline{r}) \quad (2.14b)$$

where ${}^I \underline{\omega}^R$ represents the angular velocity of the rotating reference frame with respect to the inertial one. Of course, $\frac{{}^R d\underline{r}}{dt}$ represents the change in the position vector as observed from the rotating reference frame. Thus, the kinematic expansion for inertial acceleration is written in the form:

$$\ddot{\underline{r}} = (\ddot{x} - 2n\dot{y} - n^2 x) \hat{x} + (\ddot{y} + 2n\dot{x} - n^2 y) \hat{y} + \ddot{z} \hat{z} \quad (2.15)$$

Note that the non-dimensional mean motion, n , is equal to one in non-dimensional units. Substituting the kinematic expression from Equations (2.12) and (2.13) into Equation (2.15) yields the three scalar, second differential equations of motion for P_3 in the CR3BP:

$$\begin{cases} \ddot{x} = 2n\dot{y} + n^2 x - \frac{(1 - \mu)(x + \mu)}{(r_1)^3} - \frac{\mu(x - (1 - \mu))}{(r_2)^3} & (2.16a) \\ \ddot{y} = -2n\dot{x} + n^2 y - \frac{(1 - \mu)y}{(r_1)^3} - \frac{\mu y}{(r_2)^3} & (2.16b) \\ \ddot{z} = -\frac{(1 - \mu)z}{(r_1)^3} - \frac{\mu z}{(r_2)^3} & (2.16c) \end{cases}$$

where the scalar relative distances are:

$$r_1 = \sqrt{(x + \mu)^2 + y^2 + z^2} \quad (2.17a)$$

$$r_2 = \sqrt{(x - (1 - \mu))^2 + y^2 + z^2} \quad (2.17b)$$

and all derivatives are relative to a rotating reference frame. These equations of motion are written more compactly following the introduction of a potential function:

$$V(x, y, z) = \frac{1}{2} n^2 (x^2 + y^2) + \frac{1 - \mu}{r_1} + \frac{\mu}{r_2} \quad (2.18)$$

Then, we can define centrifugal potential function as:

$$\Omega(x, y, z) = \frac{1}{2} n^2 (x^2 + y^2) + V(x, y, z) + \frac{1}{2} (1 - \mu) \mu \quad (2.19a)$$

$$= \frac{1}{2} n^2 (x^2 + y^2) + \frac{1 - \mu}{r_1} + \frac{\mu}{r_2} + \frac{1}{2} (1 - \mu) \mu \quad (2.19b)$$

Equation (2.16) appear in a more succinct form as:

$$\begin{cases} \ddot{x} = 2n\dot{y} + \frac{\partial\Omega}{\partial x} & (2.20a) \\ \ddot{y} = -2n\dot{x} + \frac{\partial\Omega}{\partial y} & (2.20b) \\ \ddot{z} = \frac{\partial\Omega}{\partial z} & (2.20c) \end{cases}$$

2.3.1 Existence and location of the libration points

System Equation (2.20) admit 5 equilibrium points, the so-called libration points or Lagrangian points. These are the roots of the equations $f(x) = 0$ and thus $\dot{x} = \dot{y} = \dot{z} = \ddot{x} = \ddot{y} = \ddot{z} = 0$.

We distinguish between collinear and equilateral triangle libration points. Consider first the collinear libration points. For these we have $y = z = 0$ and the vector equations reduces to:

$$x - \frac{(1-\mu)(x+\mu)}{|x+\mu|^3} - \frac{\mu(x-1+\mu)}{|x-(1-\mu)|^3} = 0 \quad (2.21)$$

The collinear libration points lie on the x-axis, along with the masses, which are located at $-\mu$ and $1-\mu$. Then these points are linearly ordered, and we have to consider the three cases $x < -\mu < 1-\mu$, $-\mu < x < 1-\mu$, and $-\mu < 1-\mu < x$.

In the first case we will denote the equilibrium by $x = L_3$, the second case $x = L_1$ and the third case $x = L_2$.

In the first case we have:

$$|L+\mu| = -(L+\mu) \quad (2.22a)$$

$$|L-(1-\mu)| = -(L-(1-\mu)) \quad (2.22b)$$

as $L < -\mu$, and $L < 1-\mu$ imply that $L+\mu < 0$ and $L-(1-\mu) < 0$. Then, Equation (2.22) becomes:

$$L - \frac{(1-\mu)(L+\mu)}{(-1)(L+\mu)^3} - \frac{\mu(L-1+\mu)}{(-1)(L-(1-\mu))^3} = 0 \quad (2.23)$$

or:

$$\frac{L(L+\mu)^2(L-(1-\mu))^2 + (1-\mu)(L-(1-\mu))^2 + \mu(L+\mu)^2}{(L+\mu)^2(L-(1-\mu))^2} = 0 \quad (2.24)$$

The left hand side is zero if and only if L is a root of the numerator. Expanding this gives the condition:

$$L^5 + a_L L^4 + b_L L^3 + c_L L^2 + d_L L + e_L = 0 \quad (2.25)$$

where:

$$a_{L_3} = 2(2\mu - 1) \quad (2.26a)$$

$$b_{L_3} = (1-\mu)^2 - 4\mu(1-\mu) + \mu^2 \quad (2.26b)$$

$$c_{L_3} = 2\mu(1-\mu)(1-2\mu) + 1 \quad (2.26c)$$

$$d_{L_3} = \mu^2(1-\mu)^2 + 2(\mu^2 - (1-\mu)^2) \quad (2.26d)$$

$$e_{L_3} = (1 - \mu)^3 + \mu^3 \quad (2.26e)$$

The polynomial is fifth degree in L and there is no hope of an analytic solution, therefore, a numerical method is normally used. Similar consideration of the remaining two cases show that L_1 , and L_2 satisfy the same Equation (2.25) but with some difference, for L_1 :

$$a_{L_1} = 2(2\mu - 1) \quad (2.27a)$$

$$b_{L_1} = (1 - \mu)^2 - 4\mu(1 - \mu) + \mu^2 \quad (2.27b)$$

$$c_{L_1} = 2\mu(1 - \mu)(1 - 2\mu) + 1 \quad (2.27c)$$

$$d_{L_1} = \mu^2(1 - \mu)^2 + 2(\mu^2 + (1 - \mu)^2) \quad (2.27d)$$

$$e_{L_1} = (1 - \mu)^3 - \mu^3 \quad (2.27e)$$

and for L_2 :

$$a_{L_2} = 2(2\mu - 1) \quad (2.28a)$$

$$b_{L_2} = (1 - \mu)^2 - 4\mu(1 - \mu) + \mu^2 \quad (2.28b)$$

$$c_{L_2} = 2\mu(1 - \mu)(1 - 2\mu) - 1 \quad (2.28c)$$

$$d_{L_2} = \mu^2(1 - \mu)^2 + 2(\mu^2 - (1 - \mu)^2) \quad (2.28d)$$

$$e_{L_2} = -(1 - \mu)^3 - \mu^3 \quad (2.28e)$$

The locations of the equilateral triangle libration points are much easier to compute, since they must lie at the vertex of an equilateral triangle whose base is the line between the two primaries. Since this line has length one, the distance from the primaries to either L_4 or L_5 must be one.

Since the base lies on the x -axis and the sides have length one we see that the height of the third vertex must be $y = \pm\sqrt{3}/2$. The x coordinate of either libration point must bisect the adjacent side. Since this side has length one, this coordinate must be $x = -\mu + 1/2$.

In the Figure 2.3 an example is proposed for the case Sun-(Earth-Moon).

2.3.2 The Jacobi constant

The CR3BP has one known integral of motion. The following derivation is the one most often given as it is quite elementary. Begin with the scalar combination of dynamical variables $\ddot{x}\dot{x} + \ddot{z}\dot{z} + \ddot{z}\dot{z}$. Then observe that this is:

$$\ddot{x}\dot{x} + \ddot{z}\dot{z} + \ddot{z}\dot{z} = \dot{x}(2\dot{y} + \Omega_x) + \dot{y}(-2\dot{x} + \Omega_y) + \dot{z}(\Omega_z) \quad (2.29a)$$

$$= \dot{x}\Omega_x + \dot{z}\Omega_z + \dot{z}\Omega_z \quad (2.29b)$$

$$= \frac{d\Omega}{dt} \quad (2.29c)$$

Then we observe that:

$$\frac{d}{dt} \frac{1}{2} (\dot{x}^2 + \dot{y}^2 + \dot{z}^2) = \ddot{x}\dot{x} + \ddot{z}\dot{z} + \ddot{z}\dot{z} \quad (2.30)$$

so that:

$$\frac{d}{dt} \frac{1}{2} (\dot{x}^2 + \dot{y}^2 + \dot{z}^2) = \frac{d\Omega}{dt} \quad (2.31)$$

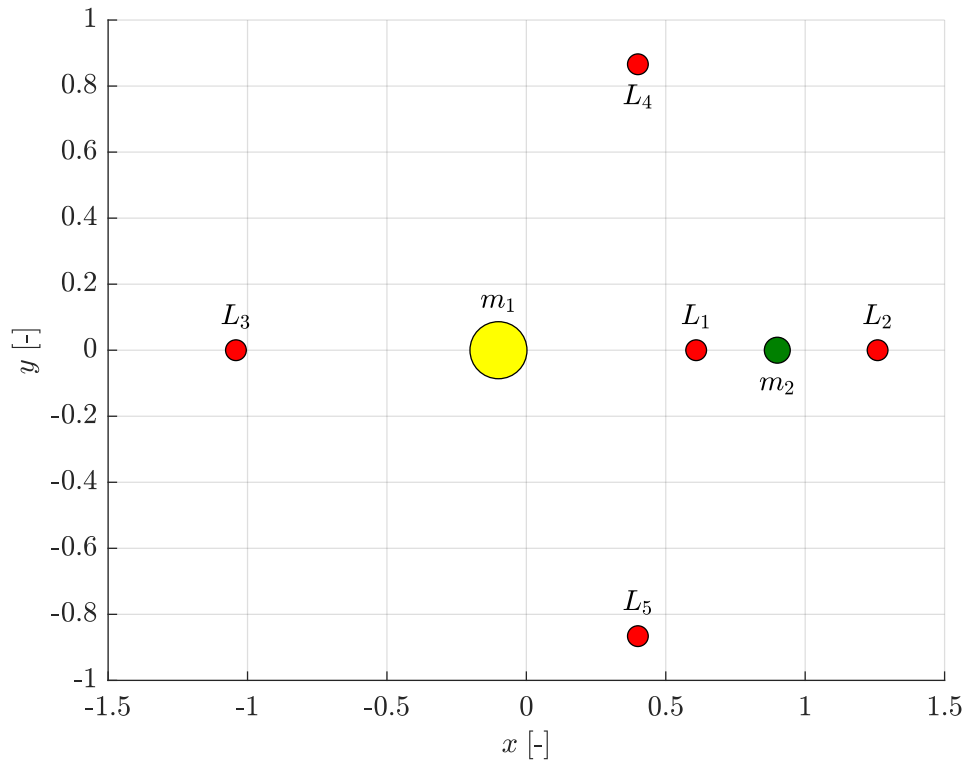


Figure 2.3: Representation of the configuration that the five Libration points have compared to the 2 main attractors.

Then:

$$\frac{d}{dt} \frac{1}{2} (\dot{x}^2 + \dot{y}^2 + \dot{z}^2) = \Omega - \frac{1}{2} J \quad (2.32)$$

where J is an arbitrary constant. Then it is the case that:

$$2\Omega - (\dot{x}^2 + \dot{y}^2 + \dot{z}^2) = J \quad (2.33)$$

or:

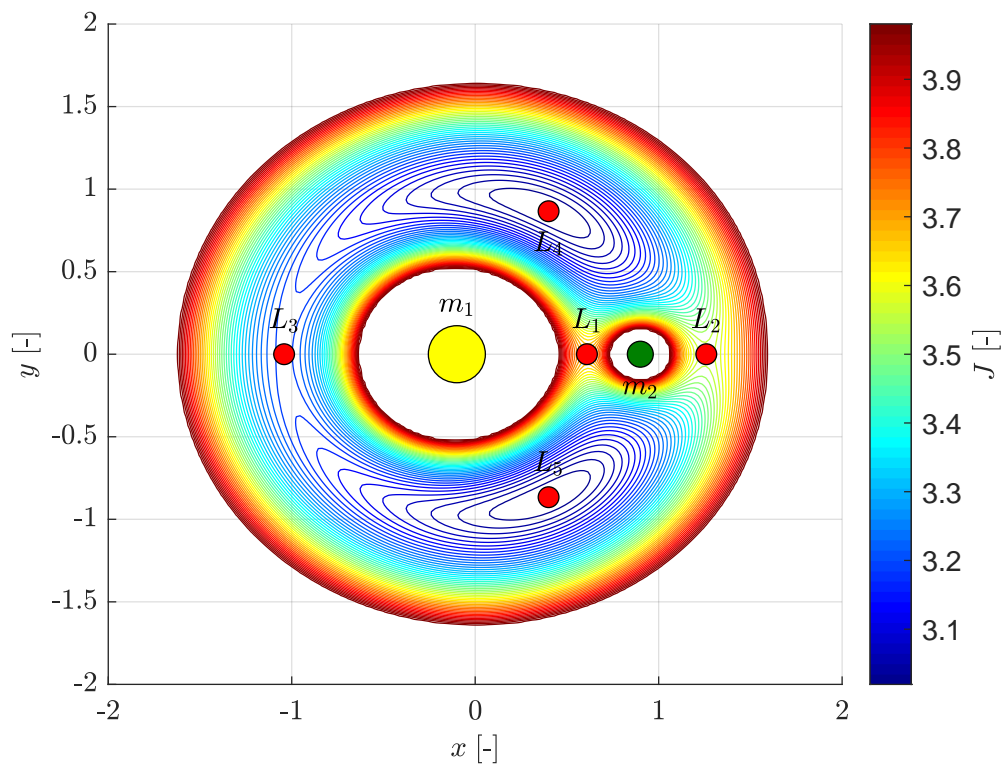
$$J = n(x^2 + y^2) + 2\frac{1-\mu}{r_1} + 2\frac{\mu}{r_2} - (\dot{x}^2 + \dot{y}^2 + \dot{z}^2) + (1-\mu)\mu \quad (2.34)$$

This constant, or conserved quantity is called the Jacobi constant/integral.

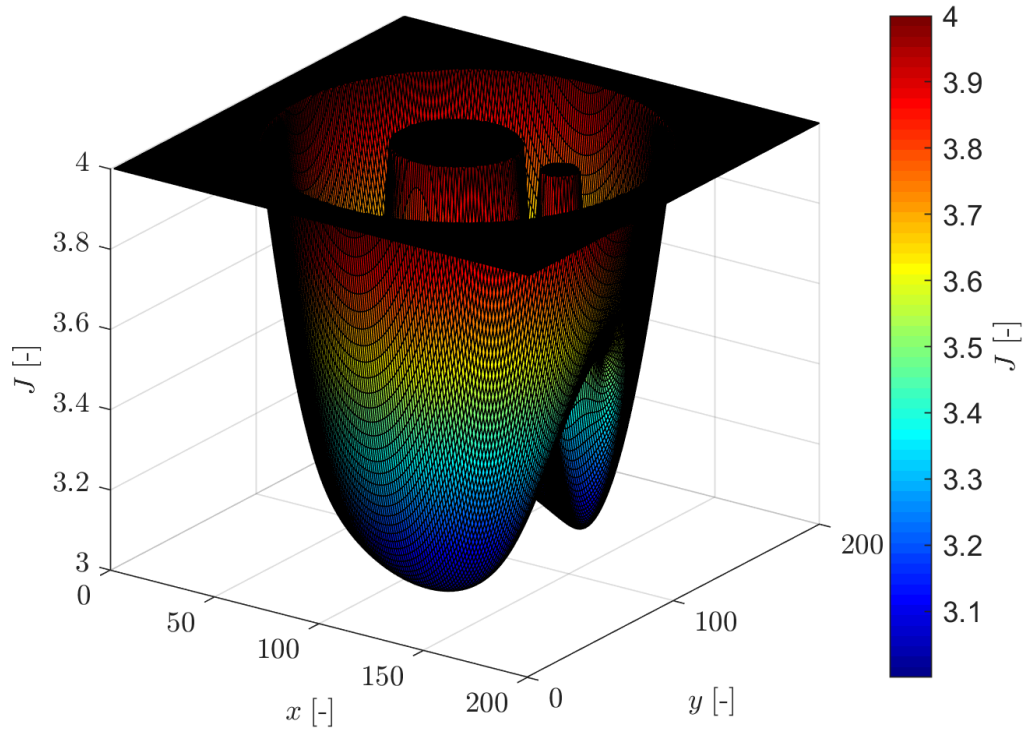
2.3.3 Zero velocity surfaces and curves

The curves, Figures 2.5 to 2.8, and surfaces, Figure 2.4, are obtained by choosing an energy level, setting the velocity terms in the Jacobi Integral to zero, and plotting the implicitly defined curve or surface so defined. The physical/dynamical significance of the Jacobi Constant is as follows; once an energy level is fixed, the magnitude of the velocity at any point is uniquely determined.

The Hill's surfaces determine the allowable regions of motion for fixed energies in the CR3BP. These allowable regions are called Hill's Regions.



(a) Hill's curve.



(b) Hill's surface.

Figure 2.4: Forbidden regions and CR3BP's curves for several values of J with $\mu=0.1$.

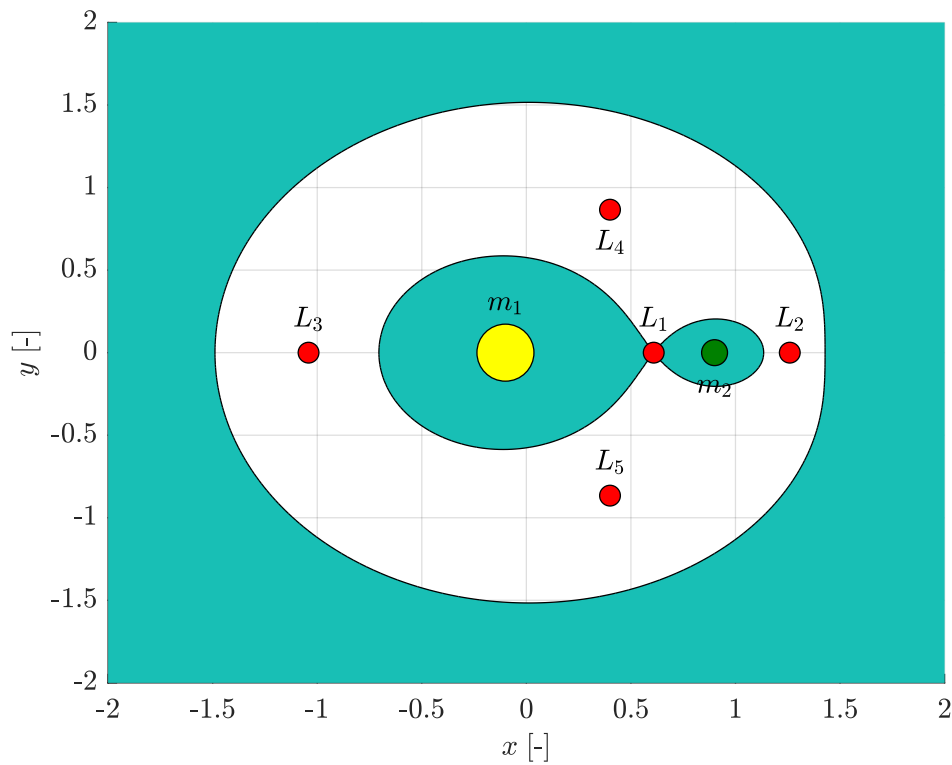


Figure 2.5: Zero Velocity Curve (black line) and and motion regions not allowed (green surface): $J=J_1$ with $\mu=0.1$.

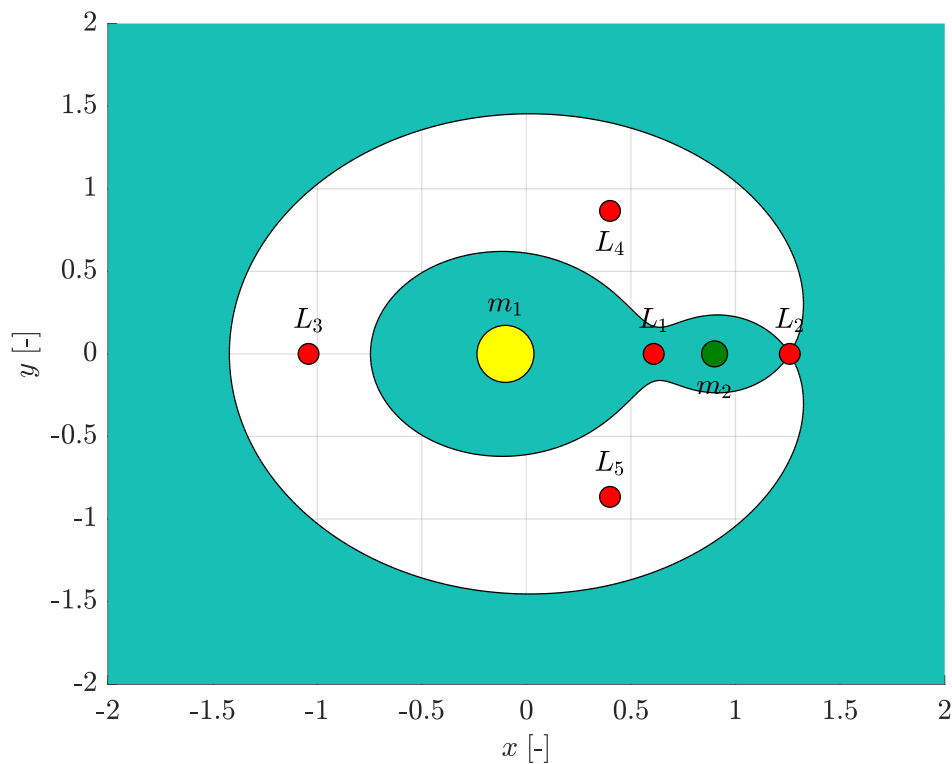


Figure 2.6: Zero Velocity Curve (black line) and and motion regions not allowed (green surface): $J=J_2$ with $\mu=0.1$.

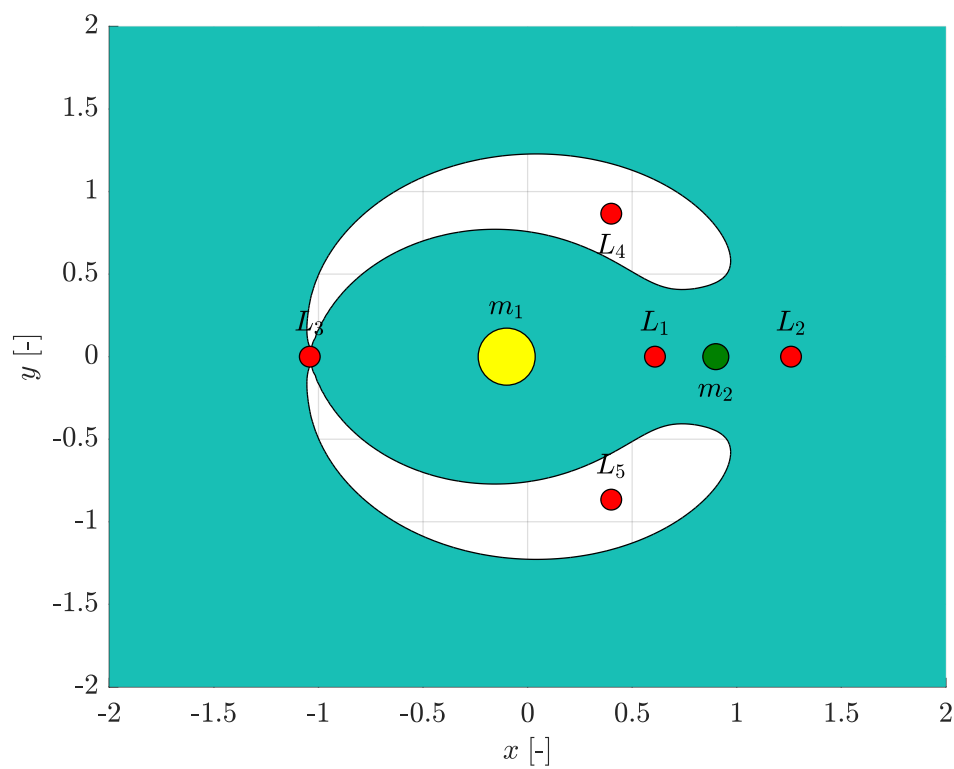


Figure 2.7: Zero Velocity Curve (black line) and motion regions not allowed (green surface): $J=J_3$ with $\mu=0.1$.

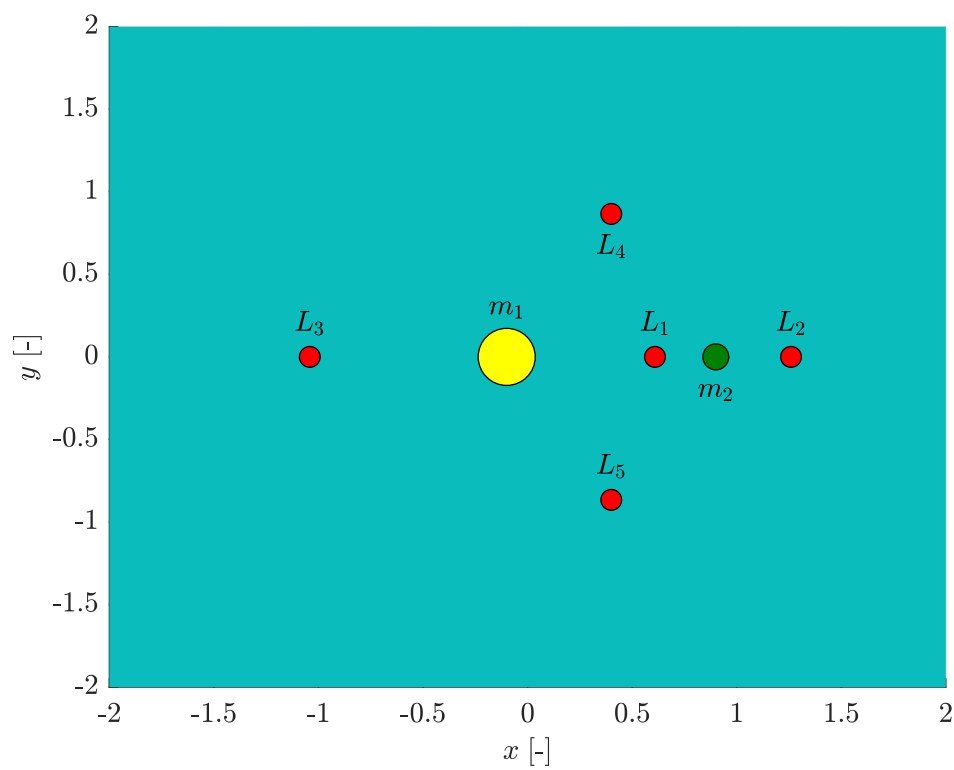


Figure 2.8: Zero Velocity Curve (black line) and motion regions not allowed (green surface): $J=J_4$ and $J=J_5$ with $\mu=0.1$.

2.4 Simplification

The CR3BP turns out to be a difficult model to solve. In this regard, it is convenient to identify two simplified models that are easier to solve. If we now consider some assumptions regarding the secondary, two simplified models can be obtained:

- Restricted Two-Body Problem in Synodic System
- Hill's problem [35, 36]
- CR3BP-1

2.4.1 Restricted two-body problem in synodic system

If we do not consider the mass of the secondary attractor:

$$\mu = 0 \quad (2.35)$$

Consequently the scalar distance becomes:

$$r_1 = \sqrt{x^2 + y^2 + z^2} \quad (2.36)$$

then, the CR3BP model of Equation (2.16) becomes:

$$\begin{cases} \ddot{x} = n^2 x + 2n\dot{y} - \frac{x}{(x^2 + y^2 + z^2)^{3/2}} & (2.37a) \\ \ddot{y} = n^2 y - 2n\dot{x} - \frac{y}{(x^2 + y^2 + z^2)^{3/2}} & (2.37b) \\ \ddot{z} = -\frac{z}{(x^2 + y^2 + z^2)^{3/2}} & (2.37c) \end{cases}$$

Which turns out to be the Restricted Keplerian Problem in a Synodic system, i.e. in a rotating coordinate system centred at the primary. Finally, the Equation (2.37) is associated with the following potential function:

$$V = \frac{1}{2}n^2(x^2 + y^2) + \frac{1}{\sqrt{x^2 + y^2 + z^2}} \quad (2.38)$$

analogously to the Equation (2.18).

2.4.2 Hill's model

If we consider the hypothesis in which the mass of the primary is sufficiently distant from the secondary:

$$\mu \rightarrow 0 \quad (2.39)$$

This leads to simplifying the problem. Despite the fact that the dynamics is still determined by the primary, the fact that we are sufficiently distant means that the secondary attractor plays an important role. So much so that this model is valid only in the vicinity of the secondary. Starting from Equation (2.16), we introduce the following coordinate change:

$$\begin{cases} \xi = x - 1 + \mu & (2.40a) \\ \eta = y & (2.40b) \\ \zeta = z & (2.40c) \end{cases}$$

so that the reference coordinate system is centred in the secondary. Substituting the Equation (2.40) in the Equation (2.16), we can obtain:

$$\left\{ \begin{array}{l} \ddot{\xi} = 2\dot{\eta}n + n^2(-\mu + \xi + 1) - \frac{\mu\xi}{(\zeta^2 + \eta^2 + \xi^2)^{3/2}} + \frac{(\mu - 1)(\xi + 1)}{(\zeta^2 + \eta^2 + (\xi + 1)^2)^{3/2}} \end{array} \right. \quad (2.41a)$$

$$\left\{ \begin{array}{l} \ddot{\eta} = -2n\dot{\xi} + \eta n^2 - \frac{\eta\mu}{(\zeta^2 + \eta^2 + \xi^2)^{3/2}} + \frac{\eta(\mu - 1)}{(\zeta^2 + \eta^2 + (\xi + 1)^2)^{3/2}} \end{array} \right. \quad (2.41b)$$

$$\left\{ \begin{array}{l} \ddot{\zeta} = \frac{\zeta(\mu - 1)}{(\zeta^2 + \eta^2 + (\xi + 1)^2)^{3/2}} - \frac{\zeta\mu}{(\zeta^2 + \eta^2 + \xi^2)^{3/2}} \end{array} \right. \quad (2.41c)$$

Now we “zoom” in the vicinity of the second body by an appropriate change of scale introducing μ^α as scale factor. Hence, the new coordinates are:

$$\left\{ \begin{array}{l} \xi = \mu^\alpha \xi \\ \eta = \mu^\alpha \eta \\ \zeta = \mu^\alpha \zeta \end{array} \right. \quad (2.42a)$$

$$\left\{ \begin{array}{l} \eta = \mu^\alpha \eta \end{array} \right. \quad (2.42b)$$

$$\left\{ \begin{array}{l} \zeta = \mu^\alpha \zeta \end{array} \right. \quad (2.42c)$$

Replacing the Equation (2.42) in the Equation (2.41), we now obtain:

$$\left\{ \begin{array}{l} \mu^\alpha \ddot{\xi} = 2\mu^\alpha \dot{\eta}n + n^2(-\mu + \mu^\alpha \xi + 1) + \\ \quad - \frac{\mu\mu^\alpha \xi}{((\mu^\alpha \zeta)^2 + (\mu^\alpha \eta)^2 + (\mu^\alpha \xi)^2)^{3/2}} + \\ \quad + \frac{(\mu - 1)(\mu^\alpha \xi + 1)}{((\mu^\alpha \zeta)^2 + (\mu^\alpha \eta)^2 + (\mu^\alpha \xi + 1)^2)^{3/2}} \end{array} \right. \quad (2.43a)$$

$$\left\{ \begin{array}{l} \mu^\alpha \ddot{\eta} = -2n\mu^\alpha \dot{\xi} + \mu^\alpha \eta n^2 - \frac{\mu^\alpha \eta \mu}{((\mu^\alpha \zeta)^2 + (\mu^\alpha \eta)^2 + \xi^2)^{3/2}} + \\ \quad + \frac{\mu^\alpha \eta (\mu - 1)}{((\mu^\alpha \zeta)^2 + (\mu^\alpha \eta)^2 + (\mu^\alpha \xi + 1)^2)^{3/2}} \end{array} \right. \quad (2.43b)$$

$$\left\{ \begin{array}{l} \mu^\alpha \ddot{\zeta} = \frac{\mu^\alpha \zeta (\mu - 1)}{((\mu^\alpha \zeta)^2 + (\mu^\alpha \eta)^2 + (\mu^\alpha \xi + 1)^2)^{3/2}} + \\ \quad - \frac{\mu^\alpha \zeta \mu}{((\mu^\alpha \zeta)^2 + (\mu^\alpha \eta)^2 + \xi^2)^{3/2}} \end{array} \right. \quad (2.43c)$$

If we now divide everything for μ^α , we get:

$$\left\{ \begin{array}{l} \ddot{\xi} = n^2 \mu^{-\alpha} (\xi \mu^\alpha - \mu + 1) + 2\dot{\eta}n - \frac{\xi \mu^{1-3\alpha}}{(\zeta^2 + \eta^2 + \xi^2)^{3/2}} + \\ \quad + \frac{(\mu - 1) \mu^{-\alpha} (\xi \mu^\alpha + 1)}{(\mu^{2\alpha} (\zeta^2 + \eta^2 + \xi^2) + 2\xi \mu^\alpha + 1)^{3/2}} \end{array} \right. \quad (2.44a)$$

$$\left\{ \begin{array}{l} \ddot{\eta} = \eta n^2 - 2n\dot{\xi} - \frac{\eta \mu^{1-3\alpha}}{(\zeta^2 + \eta^2 + \xi^2)^{3/2}} + \\ \quad + \frac{\eta (\mu - 1)}{(\mu^{2\alpha} (\zeta^2 + \eta^2 + \xi^2) + 2\xi \mu^\alpha + 1)^{3/2}} \end{array} \right. \quad (2.44b)$$

$$\left\{ \begin{array}{l} \ddot{\zeta} = \zeta \left(\frac{\mu - 1}{(\mu^{2\alpha} (\zeta^2 + \eta^2 + \xi^2) + 2\xi \mu^\alpha + 1)^{3/2}} - \frac{\mu^{1-3\alpha}}{(\zeta^2 + \eta^2 + \xi^2)^{3/2}} \right) \end{array} \right. \quad (2.44c)$$

then if we select $\alpha = 1/3$ the three forces components will have the same order of magnitude and expanding in Maclaurin series with respect to μ until 0 order and we assume $n = 1$, we obtain:

$$\left\{ \begin{array}{l} \ddot{\xi} = 2\dot{\eta} + 3\xi - \frac{\xi}{(\zeta^2 + \eta^2 + \xi^2)^{3/2}} \\ \ddot{\eta} = -2\dot{\xi} - \frac{\eta}{(\zeta^2 + \eta^2 + \xi^2)^{3/2}} \\ \ddot{\zeta} = -\zeta - \frac{\zeta}{(\zeta^2 + \eta^2 + \xi^2)^{3/2}} \end{array} \right. \quad (2.45a)$$

$$\left. \begin{array}{l} \ddot{\xi} = 2\dot{\eta} + 3\xi - \frac{\xi}{(\zeta^2 + \eta^2 + \xi^2)^{3/2}} \\ \ddot{\eta} = -2\dot{\xi} - \frac{\eta}{(\zeta^2 + \eta^2 + \xi^2)^{3/2}} \end{array} \right\} \quad (2.45b)$$

$$\left. \begin{array}{l} \ddot{\eta} = -2\dot{\xi} - \frac{\eta}{(\zeta^2 + \eta^2 + \xi^2)^{3/2}} \\ \ddot{\zeta} = -\zeta - \frac{\zeta}{(\zeta^2 + \eta^2 + \xi^2)^{3/2}} \end{array} \right\} \quad (2.45c)$$

They represent the three second order autonomous non-linear differential equations, as re-proposed by [56]. At this point the Potential function for the Hill problem can be introduced:

$$\Omega_{Hill} = \frac{1}{2} (3\xi^2 - \zeta^2) + \frac{1}{\sqrt{\xi^2 + \eta^2 + \zeta^2}} \quad (2.46)$$

Hence, the Equation (2.45) appear in a more succinct form as:

$$\left\{ \begin{array}{l} \ddot{\xi} = 2\dot{\eta} + \frac{\partial \Omega}{\partial x} \\ \ddot{\eta} = -2\dot{\xi} + \frac{\partial \Omega}{\partial y} \end{array} \right. \quad (2.47a)$$

$$\left. \begin{array}{l} \ddot{\xi} = 2\dot{\eta} + \frac{\partial \Omega}{\partial x} \\ \ddot{\eta} = -2\dot{\xi} + \frac{\partial \Omega}{\partial y} \end{array} \right\} \quad (2.47b)$$

$$\left. \begin{array}{l} \ddot{\eta} = -2\dot{\xi} + \frac{\partial \Omega}{\partial y} \\ \ddot{\zeta} = \frac{\partial \Omega}{\partial z} \end{array} \right\} \quad (2.47c)$$

Then, the Energy of the Hill system is:

$$E_{Hill} = \frac{1}{2} (\dot{\xi}^2 + \dot{\eta}^2 + \dot{\zeta}^2) + \xi\dot{\eta} - \eta\dot{\xi} - \Omega_{Hill} \quad (2.48)$$

Hill's reference frame

In the Hill reference frame the primary bodies, after the limit process, are located:

$$\left\{ \begin{array}{l} \xi|_{m_1} = -\infty \\ \xi|_{m_2} = 0 \end{array} \right. \quad (2.49a)$$

$$\left. \begin{array}{l} \xi|_{m_1} = -\infty \\ \xi|_{m_2} = 0 \end{array} \right\} \quad (2.49b)$$

The equilibrium points for Hill's model are computed as:

$$\left\{ \begin{array}{l} \dot{\xi} = 0 \\ \dot{\eta} = 0 \end{array} \right. \quad (2.50a)$$

$$\left. \begin{array}{l} \dot{\xi} = 0 \\ \dot{\eta} = 0 \end{array} \right\} \quad (2.50b)$$

$$\left. \begin{array}{l} \dot{\eta} = 0 \\ \dot{\zeta} = 0 \end{array} \right\} \quad (2.50c)$$

$$\left. \begin{array}{l} \dot{\zeta} = 0 \\ \frac{\partial \Omega}{\partial \xi} = 0 \end{array} \right\} \quad (2.50d)$$

$$\left. \begin{array}{l} \frac{\partial \Omega}{\partial \xi} = 0 \\ \frac{\partial \Omega}{\partial \eta} = 0 \end{array} \right\} \quad (2.50e)$$

$$\left. \begin{array}{l} \frac{\partial \Omega}{\partial \eta} = 0 \\ \frac{\partial \Omega}{\partial \zeta} = 0 \end{array} \right\} \quad (2.50f)$$

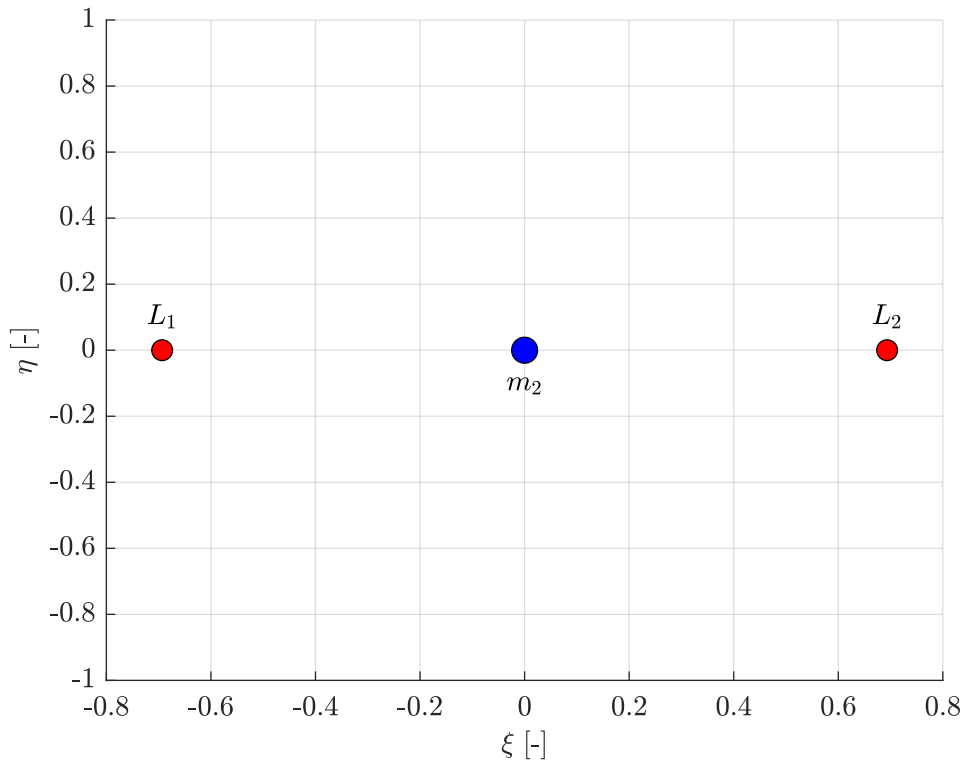


Figure 2.9: Hill's Reference System.

From the Equation (2.50), we find two collinear libration points:

$$\left\{ \begin{array}{l} L_1 = [-3^{-1/3}, 0, 0]^T \\ L_2 = [3^{-1/3}, 0, 0]^T \end{array} \right. \quad (2.51a)$$

$$\left\{ \begin{array}{l} L_1 = [-3^{-1/3}, 0, 0]^T \\ L_2 = [3^{-1/3}, 0, 0]^T \end{array} \right. \quad (2.51b)$$

The third collinear libration point does not appear in Hill's problem since m_1 moved to $-\infty$, as shown in the Figure 2.9.

Hill's Jacobi constant and zero velocity curves

The Jacobi Constant for the Hill system is:

$$\begin{aligned} J_{Hill} &= -2E \\ &= -\left(\dot{\xi}^2 + \dot{\eta}^2 + \dot{\zeta}^2\right) + \xi\dot{\eta} - \eta\dot{\xi} + (3\xi^2 - \zeta^2) + \frac{2}{\sqrt{\xi^2 + \eta^2 + \zeta^2}} \end{aligned} \quad (2.52)$$

The relative curve and surface obtained from Hill's problem are shown in Figures 2.10 to 2.12

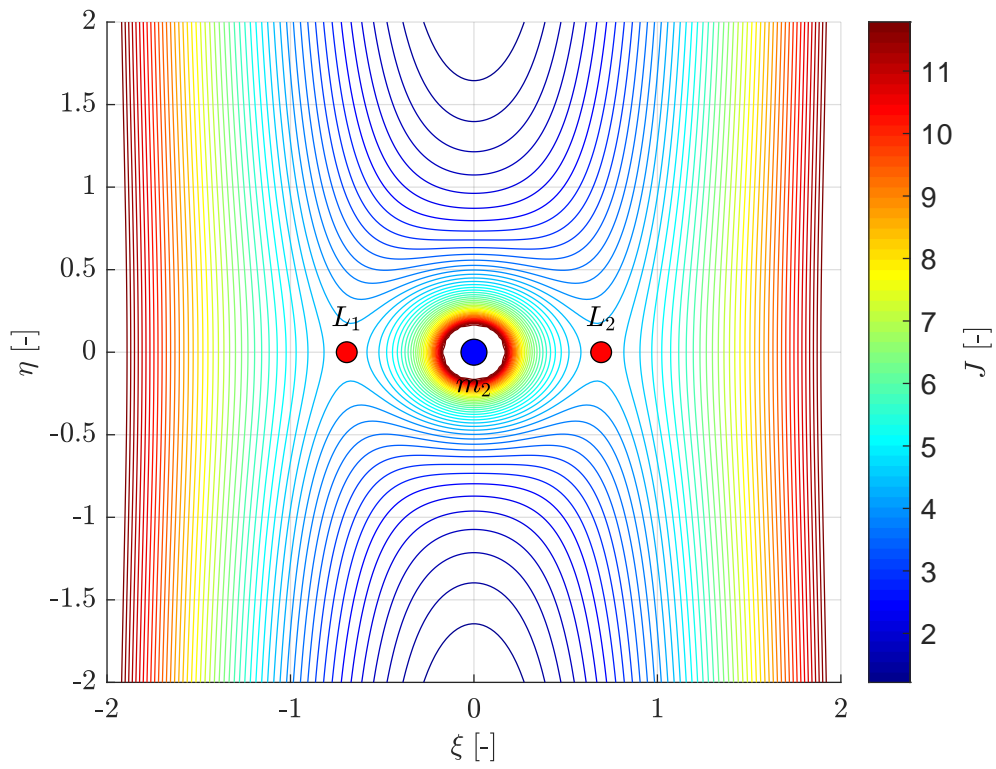


Figure 2.10: Hill's Zero Velocity Curve with $\mu=0.1$ and $n=1$.

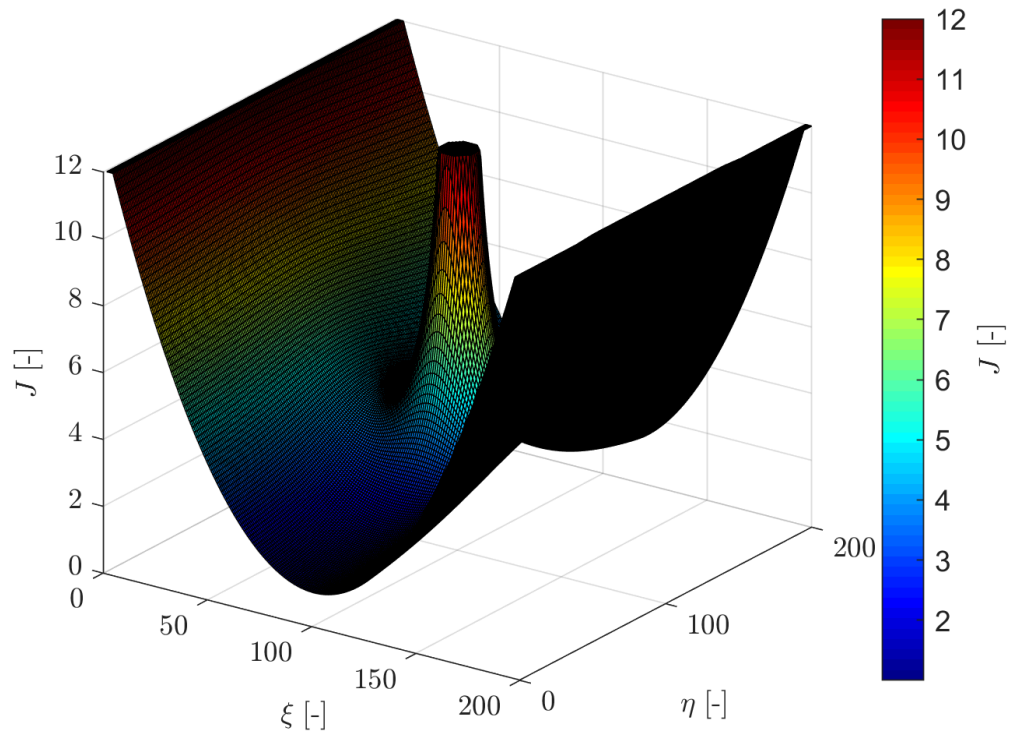


Figure 2.11: Hill's Zero Velocity Surface with $\mu=0.1$ and $n=1$.

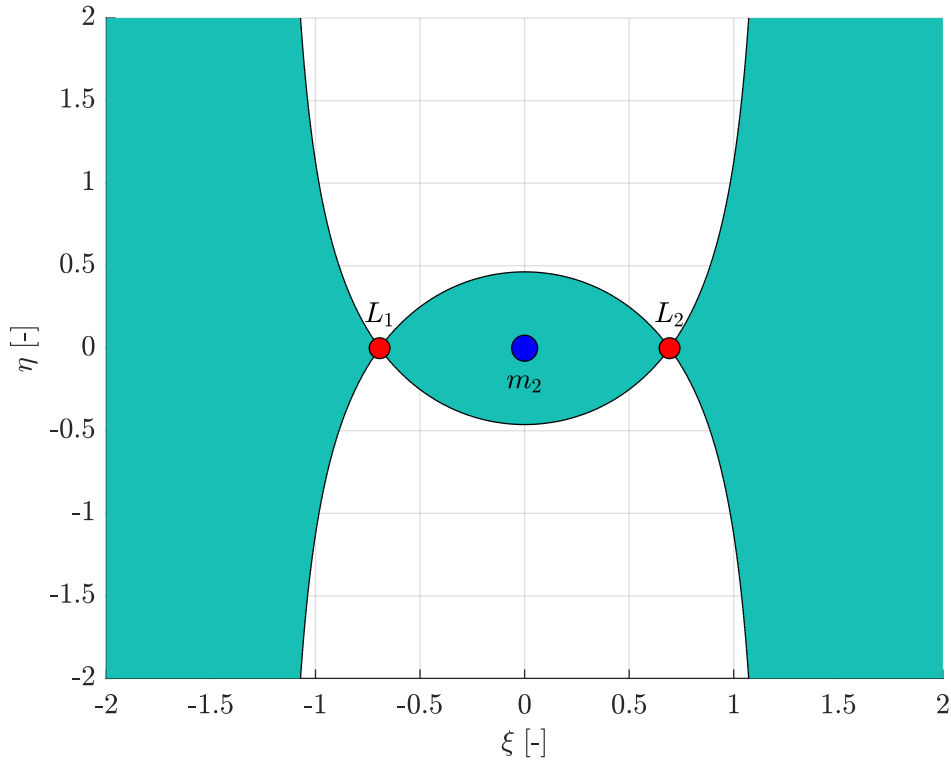


Figure 2.12: Zero Velocity Curve (black line) and and motion regions not allowed (green surface), with $\mu=0.1$ and $n=1$.

2.4.3 First term of the circular restricted three-body problem

This model is the simplified model of CR3BP. It represents a middle ground between the Hill model and the CR3BP. This is the model we will deal with later for the analytical resolution which is the purpose of the thesis. This model starts from Equation (2.44c) to which $\alpha = 1/3$ applies, as in the case of Hill, then we execute a series of Maclaurin series expansion stopped at order 1 and no longer at order 0 as Hill. As a consequence, the equations of motion are:

$$\left\{ \begin{array}{l} \ddot{\xi} = 2n\dot{\eta} + 3n^2\xi - \frac{\xi}{(\xi^2 + \eta^2 + \zeta^2)^{3/2}} + \\ \quad + 3\sqrt[3]{\mu n^2} \left(-\xi^2 + \frac{1}{2}(\eta^2 + \zeta^2) \right) + 2\sqrt[3]{\mu^2 n^2} \xi (2\xi^2 - 3(\eta^2 + \zeta^2)) + \\ \quad - \frac{\mu n^2}{8} (40\xi^4 - 120\xi^2(\eta^2 + \zeta^2) + 16\xi + 15(\eta^2 + \zeta^2)^2) \\ \ddot{\eta} = -2n\dot{\xi} - \frac{\eta}{(\xi^2 + \eta^2 + \zeta^2)^{3/2}} + 3\sqrt[3]{\mu n^2} \xi \eta + \\ \quad + 3\frac{\sqrt[3]{\mu^2 n^2}}{2} \eta (-4\xi^2 + \eta^2 + \zeta^2) + \frac{\mu n^2}{2} \eta (20\xi^3 - 15\xi(\eta^2 + \zeta^2) + 2) \\ \ddot{\zeta} = -n^2\zeta - \frac{\zeta}{(\xi^2 + \eta^2 + \zeta^2)^{3/2}} + 3\sqrt[3]{\mu n^2} \xi \zeta + \\ \quad + 3\frac{\sqrt[3]{\mu^2 n^2}}{2} \zeta (-4\xi^2 + \eta^2 + \zeta^2) + \frac{\mu n^2}{2} \zeta (20\xi^3 - 15\xi(\eta^2 + \zeta^2) + 2) \end{array} \right. \quad (2.53a)$$

(2.53b)

(2.53c)

Chapter 3

Lagrange's approach and Hamiltonian mechanics

The Lagrangian approach, compared to the Newtonian approach, seen so far, focuses exclusively on the energy of the system, losing sight of the individual constraints and reactions involved. This approach is based on the Lagrange Equation (3.2):

$$\frac{d}{dt} \left(\frac{\partial \mathcal{L}}{\partial \dot{\underline{X}}} \right) - \frac{\partial \mathcal{L}}{\partial \underline{X}} = \underline{Q} \quad (3.1)$$

which, if the system is conservative (as in the case of orbital dynamics), takes the following form:

$$\frac{d}{dt} \left(\frac{\partial \mathcal{L}}{\partial \dot{\underline{X}}} \right) - \frac{\partial \mathcal{L}}{\partial \underline{X}} = \underline{0} \quad (3.2)$$

where:

$$\mathcal{L} = T + V = T - U \quad (3.3)$$

is the Lagrange function defined as the sum of the kinetic energy and the potential function or as the difference between the kinetic energy and the potential energy, \underline{X} represents the coordinate vector and \underline{Q} is the vector of non-conservative generalist forces.

To obtain the Hamiltonian function, it can be used the variational principles (Ref. [3, 5, 6, 11]). The deduction of the equations consists essentially in constructing the Legendre transformation of the Lagrangian, using the generalized velocities as variables. In this way the phase space is introduced, and the dynamics generated by a Hamiltonian function are described. For a detailed description refer to [26].

First of all, the Lagrangian function allows us to move in phase space, thanks to conjugate moments (\underline{p}). They are so defined:

$$\left\{ \begin{array}{l} \underline{p} = \frac{\partial \mathcal{L}}{\partial \dot{\underline{q}}} \\ \underline{\dot{p}} = \frac{\partial \mathcal{L}}{\partial \underline{q}} \end{array} \right. \quad (3.4a)$$

$$\left\{ \begin{array}{l} \underline{p} = \frac{\partial \mathcal{L}}{\partial \dot{\underline{q}}} \\ \underline{\dot{p}} = \frac{\partial \mathcal{L}}{\partial \underline{q}} \end{array} \right. \quad (3.4b)$$

which allow to replace the generalized speed and bring the whole system back to a form of the first order.

The Equation (3.4) are equivalent to the Hamilton equation system in the form:

$$\begin{cases} \dot{\underline{q}} = \frac{\partial \mathcal{H}}{\partial \underline{p}} & (3.5a) \\ \dot{\underline{p}} = -\frac{\partial \mathcal{H}}{\partial \underline{q}} & (3.5b) \end{cases}$$

where the Hamiltonian function $\mathcal{H}(\underline{q}, \underline{p}, t)$ is the Legendre transformation of the Lagrangian function, called:

$$\mathcal{H}(\underline{q}, \underline{p}, t) = [\underline{p}^T \cdot \dot{\underline{q}} - \mathcal{L}(\underline{q}, \dot{\underline{q}}, t)] \Big|_{\dot{\underline{q}}=\dot{\underline{q}}(\underline{q}, \underline{p}, t)} \quad (3.6)$$

remembering that (\underline{q}) are the generalized coordinates.

3.1 CR3BP model

3.1.1 Inertial reference frame

First of all it is necessary to consider the energies that come into play which are, kinetic energy, which in the inertial case has the form:

$$T_I = \frac{1}{2}(\dot{x}^2 + \dot{y}^2 + \dot{z}^2) \quad (3.7)$$

and subsequently the potential energy is:

$$V_I = \frac{1-\mu}{R_1} + \frac{\mu}{R_2} \quad (3.8)$$

where:

$$R_1 = \sqrt{(x + \mu \cos(nt + \vartheta_0))^2 + (y + \mu \sin(nt + \vartheta_0))^2 + z^2} \quad (3.9a)$$

$$R_2 = \sqrt{(x - (1-\mu) \cos(nt + \vartheta_0))^2 + (y - (1-\mu) \sin(nt + \vartheta_0))^2 + z^2} \quad (3.9b)$$

consequently, the Lagrangian function turns out to be:

$$\mathcal{L}_I = T_I + V_I \quad (3.10a)$$

$$= \frac{1}{2}(\dot{x}^2 + \dot{y}^2 + \dot{z}^2) + \frac{1-\mu}{R_1} + \frac{\mu}{R_2} \quad (3.10b)$$

Now, by applying the Lagrange equation (Equation (3.2)), it is possible to obtain the equations of motion of the system, such as:

$$\begin{cases} \ddot{x} = -\frac{(1-\mu)(x + \mu \cos(nt + \vartheta_0))}{(R_1)^3} - \frac{\mu(x - (1-\mu) \cos(nt + \vartheta_0))}{(R_2)^3} & (3.11a) \\ \ddot{y} = -\frac{(1-\mu)(y + \mu \sin(nt + \vartheta_0))}{(R_1)^3} - \frac{\mu(y - (1-\mu) \sin(nt + \vartheta_0))}{(R_2)^3} & (3.11b) \\ \ddot{z} = -\frac{(1-\mu)z}{(R_1)^3} - \frac{\mu z}{(R_2)^3} & (3.11c) \end{cases}$$

They represent a sum between the Keplerian contribution (1st term) produced by the main (primary) attractor and a second contribution due to the secondary attractor. If

we apply Equation (3.4a) for the Lagrangian function (Equation (3.10)), it is possible to obtain the generalized speed function of the conjugated moments as:

$$p_x = \dot{x} \quad (3.12a)$$

$$p_y = \dot{y} \quad (3.12b)$$

$$p_z = \dot{z} \quad (3.12c)$$

Now replacing the definition of Equation (3.6) it is possible to write the Hamiltonian function as:

$$\mathcal{H}_I = p_x \dot{x} + p_y \dot{y} + p_z \dot{z} - \mathcal{L}_I \quad (3.13a)$$

$$= \frac{1}{2} p_x^2 + \frac{1}{2} p_y^2 + \frac{1}{2} p_z^2 - \frac{1-\mu}{R_1} - \frac{\mu}{R_2} \quad (3.13b)$$

Thus, the system of differential equations of the first order, derived from Equations (3.5) and (3.13b), is:

$$\left\{ \begin{array}{l} \dot{x} = p_x \quad (3.14a) \\ \dot{y} = p_y \quad (3.14b) \\ \dot{z} = p_z \quad (3.14c) \end{array} \right.$$

$$\left\{ \begin{array}{l} \dot{p}_x = -\frac{(1-\mu)(x + \mu \cos(nt + \vartheta_0))}{(R_1)^3} - \frac{\mu(x - (1-\mu) \cos(nt + \vartheta_0))}{(R_2)^3} \quad (3.14d) \end{array} \right.$$

$$\left\{ \begin{array}{l} \dot{p}_y = -\frac{(1-\mu)(y + \mu \sin(nt + \vartheta_0))}{(R_1)^3} - \frac{\mu(y - (1-\mu) \sin(nt + \vartheta_0))}{(R_2)^3} \quad (3.14e) \end{array} \right.$$

$$\left\{ \begin{array}{l} \dot{p}_z = -\frac{(1-\mu)z}{(R_1)^3} - \frac{\mu z}{(R_2)^3} \quad (3.14f) \end{array} \right.$$

3.1.2 Rotating reference frame

First of all, we move the reference system in the center of gravity of the CR3BP. Subsequently, we pass to a rotating reference frame using the definition in Appendix A.2. Therefore, to construct the Lagrangian function, we need kinetic energy which, through the rotation matrix just described, is written in the form:

$$T_R = \frac{1}{2}(\dot{x}^2 + \dot{y}^2 + \dot{z}^2) + nx\dot{y} - ny\dot{x} \quad (3.15)$$

On the other hand, the potential energy, once the change in the reference system has been applied, has the form:

$$V_R = \frac{1}{2}n^2(x^2 + y^2) + \frac{1-\mu}{r_1} + \frac{\mu}{r_2} \quad (3.16)$$

where:

$$r_1 = \sqrt{(x + \mu)^2 + y^2 + z^2} \quad (3.17a)$$

$$r_2 = \sqrt{(x - (1-\mu))^2 + y^2 + z^2} \quad (3.17b)$$

Hence, the Lagrangian function is:

$$\mathcal{L}_R = T_R + V_R \quad (3.18a)$$

$$= \frac{1}{2}(\dot{x}^2 + \dot{y}^2 + \dot{z}^2) + nx\dot{y} - ny\dot{x} + \frac{1}{2}n^2(x^2 + y^2) + \frac{1-\mu}{r_1} + \frac{\mu}{r_2} \quad (3.18b)$$

$$= \frac{1}{2} \left[(\dot{x} - ny)^2 + (\dot{y} + nx)^2 + \dot{z}^2 \right] + \frac{1-\mu}{r_1} + \frac{\mu}{r_2} \quad (3.18c)$$

From the Equation (3.18) it is possible, applying the Lagrange's equation, Equation (3.2), from which it is possible to obtain the equations of motion of the system as:

$$\begin{cases} \ddot{x} = 2n\dot{y} + n^2x - \frac{(1-\mu)(x+\mu)}{(r_1)^3} - \frac{\mu(x-(1-\mu))}{(r_2)^3} \end{cases} \quad (3.19a)$$

$$\begin{cases} \ddot{y} = -2n\dot{x} + n^2y - \frac{(1-\mu)y}{(r_1)^3} - \frac{\mu y}{(r_2)^3} \end{cases} \quad (3.19b)$$

$$\begin{cases} \ddot{z} = -\frac{(1-\mu)z}{(r_1)^3} - \frac{\mu z}{(r_2)^3} \end{cases} \quad (3.19c)$$

Resulting the same as Equation (2.16). If we now refer to the Lagrangian function of Equation (3.18), and remembering the definition of the conjugated moments (Equation (3.4a)), we obtain:

$$\begin{cases} p_x = \dot{x} - ny & (3.20a) \\ p_y = \dot{y} + nx & (3.20b) \\ p_z = \dot{z} & (3.20c) \end{cases}$$

and then, exploiting the definition of Equation (3.6), we get the Hamiltonian function, as:

$$\mathcal{H}_R = p_x\dot{x} + p_y\dot{y} + p_z\dot{z} - \mathcal{L}_R \quad (3.21a)$$

$$= p_x\dot{x} + p_y\dot{y} + p_z\dot{z} - \left[\frac{1}{2}(p_x^2 + p_y^2 + p_z^2) + \frac{1-\mu}{r_1} + \frac{\mu}{r_2} \right] \quad (3.21b)$$

$$= p_x(p_x + ny) + p_y(p_y - nx) + p_z(p_z) - \frac{1}{2}(p_x^2 + p_y^2 + p_z^2) + \frac{1-\mu}{r_1} + \frac{\mu}{r_2} \quad (3.21c)$$

$$= \frac{1}{2}(p_x^2 + p_y^2 + p_z^2) + n(y p_x - x p_y) - \frac{1-\mu}{r_1} - \frac{\mu}{r_2} \quad (3.21d)$$

Analogously to Equation (3.14), the following differential system of the first order is obtained:

$$\begin{cases} \dot{x} = p_x + ny & (3.22a) \end{cases}$$

$$\begin{cases} \dot{y} = p_y - nx & (3.22b) \end{cases}$$

$$\begin{cases} \dot{z} = p_z & (3.22c) \end{cases}$$

$$\begin{cases} \dot{p}_x = n p_y - \frac{(1-\mu)(\mu+x)}{(r_1)^3} - \frac{\mu(x-(1-\mu))}{(r_2)^3} \end{cases} \quad (3.22d)$$

$$\begin{cases} \dot{p}_y = -n p_x - \frac{(1-\mu)y}{(r_1)^3} - \frac{\mu y}{(r_2)^3} \end{cases} \quad (3.22e)$$

$$\begin{cases} \dot{p}_z = -\frac{(1-\mu)z}{(r_1)^3} - \frac{\mu z}{(r_2)^3} \end{cases} \quad (3.22f)$$

Finally the Hamiltonian function is related to the Jacobi constant by:

$$J_R = -2\mathcal{H}_R + (1-\mu)\mu \quad (3.23)$$

it follows:

$$\mathcal{H}_R = -\frac{1}{2}J_R + \frac{1}{2}(1-\mu)\mu \quad (3.24)$$

3.1.3 Rotating reference frame centred in the second attractor

An important variation of the current model is that in which the reference system centred in the secondary is considered. This approach is also fruitful during Hill's approximation of CR3BP. In this case the form of kinetic energy is:

$$T_{R-B2} = \frac{1}{2}(\dot{x}^2 + \dot{y}^2 + \dot{z}^2) + nxy\dot{y} - ny\dot{x} \quad (3.25)$$

Instead, the potential function becomes:

$$V_{R-B2} = n^2(1-\mu)x + \frac{1-\mu}{r_{1-B2}} + \frac{\mu}{r_{2-B2}} \quad (3.26)$$

where:

$$r_{1-B2} = \sqrt{(x+1)^2 + y^2 + z^2} \quad (3.27a)$$

$$r_{2-B2} = \sqrt{x^2 + y^2 + z^2} \quad (3.27b)$$

consequently, the Lagrangian function turns out to be:

$$\mathcal{L}_{R-B2} = \frac{1}{2}(\dot{x}^2 + \dot{y}^2 + \dot{z}^2) + nxy\dot{y} - ny\dot{x} + n^2(1-\mu)x + \frac{1-\mu}{r_{1-B2}} + \frac{\mu}{r_{2-B2}} \quad (3.28)$$

Using the Lagrange equation again, the equations of motion can be obtained as follows:

$$\begin{cases} \ddot{x} = 2ny\dot{y} + n^2x + (1-\mu)n^2 - \frac{(1-\mu)(x+1)}{(r_{1-B2})^3} - \frac{\mu x}{(r_{2-B2})^3} \end{cases} \quad (3.29a)$$

$$\begin{cases} \ddot{y} = -2n\dot{x} + n^2y - \frac{(1-\mu)y}{(r_{1-B2})^3} - \frac{\mu y}{(r_{2-B2})^3} \end{cases} \quad (3.29b)$$

$$\begin{cases} \ddot{z} = -\frac{(1-\mu)z}{(r_{1-B2})^3} - \frac{\mu z}{(r_{2-B2})^3} \end{cases} \quad (3.29c)$$

Similarly to what we did in the previous section, we can obtain the conjugated moments of the Lagrangian function of Equation (3.28), as follows:

$$\begin{cases} p_x = \dot{x} - ny \end{cases} \quad (3.30a)$$

$$\begin{cases} p_y = \dot{y} + nx \end{cases} \quad (3.30b)$$

$$\begin{cases} p_z = \dot{z} \end{cases} \quad (3.30c)$$

Hence, we have the Hamiltonian function, as:

$$\mathcal{H}_{R-B2} = \frac{1}{2}(p_x^2 + p_y^2 + p_z^2) + n(y p_x - x p_y) - n^2(1-\mu)x - \frac{1-\mu}{r_{1-B2}} - \frac{\mu}{r_{2-B2}} \quad (3.31)$$

the following differential system of the first order is obtained:

$$\begin{cases} \dot{x} = p_x + ny & (3.32a) \end{cases}$$

$$\begin{cases} \dot{y} = p_y - nx & (3.32b) \end{cases}$$

$$\begin{cases} \dot{z} = p_z & (3.32c) \end{cases}$$

$$\begin{cases} \dot{p}_x = np_y + n^2(1-\mu) - \frac{(1-\mu)(1+x)}{(r_{1-B2})^3} - \frac{\mu x}{(r_{2-B2})^3} & (3.32d) \end{cases}$$

$$\begin{cases} \dot{p}_y = -np_x - \frac{(1-\mu)y}{(r_{1-B2})^3} - \frac{\mu y}{(r_{2-B2})^3} & (3.32e) \end{cases}$$

$$\begin{cases} \dot{p}_z = -\frac{(1-\mu)z}{(r_{1-B2})^3} - \frac{\mu z}{(r_{2-B2})^3} & (3.32f) \end{cases}$$

3.2 Hill's model

The Hill model is a simplified model of CR3BP, in fact, it aims to explore the dynamics in the vicinity of the secondary attraction, placing, “virtually”, the primary attractor at an infinite distance from the secondary. This assumption means the model's inability to correctly predict the dynamics of the third body (artificial satellite) in regions far from the secondary attractor and therefore where influence of the primary attractor increasing. As described for the first time by Hill [35, 36], and reworked by Hénon [30, 31], the kinetic energy has the following form:

$$T_{Hill} = \frac{1}{2}(\dot{x}^2 + \dot{y}^2 + \dot{z}^2) + nyx - ny\dot{x} \quad (3.33)$$

instead, the potential function is written as:

$$V_{Hill} = \frac{1}{2}n^2(3x^2 - z^2) + \frac{1}{r_{2-B2}} \quad (3.34)$$

therefore, it is possible to write the Lagrangian function of the system, it follows:

$$\mathcal{L}_{Hill} = \left[\frac{1}{2}(\dot{x}^2 + \dot{y}^2 + \dot{z}^2) + nyx - n\eta\dot{x} \right] + \left[\frac{1}{2}n^2(3x^2 - z^2) + \frac{1}{r_{2-B2}} \right] \quad (3.35)$$

It is possible, applying the Lagrange equation, Equation (3.2), from which it is possible to obtain the equations of motion of the system in the form:

$$\begin{cases} \ddot{x} = 2n\dot{y} + 3n^2x - \frac{x}{(r_{2-B2})^3} & (3.36a) \end{cases}$$

$$\begin{cases} \ddot{y} = -2n\dot{x} - \frac{y}{(r_{2-B2})^3} & (3.36b) \end{cases}$$

$$\begin{cases} \ddot{z} = -n^2z - \frac{z}{(r_{2-B2})^3} & (3.36c) \end{cases}$$

the system of Equation (3.36) is identical to that of Equation (2.45). The maintenance of the variables n is for completeness, it, in the Hill model, is unitary. Following the Equation (3.4a), it is possible to obtain the generalized speed function from the

conjugated moments as:

$$\begin{cases} \dot{x} = p_x + ny & (3.37a) \\ \dot{y} = p_y - nx & (3.37b) \\ \dot{z} = p_z & (3.37c) \end{cases}$$

Now applying the definition of Equation (3.6) it is possible to write the Hamiltonian function for the Hill model as:

$$\mathcal{H}_{Hill} = \frac{1}{2} \left((p_x + ny)^2 + (p_y - nx)^2 + p_z^2 \right) - \frac{1}{2} n^2 (3x^2 - z^2) - \frac{1}{r_{2-B2}} \quad (3.38)$$

3.3 First order term of the circular restricted three-body problem model

Given the nature of the problem the kinetic energy remains almost unchanged compared to that of Section 3.2 in fact turns out to be:

$$T_{CR3BP-1} = \frac{1}{2} (\dot{x}^2 + \dot{y}^2 + \dot{z}^2) + nx\dot{y} - ny\dot{x} \quad (3.39)$$

For the CR3BP-1 model the potential function turns out to be equal to that of Hill to which some terms are added, from which it results:

$$\begin{aligned} V_{CR3BP-1} = & \frac{1}{2} n^2 (3x^2 - z^2) + \frac{1}{r_{2-B2}} + \frac{n^2}{p} \left(-x^3 + \frac{3}{2} x (y^2 + z^2) \right) + \\ & + \frac{n^2}{p^2} \left(-3x^2 (y^2 + z^2) + x^4 + \frac{3}{8} (y^2 + z^2)^2 \right) + \\ & + \frac{n^2}{p^3} \left(5x^3 (y^2 + z^2) - \frac{15}{8} x (y^2 + z^2)^2 - (x^3 + 1) x^2 + \right. \\ & \left. + \frac{1}{2} (y^2 + z^2) \right) \end{aligned} \quad (3.40)$$

where p is the non-dimensional distance between first and second attractor:

$$p = \frac{1}{\sqrt[3]{\mu}} \quad (3.41)$$

In the same way as already done, use the Equation (3.3) to obtain the Lagrangian function which has the following form:

$$\begin{aligned}
\mathcal{L}_{CR3BP-1} = & \left[\frac{1}{2} (\dot{x}^2 + \dot{y}^2 + \dot{z}^2) + n\dot{y}x - ny\dot{x} \right] + \left[\frac{1}{2} n^2 (3x^2 - z^2) + \right. \\
& + \frac{1}{r_{2-B2}} + \frac{n^2}{p} \left(-x^3 + \frac{3}{2} x (y^2 + z^2) \right) + \\
& + \frac{n^2}{p^2} \left(-3x^2 (y^2 + z^2) + x^4 + \frac{3}{8} (y^2 + z^2)^2 \right) + \\
& + \frac{n^2}{p^3} \left(5x^3 (y^2 + z^2) - \frac{15}{8} x (y^2 + z^2)^2 - (x^3 + 1) x^2 + \right. \\
& \left. \left. + \frac{1}{2} (y^2 + z^2) \right) \right] \quad (3.42)
\end{aligned}$$

From the Equation (3.42), using the well-known Lagrange Equation (3.2), we can obtain the system of second order differential equations:

$$\left\{ \begin{aligned} \ddot{x} = & 2n\dot{y} + 3n^2x - \frac{x}{(r_{2-B2})^3} + \\ & + 3\frac{n^2}{p} \left(-x^2 + \frac{1}{2} (y^2 + z^2) \right) + 2\frac{n^2}{p^2}x (2x^2 - 3(y^2 + z^2)) + \\ & - \frac{1}{8}\frac{n^2}{p^3} \left(40x^4 - 120x^2 (y^2 + z^2) + 16x + 15 (y^2 + z^2)^2 \right) \end{aligned} \right. \quad (3.43a)$$

$$\left\{ \begin{aligned} \ddot{y} = & -2n\dot{x} - \frac{y}{(r_{2-B2})^3} + 3\frac{n^2}{p}xy + \\ & + \frac{3}{2}\frac{n^2}{p^2}y (-4x^2 + y^2 + z^2) + \frac{1}{2}\frac{n^2}{p^3}y (20x^3 - 15x (y^2 + z^2) + 2) \end{aligned} \right. \quad (3.43b)$$

$$\left\{ \begin{aligned} \ddot{z} = & -n^2z - \frac{z}{(r_{2-B2})^3} + 3\frac{n^2}{p}xz + \\ & + \frac{3}{2}\frac{n^2}{p^2}z (-4x^2 + y^2 + z^2) + \frac{1}{2}\frac{n^2}{p^3}z (20x^3 - 15x (y^2 + z^2) + 2) \end{aligned} \right. \quad (3.43c)$$

similar to the Equation (2.53). Following the Equation (3.4a) for Equation (3.46), it is possible to obtain the generalized speed function of the conjugated moments, which are identical to the Equation (3.37). Applying the Equation (3.6) it is possible to write the Hamiltonian function, as:

$$\begin{aligned}
\mathcal{H}_{CR3BP-1} = & \frac{1}{2} \left((p_x + ny)^2 + (p_y - nx)^2 + p_z^2 \right) - \frac{1}{2} n^2 (3x^2 - z^2) + \\
& - \frac{1}{r_{2-B2}} + \frac{n^2}{p} x \left(x^2 - \frac{3}{2} (y^2 + z^2) \right) + \\
& - \frac{n^2}{p^2} \left(-3x^2 (y^2 + z^2) + x^4 + \frac{3}{8} (y^2 + z^2)^2 \right) + \\
& - \frac{n^2}{p^3} \left(5x^3 (y^2 + z^2) - \frac{15}{8} x (y^2 + z^2)^2 - (x^3 + 1) x^2 + \right. \\
& \left. + \frac{1}{2} (y^2 + z^2) \right) \quad (3.44)
\end{aligned}$$

3.3.1 First term of the circular restricted three-body problem model

This model represents a simplification of the CR3BP-1, where only the terms most relevant are considered. In particular, since $0 < \mu < 1$ the most important terms are those for $\sqrt[3]{\mu} = 1/p$ and therefore the remaining terms can be ignored. Consequently the kinetic energy remaining equal to the Equation (3.39), instead the potential function is reduced to:

$$V_{CR3BP-1_{13}} = \frac{1}{2}n^2(3x^2 - z^2) + \frac{1}{r_{2-B2}} + \frac{n^2}{p} \left(-x^3 + \frac{3}{2}x(y^2 + z^2) \right) \quad (3.45)$$

Hence the Lagrangian function which has the following form:

$$\begin{aligned} \mathcal{L}_{CR3BP-1_{13}} = & \left[\frac{1}{2}(\dot{x}^2 + \dot{y}^2 + \dot{z}^2) + n y \dot{x} - n y \dot{x} \right] + \left[\frac{1}{2}n^2(3x^2 - z^2) + \right. \\ & \left. + \frac{1}{r_{2-B2}} + \frac{n^2}{p} \left(-x^3 + \frac{3}{2}x(y^2 + z^2) \right) \right] \end{aligned} \quad (3.46)$$

We can obtain the equation of motion:

$$\begin{cases} \ddot{x} = 2n\dot{y} + 3n^2x - \frac{x}{(r_{2-B2})^3} + 3\frac{n^2}{p} \left(-x^2 + \frac{1}{2}(y^2 + z^2) \right) \end{cases} \quad (3.47a)$$

$$\begin{cases} \ddot{y} = -2n\dot{x} - \frac{y}{(r_{2-B2})^3} + 3\frac{n^2}{p}xy \end{cases} \quad (3.47b)$$

$$\begin{cases} \ddot{z} = -n^2z - \frac{z}{(r_{2-B2})^3} + 3\frac{n^2}{p}xz \end{cases} \quad (3.47c)$$

As done before, the conjugated moments turns out to be identical to the Equation (3.37). The Hamiltonian function is:

$$\begin{aligned} \mathcal{H}_{CR3BP-1_{13}} = & \frac{1}{2} \left((p_x + ny)^2 + (p_y - nx)^2 + p_z^2 \right) - \frac{1}{2}n^2(3x^2 - z^2) + \\ & - \frac{1}{r_{2-B2}} + \frac{n^2}{p}x \left(x^2 - \frac{3}{2}(y^2 + z^2) \right) \end{aligned} \quad (3.48)$$

Chapter 4

Perturbation approach applied to the Hill model

The study aim, as already mentioned, is to find a first approximate analytical solution for the CR3BP for the planar problem, applicable to DRO computation. In this chapter the approach proposed by Lara [38, 39] will be explained as this will be the basis for the development in the next chapter which represents the original contribution of this work. In Figure 4.1 a generic DRO and its configuration is shown. First of all, we identify some particular points on the orbit. The quadrature points, defined as ad-

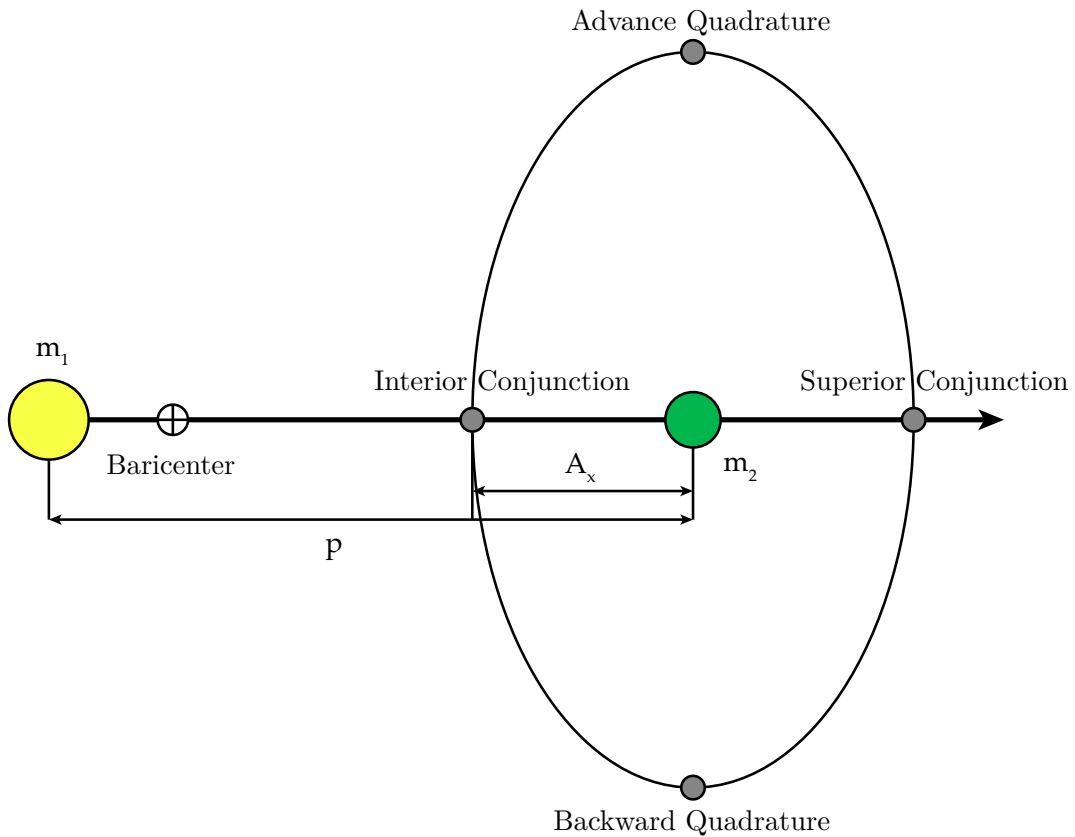


Figure 4.1: Generic configuration and features of DRO.

vance and backward, are points in which the third body moves to the most advanced or backward position with respect to the secondary attractor. Instead, we call interior and superior junction points, those points for which the third body is closer or far from the primary attractor [55]. In particular, the orbit amplitudes (A_x) is defined as the distance between the secondary attractor and the point of intersection between

the orbit and the abscissa axis in the direction of the primary attractor. Since the problem is planar, we impose $z = p_z = 0$. With this assumption Equation (3.38) is simplified as follows:

$$\mathcal{H} = \frac{1}{2} (p_x^2 + p_y^2) - nxp_y + nyp_x - n^2x^2 + \frac{1}{2}n^2y^2 - \frac{1}{\sqrt{x^2 + y^2}} \quad (4.1)$$

where p_x and p_y are the conjugate momenta and x and y coordinates in rotating reference frame and n is the non-dimensional mean motion. Another important assumption is that we are seeking solution for DRO: this means that the third body (artificial satellite) is at a considerable distance from the secondary attraction [38, 39]. This assumption allows rewriting the Hamiltonian function in the following form:

$$\mathcal{H} = \mathcal{H}_0 + \varepsilon\mathcal{H}_1 \quad (4.2)$$

where the term \mathcal{H}_0 constitutes the unperturbed Hamiltonian and $\varepsilon\mathcal{H}_1$ represents, instead, the one associated with the perturbation due to the third body. In our case the two terms have the following form:

$$\begin{cases} \mathcal{H}_0 = \frac{1}{2} (p_x^2 + p_y^2) - nxp_y + nyp_x - n^2x^2 + \frac{1}{2}n^2y^2 & (4.3a) \\ \mathcal{H}_1 = -\frac{1}{\sqrt{x^2 + y^2}} & (4.3b) \end{cases}$$

In the next sessions we will first define and find a canonical transformation, for the unperturbed part only, that will allow us to simplify the problem. In Hamiltonian mechanics, a canonical transformation is a change of canonical coordinates, which are a sets of coordinates on phase space which can be used to describe a physical system. We will subsequently apply the Lie transform, [11], which will allow us to consider the perturbing part and consequently obtain an analytical solution approaching the problem.

4.1 Canonical transformation

The study of the solutions of a system of differential equations can also take place through the search for a transformation of coordinates under whose action the system assumes a particularly simple form. In the case of the Hamiltonian formalism a transformation of coordinates must be a diffeomorphism [2, 5, 26].

First of all, the problem is to find a class of transformations $(\underline{q}, \underline{p}) = \mathcal{T}(\underline{Q}, \underline{P})$ invertible such that the system of the Hamilton equations (Equation (3.5)), relative to the Hamiltonian function $\mathcal{H}(\underline{q}, \underline{p}, t)$ is transformed into the system written in canonical variables:

$$\begin{cases} \dot{\underline{Q}} = \frac{\partial \mathcal{K}}{\partial \underline{P}} & (4.4a) \\ \dot{\underline{P}} = -\frac{\partial \mathcal{K}}{\partial \underline{Q}} & (4.4b) \end{cases}$$

which can be rewritten in an appropriate canonical Hamiltonian function $\mathcal{K}(\underline{Q}, \underline{P}, t)$, by:

$$\mathcal{K}(\underline{Q}, \underline{P}, t) = \mathcal{H}(\underline{q}, \underline{p}, t)|_{\underline{q}=\underline{Q}, \underline{p}=\underline{P}} \quad (4.5)$$

Lie condition: One criterion for the canonicity is to satisfy the Lie condition. Although this circumstance is not particularly useful, it is very useful for obtaining

the generating functions [5, 26].

The condition for the transformation is to satisfy the differential 1-form also called *1-form of Lionville*, namely:

$$p \cdot dq = P \cdot dQ + dW(\underline{Q}, \underline{P}, t) - K_0(\underline{Q}, \underline{P}, t)dt \quad (4.6)$$

for particular W and K_0 , where W is the generating function, that depends on only $2n$ independent variables and time. This fact makes that there can be 4 types of generating functions listed in the Table 4.1 [5, 26, 58].

	\underline{q}	\underline{p}	\underline{Q}	\underline{P}
$W_1(\underline{q}, \underline{Q}, t)$		$\frac{\partial W_1}{\partial \underline{q}}$		$-\frac{\partial W_1}{\partial \underline{Q}}$
$W_2(\underline{q}, \underline{P}, t)$		$\frac{\partial W_2}{\partial \underline{q}}$	$\frac{\partial W_2}{\partial \underline{P}}$	
$W_3(\underline{p}, \underline{Q}, t)$	$-\frac{\partial W_3}{\partial \underline{p}}$			$-\frac{\partial W_3}{\partial \underline{Q}}$
$W_4(\underline{p}, \underline{P}, t)$	$-\frac{\partial W_4}{\partial \underline{p}}$		$\frac{\partial W_4}{\partial \underline{P}}$	

Table 4.1: Canonical transformation in the Phase Space.

4.1.1 Hamilton-Jacobi equation

The method of the generating function makes it possible to formulate the problem of the search for a canonical transformation:

$$\begin{cases} \underline{Q} = \underline{Q}(\underline{q}, \underline{p}) & (4.7a) \\ \underline{P} = \underline{P}(\underline{q}, \underline{p}) & (4.7b) \end{cases}$$

that combines a given Hamiltonian function $\mathcal{H}(\underline{q}, \underline{p}, t)$ with a canonical Hamiltonian function $\mathcal{K}(\underline{Q}, \underline{P}, t)$.

To determine an appropriate generating function, $S(\underline{q}, \underline{P}, t)$, we must solve a partial differential equation, called (complete) Hamilton-Jacobi equation [2, 5, 26]:

$$\mathcal{H}\left(\underline{q}, \frac{\partial S}{\partial \underline{q}}, t\right) - \frac{\partial S}{\partial t} = 0 \quad (4.8)$$

which generates the time-dependent canonical transformation by inversion of the equations:

$$\begin{cases} \underline{p} = \frac{\partial S}{\partial \underline{q}} & (4.9a) \\ \underline{Q} = -\frac{\partial S}{\partial \underline{P}} & (4.9b) \end{cases}$$

which link the generating function, $S(\underline{q}, \underline{P}, t)$, to the canonical Hamiltonian function:

$$\mathcal{K} = \mathcal{H} + \frac{\partial S}{\partial t} \quad (4.10)$$

When \mathcal{H} is time-independent, then choose $S(\underline{q}; \underline{P}; t)$ in the separate form:

$$S(\underline{q}, \underline{P}, t) = W_2(\underline{q}, \underline{P}) - \mathcal{K}(\underline{P})t \quad (4.11)$$

so that W is determined by solution of the so-called Hamilton-Jacobi reduced equation:

$$\mathcal{H}\left(\underline{q}, \frac{\partial W_2}{\partial \underline{q}}\right) = \mathcal{K}(\underline{P}) \quad (4.12)$$

in which both the W_2 and the \mathcal{K} constant are unknown.

In the case of Hill's problem, what we do is look for a canonical transformation exclusively for the unperturbed part of the Hamiltonian function Equation (4.3a). Following the definition of Equation (4.12) we can write the Hamiltonian function as:

$$\begin{aligned} \frac{1}{2} \left[\left(\frac{\partial W_2}{\partial x} \right)^2 + \left(\frac{\partial W_2}{\partial y} \right)^2 \right] + ny \frac{\partial W_2}{\partial x} - nx \frac{\partial W_2}{\partial y} - n^2 x^2 + \frac{1}{2} n^2 y^2 = \\ = \mathcal{K}(\Phi, Q) \end{aligned} \quad (4.13)$$

The Equation (4.13) represents a Partial Differential Equation PDE. The most classic way to solve these equations is the method of separating the variables. It can be immediately noticed that the equation itself does not allow factoring and therefore it is not possible to separate it. However, we can exploit Equation (3.36b) (assuming the negligible the perturbing term [24]), similarly to the Clohessy-Wiltshire equations (CWE), [54], it has the following form:

$$\ddot{y} + 2n\dot{x} = 0 \quad (4.14)$$

it can be easily integrated over time, the resulting constant represents the second canonical moment (Q). The resulting equation has the form:

$$\dot{y} + 2nx = Q \quad (4.15)$$

now applying the substitution of Equation (3.37b) and then the Equation (4.9a), Equation (4.15) becomes:

$$\frac{\partial W_2}{\partial y} = Q - nx \quad (4.16)$$

which can be integrated directly by quadrature, obtaining:

$$W_2(y) = yQ - nyx \quad (4.17)$$

This solution allows us to define the second canonical momenta as follows:

$$Q = \frac{\partial W_2}{\partial y} = nx + p_y \quad (4.18)$$

Moreover, having been able to separate the equations it is possible to separate the generating functions as follows:

$$W_2(x, y) = W_2(x) + W_2(y) \quad (4.19)$$

$$W_2(x, y) = W_2(x) + yQ - nyx \quad (4.20)$$

Now, it is possible to replace the Equation (4.20) to Equation (4.13). This change leads to rewrite the Equation (4.13) as follows:

$$\frac{\partial W_2(x)}{\partial x} = \sqrt{2\mathcal{K}(\Phi, Q) - n^2 x^2 + 4nxQ - Q^2} \quad (4.21)$$

which can be easily solved by separating the variables and where (Φ) is the first canonical moment, so we finding:

$$W_2(x) = \frac{1}{2n} (A + B) \quad (4.22)$$

with:

$$A = (nx - 2Q) \sqrt{2\mathcal{K}(\Phi, Q) - n^2x^2 + 4nxQ - Q^2} \quad (4.23)$$

$$B = (2\mathcal{K}(\Phi, Q) + 3Q^2) \tan^{-1}(B_1) \quad (4.24)$$

$$B_1 = \frac{nx - 2Q}{n\sqrt{-\frac{-2\mathcal{K}(\Phi, Q) + n^2x^2 - 4nxQ + Q^2}{n^2}}} \quad (4.25)$$

However, our aim is to find a Canonical transformation that is easily invertible because we still have to treat the perturbing term of the Hamiltonian function of Equation (4.3b). The problem arises when defining the second canonical coordinate (considering the Equation (4.19)), which derives from the Equation (4.9b) and in the Hill problem takes the form:

$$q = \frac{\partial W_2(x, y)}{\partial x} = \frac{C + D}{n\sqrt{2\mathcal{K}(\Phi, Q) + n^2x^2 - 4nxQ + Q^2}} \quad (4.26)$$

with:

$$C = \frac{1}{n} \left(\left(\frac{\partial \mathcal{K}(\Phi, Q)}{\partial Q} + 3Q \right) \tan^{-1}(C_1) \right) \quad (4.27)$$

$$C_1 = \frac{nx - 2Q}{\sqrt{2\mathcal{K}(\Phi, Q) - n^2x^2 + 4nxQ - Q^2}} \quad (4.28)$$

$$D = Q\sqrt{2\mathcal{K}(\Phi, Q) - n^2x^2 + 4nxQ - Q^2} \quad (4.29)$$

From the Equation (4.26) we note that the term Equation (4.27) produces a trigonometric coupling which leads an impossibility to reverse the transformation. However, since we still have to get the $\mathcal{K}(\Phi, Q)$ this allows us to have a degree of freedom to handle this problem. In most cases, by custom, we select $\mathcal{K}(\Phi, Q) = n\Phi$. But in this case we decide to impose the term Equation (4.27) at zero, so we find the following equation:

$$\frac{\partial \mathcal{K}(\Phi, Q)}{\partial Q} = -3Q \quad (4.30)$$

The Equation (4.30) is easily solved by quadrature:

$$\mathcal{K}(Q) = -\frac{3}{2}Q^2 \quad (4.31)$$

As a consequence, the canonical Hamiltonian function can be separated and therefore can be defined as:

$$\mathcal{K}(\Phi, Q) = \mathcal{K}(\Phi) + \mathcal{K}(Q) \quad (4.32)$$

and so:

$$\mathcal{K}(\Phi, Q) = n\Phi - \frac{3}{2}Q^2 \quad (4.33)$$

Replacing the Equation (4.33) in the Equation (4.22) results in the final generating function, can be written as:

$$W_2(x, y) = \frac{(nx - 2Q)}{2n} \sqrt{2n\Phi - (nx - 2Q)^2} + y(Q - nx) + \Phi \tan^{-1} \left(\frac{nx - 2Q}{\sqrt{2n\Phi - (nx - 2Q)^2}} \right) \quad (4.34)$$

from which applying the definition of Equation (4.9) it is possible to obtain the inverse canonical transformation as:

$$\left\{ \begin{array}{l} \phi = -\tan^{-1} \left(\frac{nx + 2p_y}{ny + p_x} \right) \end{array} \right. \quad (4.35a)$$

$$\left\{ \begin{array}{l} q = \frac{-ny - 2p_x}{n} \end{array} \right. \quad (4.35b)$$

$$\left\{ \begin{array}{l} \Phi = \frac{n^2 y^2 + (nx + 2p_y)^2 + 2nyp_x + p_x^2}{2n} \end{array} \right. \quad (4.35c)$$

$$\left\{ \begin{array}{l} Q = nx + p_y \end{array} \right. \quad (4.35d)$$

where, we can introduce the epicyclic variables. The Equation (4.35) are therefore easily invertible, in fact the canonical transformation [2, 3, 5, 26] has the following form:

$$\left\{ \begin{array}{l} x = \frac{2Q}{n} + \sqrt{\frac{2\Phi}{n}} \sin(\phi) \end{array} \right. \quad (4.36a)$$

$$\left\{ \begin{array}{l} y = q + 2\sqrt{\frac{2\Phi}{n}} \cos(\phi) \end{array} \right. \quad (4.36b)$$

$$\left\{ \begin{array}{l} p_x = -nq - \sqrt{2n\Phi} \cos(\phi) \end{array} \right. \quad (4.36c)$$

$$\left\{ \begin{array}{l} p_y = -Q - \sqrt{2n\Phi} \sin(\phi) \end{array} \right. \quad (4.36d)$$

if we apply the Canonical transformation of Equation (4.36) to Equation (4.3b) we obtain:

$$\mathcal{K}_0 = n\Phi - \frac{3}{2}Q^2 \quad (4.37)$$

4.2 Unperturbed solution

Before solving the perturbed problem we can solve the unperturbed one as [3, 10, 11, 38, 39]. Given the canonical Hamiltonian function of Equation (4.37) we can apply the definition of Equation (4.4), we can obtain the equations of motion for the simple problem of Hill not perturbed, which are:

$$\left\{ \begin{array}{l} \dot{\phi} = n \end{array} \right. \quad (4.38a)$$

$$\left\{ \begin{array}{l} \dot{q} = -3Q \end{array} \right. \quad (4.38b)$$

$$\left\{ \begin{array}{l} \dot{\Phi} = 0 \end{array} \right. \quad (4.38c)$$

$$\left\{ \begin{array}{l} \dot{Q} = 0 \end{array} \right. \quad (4.38d)$$

whose integration by quadrature is of immediate writing as follows:

$$\begin{cases} \phi = \phi_0 + nt & (4.39a) \\ q = q_0 - 3Q_0t & (4.39b) \\ \Phi = \Phi_0 & (4.39c) \\ Q = Q_0 & (4.39d) \end{cases}$$

once the previous equations have been recovered it is possible to obtain the solution of the unperturbed problem in the original physical coordinates by applying the Canonical transformation of Equation (4.36d), whose solution has the following form:

$$\begin{cases} x = \frac{\sqrt{2n\Phi_0} \sin(\phi_0 + nt) + 2Q_0}{n} & (4.40a) \end{cases}$$

$$\begin{cases} y = 2\sqrt{\frac{2\Phi_0}{n}} \cos(\phi_0 + nt) - 3tQ_0 & (4.40b) \end{cases}$$

$$\begin{cases} p_x = -nq_0 - \sqrt{2n\Phi_0} \cos(\phi_0 + nt) + 3ntQ_0 & (4.40c) \end{cases}$$

$$\begin{cases} p_y = -\sqrt{2n\Phi_0} \sin(\phi_0 + nt) - Q_0 & (4.40d) \end{cases}$$

From the Equation (4.40) it is therefore possible to identify the semi-major axis (a) and semi-minor axis (b), recognizable in the Figure 4.2, of equation:

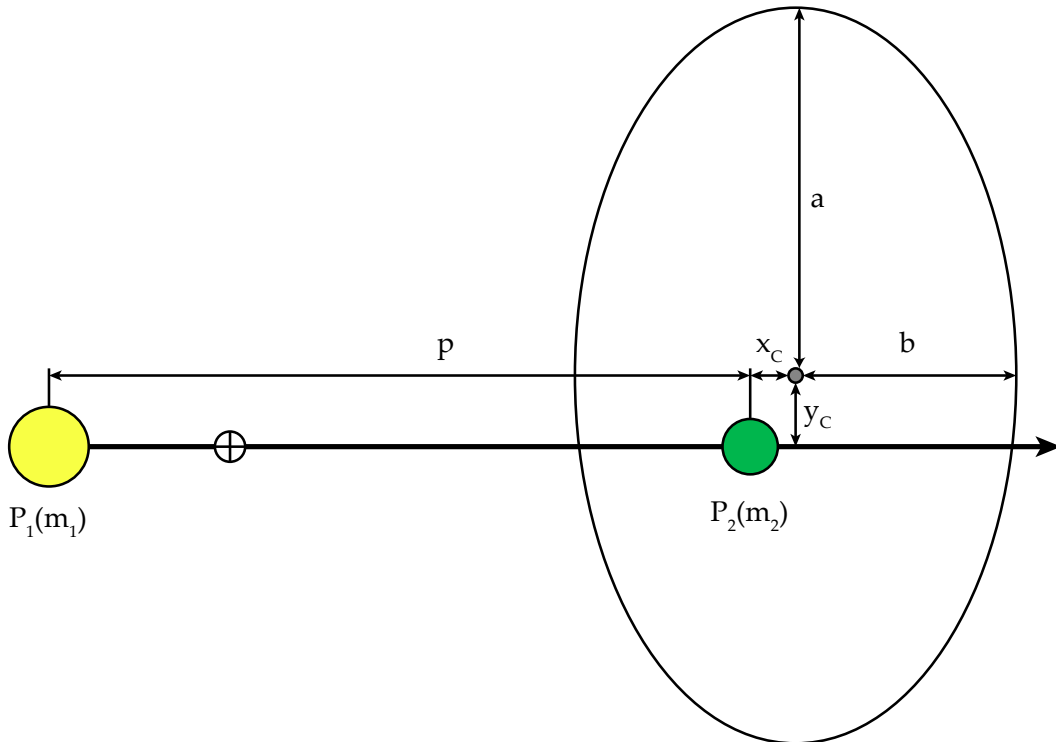


Figure 4.2: Geometric meaning of the auxiliary variables.

$$\begin{cases} a = 2\sqrt{\frac{2Q}{n}} & (4.41a) \end{cases}$$

$$\begin{cases} b = \sqrt{\frac{2Q}{n}} & (4.41b) \end{cases}$$

It is therefore possible to see the behaviour of Equation (4.40) on an DRO, with the following initial conditions:

$$\begin{cases} x_0 = 0 & (4.42a) \\ y_0 = 10 & (4.42b) \\ \dot{x}_0 = 9.5 & (4.42c) \\ \dot{y}_0 = -0.1 & (4.42d) \end{cases} \quad \begin{cases} x_0 = 0.1 & (4.43a) \\ y_0 = 20 & (4.43b) \\ \dot{x}_0 = 9.5 & (4.43c) \\ \dot{y}_0 = -0.2 & (4.43d) \end{cases}$$

The behaviour is shown Figure 4.3 where *nHill* is the numerical Hill's model and *aHill UnPert* the solution of Equation (4.40). The un-perturbed solution is shown to show how the behaviour is very different with respect to the perturbed solution obtained later. This is because the influence of the secondary attractor is not negligible. By convention, in this work, we will use the letter "n", in front of the name of the model, to say that it is a numerical integration, vice versa, we will use the letter "a" to say that it is the analytical solution.

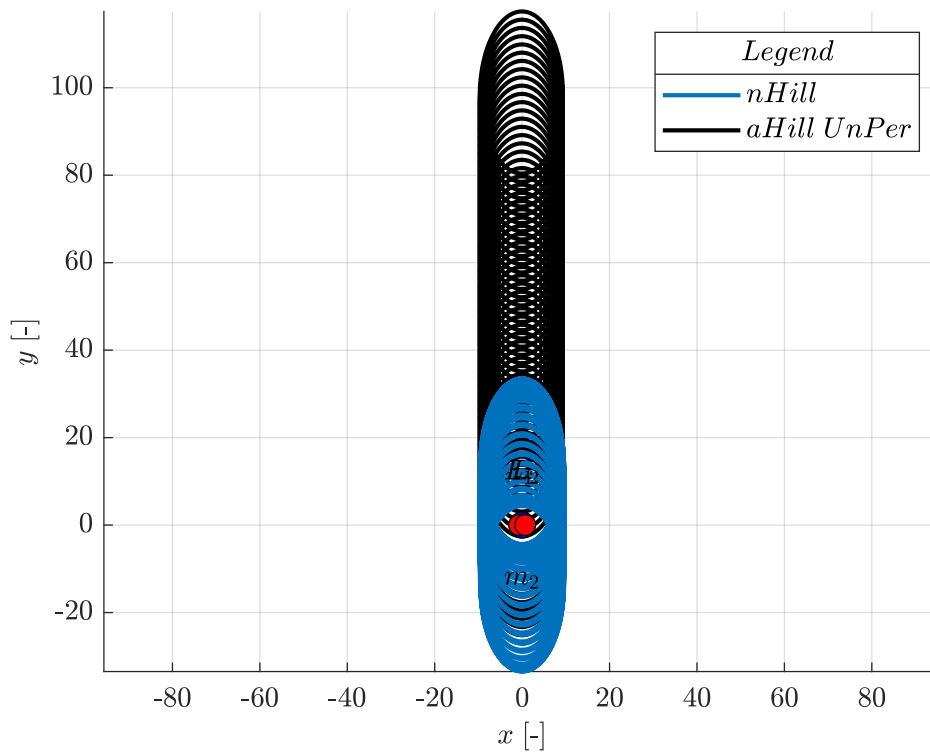


Figure 4.3: Comparison between the numerical Hill model and the analytical solution of the unperturbed part of Equation (4.40) with IC of Equation (4.42).

4.3 Perturbed solution

In this part we will go to exploit the canonical transformation normalised by a factor $k = \sqrt{\frac{3}{4}}$ as described in [38]. It has the following form:

$$\left\{ \begin{array}{l} x = \frac{Q + k\sqrt{2n\Phi} \sin(\phi)}{kn} \end{array} \right. \quad (4.44a)$$

$$\left\{ \begin{array}{l} y = 2kq + 2\sqrt{\frac{2\Phi}{n}} \cos(\phi) \end{array} \right. \quad (4.44b)$$

$$\left\{ \begin{array}{l} p_x = -2knq - \sqrt{2n\Phi} \cos(\phi) \end{array} \right. \quad (4.44c)$$

$$\left\{ \begin{array}{l} p_y = \frac{-Q - 2k\sqrt{2n\Phi} \sin(\phi)}{2k} \end{array} \right. \quad (4.44d)$$

It is very similar to the Equation (4.36).

Starting from the Equation (4.3) we have to introduce some support variables to scale the problem. The DROs have an elliptical shape and the centre at the following coordinates with respect to the secondary mass:

$$\left\{ \begin{array}{l} x_c = \frac{Q}{kn} \end{array} \right. \quad (4.45a)$$

$$\left\{ \begin{array}{l} y_c = 2kq \end{array} \right. \quad (4.45b)$$

introducing the following auxiliary variables:

$$\chi = \frac{y_c}{a} = \frac{2k}{a} q \quad (4.46)$$

$$\sigma = \frac{x_c}{2b} = \frac{Q}{2kB} \quad (4.47)$$

$$\gamma = \frac{1}{an\Phi} \quad (4.48)$$

$$a = 2b \quad (4.49)$$

$$B = bn \quad (4.50)$$

$$b = \sqrt{\frac{2\Phi}{n}} \quad (4.51)$$

where b is the semi-minor axis of the DRO, a is the semi-major axis, in Figure 4.2 the reader can see what the geometric interpretation of the variables that have just been described is. Similar to the Equation (4.2), the canonical Hamiltonian function is scaled, it has the following form:

$$\mathcal{K} = \mathcal{K}_0 + \varepsilon\mathcal{K}_1 \quad (4.52)$$

Using the Equation (4.44) and Equations (4.46) to (4.51) where:

$$\left\{ \begin{array}{l} \mathcal{K}_0 \text{ Hill} = n\Phi (1 - 3\sigma^2) \end{array} \right. \quad (4.53a)$$

$$\left\{ \begin{array}{l} \mathcal{K}_1 \text{ Hill} = -\frac{(n\Phi)\gamma}{\sqrt{\sigma^2 + \chi^2 + \sigma \sin(\phi) + 2\chi \cos(\phi) + \Delta^2}} \end{array} \right. \quad (4.53b)$$

with:

$$\Delta^2 = 1 - \frac{3}{4} \sin(\phi)^2 \quad (4.54)$$

4.4 Lie transform perturbation theory

The Lie transformation method consists in expanding the canonical Hamiltonian function in order to add the perturbation terms becoming, gradually, less important. This is obtained by analogously looking for the terms of the generating function for all the perturbation terms which we wish to retain in mind [3, 11, 15, 16].

4.4.1 Deprit's method to the Hamiltonian system

In this section we will see the procedure of Deprit's method through the general formulation of Kamel. Hence, we define the coefficients of the expansion of Lie with the Deprit's method (ref. [11, 21, 22]) which has the following form:

$$\mathbb{H}(\underline{Q}, \underline{P}, t, \varepsilon) = \sum_{m=0}^{\infty} \frac{\varepsilon^m}{m!} \mathbb{H}_m(\underline{Q}, \underline{P}, t) \quad (4.55)$$

We must also remember that each term multiplying a factor of $1/m!$. Then, it is necessary to rewrite Equation (4.55) in the following form:

$$\mathcal{K}(\underline{Q}, \underline{P}, t, \varepsilon) = \sum_{n=0}^{\infty} \frac{\varepsilon^n}{n!} \mathcal{K}_n(\underline{Q}, \underline{P}, t) \quad (4.56)$$

The terms of the above equation can be written in the following form:

$$\mathcal{K}_n = \mathbb{H}_n + \sum_{j=0}^{n-1} \left[\binom{n-1}{j-1} L'_j \mathbb{H}_{n-j} + \binom{n-1}{j} \mathcal{K}_{j,n-j} \right] - \frac{\mathcal{D}S_n}{\mathcal{D}t} \quad (4.57)$$

where:

$$\left\{ \begin{array}{l} L'_j f = \{f, S_j\}_{\underline{Q}, \underline{P}} = \frac{\partial f}{\partial \underline{Q}} \cdot \frac{\partial S_j}{\partial \underline{P}} - \frac{\partial f}{\partial \underline{P}} \cdot \frac{\partial S_j}{\partial \underline{Q}} \end{array} \right. \quad (4.58a)$$

$$\left\{ \begin{array}{l} \frac{\mathcal{D}S_n}{\mathcal{D}t} = \frac{\partial S_n}{\partial t} - L'_n \mathcal{H}_0 \end{array} \right. \quad (4.58b)$$

$$\left\{ \begin{array}{l} \mathcal{K}_{j,i} = L'_j \mathcal{K}_i - \sum_{m_j=1}^{j-1} \binom{j-1}{m_j-1} L'_j \mathcal{K}_{j-m_j,i} \end{array} \right. \quad (4.58c)$$

the Equation (4.58a) represent the Poisson bracket and L'_j is called Lie operator. For completeness we also remind the binomial form:

$$\binom{n}{m} = \frac{n!}{(n-m)!m!} \quad (4.59)$$

To eliminate the short-terms, an average procedure is performed on the angular part of the epicyclic variables, obtaining a canonical Hamiltonian function, stopped at the M order, in the following form:

$$\bar{\mathcal{K}}(\underline{Q}, \underline{P}, t, \varepsilon) = \sum_{n=0}^M \frac{\varepsilon^n}{n!} \langle \mathcal{K}_n \rangle + \mathcal{O}(\varepsilon^{M+1}) \quad (4.60)$$

where $\langle \mathcal{K}_n \rangle$ is the mean performed on the angular variable (ϕ):

$$\langle \mathcal{K}_n \rangle = \frac{1}{2\pi} \int \mathcal{K}_n|_{S_n=0} d\phi \quad (4.61)$$

At this point it is possible to obtain the terms of the generating function S_n up to the n order. To do this, we need to solve the PDE, Equation (4.62), thanks to the equality between Equations (4.57) and (4.61), i.e.:

$$\langle \mathcal{K}_n \rangle = \mathcal{K}_n \quad (4.62)$$

However, to guarantee that $\langle S_n \rangle = 0$ we must add a constant term, which has no effect on the solution of the homological equation Equation (4.63).

$$\{\mathcal{K}_0, S_n\} = \langle \mathcal{K}_n \rangle - \mathcal{K}_n \quad (4.63)$$

4.4.2 Lie transformation applied to the Hill problem

Applying what we have just introduced, once the equation Equation (4.52) is defined, we can expand into Maclaurin series for $\chi \rightarrow 0$, assuming also that $\sigma = \mathcal{O}[\chi^2]$. These assumptions are defined in DRO because the abscissa of the centre of the ellipse (x_c) suffers a small variation, secondly χ remains limited and less than 1. In addition, to ensure that the perturbing term is of a lower order than the non-perturbation one, we introduce the following assumption $\gamma = \mathcal{O}[\chi^4]$. With these assumptions we can apply the following replacement, like Lara in [38, 39]:

$$\begin{cases} \chi = \varepsilon \chi & (4.64a) \\ \sigma = \varepsilon^2 \sigma & (4.64b) \\ \gamma = \varepsilon^4 \gamma & (4.64c) \end{cases}$$

once the Maclaurin series expansion has been developed for both Equation (4.53), we order the system to obtain a similar form of the Equation (4.55).

In this study it was decided, by Lara [38, 39], to stop the expansion to the order 9 equivalent to neglecting the terms $\mathcal{O}[\varepsilon^{10}]$ for $\varepsilon \rightarrow 0$ obtaining a following form:

$$H = \sum_{n=0}^9 \frac{\varepsilon^n}{n!} H_n \quad (4.65)$$

To simplify the equations we introduce the following notation:

$$\begin{aligned} \cos(i\phi) &= c_i \\ \sin(i\phi) &= s_i \end{aligned} \quad (4.66)$$

with i positive integer number. Hence, in the case of Hill's problem the terms H_n , with $m = 0, \dots, 9$ of the McLaurin series, are:

$$H_0 \text{ Hill}_0 = n\Phi \quad (4.67a)$$

$$H_1 \text{ Hill}_0 = 0 \quad (4.67b)$$

$$H_2 \text{ Hill}_0 = 0 \quad (4.67c)$$

$$H_3 \text{ Hill}_0 = 0 \quad (4.67d)$$

$$H_4 \text{ Hill}_0 = 4! (n\Phi) (-3\sigma^2) \quad (4.67e)$$

$$H_4 \text{ Hill}_1 = 4! (n\Phi) \left(-\frac{\gamma}{\Delta}\right) \quad (4.67f)$$

$$H_5 \text{ Hill}_1 = 5! (n\Phi) \frac{\gamma\chi}{\Delta^3} c_1 \quad (4.67g)$$

$$H_6 \text{ Hill}_1 = 6! (n\Phi) \gamma \left[\frac{\chi^2 (-3c_2 + 2\Delta^2 - 3) + 2\Delta^2 \sigma s_1}{4\Delta^5} \right] \quad (4.67h)$$

$$H_7 \text{ Hill}_1 = 7! (n\Phi) \gamma \left[\frac{c_1 \chi (\chi^2 (5c_2 - 6\Delta^2 + 5) - 6\Delta^2 \sigma s_1)}{4\Delta^7} \right] \quad (4.67i)$$

$$H_8 \text{ Hill}_1 = 8! \frac{(n\Phi) \gamma}{64\Delta^9} \left[4c_2 (3\Delta^4 \sigma^2 + 5 (6\Delta^2 - 7) \chi^4) + 4 (8\Delta^2 - 3) \Delta^4 \sigma^2 + \right. \\ \left. + 24\Delta^2 \sigma s_1 \chi^2 (5c_2 - 2\Delta^2 + 5) - 3 (8 (\Delta^2 - 5) \Delta^2 + 35) \chi^4 - 35c_4 \chi^4 \right] \quad (4.67j)$$

$$H_9 \text{ Hill}_1 = 9! (n\Phi) \frac{\gamma c_1 \chi}{64\Delta^{11}} \left[-4c_2 (15\Delta^4 \sigma^2 + 7 (10\Delta^2 - 9) \chi^4) + 63c_4 \chi^4 + \right. \\ \left. - 40\Delta^2 \sigma s_1 \chi^2 (7c_2 - 6\Delta^2 + 7) + (40 (3\Delta^2 - 7) \Delta^2 + 189) \chi^4 + \right. \\ \left. + 12 (5 - 8\Delta^2) \Delta^4 \sigma^2 \right] \quad (4.67k)$$

where the word “*Hill*₀” refers to the potential of the primary, Equation (4.53a), and “*Hill*₁” to the potential of the secondary attractor, Equation (4.53b). To better understand the assumptions of Equation (4.64), Figure 4.4 shows the trend of the absolute maximum value on one orbit period of the terms of Equations (4.67a) to (4.67k) on a logarithmic scale as the size of the orbit increases.

$$\max(|H_n|) = \max(|H_n(0 \rightarrow t_{2\pi})|) \quad (4.68)$$

We immediately notice that the DROs are sufficiently large, so the terms referring to the potential of the primary attractor Equation (4.53a), are predominant compared to the others, which refer to the potential of the secondary attractor, Equation (4.53b). Now, before using the Lie transform method, to simplify the notation, we introduce the following auxiliary variables $\tilde{K} = K(k^2)/\pi$ and $\tilde{E} = E(k^2)/\pi$ and the auxiliary functions:

$$F^* = 2\phi \tilde{K} - F(\phi | k^2) \quad (4.69)$$

$$E^* = 2\phi \tilde{E} - E(\phi | k^2) \quad (4.70)$$

$$P^* = 2\phi + 2 \tan^{-1}(2 \cot(\phi)) \sim 2\phi - \Pi(k^2; \phi | 0) \quad (4.71)$$

where $K(k^2)$, $E(k^2)$ represent complete elliptic integrals of the first and second types and $F(\phi | k^2)$, $E(\phi | k^2)$ and $\Pi(k^2; \phi | 0)$ represent incomplete elliptic integrals of the first, second and third types, [4]. Note that F^* , E^* and P^* , are periodic function of ϕ with period π .

By observing the coefficients Equation (4.67), one immediately notices that:

$$\langle \mathcal{K}_0 \text{ Hill} \rangle_\phi = n\Phi \quad (4.72)$$

Subsequently, due to the fact that the Equations (4.67b) to (4.67d) are null, then we have $S_1 \text{ Hill} = S_2 \text{ Hill} = S_3 \text{ Hill} = 0$ and as a consequence also $\langle \mathcal{K}_1 \text{ Hill} \rangle_\phi = \langle \mathcal{K}_2 \text{ Hill} \rangle_\phi = \langle \mathcal{K}_3 \text{ Hill} \rangle_\phi = 0$.

Now, applying the Equations (4.57), (4.61) and (4.62) with $n = 4$ we get:

$$\langle \mathcal{K}_4 \text{ Hill} \rangle_\phi = -12 \left(Q^2 + \sqrt{\frac{2}{n\Phi}} \tilde{K} \right) \quad (4.73)$$

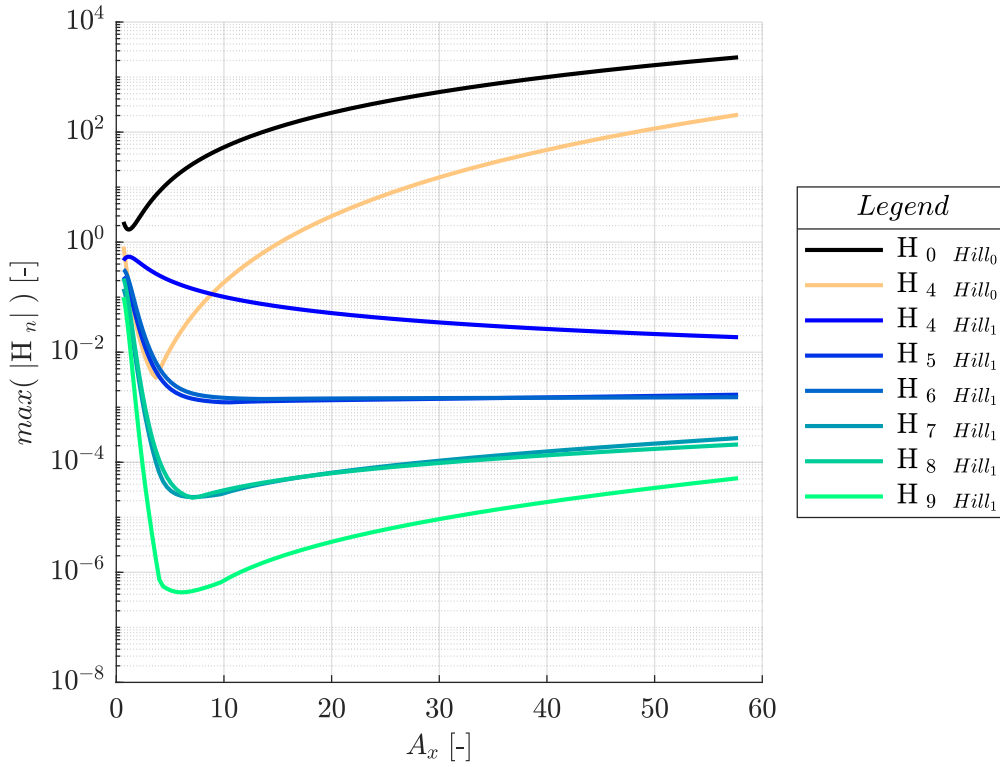


Figure 4.4: Trend of the maximum in absolute value of the terms of Equations (4.67a) to (4.67k) in MD.

$$S_{4 \text{ Hill}} = 6\sqrt{\frac{2}{n\Phi}}F^* \quad (4.74)$$

Subsequently for $n = 5$ it will have:

$$\langle \mathcal{K}_{5 \text{ Hill}} \rangle_\phi = 0 \quad (4.75)$$

$$S_{5 \text{ Hill}} = 15\sqrt{3}\frac{q}{\Phi\Delta}s_1 \quad (4.76)$$

with $n = 6$:

$$\langle \mathcal{K}_{6 \text{ Hill}} \rangle_\phi = 90q^2\sqrt{2\frac{n^3}{\Phi^3}}(\tilde{E} - \tilde{K}) \quad (4.77)$$

$$S_{6 \text{ Hill}} = 45q^2\sqrt{\frac{2n}{\Phi^3}}(F^* - E^*) - \frac{15c_1(512\sqrt{3}\Delta^2k^3\sigma + 9(23s_1 + 3s_3)\chi^2)}{16b\Delta^3k^2n} \quad (4.78)$$

then, with $n = 7$:

$$\langle \mathcal{K}_{7 \text{ Hill}} \rangle_\phi = 0 \quad (4.79)$$

$$S_{7 \text{ Hill}} = \frac{105\chi(-1536c_2k^3\sigma - 2560k^3\sigma + 3\sqrt{3}(138s_1 + 175s_3 + 21s_5)\chi^2)}{256b\Delta^5k^3n} + \quad (4.80)$$

$$- 1680\sqrt{\frac{2}{n\Phi^3}}qQ\tilde{E}$$

with $n = 8$:

$$\langle \mathcal{K}_8 \text{ Hill} \rangle_\phi = 8! \left[\frac{(1 - 2\tilde{K}^2)}{8\Phi^2} + \frac{(14\tilde{E} - 11\tilde{K})}{128} \sqrt{\frac{n^5}{2\Phi^5}} q^4 + \frac{(\tilde{K} - 4\tilde{E})}{9\sqrt{2n\Phi^3}} Q^2 \right] \quad (4.81)$$

$$\begin{aligned} S_8 \text{ Hill} = & -\frac{2520}{n\Phi^2} P^* + \frac{35(256Q^2\Phi - 63n^3q^4)}{\sqrt{2n^3\Phi^5}} E^* + \\ & + \left(\frac{2520}{n\Phi^2} \tilde{K} + \frac{35(99n^3q^4 + 32(\frac{9}{2}\sqrt{\frac{n\Phi}{2}}\frac{1}{\Delta} - 4Q^2\Phi))}{2\sqrt{2n^3\Phi^5}} \right) F^* + \\ & - \frac{105c_1}{16384\sqrt{2n^3\Phi^5}\Delta^7} \left[768\sqrt{6n^3\Phi}(271c_2 + 96c_4 + 9c_6 + 136)q^2Q + \right. \\ & + 9n^3q^4(5945s_1 + 9(1393s_3 + 277s_5 + 21s_7)) + \\ & \left. - 65536\Delta^4Q^2(11s_1 + 3s_3)\Phi \right] \end{aligned} \quad (4.82)$$

and finally with $n = 9$ we have:

$$\langle \mathcal{K}_9 \text{ Hill} \rangle_\phi = 0 \quad (4.83)$$

it is important to note that the mediated terms, deriving from the perturbative part of the Hamiltonian, are all of odd order.

4.5 Motion described by analytical solution

In this section, we will get the differential equations associated with the average Hamiltonian stopped at 7th and 9th order. Then we will get the analytical solution.

4.5.1 Solution of the 7th order

On a DROs, being very large and distant from the secondary attractor, remove the third body (artificial satellite) moves slowly. Consequently, a first low-level solution can already simulate long-term dynamics well even if the short-term effects are very neglected.

In this first solution we neglect the terms of order above 6, consequently we will have the Equation (4.60) with $M = 7$. The canonical Hamiltonian function, obtained, is the sum of Equations (4.72), (4.73), (4.75), (4.77) and (4.79), obtaining:

$$\bar{\mathcal{K}}_7 \text{ Hill} = n\Phi - \frac{1}{2}Q^2 - \sqrt{\frac{n}{2\Phi}} \tilde{K} + \frac{1}{4}\sqrt{\frac{n^3}{2\Phi^3}} (\tilde{E} - \tilde{K}) q^2 \quad (4.84)$$

from Equation (4.84) applying the definition Equation (4.4) it is possible to obtain the equations of motion for this system, which have the following form:

$$\begin{cases} \dot{\phi} = \tilde{C}_{\phi-a} + \tilde{C}_{\phi-b}q^2 & (4.85a) \\ \dot{q} = \tilde{C}_{q-a}Q & (4.85b) \\ \dot{\Phi} = 0 & (4.85c) \\ \dot{Q} = \tilde{C}_{Q-a}q & (4.85d) \end{cases}$$

where:

$$\tilde{C}_{q-a} = -1 \quad (4.86)$$

$$\tilde{C}_{Q-a} = \frac{1}{2} \sqrt{\frac{n^3}{2\Phi^3}} (\tilde{K} - \tilde{E}) \quad (4.87)$$

$$\tilde{C}_{\phi-a} = n + \frac{1}{2} \sqrt{\frac{n}{2\Phi^3}} \tilde{K} \quad (4.88)$$

$$\tilde{C}_{\phi-b} = \frac{3}{8} \sqrt{\frac{n^3}{2\Phi^5}} (\tilde{K} - \tilde{E}) \quad (4.89)$$

as expected, the Equation (4.85c) is null, this is due to the fact that having averaged the ϕ variable was made cyclic. Subsequently, we can see how the Equations (4.85b) and (4.85d) are coupling, even if easily solved because they are linear ODE. Instead, Equation (4.85a) turns out to be a separate equation solvable by quadrature. Before giving the solution of the system we introduce a support variable, hereafter defined as:

$$\Lambda = \left(\frac{n}{2\Phi}\right)^{3/4} \sqrt{\tilde{K} - \tilde{E}} \quad (4.90)$$

Having said that the solution of the system as for the [38, 39], becomes:

$$\left\{ \begin{array}{l} \phi = \frac{\tilde{C}_{\phi-b} (\tilde{C}_{q-a} Q_0^2 + \tilde{C}_{Q-a} q_0^2)}{4\sqrt{\tilde{C}_{q-a} \tilde{C}_{Q-a}^3}} \sinh(2\Lambda t) + \frac{\tilde{C}_{\phi-b} q_0 Q_0}{2\tilde{C}_{Q-a}} \cosh(2\Lambda t) + \\ \frac{2\tilde{C}_{Q-a} (\tilde{C}_{\phi-a} t + \phi_0) + \tilde{C}_{\phi-b} (-\tilde{C}_{q-a} Q_0^2 t + \tilde{C}_{Q-a} q_0^2 t - q_0 Q_0)}{2\tilde{C}_{Q-a}} \end{array} \right. \quad (4.91a)$$

$$q = Q_0 \sqrt{\frac{\tilde{C}_{q-a}}{\tilde{C}_{Q-a}}} \sinh(\Lambda \tau) + q_0 \cosh(\Lambda \tau) \quad (4.91b)$$

$$\Phi = \Phi_0 \quad (4.91c)$$

$$Q = q_0 \sqrt{\frac{\tilde{C}_{Q-a}}{\tilde{C}_{q-a}}} \sinh(\Lambda \tau) + Q_0 \cosh(\Lambda \tau) \quad (4.91d)$$

from Equation (4.91), using the canonical transformation of Equation (4.36) it is possible to obtain the solution in original coordinates.

Exploiting the initial conditions of Equation (4.42) propagated through the Equation (4.91), we obtain the trend of Figures 4.5 and 4.6 and we make a comparison between the numerical model and the 7th order. The images on the left show the behavior that the model predicts, on the right instead the dynamics of the center of the orbit. We see how the analytical solution (red line) has a behavior that follows, on average, that of the numerical solution (blue line). However, the short-term oscillation, which have been suppressed with the average process, are not included in the analytical model.

<i>Legend</i>
— <i>nHill</i> - - - <i>aHill 7</i>

<i>Legend</i>
— <i>nHill</i> — <i>aHill 7</i>

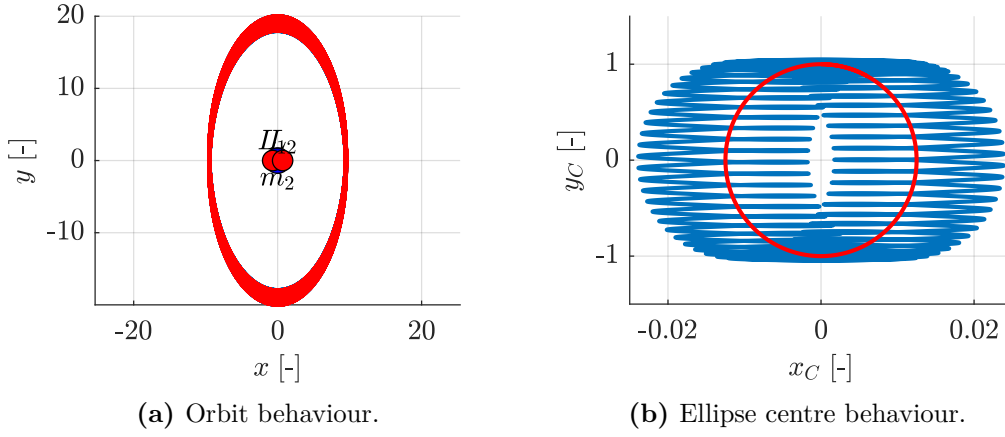


Figure 4.5: Comparison between the numerical Hill model and the analytical 7th order solution with IC of Equation (4.43).

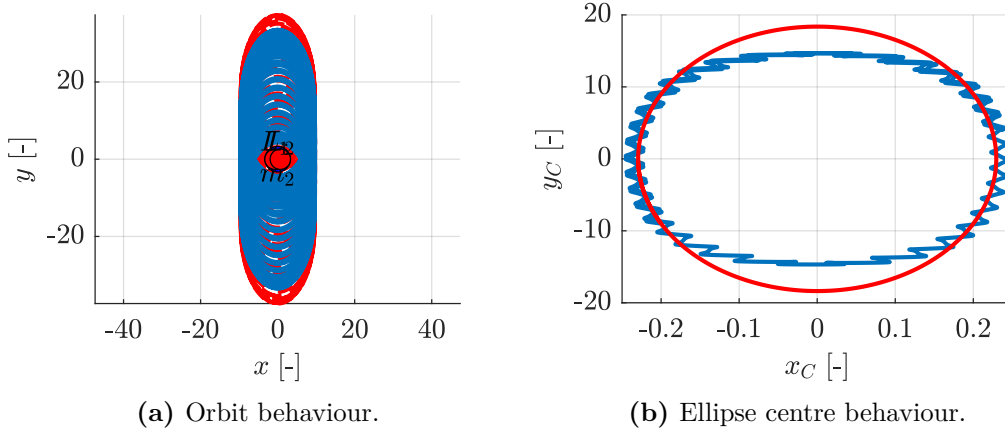


Figure 4.6: Comparison between the numerical Hill model and the analytical 7th order solution with IC of Equation (4.42).

4.5.2 Solution of the 9th order

To obtain a solution that is better able to simulate the short term terms we can solve the system obtained for the Lie series of the canonical Hamiltonian function. Since the odd order terms are null, as shown by the Equations (4.75), (4.79) and (4.83), then the order Lie series 9th order is the same as the 8th. Consequently we can write the canonical Hamiltonian function of 8th order as:

$$\bar{\mathcal{K}}_9_{Hill} = \bar{\mathcal{K}}_7_{Hill} + \frac{(1 - 2\tilde{K}^2)}{8\Phi^2} + \frac{(14\tilde{E} - 11\tilde{K})}{128} \sqrt{\frac{n^5}{2\Phi^5}} q^4 + \frac{(\tilde{K} - 4\tilde{E})}{9\sqrt{2n\Phi^3}} Q^2 \quad (4.92)$$

from Equation (4.92) by applying the Equation (4.4) it is possible to obtain the equations of motion of the system. However, before writing them we introduce some support variables in order to simplify the notation as they appear to be constant. They are:

$$\tilde{C}_{q-a\varepsilon} = \frac{1}{9} \sqrt{\frac{2}{n\Phi^3}} (\tilde{K} - 4\tilde{E}) \quad (4.93)$$

Equating coefficients of powers of ε on both sides of Equation (4.100) yields:

$$\left\{ \begin{array}{l} Q_{9,0}(\tau)\tilde{C}_{q-a} + \dot{q}_{9,0}(\tau) = 0 \quad (4.101a) \\ -Q_{9,1}(\tau)\tilde{C}_{q-a} + Q_{9,0}(\tau)\left(-\tilde{C}_{q-a\varepsilon}\right) + \omega_1\dot{q}_{9,0}(\tau) + \dot{q}_{9,1}(\tau) = 0 \quad (4.101b) \\ \dot{Q}_{9,0}(\tau) - q_{9,0}(\tau)\tilde{C}_{Q-a} = 0 \quad (4.101c) \\ -q_{9,1}(\tau)\tilde{C}_{Q-a} + q_{9,0}(\tau)^3\left(-\tilde{C}_{Q-a\varepsilon}\right) + \omega_1\dot{Q}_{9,0}(\tau) + \dot{Q}_{9,1}(\tau) = 0 \quad (4.101d) \end{array} \right.$$

the zero-order equation, can be expressed as:

$$\left\{ \begin{array}{l} q_{9,0}(\tau) = Q_0 \frac{\sqrt{\tilde{C}_{q-a}} \sinh(\Lambda\tau)}{\sqrt{\tilde{C}_{Q-a}}} + q_0 \cosh(\Lambda\tau) \quad (4.102a) \end{array} \right.$$

$$\left\{ \begin{array}{l} Q_{9,0}(\tau) = q_0 \frac{\sqrt{\tilde{C}_{Q-a}} \sinh(\Lambda\tau)}{\sqrt{\tilde{C}_{q-a}}} + Q_0 \cosh(\Lambda\tau) \quad (4.102b) \end{array} \right.$$

We have expressed q_0 and Q_0 as a pure function so that we can evaluate its derivatives in the higher-order problems. Substituting the Equation (4.102) into Equations (4.101b) and (4.101d), the first-order equation, yields:

$$\left\{ \begin{array}{l} \frac{\left(\tilde{C}_{q-a\varepsilon} - \omega_1\tilde{C}_{q-a}\right)\left(q_0\sqrt{\tilde{C}_{Q-a}}\sinh(\Lambda\tau) + Q_0\sqrt{\tilde{C}_{q-a}}\cosh(\Lambda\tau)\right)}{\sqrt{\tilde{C}_{q-a}}} = \quad (4.103a) \end{array} \right.$$

$$\left\{ \begin{array}{l} -Q_{9,1}(\tau)\tilde{C}_{q-a} + \dot{q}_{9,1} \\ \omega_1\left(q_0\tilde{C}_{Q-a}\cosh(\Lambda\tau) + \Lambda Q_0\sinh(\Lambda\tau)\right) + \dot{Q}_{9,1}(\tau) = \\ \tilde{C}_{Q-a\varepsilon}\left(\frac{Q_0\sqrt{\tilde{C}_{q-a}}\sinh(\Lambda\tau)}{\sqrt{\tilde{C}_{Q-a}}} + q_0\cosh(\Lambda\tau)\right)^3 + q_{9,1}(\tau)\tilde{C}_{Q-a} \quad (4.103b) \end{array} \right.$$

which particular solution is:

$$\left. \begin{aligned}
 q_{9,1}(\tau) &= \frac{e^{-3\Lambda\tau}}{64\tilde{C}_{q-a}\tilde{C}_{Q-a}^{5/2}} \left(2e^{2\Lambda\tau} \left(q_0\sqrt{\tilde{C}_{Q-a}} - Q_0\sqrt{\tilde{C}_{q-a}} \right) \left(2\Lambda\tau \right. \right. \\
 &\quad \left. \left. \left(-4\tilde{C}_{Q-a}^2\tilde{C}_{q-a\varepsilon} - 3q_0^2\tilde{C}_{q-a}\tilde{C}_{Q-a}\tilde{C}_{Q-a\varepsilon} + 3Q_0^2\tilde{C}_{q-a}^2\tilde{C}_{Q-a\varepsilon} \right) + \right. \right. \\
 &\quad \left. \left. + 4\tilde{C}_{Q-a}^2\tilde{C}_{q-a\varepsilon} - 3q_0^2\tilde{C}_{q-a}\tilde{C}_{Q-a}\tilde{C}_{Q-a\varepsilon} + 3Q_0^2\tilde{C}_{q-a}^2\tilde{C}_{Q-a\varepsilon} + \right. \right. \\
 &\quad \left. \left. + 16\tau\omega_1\tilde{C}_{q-a}^{3/2}\tilde{C}_{Q-a}^{5/2} \right) + 2e^{4\Lambda\tau} \left(q_0\sqrt{\tilde{C}_{Q-a}} + Q_0\sqrt{\tilde{C}_{q-a}} \right) \left(2\Lambda\tau \right. \right. \\
 &\quad \left. \left. \left(4\tilde{C}_{Q-a}^2\tilde{C}_{q-a\varepsilon} + 3q_0^2\tilde{C}_{q-a}\tilde{C}_{Q-a}\tilde{C}_{Q-a\varepsilon} - 3Q_0^2\tilde{C}_{q-a}^2\tilde{C}_{Q-a\varepsilon} \right) + \right. \right. \\
 &\quad \left. \left. + 4\tilde{C}_{Q-a}^2\tilde{C}_{q-a\varepsilon} - 3q_0^2\tilde{C}_{q-a}\tilde{C}_{Q-a}\tilde{C}_{Q-a\varepsilon} + 3Q_0^2\tilde{C}_{q-a}^2\tilde{C}_{Q-a\varepsilon} + \right. \right. \\
 &\quad \left. \left. - 16\tau\omega_1\tilde{C}_{q-a}^{3/2}\tilde{C}_{Q-a}^{5/2} \right) + e^{6\Lambda\tau}\tilde{C}_{q-a}\tilde{C}_{Q-a\varepsilon} \left(q_0\sqrt{\tilde{C}_{Q-a}} + \right. \right. \\
 &\quad \left. \left. + Q_0\sqrt{\tilde{C}_{q-a}} \right)^3 + \tilde{C}_{q-a}\tilde{C}_{Q-a\varepsilon} \left(q_0\sqrt{\tilde{C}_{Q-a}} - Q_0\sqrt{\tilde{C}_{q-a}} \right)^3 \right) \\
 Q_{9,1}(\tau) &= \frac{e^{-3\Lambda\tau}}{64\tilde{C}_{q-a}^{3/2}\tilde{C}_{Q-a}^2} \left(2e^{2\Lambda\tau} \left(q_0\sqrt{\tilde{C}_{Q-a}} - Q_0\sqrt{\tilde{C}_{q-a}} \right) \left(2\Lambda\tau \right. \right. \\
 &\quad \left. \left. \left(4\tilde{C}_{Q-a}^2\tilde{C}_{q-a\varepsilon} + 3q_0^2\tilde{C}_{q-a}\tilde{C}_{Q-a}\tilde{C}_{Q-a\varepsilon} - 3Q_0^2\tilde{C}_{q-a}^2\tilde{C}_{Q-a\varepsilon} \right) + \right. \right. \\
 &\quad \left. \left. + 4\tilde{C}_{Q-a}^2\tilde{C}_{q-a\varepsilon} - 3q_0^2\tilde{C}_{q-a}\tilde{C}_{Q-a}\tilde{C}_{Q-a\varepsilon} + 3Q_0^2\tilde{C}_{q-a}^2\tilde{C}_{Q-a\varepsilon} + \right. \right. \\
 &\quad \left. \left. - 16\tau\omega_1\tilde{C}_{q-a}^{3/2}\tilde{C}_{Q-a}^{5/2} \right) - 2e^{4\Lambda\tau} \left(q_0\sqrt{\tilde{C}_{Q-a}} + Q_0\sqrt{\tilde{C}_{q-a}} \right) \left(2\Lambda\tau \right. \right. \\
 &\quad \left. \left. \left(-4\tilde{C}_{Q-a}^2\tilde{C}_{q-a\varepsilon} - 3q_0^2\tilde{C}_{q-a}\tilde{C}_{Q-a}\tilde{C}_{Q-a\varepsilon} + 3Q_0^2\tilde{C}_{q-a}^2\tilde{C}_{Q-a\varepsilon} \right) + \right. \right. \\
 &\quad \left. \left. + 4\tilde{C}_{Q-a}^2\tilde{C}_{q-a\varepsilon} - 3q_0^2\tilde{C}_{q-a}\tilde{C}_{Q-a}\tilde{C}_{Q-a\varepsilon} + 3Q_0^2\tilde{C}_{q-a}^2\tilde{C}_{Q-a\varepsilon} + \right. \right. \\
 &\quad \left. \left. + 16\tau\omega_1\tilde{C}_{q-a}^{3/2}\tilde{C}_{Q-a}^{5/2} \right) + 3e^{6\Lambda\tau}\tilde{C}_{q-a}\tilde{C}_{Q-a\varepsilon} \left(q_0\sqrt{\tilde{C}_{Q-a}} + \right. \right. \\
 &\quad \left. \left. + Q_0\sqrt{\tilde{C}_{q-a}} \right)^3 + 3\tilde{C}_{q-a}\tilde{C}_{Q-a\varepsilon} \left(Q_0\sqrt{\tilde{C}_{q-a}} - q_0\sqrt{\tilde{C}_{Q-a}} \right)^3 \right)
 \end{aligned} \right\} \quad (4.104a)$$

$$\left. \begin{aligned}
 &\quad \left(-4\tilde{C}_{Q-a}^2\tilde{C}_{q-a\varepsilon} - 3q_0^2\tilde{C}_{q-a}\tilde{C}_{Q-a}\tilde{C}_{Q-a\varepsilon} + 3Q_0^2\tilde{C}_{q-a}^2\tilde{C}_{Q-a\varepsilon} \right) + \\
 &\quad + 4\tilde{C}_{Q-a}^2\tilde{C}_{q-a\varepsilon} - 3q_0^2\tilde{C}_{q-a}\tilde{C}_{Q-a}\tilde{C}_{Q-a\varepsilon} + 3Q_0^2\tilde{C}_{q-a}^2\tilde{C}_{Q-a\varepsilon} + \\
 &\quad + 16\tau\omega_1\tilde{C}_{q-a}^{3/2}\tilde{C}_{Q-a}^{5/2} \right) + 3e^{6\Lambda\tau}\tilde{C}_{q-a}\tilde{C}_{Q-a\varepsilon} \left(q_0\sqrt{\tilde{C}_{Q-a}} + \right. \\
 &\quad \left. + Q_0\sqrt{\tilde{C}_{q-a}} \right)^3 + 3\tilde{C}_{q-a}\tilde{C}_{Q-a\varepsilon} \left(Q_0\sqrt{\tilde{C}_{q-a}} - q_0\sqrt{\tilde{C}_{Q-a}} \right)^3 \right) \\
 &\quad \left(-4\tilde{C}_{Q-a}^2\tilde{C}_{q-a\varepsilon} - 3q_0^2\tilde{C}_{q-a}\tilde{C}_{Q-a}\tilde{C}_{Q-a\varepsilon} + 3Q_0^2\tilde{C}_{q-a}^2\tilde{C}_{Q-a\varepsilon} \right) + \\
 &\quad + 4\tilde{C}_{Q-a}^2\tilde{C}_{q-a\varepsilon} - 3q_0^2\tilde{C}_{q-a}\tilde{C}_{Q-a}\tilde{C}_{Q-a\varepsilon} + 3Q_0^2\tilde{C}_{q-a}^2\tilde{C}_{Q-a\varepsilon} + \\
 &\quad + 16\tau\omega_1\tilde{C}_{q-a}^{3/2}\tilde{C}_{Q-a}^{5/2} \right) + 3e^{6\Lambda\tau}\tilde{C}_{q-a}\tilde{C}_{Q-a\varepsilon} \left(q_0\sqrt{\tilde{C}_{Q-a}} + \right. \\
 &\quad \left. + Q_0\sqrt{\tilde{C}_{q-a}} \right)^3 + 3\tilde{C}_{q-a}\tilde{C}_{Q-a\varepsilon} \left(Q_0\sqrt{\tilde{C}_{q-a}} - q_0\sqrt{\tilde{C}_{Q-a}} \right)^3 \right)
 \end{aligned} \right\} \quad (4.104b)$$

It is clear that Equation (4.104) contains a mixed-long term, which makes the expansion non-uniform. Now, we can choose the parameter ω_1 to eliminate the secular term, by eliminating the terms proportional to τ and then finding an appropriate ω_1 . Consequently ω_1 is:

$$\omega_1 = \frac{4\tilde{C}_{Q-a}^2\tilde{C}_{q-a\varepsilon} + 3q_0^2\tilde{C}_{q-a}\tilde{C}_{Q-a}\tilde{C}_{Q-a\varepsilon} - 3Q_0^2\tilde{C}_{q-a}^2\tilde{C}_{Q-a\varepsilon}}{8\tilde{C}_{q-a}\tilde{C}_{Q-a}^2} \quad (4.105)$$

Substituting Equation (4.105) into Equation (4.104b), we have:

$$\left\{ \begin{array}{l}
q(\tau) = \frac{\left(Q_0 \sqrt{\tilde{C}_{q-a}} \sinh(\Lambda\tau) + q_0 \sqrt{\tilde{C}_{Q-a}} \cosh(\Lambda\tau) \right)}{32 \tilde{C}_{q-a} \tilde{C}_{Q-a}^{5/2}} \\
\left(4q_0 Q_0 \tilde{C}_{q-a}^{3/2} \sqrt{\tilde{C}_{Q-a}} \tilde{C}_{Q-a\varepsilon} \sinh(2\Lambda\tau) + 2\tilde{C}_{q-a} \tilde{C}_{Q-a\varepsilon} \cosh(2\Lambda\tau) \right) \quad (4.106a) \\
\left(q_0^2 \tilde{C}_{Q-a} + Q_0^2 \tilde{C}_{q-a} \right) + 8\tilde{C}_{Q-a}^2 \tilde{C}_{q-a\varepsilon} - 7q_0^2 \tilde{C}_{q-a} \tilde{C}_{Q-a} \tilde{C}_{Q-a\varepsilon} + \\
+ 7Q_0^2 \tilde{C}_{q-a}^2 \tilde{C}_{Q-a\varepsilon} \\
Q(\tau) = \frac{\left(q_0 \sqrt{\tilde{C}_{Q-a}} \sinh(\Lambda\tau) + Q_0 \sqrt{\tilde{C}_{q-a}} \cosh(\Lambda\tau) \right)}{32 \tilde{C}_{q-a}^{3/2} \tilde{C}_{Q-a}^2} \\
\left(12q_0 Q_0 \tilde{C}_{q-a}^{3/2} \sqrt{\tilde{C}_{Q-a}} \tilde{C}_{Q-a\varepsilon} \sinh(2\Lambda\tau) + 6\tilde{C}_{q-a} \tilde{C}_{Q-a\varepsilon} \cosh(2\Lambda\tau) \right) \quad (4.106b) \\
\left(q_0^2 \tilde{C}_{Q-a} + Q_0^2 \tilde{C}_{q-a} \right) - 8\tilde{C}_{Q-a}^2 \tilde{C}_{q-a\varepsilon} + 9q_0^2 \tilde{C}_{q-a} \tilde{C}_{Q-a} \tilde{C}_{Q-a\varepsilon} + \\
- 9Q_0^2 \tilde{C}_{q-a}^2 \tilde{C}_{Q-a\varepsilon}
\end{array} \right.$$

The final solution is obtained as:




$$\left\{ \begin{array}{l}
q(\tau) = q_{9,0}(\tau) + q_{9,1}(\tau) \quad (4.107a) \\
Q(\tau) = Q_{9,0}(\tau) + Q_{9,1}(\tau) \quad (4.107b)
\end{array} \right.$$




At the end, replacing τ with $(\omega_0 + \varepsilon\omega_1)t$, imposing $\omega_0 = 1$, we obtain the complete equation of motion.

$$\left\{ \begin{array}{l}
q(t) = q_{9,0}(1 + \omega_1 t) + q_{9,1}(1 + \omega_1 t) \quad (4.108a) \\
Q(t) = Q_{9,0}(1 + \omega_1 t) + Q_{9,1}(1 + \omega_1 t) \quad (4.108b)
\end{array} \right.$$

At the end, it is possible to solve the Equation (4.85a) by quadrature after replacing the Equation (4.108) into Equation (4.85a), Equal to Lara [38, 39].

Similar to the 7th order solution, through the initial conditions of Equation (4.42) propagated through the Equation (4.108) we obtain the trend of Figures 4.7 and 4.8 and we make a comparison between the numerical model, the 7th order and the 9th order, equal to the [39]. In the figures on the left we see the behaviour that the model predicts, instead in the right plots the dynamic of the centre of the DRO. The new analytical solution, of order 9, (green line) does not show a particular improvement compared to the analytical solution of 7th order previously obtained. Also in this case the short-term oscillation are lost and the improvement is not perceptible.

Legend	
	<i>nHill</i>
	<i>aHill 7</i>
	<i>aHill 9</i>

Legend	
	<i>nHill</i>
	<i>aHill 7</i>
	<i>aHill 9</i>

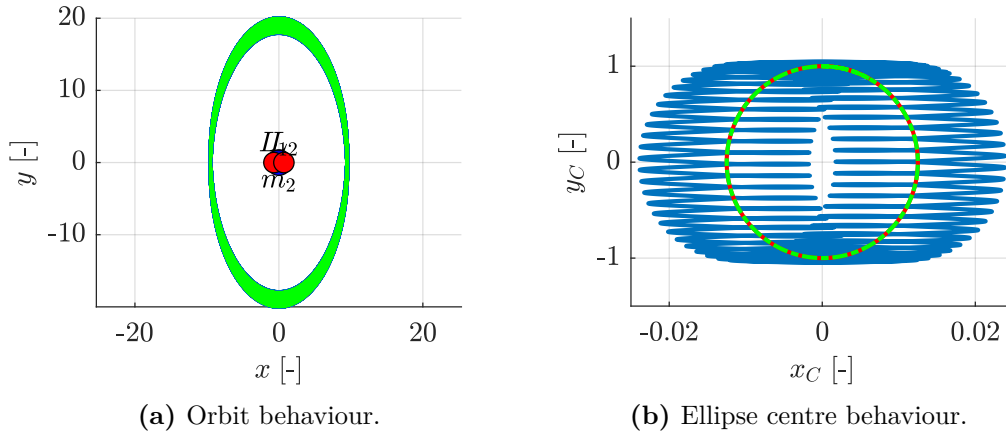


Figure 4.7: Comparison between the numerical Hill's model and the analytical 7th and 9th order solution with IC of Equation (4.43).

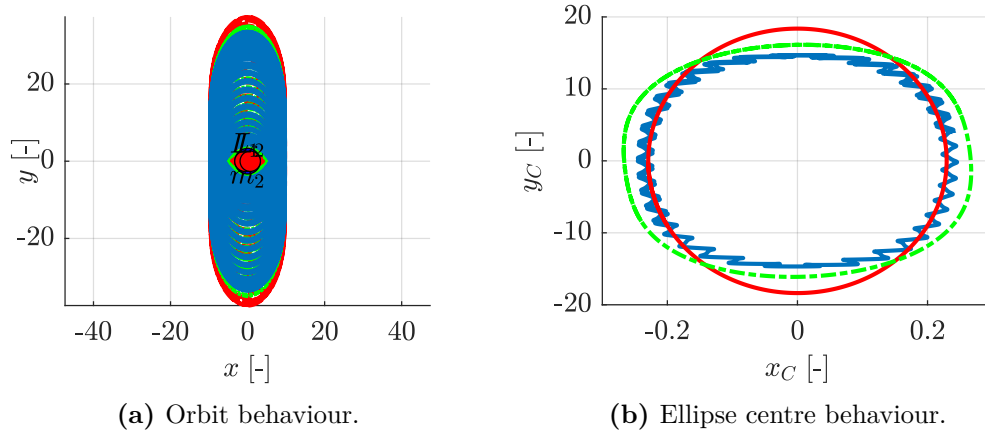


Figure 4.8: Comparison between the numerical Hill's model and the analytical 7th and 9th order solution with IC of Equation (4.42).

4.6 Short-periodic correction

One of the main problems that can be encountered through the method proposed in the Section 4.4.2 is the suppression of short term terms and this is the reason why adding this passage to the solutions, found above, is crucial to obtaining a more accurate model even in the short term. But thanks to the Deprit's triangle, as proposed in [11], it is possible to correct the values through the short-periodic correction. It consists of applying the following equations:

$$\underline{Q} = \tilde{Q} + \sum_{n=1}^{\infty} \frac{\varepsilon^n}{n!} \underline{Q}^{(n)} (S, \tilde{Q}, \tilde{P}, t) \quad (4.109)$$

with:

$$\left\{ \begin{array}{l} \underline{Q}^{(n)} = \frac{\partial S_n}{\partial \underline{P}} + \sum_{j=1}^{n-1} \binom{n-1}{j} \underline{Q}_{j,n-j} \end{array} \right. \quad (4.110a)$$

$$\left\{ \begin{array}{l} \underline{Q}_{j,i} = L'_j \underline{Q}^{(i)} - \sum_{m_j=1}^{j-1} \binom{j-1}{m_j-1} L'_m \underline{Q}_{j-m_j,i} \end{array} \right. \quad (4.110b)$$

in a similar way also for conjugate moments, we have:

$$\underline{P} = \tilde{\underline{P}} + \sum_{n=1}^{\infty} \frac{\varepsilon^n}{n!} \underline{P}^{(n)} \left(S, \tilde{\underline{Q}}, \tilde{\underline{P}}, t \right) \quad (4.111)$$

with:

$$\left\{ \begin{array}{l} \underline{P}^{(n)} = -\frac{\partial S_n}{\partial \underline{Q}} + \sum_{j=1}^{n-1} \binom{n-1}{j} \underline{P}_{j,n-j} \\ \underline{P}_{j,i} = L'_j \underline{P}^{(i)} - \sum_{m_j=1}^{j-1} \binom{j-1}{m_j-1} L'_{m_j} \underline{P}_{j-m_j,i} \end{array} \right. \quad (4.112a)$$

$$\quad (4.112b)$$

where \underline{Q} and \underline{P} are the correct terms with the short-periodic correction instead $\tilde{\underline{Q}}$ and $\tilde{\underline{P}}$ are long-term terms obtained through the equations solved in the previous sections as Equations (4.91) and (4.108). The one just described, turns out to be the correction of the direct transformation, however, for the correction of the initial conditions, we should have the correction for the inverse transformation. To obtain it, we use a new generating function S_n^{-1} , defined:

$$S_n^{-1} = -S_n \quad (4.113)$$

then the Deprit's triangle is applied exactly as the direct transformation seen above. It consists of applying the following equations:

$$\tilde{\underline{Q}}_0 = \underline{Q}_0 + \sum_{n=1}^{\infty} \frac{\varepsilon^n}{n!} \underline{Q}'^{(n)} \left(S^{-1}, \underline{Q}_0, \underline{P}_0, t \right) \quad (4.114)$$

and:

$$\tilde{\underline{P}}_0 = \underline{P}_0 + \sum_{n=1}^{\infty} \frac{\varepsilon^n}{n!} \underline{P}'^{(n)} \left(S^{-1}, \underline{Q}_0, \underline{P}_0, t \right) \quad (4.115)$$

with $\tilde{\underline{Q}}_0$ and $\tilde{\underline{P}}_0$ are the new initial conditions that should be used in Equations (4.91) and (4.108).

4.6.1 Short-periodic correction until 7th order

Without worrying too much on how the terms have been obtained, it is sufficient to apply the above formulas from which the terms of corrections for the direct transformation are obtained. It turns out that the terms up to the order 3 are null, instead for the others we have:

$$\phi_{Hill}^{(4)} = -\frac{1}{2b^3 n^2} F^* \quad (4.116a)$$

$$q_{Hill}^{(4)} = 0 \quad (4.116b)$$

$$\Phi_{Hill}^{(4)} = \frac{1}{bn} \left(\frac{1}{2\Delta} - \tilde{K} \right) \quad (4.116c)$$

$$Q_{Hill}^{(4)} = 0 \quad (4.116d)$$

$$\phi_{Hill}^{(5)} = -\frac{\sqrt{3}s_1\chi}{2b^3 \Delta kn^2} \quad (4.116e)$$

$$q_{Hill}^{(5)} = 0 \quad (4.116f)$$

$$\Phi_{Hill}^{(5)} = -\frac{\sqrt{3}c_1\chi}{4b\Delta^3kn} \quad (4.116g)$$

$$Q_{Hill}^{(5)} = -\frac{\sqrt{3}s_1}{4b^2\Delta n} \quad (4.116h)$$

$$\phi_{Hill}^{(6)} = \frac{3\chi}{4b^3k^2n^2}(E^* - F^*) + \frac{c_1(1024\sqrt{3}\Delta^2k^3\sigma + 27(23s_1 + 3s_3)\chi^2)}{768b^3\Delta^3k^2n^2} \quad (4.116i)$$

$$q_{Hill}^{(6)} = -\frac{c_1}{\sqrt{3}b^2\Delta n^2} \quad (4.116j)$$

$$\Phi_{Hill}^{(6)} = \frac{3\chi^2(64\Delta^5(\tilde{E} - \tilde{K}) + 21) + 81c_2\chi^2 - 4\sqrt{3}k^3\sigma(7s_1 + 3s_3)}{384b\Delta^5k^2n} \quad (4.116k)$$

$$Q_{Hill}^{(6)} = -\frac{\chi}{2b^2kn}(F^* - E^*) + \frac{3(3c_2 + 13)s_2\chi}{128b^2\Delta^3kn} \quad (4.116l)$$




$$\phi_{Hill}^{(7)} = \frac{\chi}{1024b^3\Delta^5k^3n^2} \left[64k^3\sigma(6c_2 - 2\tilde{E}(3c_2 + 5)^2\Delta) + 640k^3\sigma - \sqrt{3}(138s_1 + 175s_3 + 21s_5)\chi^2 \right] \quad (4.116m)$$




$$q_{Hill}^{(7)} = \frac{\chi}{6b^2\Delta^3kn^2}(1 - 8\tilde{E}\Delta^3) \quad (4.116n)$$

$$\Phi_{Hill}^{(7)} = \frac{3c_1\chi(4k^3\sigma(7s_1 + 3s_3) - \sqrt{3}(11c_2 + 5)\chi^2)}{256b\Delta^7k^3n} \quad (4.116o)$$

$$Q_{Hill}^{(7)} = -\frac{1536\tilde{E}c_2(3c_2 + 10)\Delta k^3\sigma + 2560k^3\sigma(5\tilde{E}\Delta - 1)}{12288b^2\Delta^5k^2n} + \frac{9\sqrt{3}(138s_1 + 175s_3 + 21s_5)\chi^2}{12288b^2\Delta^5k^2n} \quad (4.116p)$$

now applying the direct transformation Equation (4.109) for the correction of the variables obtained from Equation (4.91) and the inverse transformation to the initial conditions (note that up to this point, since the inverse transformation is coupled, it turns out to be exactly the opposite of the direct one), we obtain the short periodic correction of 7th order. To better visualise how much this correction effects, we reproduce the images similar to those of Figures 4.5 and 4.6. In the Figures 4.9 and 4.10, it is possible to see, very well, how the correction allows, especially in the periodic orbits, an already very good correction and it can be seen how the solution predicts and follows the numerical model, equal to the Lara [39]. In the figures to the left we see the behaviour that the model predicts, instead in the graph on the right the dynamics of the DRO centre. However, in this case the short-term oscillations have been considered (green line) with respect to the average solution only (red line), consequently the behaviour of the centre of the DRO (green line) is described much better than the previous cases (red line).

<i>Legend</i>	
	<i>nHill</i>
	<i>aHill 7</i>
	<i>aHill 7 SPC</i>

<i>Legend</i>	
	<i>nHill</i>
	<i>aHill 7</i>
	<i>aHill 7 SPC</i>

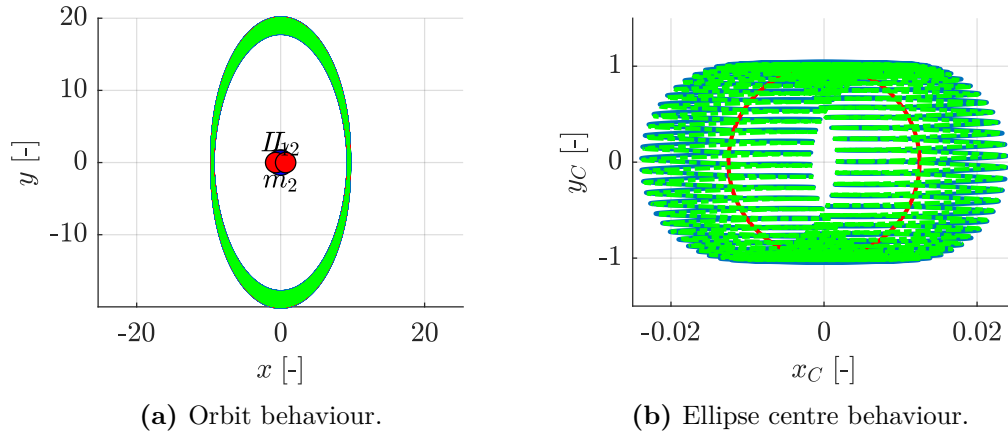


Figure 4.9: Comparison between the numerical Hill's model and the analytical 7th order solution with and without SPC with IC of Equation (4.43).

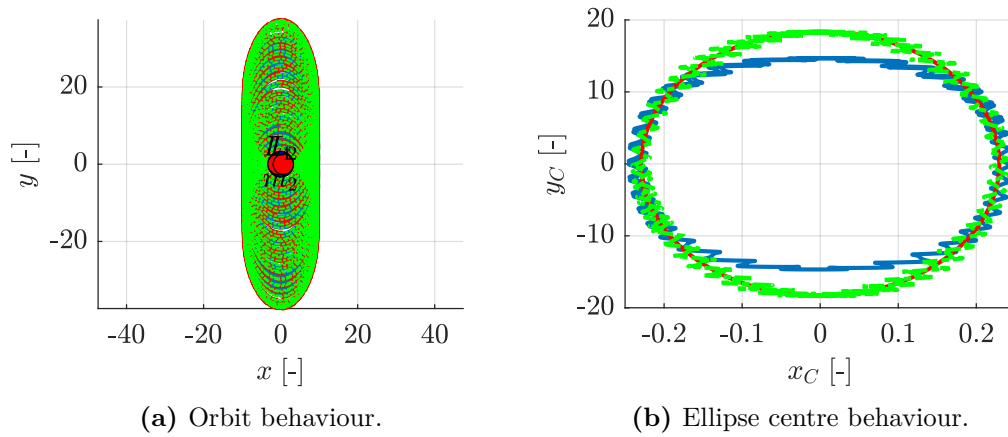


Figure 4.10: Comparison between the numerical Hill's model and the analytical 7th order solution with and without SPC with IC of Equation (4.42).

4.6.2 Short-periodic correction of the 8th-9th orders

The same way as in the Section 4.6.1, we obtain the equations of the short-periodic correction terms for both 8th and 9th order. The following are the terms of the direct transformation:

$$\begin{aligned}
 \phi_{Hill}^{(8)} = & \frac{P^*}{b^6 n^4} + \frac{(105\chi^4 - 512k^6\sigma^2)}{96b^3k^4n^2} E^* + \frac{F^*}{192b^6n^4} \left[-288\tilde{K} - \frac{48}{\Delta} + \right. \\
 & \left. + \frac{b^3n^2(256k^6\sigma^2 - 165\chi^4)}{k^4} \right] + \frac{c_1}{524288b^3\Delta^7k^4n^2} \left[2048\sqrt{3} \left(271c_2 + \right. \right. \\
 & \left. \left. + 96c_4 + 9c_6 + 136 \right) k^3\sigma\chi^2 - 131072\Delta^4k^6\sigma^2(11s_1 + 3s_3) + \right. \\
 & \left. + 15(5945s_1 + 9(1393s_3 + 277s_5 + 21s_7))\chi^4 \right] \quad (4.117a)
 \end{aligned}$$

$$q_{Hill}^{(8)} = \frac{4k\sigma}{9b^2n^2} (4E^* - F^*) + \frac{(13c_1 + 3c_3)}{6144b^2\Delta^7k^2n^2} \left[2k^3\sigma (86s_1 + 9(7s_3 + s_5)) + \right. \\ \left. - 3\sqrt{3} (22c_2 + 3c_4 + 7) \chi^2 \right] \quad (4.117b)$$

$$\Phi_{Hill}^{(8)} = \frac{(63\chi^4 - 512k^6\sigma^2)}{144bk^4n} \tilde{E} - \frac{3s_2}{32b^4\Delta^3n^3} F^* + \frac{\tilde{K}}{288b^4n^3} \left[288\tilde{K} + \frac{144}{\Delta} + \right. \\ \left. + \frac{b^3n^2(256k^6\sigma^2 - 99\chi^4)}{k^4} \right] + \frac{1}{196608b^4\Delta^{10}k^4n^3} \left[3c_2 \right. \\ \left. (-10688b^3\Delta k^6n^2\sigma^2 + 9000b^3\Delta n^2\chi^4 + 3375k^4) - 18b^3\Delta n^2 \left(c_4 \right. \right. \\ \left. \left. (704k^6\sigma^2 - 681\chi^4) + 8k^3\sigma \left(12c_6k^3\sigma + \sqrt{3} \left(142s_1 + 209s_3 + \right. \right. \right. \right. \\ \left. \left. \left. + 51s_5 \right) \chi^2 \right) \right) \right] - 19072b^3\Delta k^6n^2\sigma^2 + 16038b^3\Delta n^2\chi^4 + 729c_2^5k^4 + \\ \left. + 5103c_2^4k^4 + 13770c_2^3k^4 + 8775(c_4 + 1)k^4 + 1875k^4 \right] \quad (4.117c)$$

$$Q_{Hill}^{(8)} = \frac{\chi^3}{16b^2k^3n} (14E^* - 11F^*) + \frac{c_1\chi}{131072b^2\Delta^7n} \left[256\sqrt{3} \left(271c_2 + 96c_4 + \right. \right. \\ \left. \left. + 9c_6 + 136 \right) \sigma + \frac{3(5945s_1 + 9(1393s_3 + 277s_5 + 21s_7))\chi^2}{k^3} \right] \quad (4.117d)$$

Unfortunately, in this case the inverse transformation is not exactly the opposite of the direct one because of the terms used. As a result, the terms for the inverse transformation are:

$$\phi_{Hill}^{(8)} = \frac{(1 - 2\Delta\tilde{K})}{2\pi^2 b^6 \Delta n^4} F^* - \phi_{Hill}^{(8)} \quad (4.118a)$$

$$\Phi_{Hill}^{(8)} = -\frac{3s_2}{32b^4 \Delta^3 n^3} F^* + \frac{(3c_2 + 5)(-\Delta)\tilde{K}^2 + (3c_2 + 5)\tilde{K} - 2\Delta}{8b^4 \Delta^3 n^3} - \Phi_{Hill}^{(8)} \quad (4.118b)$$

$$\phi_{Hill}^{(9)} = \frac{\chi(-2\tilde{K}(7s_1 + 3s_3) + 16\Delta s_1 - F^* c_1)}{6\sqrt{3}b^6 \Delta^3 k n^4} - \phi_{Hill}^{(9)} \quad (4.118c)$$

$$\Phi_{Hill}^{(9)} = \frac{\chi((13c_1 + 3c_3)(-28\Delta\tilde{K} + 3c_2 + 11) - 10\Delta F^*(s_1 + 3s_3))}{192\sqrt{3}b^4 \Delta^6 k n^3} + \quad (4.118d)$$

$$- \Phi_{Hill}^{(9)}$$

$$Q_{Hill}^{(9)} = \frac{5((7s_1 + 3s_3)(1 - 2\Delta\tilde{K}) + 8\pi c_1 \Delta F^*)}{96\sqrt{3}b^5 \Delta^4 n^3} - Q_{Hill}^{(9)} \quad (4.118e)$$

So, thanks to the 9th order and the short-term correction just mentioned, it is possible to get a simulation even more similar to the numerical one. As for the other times we propose the Figures 4.11 and 4.12 in which we compare the solution of the 9th and the 9th with the short-periodic correction, equal [39]. In the figures to the left we see the behaviour that the model foresees, instead in the graph on the right the dynamics of the DRO centre. In this case the short-term oscillations (green line) were considered until 9th order, of consequence the dynamic of the centre of the DRO is described even better than before in fact the green line follows perfectly the numerical solution (blue line).

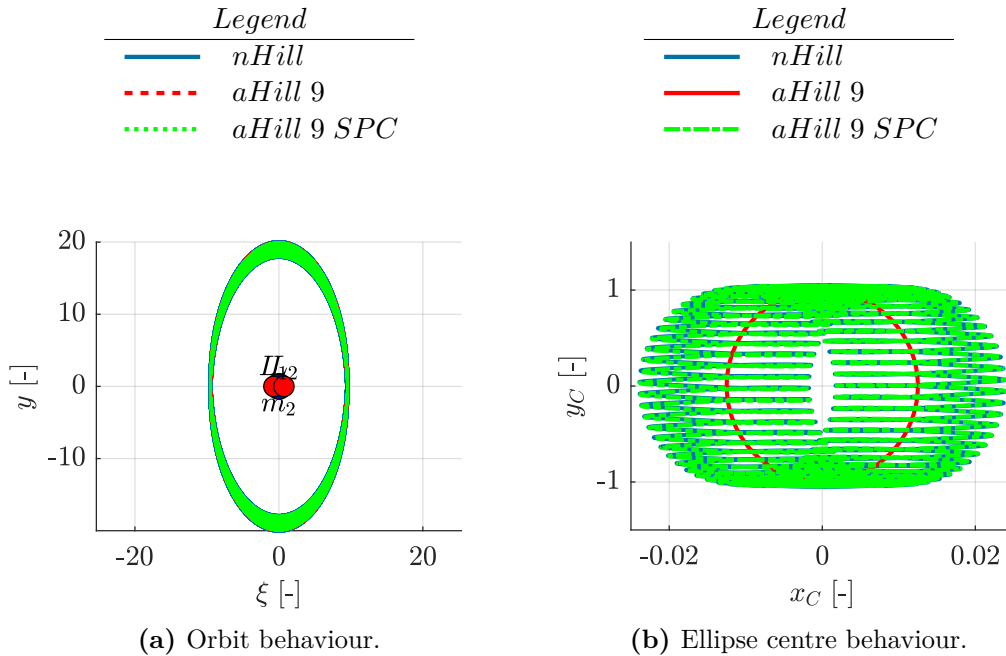


Figure 4.11: Comparison between the numerical Hill's model and the analytical 9th order solution with and without SPC with IC of Equation (4.43).

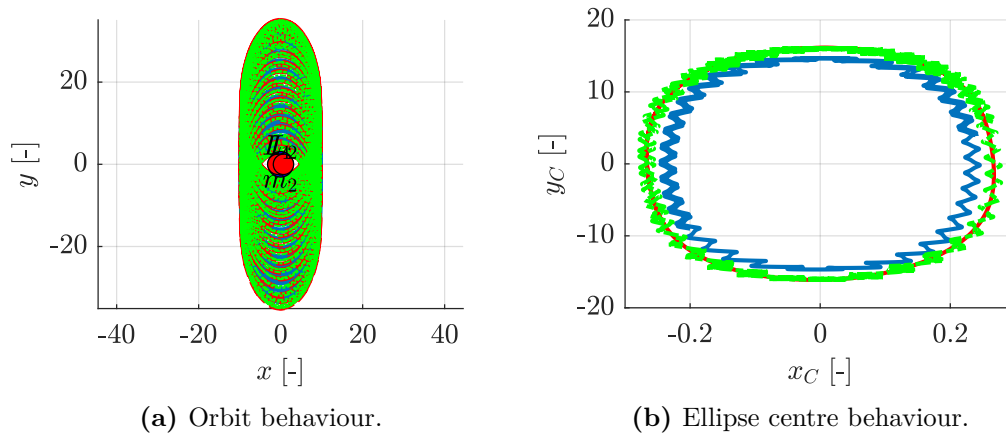


Figure 4.12: Comparison between the numerical Hill's model and the analytical 7th order solution with and without SPC with IC of Equation (4.42).

Chapter 5

Perturbation approach applied to the first term of the circular restricted three-body problem

As already mentioned above, the aim of this thesis is to provide a solution that is a intermediate stage between the Hill model and the CR3BP. The problem we are dealing with in this thesis is called CR3BP-1₁₃. As already seen in the Section 3.3.1 this model represents a higher order approximation, in mass, than the Hill model. In fact, it is similar to the Hill model to which are added the most relevant terms of the CR3BP-1. To deal with this new model we will take into consideration everything we have said and obtained in the Chapter 4 for the Hill model. Consequently, as we did previously, we start with the Hamiltonian function (Equation (3.48)). Given that, in this work we will deal exclusively with the planar case, we impose the hypotheses necessary for the Equation (3.48), thus obtaining:

$$\begin{aligned} \mathcal{H} = & \frac{1}{2} (p_x^2 + p_y^2) - nxp_y + nyp_x - n^2 \left(x^2 + \frac{1}{2}y^2 \right) - \frac{1}{\sqrt{x^2 + y^2}} + \\ & + \frac{n^2}{p} x \left(x^2 - \frac{3}{2}y^2 \right) \end{aligned} \quad (5.1)$$

where p_x and p_y are the conjugate momenta and x and y coordinates in rotating reference frame and n is the non-dimensional mean motion.

5.1 Canonical Hamiltonian

Our goal, now, is to simplify the problem through a canonical transformation however, since the problem is very similar to the one treated in Chapter 4, we can say that the new part of the Hamiltonian turns out to be a perturbing term to the main one. This assumption allows us to take advantage of still exploiting the canonical transformation, found in the previous chapter in Equation (4.44). This transformation, having been obtained with a generation function, already satisfies the canonicity criteria and consequently the Lie condition ??.

Consequently, if we apply this canonical transformation to Equation (5.1) what we get is the canonical Hamiltonian function :

$$\begin{aligned} \mathcal{K} = & \mathcal{K}_{0 \text{ Hill}} + \mathcal{K}_{1 \text{ Hill}} + \\ & \frac{1}{2kp} n \left[\left(\sqrt{2}k\sqrt{n}\sqrt{\Phi} \sin(\phi) + Q \right) \left(\frac{2 \left(\sqrt{2}k\sqrt{n}\sqrt{\Phi} \sin(\phi) + Q \right)^2}{k^2 n^2} + \right. \right. \\ & \left. \left. - 12 \left(kq + \frac{\sqrt{2}\sqrt{\Phi} \cos(\phi)}{\sqrt{n}} \right)^2 \right) \right] \end{aligned} \quad (5.2)$$

which turns out to be a linear combination of the terms of Equation (4.53) and the new terms. Now, as previously done, we introduce the same variable Equations (4.46) to (4.51) with which the previous equation:

$$\begin{aligned} \mathcal{K} = & \mathcal{K}_{0 \text{ Hill}} + \mathcal{K}_{1 \text{ Hill}} - \frac{b(2\sigma + \sin(\phi))}{p} \left(-8\sigma^2 - 8\sigma \sin(\phi) + 12\chi^2 + \right. \\ & \left. + 24\chi \cos(\phi) + 7 \cos(2\phi) + 5 \right) \end{aligned} \quad (5.3)$$

5.2 Lie transformation applied on the CR3BP-1₁₃

The procedure that we are going to perform is completely analogous to the one proposed in the previous chapter, Section 4.4, so as to obtain an equation with a form similar to that of Equation (4.55). To do this we maintain the assumptions of Equation (4.64) and add a hypothesis. This hypothesis concerns the distance between the primaries, in fact, it must be sufficiently large compared to the osculation of the center of the orbit. This assumption in normalised terms translates into the form $b/p = \mathcal{O}[\chi^j]$. During the work several values of the parameter j were taken into consideration to find the best one and some results will be presented later. In this part we will deal only with the case $b/p = \mathcal{O}[\chi^2]$ for which the most interesting results are obtained, consequently applying this assumption in the following way:

$$\frac{b}{p} = \varepsilon^2 \frac{b}{p} \quad (5.4)$$

applying the assumptions of Equations (4.64) and (5.4) and performing the expansion, the new terms of the summation have the following form:

$$\mathbf{H}_{1 \text{ CR3BP-1}_{13}} = -\frac{b}{2p} (3 \sin(\phi) + 7 \sin(3\phi)) \quad (5.5a)$$

$$\mathbf{H}_{2 \text{ CR3BP-1}_{13}} = -12 \frac{b\chi}{p} \sin(2\phi) \quad (5.5b)$$

$$\mathbf{H}_{3 \text{ CR3BP-1}_{13}} = -\frac{6b}{p} (\sigma (3 \cos(2\phi) + 1) + 2\chi^2 \sin(\phi)) \quad (5.5c)$$

$$\mathbf{H}_{4 \text{ CR3BP-1}_{13}} = -48 \frac{b\sigma\chi}{p} \cos(\phi) \quad (5.5d)$$

$$\mathbf{H}_{5 \text{ CR3BP-1}_{13}} = 24 \frac{b\sigma}{p} (\sigma \sin(\phi) - \chi^2) \quad (5.5e)$$

$$\mathbf{H}_{6 \text{ CR3BP-1}_{13}} = \frac{16b\sigma^3}{p} \quad (5.5f)$$

As done in the previous chapter, to better understand the assumption of Equation (5.4) we are going to show, Figure 5.1, the contributions of the terms of Equation (5.5) just obtained with respect to those of the Hill problem alone. It should be noted, from the Figure 5.1 that the terms of Equations (5.5a) and (5.5c) are of a higher order than compared to the first perturbing term associated with the secondary attractor, Equation (4.67e), this results from the fact that the dynamics is governed mainly by the primary attractor, consequently the corresponding terms are more influential than those of the secondary attractor. Finally, the terms of the summation of

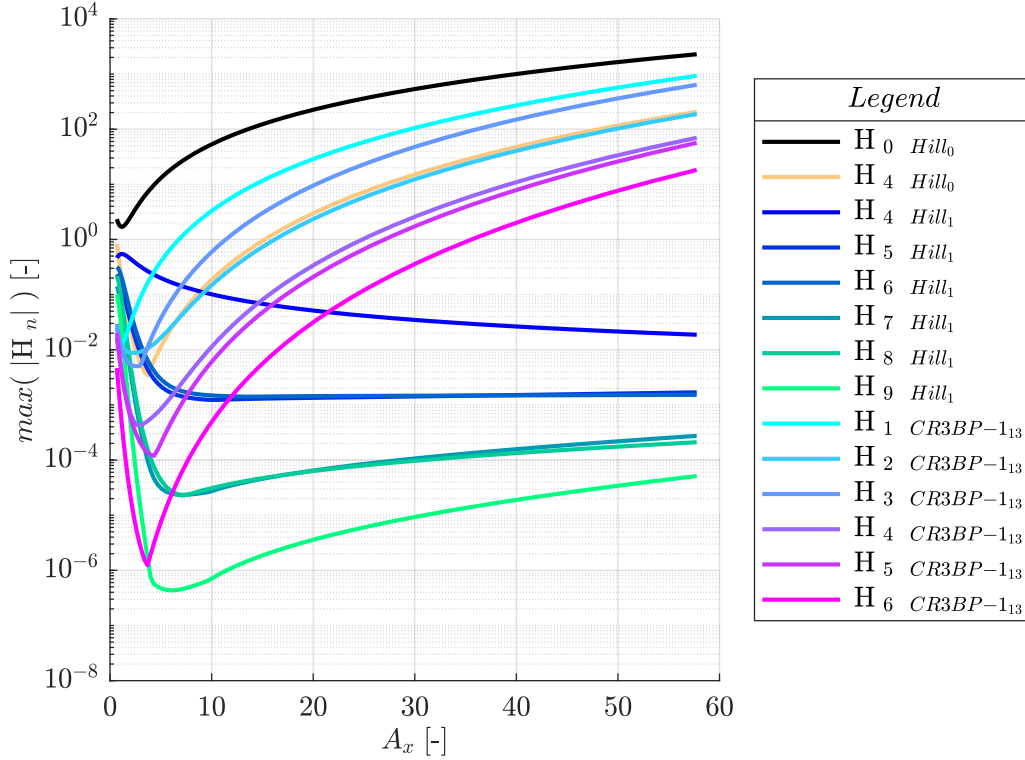


Figure 5.1: Trend of the maximum in absolute value of the terms of Equation (5.5) in MD.

Equation (4.65), for the complete problem, turn out to be:

$$\tilde{\mathbf{H}}_0_{CR3BP-113} = \mathbf{H}_0_{Hill_0} \quad (5.6a)$$

$$\tilde{\mathbf{H}}_1_{CR3BP-113} = \mathbf{H}_1_{Hill_0} \quad (5.6b)$$

$$\tilde{\mathbf{H}}_2_{CR3BP-113} = \mathbf{H}_2_{Hill_0} + \mathbf{H}_1_{CR3BP-113} \quad (5.6c)$$

$$\tilde{\mathbf{H}}_3_{CR3BP-113} = \mathbf{H}_3_{Hill_0} + \mathbf{H}_2_{CR3BP-113} \quad (5.6d)$$

$$\tilde{\mathbf{H}}_4_{CR3BP-113} = \mathbf{H}_4_{Hill_0} + \mathbf{H}_4_{Hill_1} + \mathbf{H}_3_{CR3BP-113} \quad (5.6e)$$

$$\tilde{\mathbf{H}}_5_{CR3BP-113} = \mathbf{H}_5_{Hill_1} + \mathbf{H}_4_{CR3BP-113} \quad (5.6f)$$

$$\tilde{\mathbf{H}}_6_{CR3BP-113} = \mathbf{H}_6_{Hill_1} + \mathbf{H}_5_{CR3BP-113} \quad (5.6g)$$

$$\tilde{\mathbf{H}}_7_{CR3BP-113} = \mathbf{H}_7_{Hill_1} \quad (5.6h)$$

$$\tilde{\mathbf{H}}_8_{CR3BP-113} = \mathbf{H}_8_{Hill_1} + \mathbf{H}_6_{CR3BP-113} \quad (5.6i)$$

Now, by applying the general method of Kamel derived from the Deprit triangle for the Hamiltonian systems, i.e. by applying the procedure seen in Section 4.4.1, we can

obtain the averaged Hamiltonian terms and the corresponding generating function. However, thanks to the fact that the one part of the problem turns out to be equal to that of Hill, treated in the previous chapter, one part turns out to be identical, consequently:

$$\langle \mathcal{K}_0 CR3BP-113 \rangle_\phi = \langle \mathcal{K}_0 Hill \rangle_\phi \quad (5.7)$$

with $n = 1$:

$$\langle \mathcal{K}_1 CR3BP-113 \rangle_\phi = \langle \mathcal{K}_1 Hill \rangle_\phi \quad (5.8)$$

$$S_1 CR3BP-113 = S_1 Hill \quad (5.9)$$

for $n = 2$ we have:

$$\langle \mathcal{K}_2 CR3BP-113 \rangle_\phi = \langle \mathcal{K}_2 Hill \rangle_\phi \quad (5.10)$$

$$S_2 CR3BP-113 = S_2 Hill + \frac{\sqrt{2}\Phi^{3/2}}{3\sqrt{np}}(9 \cos(\phi) + 7 \cos(3\phi)) \quad (5.11)$$

with $n = 3$:

$$\langle \mathcal{K}_3 CR3BP-113 \rangle_\phi = \langle \mathcal{K}_3 Hill \rangle_\phi \quad (5.12)$$

$$S_3 CR3BP-113 = S_3 Hill + \frac{18\sqrt{3}q\Phi \cos(2\phi)}{p} \quad (5.13)$$

and with $n = 4$:

$$\langle \mathcal{K}_4 CR3BP-113 \rangle_\phi = \langle \mathcal{K}_4 Hill \rangle_\phi - \frac{522\Phi^2}{p^2} - \frac{48\sqrt{3}Q\Phi}{p} \quad (5.14)$$

$$S_4 CR3BP-113 = S_4 Hill + \frac{108\sqrt{2}\sqrt{n}q^2\sqrt{\Phi} \cos(\phi)}{p} + \frac{9\Phi \sin(2\phi)}{np} \left(\frac{7\Phi(\cos(2\phi) + 4)}{p} + 8\sqrt{3}Q \right) \quad (5.15)$$

then, with $n = 5$:

$$\langle \mathcal{K}_5 CR3BP-113 \rangle_\phi = \langle \mathcal{K}_5 Hill \rangle_\phi \quad (5.16)$$

$$S_5 CR3BP-113 = S_5 Hill - \frac{72\sqrt{2}q}{p} s_1 \sqrt{\frac{\Phi}{n}} \left(\frac{\sqrt{3}c_2\Phi}{p} + \frac{67\sqrt{3}\Phi}{p} + 20Q \right) \quad (5.17)$$

and with $n = 6$, we have:

$$\langle \mathcal{K}_6 CR3BP-113 \rangle_\phi = \langle \mathcal{K}_6 Hill \rangle_\phi - \frac{1080nq^2}{p} \left(\frac{45\Phi}{p} + 2\sqrt{3}Q \right) \quad (5.18)$$

$$\begin{aligned}
S_{6 \text{ CR3BP-113}} = & S_{6 \text{ Hill}} - \frac{1040\sqrt{3}}{np} \log \left(\sqrt{6}c_1 + \sqrt{3c_2 + 5} \right) + \\
& + \frac{60F^* (3s_1 + 7s_3)}{np} - \frac{120 (9c_1 + 7c_3)}{np} \tilde{K} + \\
& + \frac{3\sqrt{2}c_1}{\sqrt{\Delta^2 n^{3/2} p}} \left(- \frac{18\sqrt{2}\Delta\Phi}{p} \left(\frac{91\sqrt{2}c_4\Phi^{3/2}}{p} + \right. \right. \\
& \left. \left. + 230n^{3/2}q^2s_1 \right) + 7\sqrt{2}c_2 \left(20\sqrt{n} + \frac{2\sqrt{2}\Delta\Phi^{3/2}}{p} \right. \right. \\
& \left. \left. \left(\frac{697\Phi}{p} + 40\sqrt{3}Q \right) \right) + 4\sqrt{2} \left(85\sqrt{n} + 2\sqrt{2}\Delta\sqrt{\Phi} \right. \right. \\
& \left. \left. \left(\frac{1027\Phi^2}{p^2} + \frac{250\sqrt{3}Q\Phi}{p} - 60Q^2 \right) \right) \right) - \frac{825760\sqrt{3}}{2291np}
\end{aligned} \tag{5.19}$$

for $n = 7$:

$$\langle \mathcal{K}_{7 \text{ CR3BP-113}} \rangle_\phi = \langle \mathcal{K}_{7 \text{ Hill}} \rangle_\phi + \frac{136080\Phi^2}{p^2} \tag{5.20}$$

$$\begin{aligned}
S_{7 \text{ CR3BP-113}} = & S_{7 \text{ Hill}} + \frac{2160\sqrt{6}F^*qs_2}{p\sqrt{n}\Phi} - \frac{432\sqrt{3}q}{np\sqrt{\Phi}} \left(10\sqrt{2}c_2\sqrt{n} + \right. \\
& \left. + \frac{(120s_1 + 5s_3 + 21s_5)\sqrt{\Phi}}{p} \right) \tilde{K} + \frac{1}{n^{3/2}p\sqrt{\Phi}} \\
& \left(- \frac{421200\sqrt{3}c_4\sqrt{n}q\Phi^{5/2}}{p^2} + 135c_2\sqrt{n}q \left(3\sqrt{3} \right. \right. \\
& \left. \left. \left(\frac{4528\Phi^{5/2}}{p^2} - \frac{31\sqrt{n}}{16\sqrt{2}\Delta^3} \right) + \frac{2720Q\Phi^{3/2}}{p} \right) + \right. \\
& - \frac{6345\sqrt{\frac{3}{2}}c_4nq}{8\Delta^3} - \frac{4725\sqrt{\frac{3}{2}}c_6nq}{16\Delta^3} + \frac{103680\sqrt{2}c_1\Phi^3}{p^2} + \\
& + \frac{25920\sqrt{2}c_3\Phi^3}{p^2} + \frac{36288\sqrt{2}c_5\Phi^3}{p^2} + \\
& - \frac{106920\sqrt{6}n^2q^3s_1\Phi}{p} + \frac{1469340\sqrt{3}\sqrt{n}q\Phi^{5/2}}{p^2} + \\
& + \frac{276480\sqrt{n}qQ\Phi^{3/2}}{p} + \frac{45360\sqrt{n}s_2\Phi^{5/2}}{p} + \\
& - \frac{4860\sqrt{n}s_4\Phi^{5/2}}{p} - \frac{8375\sqrt{\frac{3}{2}}nq}{8\Delta^3} - 2605\sqrt{15}nq + \\
& + 7560\sqrt{3}\sqrt{n}Qs_2\Phi^{3/2} + \frac{13906080\sqrt{6}qs_1\Phi^3}{p^3} + \\
& - \frac{751680\sqrt{6}qs_3\Phi^3}{p^3} - \frac{526176\sqrt{6}qs_5\Phi^3}{p^3} + \\
& \left. + \frac{1399680\sqrt{2}qQs_1\Phi^2}{p^2} - \frac{51840\sqrt{2}qQs_3\Phi^2}{p^2} \right)
\end{aligned} \tag{5.21}$$

and finally with $n = 8$ we have:

$$\begin{aligned}
 \langle \mathcal{K}_8 CR3BP_{-113} \rangle_\phi = & \langle \mathcal{K}_8 Hill \rangle_\phi + \frac{28}{3np} \left(30 \left(-27 \left(\frac{54n^3 q^4}{p} + \right. \right. \right. \\
 & - \frac{91854nq^2 \Phi^2}{p^3} + \frac{39191 \Phi^3}{p^3} \left. \left. \left. \right) + \frac{324\sqrt{3}Q\Phi}{p^2} \right. \right. \\
 & \left. \left. \left(36nq^2 - 509\Phi \right) - \frac{29376Q^2\Phi}{p} + 128\sqrt{3}Q^3 \right) + \right. \\
 & - \sqrt{\frac{2n}{\Phi}} \left(\frac{\Phi}{p} \left(222208\tilde{E} - 95455\tilde{K} \right) + 40\sqrt{3}Q \left(2216\tilde{E} + \right. \right. \\
 & \left. \left. - 1259\tilde{K} \right) \right) \left. \right) + \\
 & - \frac{1260\sqrt{2}\tilde{K}}{\sqrt{np}\sqrt{\Phi}} \left(\frac{81nq^2}{p} - \frac{1344\Phi}{p} - 32\sqrt{3}Q \right)
 \end{aligned} \tag{5.22}$$

5.3 Motion by full normalised Hamiltonian in canonical form (8th order)

In this case the Hamiltonian function turns out to be:

$$\begin{aligned}
 \bar{\mathcal{K}}_{CR3BP_{-113}} = & \bar{\mathcal{K}}_{9 Hill} + \frac{1}{4320np^4\sqrt{\Phi}} \left[40\sqrt{3}p^3Q \left(\sqrt{2}\sqrt{n}(1367\tilde{K} + \right. \right. \\
 & \left. \left. - 2216\tilde{E}) + 12\sqrt{\Phi} (8Q^2 - 27n^2q^2) - 216n\Phi^{3/2} \right) - p^2 \right. \\
 & \left(5\sqrt{2}\sqrt{n}\tilde{K} (2187nq^2 - 55379\Phi) + 4\sqrt{\Phi} (55552\sqrt{2}\tilde{E}\sqrt{n}\sqrt{\Phi} + \right. \\
 & \left. + 405 (27n^3q^4 + 180n^2q^2\Phi - 14n\Phi^2 + 544Q^2\Phi) \right) \left. \right) + \\
 & + 9720\sqrt{3}pQ\Phi^{3/2} (36nq^2 - 509\Phi) + 810\Phi^{5/2} \\
 & \left. \left(91854nq^2 - 39191\Phi \right) \right]
 \end{aligned} \tag{5.23}$$

from which, by applying Equation (4.4), we obtain the following system of differential equations of the first order:

$$\begin{cases} \dot{\phi} = C_{\phi-a} + C_{\phi-b}q^2 + C_{\phi-c}q^4 + C_{\phi-d}Q + C_{\phi-e}Q^2 + C_{\phi-f}q^2Q & (5.24a) \\ \dot{q} = C_{q-a} + C_{q-b}Q + \varepsilon (C_{q-a\varepsilon} + C_{q-b\varepsilon}q^2 + C_{q-c\varepsilon}Q + C_{q-d\varepsilon}Q^2) & (5.24b) \\ \dot{\Phi} = 0 & (5.24c) \\ \dot{Q} = C_{Q-a}q + \varepsilon (C_{Q-a\varepsilon}q + C_{Q-b\varepsilon}q^3 + C_{Q-c\varepsilon}qQ) & (5.24d) \end{cases}$$

where:

$$C_{\phi-a} = \tilde{C}_{\phi_9-a} + \frac{1}{8640p^4} \left[\frac{\sqrt{2}p^2 (276895\tilde{K} - 222208\tilde{E})}{\sqrt{n\Phi}} - \frac{190468260\Phi^2}{n} + 90720p^2\Phi \right] \quad (5.25a)$$

$$C_{\phi-b} = \tilde{C}_{\phi-b} + \frac{27}{64p^4\Phi^{3/2}} \left[3\sqrt{2}\sqrt{np^2}\tilde{K} + 16\Phi^{3/2} (5103\Phi - 10np^2) \right] \quad (5.25b)$$

$$C_{\phi-c} = \tilde{C}_{\phi-c} \quad (5.25c)$$

$$C_{\phi-d} = \frac{1}{72\sqrt{3}} \left[\frac{\sqrt{2} (2216\tilde{E} - 1367\tilde{K})}{\sqrt{np}\Phi^{3/2}} - \frac{494748\Phi}{np^3} - \frac{432}{p} \right] \quad (5.25d)$$

$$C_{\phi-e} = \tilde{C}_{\phi-d} - \frac{204}{np^2} \quad (5.25e)$$

$$C_{\phi-f} = \frac{81\sqrt{3}}{p^3} \quad (5.25f)$$

$$C_{q-a} = -\frac{2\sqrt{3}\Phi}{p} \quad (5.25g)$$

$$C_{q-b} = \tilde{C}_{q-a} \quad (5.25h)$$

$$C_{q-a\varepsilon} = \frac{(1367\tilde{K} - 2216\tilde{E})}{18\sqrt{6}p\sqrt{n\Phi}} - \frac{4581\sqrt{3}\Phi^2}{4np^3} \quad (5.25i)$$

$$C_{q-b\varepsilon} = -\frac{3\sqrt{3}(np^2 - 27\Phi)}{p^3} \quad (5.25j)$$

$$C_{q-c\varepsilon} = \tilde{C}_{q-a\varepsilon} - \frac{408\Phi}{np^2} \quad (5.25k)$$

$$C_{q-d\varepsilon} = \frac{8}{\sqrt{3}np} \quad (5.25l)$$

$$C_{Q-a} = \tilde{C}_{Q-a} \quad (5.25m)$$

$$C_{Q-a\varepsilon} = \frac{27}{16p^4\sqrt{\Phi}} \left[3\sqrt{2}\sqrt{np^2}\tilde{K} + 4\Phi^{3/2} (20np^2 - 5103\Phi) \right] \quad (5.25n)$$

$$C_{Q-b\varepsilon} = \tilde{C}_{Q-a\varepsilon} + \frac{81n^2}{2p^2} \quad (5.25o)$$

$$C_{Q-c\varepsilon} = \frac{6\sqrt{3}(np^2 - 27\Phi)}{p^3} \quad (5.25p)$$

This represents a system of ODE that can not be solved by classical methods. As we did in the case of Hill, we apply the Lindstedt-Poincaré technique, from which, without proposing all the steps, we obtain the following equations:

$$\left\{ \begin{array}{l} q = G_{q-a} \cosh(t\bar{\Lambda}) + G_{q-b} \cosh(2t\bar{\Lambda}) + G_{q-c} \cosh(3t\bar{\Lambda}) + \\ \quad + G_{q-d} \sinh(t\bar{\Lambda}) + G_{q-e} \sinh(2t\bar{\Lambda}) + G_{q-f} \sinh(3t\bar{\Lambda}) \\ Q = G_{Q-b} \cosh(t\bar{\Lambda}) + G_{Q-c} \cosh(2t\bar{\Lambda}) + G_{Q-d} \cosh(3t\bar{\Lambda}) + \\ \quad + G_{Q-e} \sinh(t\bar{\Lambda}) + G_{Q-f} \sinh(2t\bar{\Lambda}) + G_{Q-g} \sinh(3t\bar{\Lambda}) + G_{Q-a} \end{array} \right. \quad (5.26a)$$

$$\left\{ \begin{array}{l} Q = G_{Q-b} \cosh(t\bar{\Lambda}) + G_{Q-c} \cosh(2t\bar{\Lambda}) + G_{Q-d} \cosh(3t\bar{\Lambda}) + \\ \quad + G_{Q-e} \sinh(t\bar{\Lambda}) + G_{Q-f} \sinh(2t\bar{\Lambda}) + G_{Q-g} \sinh(3t\bar{\Lambda}) + G_{Q-a} \end{array} \right. \quad (5.26b)$$

with:

$$\begin{aligned} \bar{\Lambda} = & \frac{1}{8C_{Q-a}^{3/2}C_{q-b}^{3/2}} \left[C_{q-b} (4C_{Q-a}^2C_{q-c\varepsilon} - C_{q-a} (3C_{q-a}C_{Q-b\varepsilon} + 4C_{Q-a}C_{Q-c\varepsilon})) + \right. \\ & + C_{q-b}^2 (C_{Q-a} (4C_{Q-a\varepsilon} + 8C_{Q-a} + 3q_0^2C_{Q-b\varepsilon}) - 6Q_0C_{q-a}C_{Q-b\varepsilon}) + \\ & \left. - 8C_{q-a}C_{Q-a}^2C_{q-d\varepsilon} - 3Q_0^2C_{q-b}^3C_{Q-b\varepsilon} \right] \end{aligned} \quad (5.27)$$

and:

$$\begin{aligned} G_{q-a} = & \frac{q_0}{16C_{Q-a}^2C_{q-b}^2} \left[C_{Q-a}C_{q-b} (4C_{q-a}C_{Q-c\varepsilon} - C_{q-b} (4C_{Q-a\varepsilon} + \right. \\ & + 3q_0^2C_{Q-b\varepsilon})) + 3C_{q-b}C_{Q-b\varepsilon} (C_{q-a} + Q_0C_{q-b})^2 + 4C_{Q-a}^2 (C_{q-b} \\ & \left. (4C_{q-b} + C_{q-c\varepsilon}) - 2C_{q-a}C_{q-d\varepsilon}) \right] \end{aligned} \quad (5.28a)$$

$$G_{q-b} = \frac{q_0 (C_{q-a} + Q_0C_{q-b}) (2C_{Q-a}C_{q-d\varepsilon} + C_{q-b} (C_{Q-c\varepsilon} + 2C_{q-b\varepsilon}))}{3C_{Q-a}C_{q-b}^2} \quad (5.28b)$$

$$G_{q-c} = \frac{q_0C_{Q-b\varepsilon} (q_0^2C_{Q-a}C_{q-b} + 3 (C_{q-a} + Q_0C_{q-b})^2)}{32C_{Q-a}^2C_{q-b}} \quad (5.28c)$$

$$\begin{aligned} G_{q-d} = & \frac{(C_{q-a} + Q_0C_{q-b})}{16C_{Q-a}^{5/2}C_{q-b}^{5/2}} \left[C_{Q-a}C_{q-b} (4C_{q-a}C_{Q-c\varepsilon} - C_{q-b} (4C_{Q-a\varepsilon} + \right. \\ & + 3q_0^2C_{Q-b\varepsilon})) + 3C_{q-b}C_{Q-b\varepsilon} (C_{q-a} + Q_0C_{q-b})^2 + 4C_{Q-a}^2 (C_{q-b} \\ & \left. (4C_{q-b} + C_{q-c\varepsilon}) - 2C_{q-a}C_{q-d\varepsilon}) \right] \end{aligned} \quad (5.28d)$$

$$\begin{aligned} G_{q-e} = & \frac{(q_0^2C_{Q-a}C_{q-b} + (C_{q-a} + Q_0C_{q-b})^2)}{6C_{Q-a}^{3/2}C_{q-b}^{5/2}} \left[2C_{Q-a}C_{q-d\varepsilon} + \right. \\ & \left. + C_{q-b} (C_{Q-c\varepsilon} + 2C_{q-b\varepsilon}) \right] \end{aligned} \quad (5.28e)$$

$$G_{q-f} = \frac{C_{Q-b\varepsilon} (C_{q-a} + Q_0C_{q-b}) (3q_0^2C_{Q-a}C_{q-b} + (C_{q-a} + Q_0C_{q-b})^2)}{32C_{Q-a}^{5/2}C_{q-b}^{3/2}} \quad (5.28f)$$

$$\begin{aligned} G_{Q-a} = & \frac{1}{2C_{Q-a}C_{q-b}^3} \left[C_{q-b} (- C_{Q-a}C_{q-b} (Q_0^2C_{q-d\varepsilon} + 2C_{q-a\varepsilon} + C_{q-b\varepsilon}q_0^2) + \right. \\ & + q_0^2C_{Q-a}^2C_{q-d\varepsilon} + C_{q-b\varepsilon}Q_0^2C_{q-b}^2) + 2C_{q-a}C_{q-b} (C_{q-b} (C_{q-b\varepsilon}Q_0 + \\ & - C_{Q-a}) + C_{Q-a} (C_{q-c\varepsilon} - Q_0C_{q-d\varepsilon})) + C_{q-a}^2 (C_{q-b\varepsilon}C_{q-b} + \\ & \left. - 3C_{Q-a}C_{q-d\varepsilon}) \right] \end{aligned} \quad (5.28g)$$

$$\begin{aligned} G_{Q-b} = & \frac{(C_{q-a} + Q_0C_{q-b})}{16C_{Q-a}^2C_{q-b}^3} \left[C_{Q-a}C_{q-b} (C_{q-b} (4C_{Q-a\varepsilon} + 3q_0^2C_{Q-b\varepsilon}) + \right. \\ & - 4C_{q-a}C_{Q-c\varepsilon}) - 3C_{q-b}C_{Q-b\varepsilon} (C_{q-a} + Q_0C_{q-b})^2 + 4C_{Q-a}^2 \\ & \left. (2C_{q-a}C_{q-d\varepsilon} - C_{q-b}C_{q-c\varepsilon} + 4C_{q-b}^2) \right] \end{aligned} \quad (5.28h)$$

$$\begin{aligned} G_{Q-c} = & \frac{(q_0^2C_{Q-a}C_{q-b} + (C_{q-a} + Q_0C_{q-b})^2)}{6C_{Q-a}C_{q-b}^3} \left[C_{Q-a}C_{q-d\varepsilon} + C_{q-b} \right. \\ & \left. (2C_{Q-c\varepsilon} + C_{q-b\varepsilon}) \right] \end{aligned} \quad (5.28i)$$

$$G_{Q-d} = \frac{3C_{Q-b\varepsilon} (C_{q-a} + Q_0 C_{q-b}) (3q_0^2 C_{Q-a} C_{q-b} + (C_{q-a} + Q_0 C_{q-b})^2)}{32C_{Q-a}^2 C_{q-b}^2} \quad (5.28j)$$

$$G_{Q-e} = \frac{q_0}{16C_{Q-a}^{3/2} C_{q-b}^{5/2}} \left[C_{Q-a} C_{q-b} (C_{q-b} (4C_{Q-a\varepsilon} + 3q_0^2 C_{Q-b\varepsilon}) + \right. \\ \left. - 4C_{q-a} C_{Q-c\varepsilon}) - 3C_{q-b} C_{Q-b\varepsilon} (C_{q-a} + Q_0 C_{q-b})^2 + 4C_{Q-a}^2 \right. \\ \left. (2C_{q-a} C_{q-d\varepsilon} - C_{q-b} C_{q-c\varepsilon} + 4C_{q-b}^2) \right] \quad (5.28k)$$

$$G_{Q-f} = \frac{q_0 (C_{q-a} + Q_0 C_{q-b}) (C_{Q-a} C_{q-d\varepsilon} + C_{q-b} (2C_{Q-c\varepsilon} + C_{q-b\varepsilon}))}{3\sqrt{C_{Q-a} C_{q-b}^5}} \quad (5.28l)$$

$$G_{Q-g} = \frac{3q_0 C_{Q-b\varepsilon} (q_0^2 C_{Q-a} C_{q-b} + 3 (C_{q-a} + Q_0 C_{q-b})^2)}{32C_{Q-a}^{3/2} C_{q-b}^{3/2}} \quad (5.28m)$$

Once the solution for the Equations (5.24b) and (5.24d) has been obtained, the Equation (5.26) are replaced in the Equation (5.24a), where it appears to be a simple differential equation with separable variables, which can be integrated by quadrature.

5.4 Short-periodic correction

In a completely analogous way to Hill's model of the previous chapter we obtain the short-term correction.

5.4.1 Short-periodic correction 7th order

In a similar way to the previous case, the first 3 coefficients are zero, the others are:

$$\phi_{CR3BP-113}^{(2)} = \phi_{Hill}^{(2)} + \frac{(9c_1 + 7c_3) \sqrt{\Phi}}{2\sqrt{2}\sqrt{np}} \quad (5.29a)$$

$$q_{CR3BP-113}^{(2)} = q_{Hill}^{(2)} \quad (5.29b)$$

$$\Phi_{CR3BP-113}^{(2)} = \Phi_{Hill}^{(2)} + \frac{\sqrt{2} (3s_1 + 7s_3) \Phi^{3/2}}{2\sqrt{np}} \quad (5.29c)$$

$$Q_{CR3BP-113}^{(2)} = Q_{Hill}^{(2)} \quad (5.29d)$$

$$\phi_{CR3BP-113}^{(3)} = \phi_{Hill}^{(3)} + \frac{3\sqrt{3}c_2 q}{p} \quad (5.29e)$$

$$q_{CR3BP-113}^{(3)} = q_{Hill}^{(3)} \quad (5.29f)$$

$$\Phi_{CR3BP-113}^{(3)} = \Phi_{Hill}^{(3)} + \frac{6\sqrt{3}q s_2 \Phi}{p} \quad (5.29g)$$

$$Q_{CR3BP-113}^{(3)} = Q_{Hill}^{(3)} - \frac{3\sqrt{3}c_2 \Phi}{p} \quad (5.29h)$$

$$\phi_{CR3BP-113}^{(4)} = \phi_{Hill}^{(4)} + \frac{c_1}{4np} \left(\frac{9\sqrt{2}n^{3/2}q^2}{\sqrt{\Phi}} - s_1 \left(\frac{(126c_2 + 49c_4 + 227) \Phi}{p} + \right. \right. \\ \left. \left. + 24\sqrt{3}Q \right) \right) \quad (5.29i)$$

$$q_{CR3BP-113}^{(4)} = q_{Hill}^{(4)} - \frac{3\sqrt{3}s_2 \Phi}{np} \quad (5.29j)$$

$$\Phi_{CR3BP-113}^{(4)} = \Phi_{Hill}^{(4)} + \frac{3}{4np} \left(\frac{(56c_2 + 14c_4 + 29)\Phi^2}{p} + 8\sqrt{3}c_2Q\Phi + 6\sqrt{2}n^{3/2}q^2s_1\sqrt{\Phi} \right) \quad (5.29k)$$

$$Q_{CR3BP-113}^{(4)} = Q_{Hill}^{(4)} - \frac{9\sqrt{2}c_1\sqrt{n}q\sqrt{\Phi}}{p} \quad (5.29l)$$

$$\phi_{CR3BP-113}^{(5)} = \phi_{Hill}^{(5)} - \frac{3qs_1}{\sqrt{2}\sqrt{np}\sqrt{\Phi}} \left(\frac{\sqrt{3}(13c_2 + 7c_4 + 48)\Phi}{p} + 4Q \right) \quad (5.29m)$$

$$q_{CR3BP-113}^{(5)} = q_{Hill}^{(5)} - \frac{12\sqrt{2}qs_1\sqrt{\Phi}}{\sqrt{np}} \quad (5.29n)$$

$$\Phi_{CR3BP-113}^{(5)} = \Phi_{Hill}^{(5)} + \frac{3\sqrt{2}c_1q\sqrt{\Phi}}{\sqrt{np}} \left(\frac{\sqrt{3}(3c_2 + 25)\Phi}{p} + 4Q \right) \quad (5.29o)$$

$$Q_{CR3BP-113}^{(5)} = Q_{Hill}^{(5)} + \frac{6\sqrt{2}s_1\sqrt{\Phi}}{\sqrt{np}} \left(\frac{\sqrt{3}(c_2 + 7)\Phi}{p} + 2Q \right) \quad (5.29p)$$

$$\begin{aligned} \phi_{CR3BP-113}^{(6)} = & \phi_{Hill}^{(6)} + \frac{1}{192\sqrt{2}\Delta n^{3/2}p\Phi} \left[3\sqrt{2}c_1 \left(-72\Delta\sqrt{n}\tilde{K} + 36\sqrt{n} + \right. \right. \\ & \left. \left. + 2\sqrt{2}\Delta\sqrt{\Phi} \left(\frac{6093\Phi^2}{p^2} + \frac{840\sqrt{3}Q\Phi}{p} - 64Q^2 \right) \right) + \right. \\ & \left. + 12c_3 \left(-14\sqrt{2}\Delta\sqrt{n}\tilde{K} + 7\sqrt{2}\sqrt{n} + \frac{2\Delta\Phi^{3/2}}{p} \right) \right. \\ & \left. \left(\frac{543\Phi}{p} - 16\sqrt{3}Q \right) \right) - \frac{28\Delta\Phi^{3/2}}{p} \\ & \left. \left(\frac{7(27c_7 + 7c_9)\Phi}{p} + 9c_5 \left(\frac{81\Phi}{p} + 8\sqrt{3}Q \right) \right) \right) + \\ & \left. + 36\sqrt{2}\Delta\sqrt{n} \left(F^* (3s_1 + 7s_3) - \frac{6nq^2(24s_2 + 19s_4)\Phi}{p} \right) \right] \quad (5.29q) \end{aligned}$$

$$q_{CR3BP-113}^{(6)} = q_{Hill}^{(6)} - \frac{4\sqrt{2}c_1\sqrt{\Phi}}{3n^{3/2}p} \left(\frac{\sqrt{3}(c_2 - 5)\Phi}{p} + 6Q \right) \quad (5.29r)$$

$$\begin{aligned}
\Phi_{CR3BP-113}^{(6)} = & \Phi_{Hill}^{(6)} + \frac{1}{720} \left[\frac{15}{p} \left[-\frac{36(3s_1 + 7s_3)\tilde{K}}{n} + \frac{18c_1^2}{\Delta^3 n^{3/2}} \right. \right. \\
& \left. \left[\frac{168\Delta^3 n^{3/2} q^2 \Phi}{p} + s_1 \left[(21\Delta^2 - 4)\sqrt{n} + \frac{20\sqrt{2}\Delta^3 \Phi^{3/2}}{p} \right. \right. \right. \\
& \left. \left. \left(\frac{42\Phi}{p} + \sqrt{3}Q \right) \right] + \frac{805\sqrt{2}\Delta^3 s_1^3 \Phi^{5/2}}{p^2} \right] + \\
& - \frac{7245\sqrt{2}c_1^4 s_1 \Phi^{5/2}}{n^{3/2} p^2} - \frac{416\sqrt{3}c_1 s_1}{\sqrt{6}c_1 \sqrt{3}c_2 + 5n + 8\Delta^2 n} + \\
& - \frac{208s_1}{\sqrt{3}c_1 n + 2\Delta n} - \frac{1449\sqrt{2}s_1^5 \Phi^{5/2}}{n^{3/2} p^2} - \frac{7!\sqrt{2}s_1^3 \Phi^{5/2}}{n^{3/2} p^2} + \\
& + \frac{7605\sqrt{2}s_1 \Phi^{5/2}}{n^{3/2} p^2} - \frac{120\sqrt{6}Q s_1^3 \Phi^{3/2}}{n^{3/2} p} + \\
& + \frac{1368\sqrt{6}Q s_1 \Phi^{3/2}}{n^{3/2} p} - \frac{192\sqrt{2}Q^2 s_1 \sqrt{\Phi}}{n^{3/2}} + \frac{24s_1^3}{\Delta^3 n} - \frac{24s_1}{\Delta^3 n} + \\
& - \frac{126s_1^3}{\Delta n} + \frac{182s_1}{\Delta n} + \frac{3240q^2 \Phi}{p} - \frac{3024q^2 s_1^2 \Phi}{p} \left. \right] + \\
& - \frac{270(c_1 + 7c_3)F^*}{np} \left. \right]
\end{aligned} \tag{5.29s}$$

$$Q_{CR3BP-113}^{(6)} = Q_{Hill}^{(6)} + \frac{45qs_2\Phi}{2p^2} \tag{5.29t}$$

$$\begin{aligned}
 \phi_{CR3BP-113}^{(7)} = & \phi_{Hill}^{(7)} + \frac{1}{96768\sqrt{2}n^{3/2}p^4\Delta^3\Phi^{3/2}} \left[23982\sqrt{3}nqp^3 + \right. \\
 & + 106240\sqrt{3}nq\Delta\tilde{E}p^3 + 17955\sqrt{3}nqc_2p^3 + \\
 & + 63744\sqrt{3}nq\Delta\tilde{E}c_2p^3 - 43470\sqrt{3}nqc_4p^3 - 11907\sqrt{3}nqc_6p^3 + \\
 & + 90720\sqrt{6}\sqrt{n}Q\Delta\Phi^{3/2}s_2p^3 - 90720\sqrt{3}nq\Delta F(\phi|k^2)s_2p^3 + \\
 & + 27216\sqrt{6}\sqrt{n}Q\Delta\Phi^{3/2}s_4p^3 - 27216\sqrt{3}nq\Delta F(\phi|k^2)s_4p^3 + \\
 & - 32\sqrt{3}nq\Delta\tilde{K}(1443c_2 - 5670\phi s_2 - 1701\phi s_4 + 2405)p^3 + \\
 & + 1150848\sqrt{2}\sqrt{n}qQ\Delta\Phi^{3/2}p^2 + 3390336\sqrt{2}\sqrt{n}qQ\Delta\Phi^{3/2}c_2p^2 \\
 & - 1596672\sqrt{2}\sqrt{n}qQ\Delta\Phi^{3/2}c_4p^2 - 870912\sqrt{2}\sqrt{n}qQ\Delta\Phi^{3/2}c_6p^2 + \\
 & - 1388016\sqrt{3}n^2q^3\Delta\Phi s_1p^2 + 1088640\sqrt{2}\sqrt{n}\Delta\Phi^{5/2}s_2p^2 + \\
 & - 1306368\sqrt{3}n^2q^3\Delta\Phi s_3p^2 + 326592\sqrt{2}\sqrt{n}\Delta\Phi^{5/2}s_4p^2 + \\
 & - 244944\sqrt{3}n^2q^3\Delta\Phi s_5p^2 + 984636\sqrt{6}\sqrt{n}q\Delta\Phi^{5/2}p + \\
 & - 333396\sqrt{6}\sqrt{n}q\Delta\Phi^{5/2}\cos(10\phi)p + 8553600\Delta\Phi^3c_1p + \\
 & + 21038616\sqrt{6}\sqrt{n}q\Delta\Phi^{5/2}c_2p + 4074624\Delta\Phi^3c_3p + \\
 & - 10314864\sqrt{6}\sqrt{n}q\Delta\Phi^{5/2}c_4p + 2643840\Delta\Phi^3c_5p + \\
 & - 8470980\sqrt{6}\sqrt{n}q\Delta\Phi^{5/2}c_6p + 653184\Delta\Phi^3c_7p + \\
 & - 1825740\sqrt{6}\sqrt{n}q\Delta\Phi^{5/2}c_8p + 34712064qQ\Delta\Phi^2s_1p + \\
 & + 13250304qQ\Delta\Phi^2s_3p - 559872qQ\Delta\Phi^2s_5p + \\
 & + 570525120\sqrt{3}q\Delta\Phi^3s_1 + 195737472\sqrt{3}q\Delta\Phi^3s_3 + \\
 & \left. - 45100800\sqrt{3}q\Delta\Phi^3s_5 - 9471168\sqrt{3}q\Delta\Phi^3s_7 \right] \tag{5.29u}
 \end{aligned}$$

$$\begin{aligned}
 q_{CR3BP-113}^{(7)} = & q_{Hill}^{(7)} + \frac{3}{14n^{3/2}p^3} \left[140c_2\sqrt{n}pq\Phi + \sqrt{n}p\Phi \left(7\sqrt{3}ps_2 + \right. \right. \\
 & \left. \left. - 264q \right) + 48\sqrt{2}q(27s_1 - s_3)\Phi^{3/2} \right] \tag{5.29v}
 \end{aligned}$$

$$\begin{aligned}
 \Phi_{CR3BP-113}^{(7)} = & \Phi_{Hill}^{(7)} + \frac{1}{57344\Delta^5n^{3/2}p^4\sqrt{\Phi}} \left[12288c_1\Delta^5q \left[4\sqrt{3}p^2\tilde{K} \left(3 \left(7c_4 + \right. \right. \right. \right. \\
 & \left. \left. \left. - 6c_2 \right) \sqrt{n}\sqrt{\Phi} + 21\sqrt{n}\sqrt{\Phi} - 7\sqrt{2}nps_1 \right) + \right. \\
 & \left. + 3 \left[\sqrt{6} \left[63n^2p^2q^2\Phi - 4292\Phi^3 \right] - 432\sqrt{2}pQ\Phi^2 \right] \right] + \\
 & + 7\sqrt{6}np^3q \left(2102s_2 - 3 \left(4096c_2\Delta^5F^* + 194s_4 + 390s_6 + \right. \right. \\
 & \left. \left. + 63s_8 \right) \right) - 86016\Delta^5\sqrt{n}p\Phi^{3/2} \left(2\sqrt{3}c_2p^2Q + 4p \left(3c_2\Phi \right. \right. \\
 & \left. \left. - 34qQs_2 \right) + 5\sqrt{3}q(38s_4 - 167s_2)\Phi \right) \\
 & + 147456\sqrt{2}\Delta^5\Phi^2 \left(6c_3q \left(29\sqrt{3}\Phi + 2pQ \right) + \right. \\
 & \left. + 203\sqrt{3}c_5q\Phi + 2p(4s_1 + 3s_3 + 7s_5)\Phi \right) + \\
 & \left. - 1548288\Delta^5\sqrt{n}p^2\Phi^{5/2} \right] \tag{5.29w}
 \end{aligned}$$

$$\begin{aligned}
Q_{CR3BP-113}^{(7)} = & Q_{Hill}^{(7)} + \frac{1}{60480\Delta^3 n^{3/2} p^4 \sqrt{\Phi}} \left[32\sqrt{3}\Delta^3 p^2 \tilde{K} \left(2835\sqrt{2}c_2 np + \right. \right. \\
& - 2405\sqrt{2}np + 19440\sqrt{n}s_1\sqrt{\Phi} + 810\sqrt{n}s_3\sqrt{\Phi} + \\
& \left. \left. + 3402\sqrt{n}s_5\sqrt{\Phi} \right) + 106240\sqrt{6}\tilde{E}\Delta^3 np^3 - 8505\sqrt{6}c_4 np^3 + \right. \\
& - 15120c_2\sqrt{np} \left(\sqrt{6}\sqrt{np^2} + 3\Delta^3\Phi^{3/2} \left(217\sqrt{3}\Phi + \right. \right. \\
& \left. \left. + 40pQ \right) \right) + \Delta^3 \left[226800\sqrt{3n}\Phi^5 c_4 p - 45360\sqrt{6}F^* np^3 s_2 \right] + \quad (5.29x) \\
& + 3265920\sqrt{6}\Delta^3 n^2 p^2 q^2 s_1 \Phi + 105\sqrt{6}np^3 + \\
& + 155520\Delta^3 \sqrt{np^2} Q \Phi^{3/2} + 5968080\sqrt{3}\Delta^3 \sqrt{np}\Phi^{5/2} + \\
& - 16796160\sqrt{2}\Delta^3 p Q s_1 \Phi^2 + 622080\sqrt{2}\Delta^3 p Q s_3 \Phi^2 + \\
& - 166872960\sqrt{6}\Delta^3 s_1 \Phi^3 + 9020160\sqrt{6}\Delta^3 s_3 \Phi^3 + \\
& \left. + 6314112\sqrt{6}\Delta^3 s_5 \Phi^3 \right]
\end{aligned}$$

In this case the coupling, between the terms of the Hill model, obtained in the previous chapter, and the new terms that have been added, occurs at lower orders than in the case of Hill only. In a similar way to the Hill's problem, the inverse short-periodic correction result to be:

$$\phi_{CR3BP-113}^{(4)} = -\frac{c_1(34s_1 + 35s_3 + 49s_5)\Phi}{4np^2} - \phi_{CR3BP-113}^{(4)} \quad (5.30a)$$

$$\Phi_{CR3BP-113}^{(4)} = \frac{3(28c_2 + 7c_4 + 29)\Phi^2}{2np^2} - \Phi_{CR3BP-113}^{(4)} \quad (5.30b)$$

$$\phi_{CR3BP-113}^{(5)} = -\frac{3\sqrt{6}(62c_2 + 35c_4 + 39)qs_1\sqrt{\frac{\Phi}{n}}}{5p^2} - \phi_{CR3BP-113}^{(5)} \quad (5.30c)$$

$$\Phi_{CR3BP-113}^{(5)} = \frac{72\sqrt{6}c_1(c_2 + 5)q\Phi^{3/2}}{5\sqrt{np^2}} - \Phi_{CR3BP-113}^{(5)} \quad (5.30d)$$

$$Q_{CR3BP-113}^{(5)} = \frac{18\sqrt{6}(3c_2 + 1)s_1\Phi^{3/2}}{5\sqrt{np^2}} - Q_{CR3BP-113}^{(5)} \quad (5.30e)$$

$$\begin{aligned}
\phi_{CR3BP-113}^{(6)} = & -\frac{1}{16\Delta n^{3/2} p \Phi} \left[4(9c_1 + 7c_3)\Delta\sqrt{n}\tilde{K} + 2c_1 \left[-2c_2 \left(7\sqrt{n} + \right. \right. \right. \\
& \left. \left. \left. + \frac{2\sqrt{2}\Phi^3\Delta \left(6\sqrt{3}Q - \frac{119\Phi}{p} \right)}{p} \right) + \frac{147\sqrt{2}\Phi^5 c_6 \Delta}{p^2} + \right. \right. \\
& \left. \left. + \frac{7\sqrt{2}c_4\Delta\Phi^{3/2} \left(\frac{79\Phi}{p} + 24\sqrt{3}Q \right)}{p} + \right. \right. \\
& \left. \left. - \frac{372\Delta n^{3/2} q^2 s_1 \Phi}{p} + \frac{684\Delta n^{3/2} q^2 s_3 \Phi}{p} + \right. \right. \\
& \left. \left. - 2\sqrt{n} + \frac{784\sqrt{2}\Delta\Phi^{5/2}}{p^2} + \frac{48\sqrt{6}\Delta Q\Phi^{3/2}}{p} \right] + \right. \\
& \left. - 6\Delta F^* \sqrt{n}(3s_1 + 7s_3) \right] - \phi_{CR3BP-113}^{(6)} \quad (5.30f)
\end{aligned}$$

$$Q_{CR3BP-113}^{(6)} = -\frac{4\sqrt{6}c_1(3c_2 + 5)\left(\frac{\Phi}{n}\right)^{3/2}}{p^2} - Q_{Hill}^{(6)} \quad (5.30g)$$

$$\begin{aligned} \Phi_{CR3BP-113}^{(6)} = & \frac{1}{384\Delta^3 n^{3/2} p} \left[-2\sqrt{n} \left(32\Delta^3 (3s_1 + 7s_3) \tilde{K} + 3(34c_1 + 73c_3 + \right. \right. \\ & \left. \left. + 21c_5) \Delta F^* - 54s_1 - 133s_3 - 63s_5 \right) + \frac{48(3c_2 + 5) \Delta \Phi}{p} \right. \\ & \left. \left(57c_2 n^{3/2} q^2 + 135n^{3/2} q^2 + \sqrt{6} Q (19s_1 - 9s_3) \sqrt{\Phi} \right) + \right. \\ & \left. - \frac{21\sqrt{2}\Delta\Phi^{5/2}}{p^2} (-253s_1 + 540s_3 + 286s_5 + 21s_7) \right] + \end{aligned} \quad (5.30h)$$

$$Q_{CR3BP-113}^{(6)} = -\frac{24qs_2\Phi}{p^2} - Q_{CR3BP-113}^{(6)} \quad (5.30i)$$

$$\begin{aligned} \phi_{CR3BP-113}^{(7)} = & -\frac{1}{56\Delta np^2 \Phi} \left[63c_1 p (2\Delta \tilde{K} - 1) + 49c_3 p (2\Delta \tilde{K} - 1) + \right. \\ & \left. + 3\Delta \left(4\sqrt{6}\sqrt{n}q (23s_1 + 36s_3 + 49s_5) \Phi^{3/2} - 7F^* p \right. \right. \\ & \left. \left. (3s_1 + 7s_3) \right) \right] - \phi_{CR3BP-113}^{(7)} \end{aligned} \quad (5.30j)$$

$$\begin{aligned} \Phi_{CR3BP-113}^{(7)} = & \frac{1}{20160\Delta^3 np^2} \left[2700\sqrt{6} (490c_1 + 141c_3 + 9c_5) \Delta \sqrt{n} q \Phi^{3/2} + \right. \\ & - 45p \left(6s_1 (70\Delta \tilde{K} - 39) + s_3 (790\Delta \tilde{K} - 503) + \right. \\ & \left. \left. + 21s_5 (10\Delta \tilde{K} - 9) + 144(c_1 + 7c_3) \Delta^3 F^* \right) \right] - \Phi_{CR3BP-113}^{(7)} \end{aligned} \quad (5.30k)$$

$$Q_{CR3BP-113}^{(7)} = -\frac{12\sqrt{6}(s_1 - 3s_3) \Phi^{3/2}}{7\sqrt{n}p^2} - Q_{CR3BP-113}^{(7)} \quad (5.30l)$$

5.4.2 Short-periodic correction 8th order

Because of the size of the formulas of the direct and the inverse transformation it is not convenient to show them, in any case, the procedure for obtaining them is identical to that seen in the case of Hill in the Section 4.6.2.

Given that what we have just obtained is the object of this thesis work, the whole comparison and verification phase will be dealt with in a more exhaustive way in the following chapter.

Chapter 6

Model comparison

In this chapter we will compare both numerical and analytical models with respect to the numerical CR3BP where in this thesis it is taken as a reference. In this analysis we will take into consideration the family- f of Hénon, also called DRO, in different synodic systems.

For the construction of the families we take a set of orbit amplitudes (A_x) in the Hill model from [30], subsequently they will be corrected by the method described in the Appendix B. This applies to every model, in the particular case of CR3BP the initial conditions for the Hill's problem are first reported in the correct system, through the conversion, Equations (2.40) and (2.42), and then run with the differential method in Appendix B .

6.1 Jacobi constant

First of all, we look at the progress of the Jacobi constant referring to the Hill model for various synodic systems. The Figure 6.1 shows the trend of the Jacobi Constant (J_{Hill}) of the Hill system with respect to the initial position along the abscissas axis (x_0).

6.2 Numerical comparison CR3BP vs. CR3BP-1, CR3BP-1₁₃ and Hill

For a better understanding the difference between the proposed models, a series of graphs are proposed that represent numerical simulation of the DROs for different sizes. It is noted that as the A_x increases, the 3 models deviate from the behaviour of the CR3BP.

6.2.1 Error comparison

The problem is reduced by representing it in 2-D transforming each orbit into a point. To do this, we introduce the following variables:

Absolute Error: It represents the absolute error obtained in position with respect to the correct numerical model on one orbital period:

$$\varepsilon_{abs, \underline{r}}(0 \rightarrow t_{2\pi}) = \|\underline{r}(0 \rightarrow t_{2\pi}) - \underline{r}_{true}(0 \rightarrow t_{2\pi})\| \quad (6.1)$$

Relative Error: It represents the relative error obtained in position with respect to the correct numerical model on one orbital period:

$$\varepsilon_{rel, \underline{r}}(0 \rightarrow t_{2\pi}) = \frac{\varepsilon_{abs, \underline{r}}(0 \rightarrow t_{2\pi})}{\|\underline{r}_{true}(0 \rightarrow t_{2\pi})\|} \quad (6.2)$$

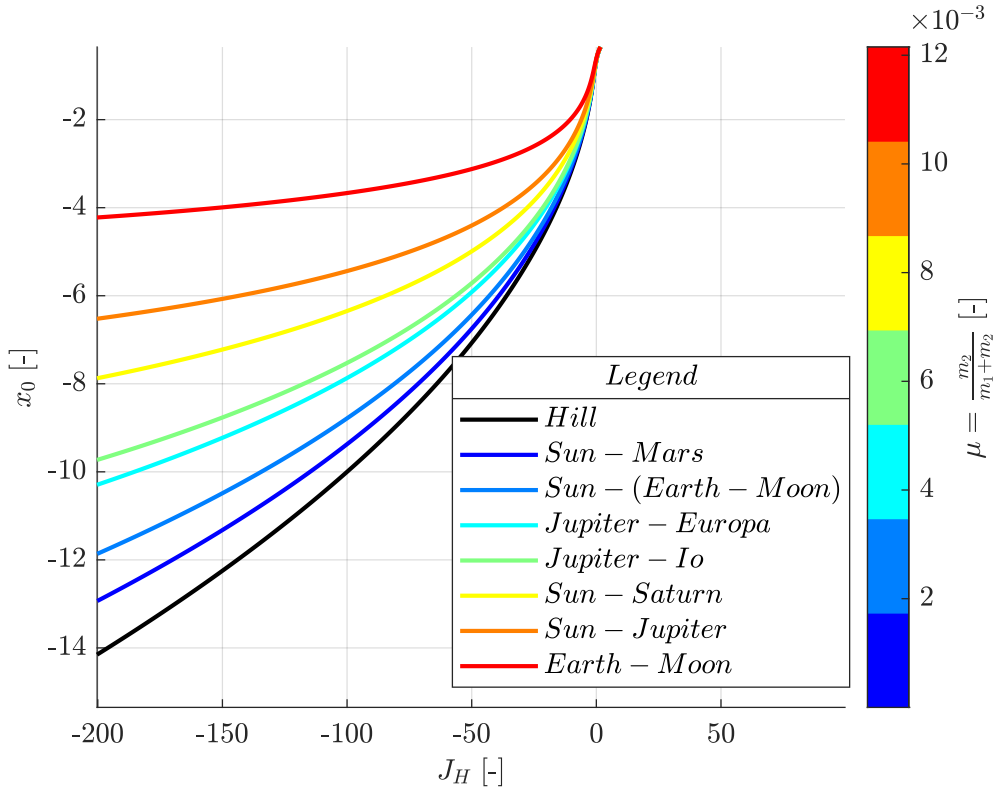


Figure 6.1: Jacobi constant trend vs. initial condition along x direction with varying mass ratio.

Maximum Error: It represents the maximum of the relative error along one orbit:

$$\varepsilon_{rel-max, \tau} = \max(\varepsilon_{rel, \tau}(0 \rightarrow t_{2\pi})) \quad (6.3)$$

Thanks to the definitions of the errors introduced, we can now show the comparison between the various models. As can be seen from the Figure 6.7, which represents the trend of the maximum error as the size of the orbits increases, the CR3BP is used as a basis for comparison. We note how the model that turns out to be worse is that of Hill, vice versa the more terms are added the more the model has a greater accuracy. Due to the fact that the Hill model considers the primary attractor placed at an infinite distance of the secondary, it is less reliable the more the size of the orbits increase. This becomes easy to see in the quadrature points, Figures 6.2 to 6.6, which are the farthest points of the secondary attractor. In these figures on the left the behaviors that the various numerical models predict are proposed, on the right instead the relative error along an orbital period of the three models compared to the CR3BP.

<i>Legend</i>	<i>Legend</i>
— <i>nCR3BP</i>	- - - <i>nCR3BP vs nCR3BP - 1</i>
- - - <i>nCR3BP - 1</i>	- . - . <i>nCR3BP vs nCR3BP - 1₁₃</i>
- . - . <i>nCR3BP - 1₁₃</i>	— <i>nCR3BP vs nHill</i>
- - - <i>nHill</i>	

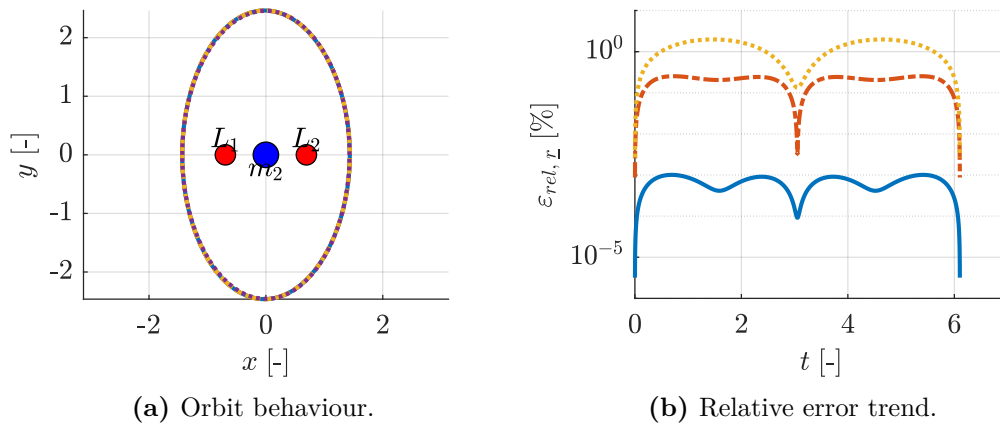


Figure 6.2: Comparison for DROs in rotating reference frame in SEM with $A_x=1.4311$ between CR3BP, CR3BP-1, CR3BP-1₁₃ and Hill's model.

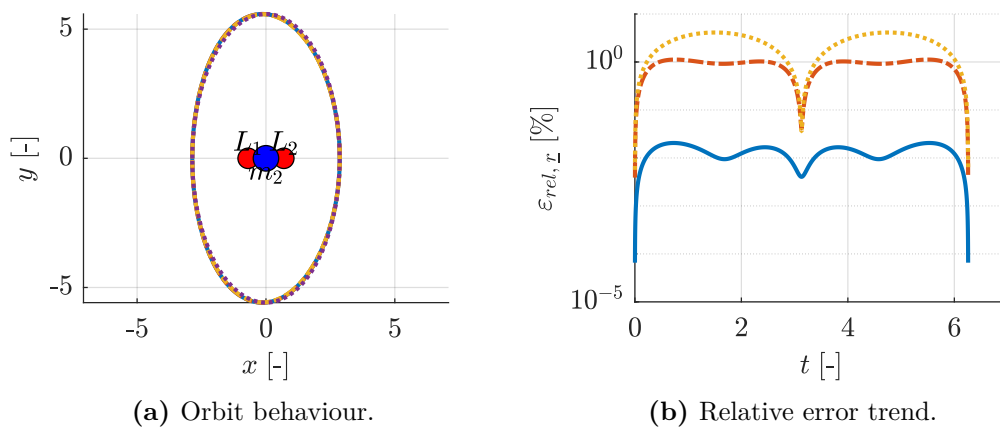


Figure 6.3: Comparison for DROs in rotating reference frame in SEM with $A_x=2.8593$ between CR3BP, CR3BP-1, CR3BP-1₁₃ and Hill's model.

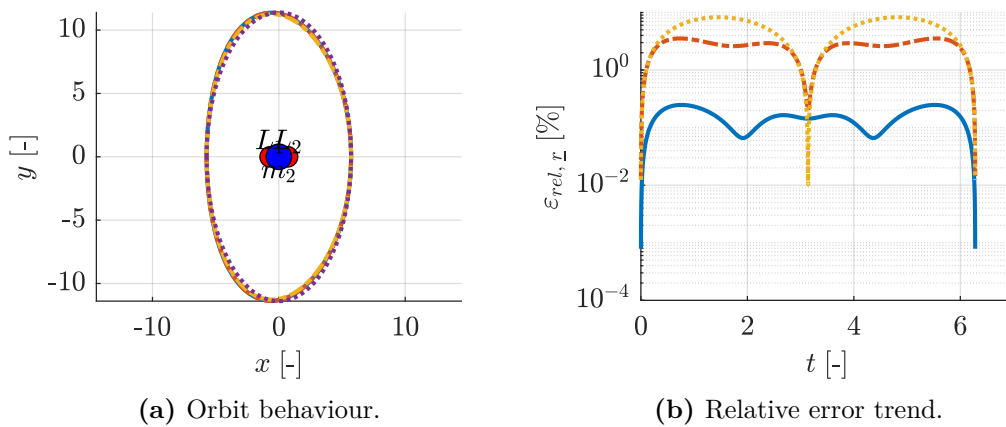


Figure 6.4: Comparison for DROs in rotating reference frame in SEM with $A_x=5.7129$ between CR3BP, CR3BP-1, CR3BP-1₁₃ and Hill's model.

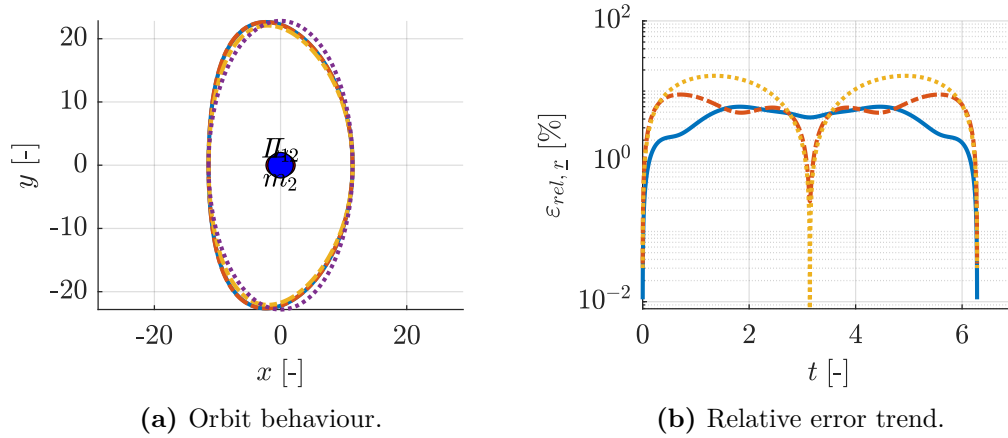


Figure 6.5: Comparison for DROs in rotating reference frame in SEM with $A_x=11.4146$ between CR3BP, CR3BP-1, CR3BP-1₁₃ and Hill's model.

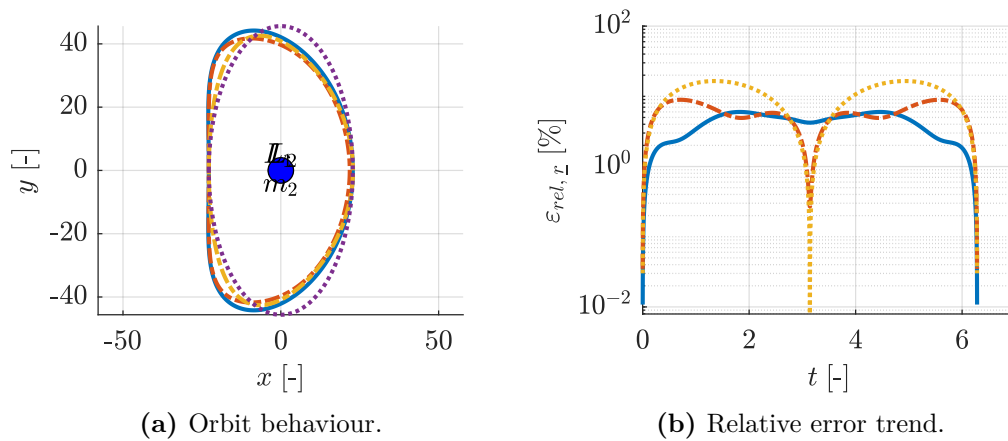


Figure 6.6: Comparison for DROs in rotating reference frame in SEM with $A_x=22.8066$ between CR3BP, CR3BP-1, CR3BP-1₁₃ and Hill's model.

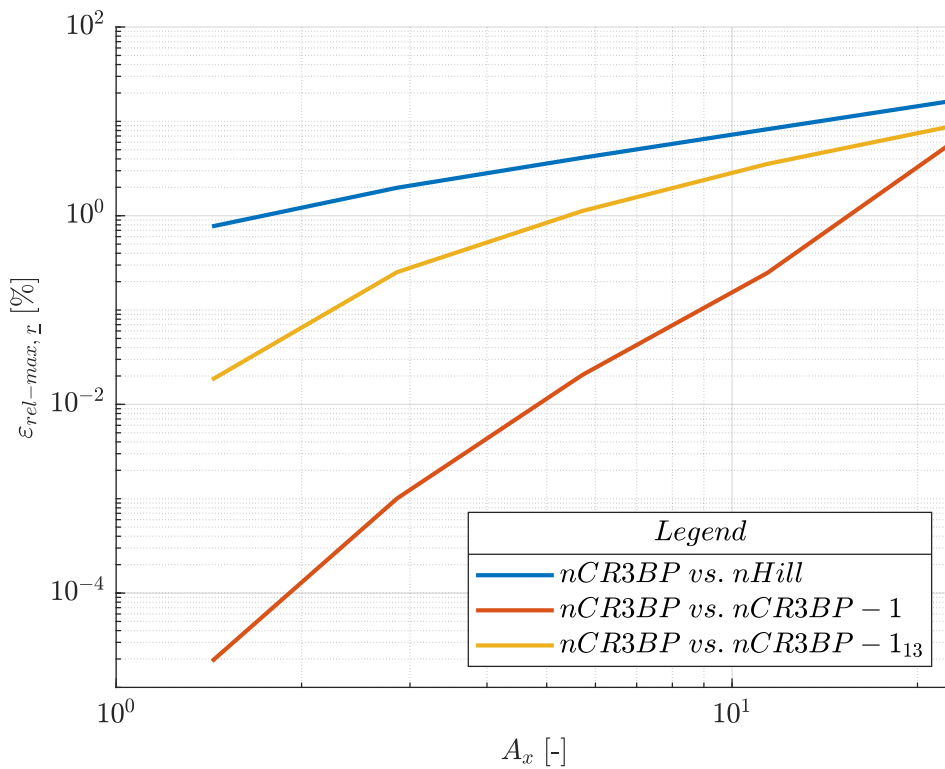


Figure 6.7: Maximum error trend between Hill, CR3BP-1₁₃ and CR3BP-1 models compared to CR3BP with increasing orbit dimensions in the SEM.

6.3 Comparison CR3BP vs. Hill

The models that we will compare in this section are: the numerical Hill's model and the analytical one. They are compared to the CR3BP, similarly to before. In particular in Figures 6.8 to 6.12 on the left the behaviour that each model predicts with the same initial conditions, on the right instead, the relative error of the analytical solutions, obtained above, 7th and 9th order with and without the short-term correction, with respect to the numerical Hill model. As expected the higher the order of approximation the more the error decreases. In Figure 6.13 we can see the various analytical solutions compared with the numerical Hill model, in terms of maximum error along an orbital period. From Figure 6.13, we note that the analytical models converge in the numerical one. This is due to the fact that the potential of the primary attractor is correct and the influence of the secondary decreases. Consequently, the hypothesis of perturbation is true and therefore the approximation is acceptable. All of this is also deducible from Figure 6.14, where the analytical and numerical Hill models are compared to the CR3BP. In this figure, we can see that analytical models converge to the numerical one, as has been said previously. In particular the analytical solutions of the Hill problem for which short-periodic corrections have been added converge faster. In particular the solution with SPC converges eg $A_x=5$ instead the one without SPC to $A_x=10$. The speed of convergence with respect to the size of the orbit depends on the system taken into consideration, e.g. MD which mass ratio is much lower than SEM, the Hill's model will be a good approximation for a greater orbit range.

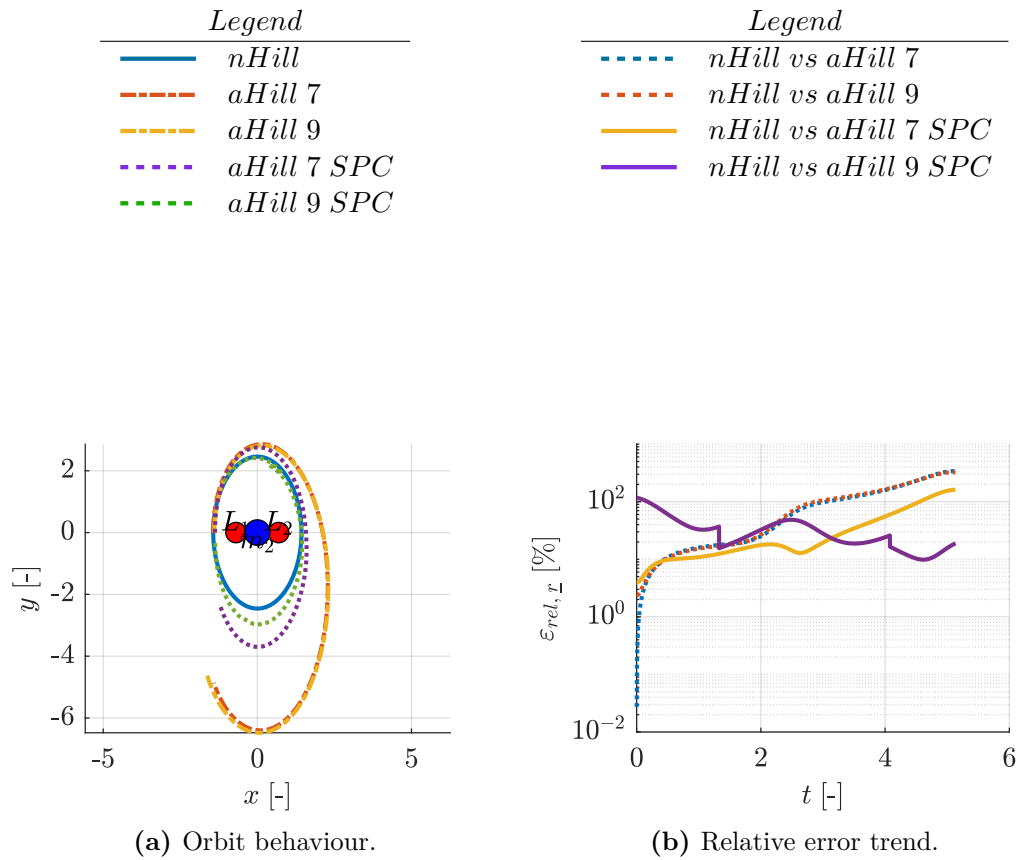


Figure 6.8: Comparison for DROs in rotating reference frame with $A_x=1.4311$ between numerical Hill model's and analytical one.

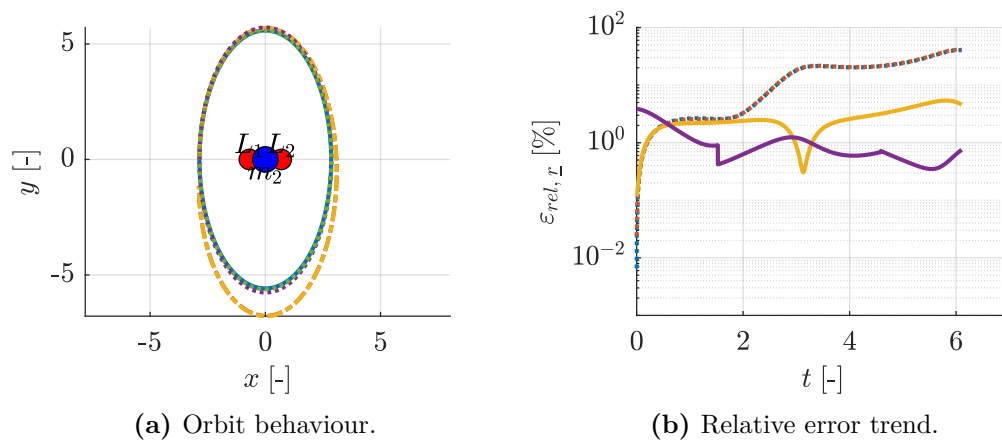


Figure 6.9: Comparison for DROs in rotating reference frame with $A_x=2.8593$ between numerical Hill's model and analytical one.

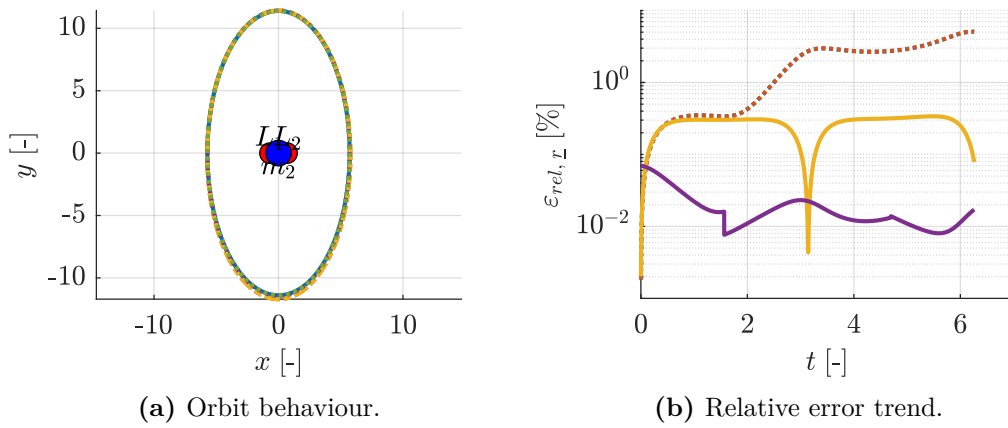


Figure 6.10: Comparison for DROs in rotating reference frame with $A_x=5.7129$ between numerical Hill's model and analytical one.

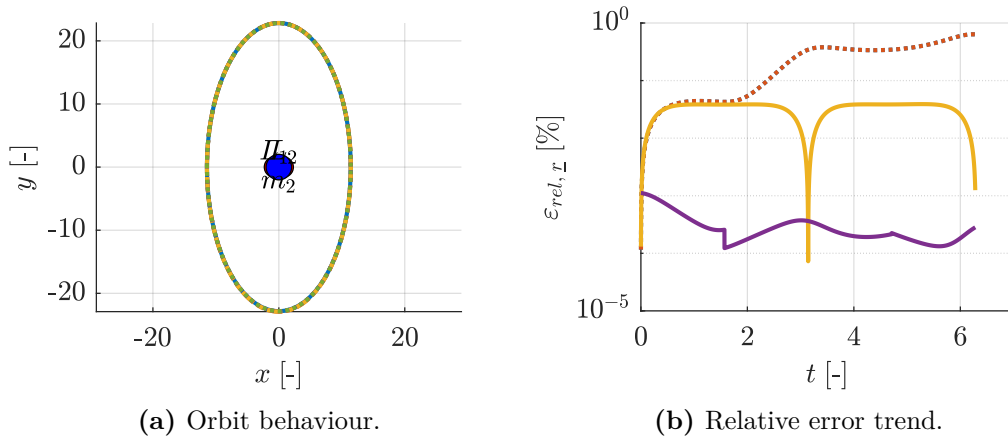


Figure 6.11: Comparison for DROs in rotating reference frame with $A_x=11.4146$ between numerical Hill's model and analytical one.

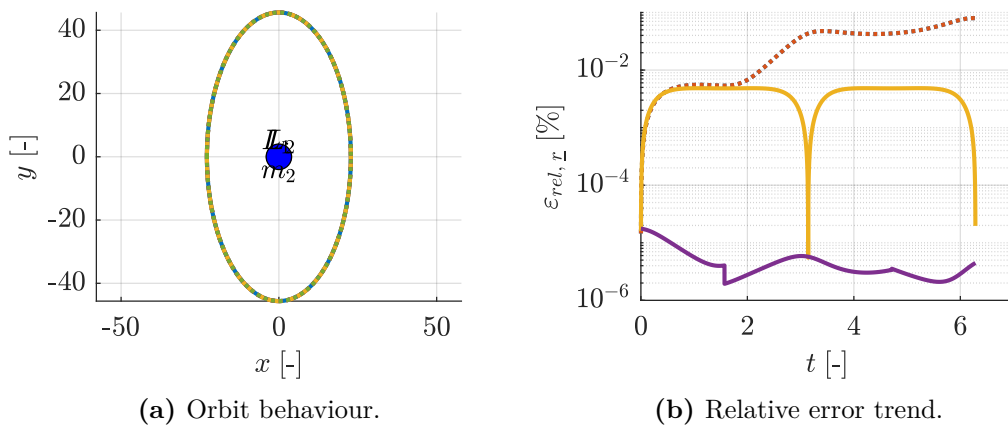


Figure 6.12: Comparison for DROs in rotating reference frame with $A_x=22.8066$ between numerical Hill's model and analytical one.

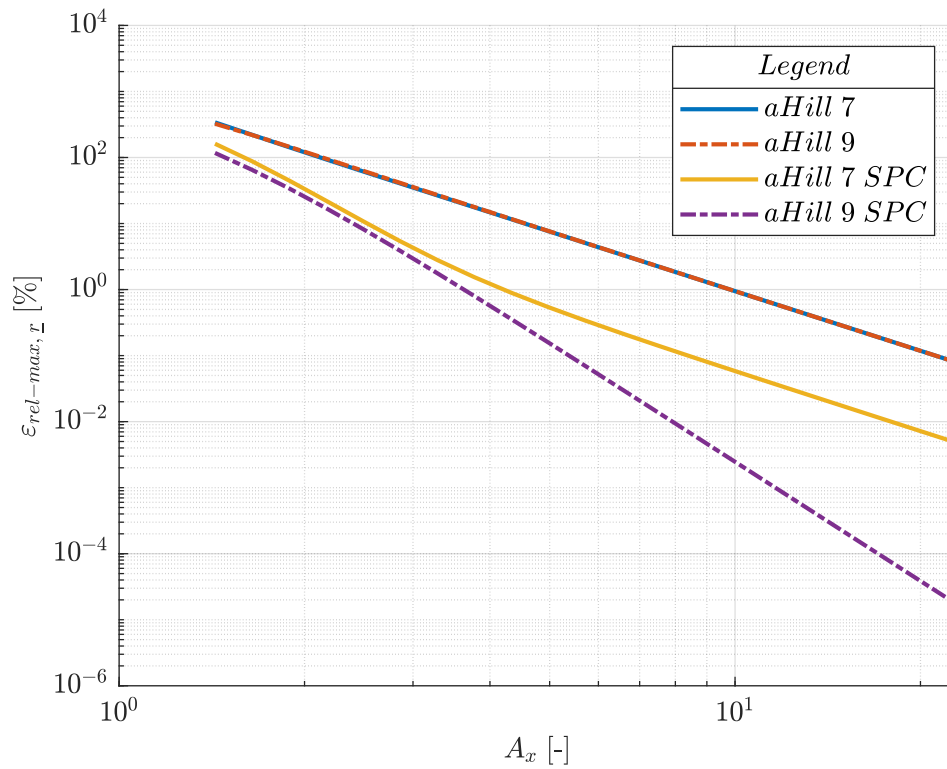


Figure 6.13: Maximum error trend of analytical Hill's model and numerical.

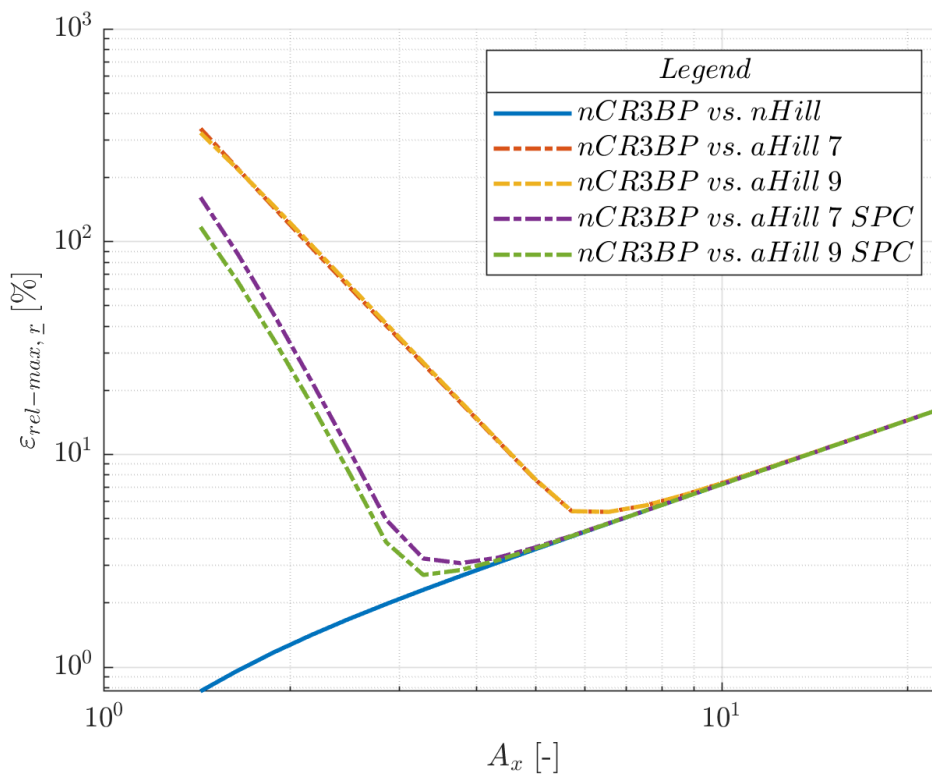


Figure 6.14: Maximum error trend of the numerical/analytical Hill's model vs. CR3BP.

6.3.1 Run time comparison

One of the characteristic that needs to be analysed is surely the computational time used by the computer. The “Run Time” represents precisely the time that the Matlab compiler uses to perform the numerical integration and the calculation of the analytical solution proposed in the previous chapters. To make the better comparison we will use graphs showing the “Run Time” for the family- f of Hénon (DRO) orbit family. The plot allows us to understand the general trends that the compiler produces as the size of the orbit increases. Figure 6.15 shows the comparison between the “Run Time” of the numerical Hill model and the analytical solutions proposed in Chapter 4. What can be seen right away is that, the analytical model has a reduction of the “Run Time” of 200 times, compared to the numerical one. This fact will be crucial if the problem is part of an optimisation system or in any case a more complex calculation scheme. However, due to the computation of the incomplete elliptic integrals the computational time, for the solution to which the short-periodic correction applies, is much higher. This is due mainly to the fact that the algorithms already present in Matlab have been exploited to obtain the values of the elliptical integrals, and these prove to be very inefficient.

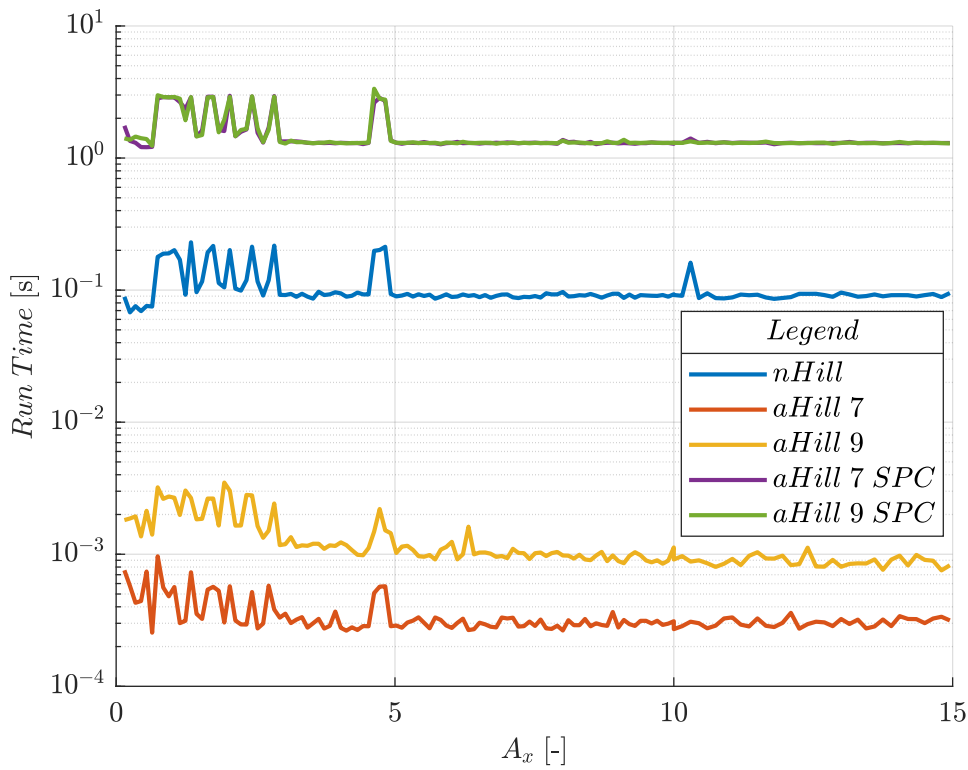


Figure 6.15: “Run Time” trend of the Hill’s numerical model and analytical.

6.4 Comparison CR3BP vs. analytical CR3BP-1₁₃ and Hill

As already mentioned earlier during the work of this thesis, different models were produced. In addition to the one proposed in the previous chapter, it obtained with hypothesis $b/p = \mathcal{O}[\chi^5]$ the $b/p = \mathcal{O}[\chi^3]$, $b/p = \mathcal{O}[\chi^1]$ and $b/p = \mathcal{O}[\chi^1]$ were also

considered. These assumptions have been tested observing the validity limits. The verification phase consists of simulating the different models obtained for various systems, that is to say, when the mass parameter μ varies, in particular values corresponding to the Sun-(Earth-Moon) system (about 10^{-6}), Mars-Deimos (about 10^{-9}) and later for Sun-Alauda ($\mu = 10^{-12}$). To better understand the validity of these assumptions, observe the Figures 6.16 to 6.18. These images represent the trend of the assumptions, previously reported, when the orbit size (A_x) increases and the mass parameter μ varies. Each line represent the evaluation of the Big O assumptions ($b/p = \mathcal{O}[\chi^j]$) where the colour is associated to a order, j , at witch the expansion is arrested. From these figures it can be deduced that the more j is small, the more the $\mathcal{O}[\chi^j]$ assumption is verified. This can be explained by the fact that the more the orbit increases in size, the closer it will be to the primary attractor and consequently the dynamic brings the deviation of the centre of the orbit to be more and more comparable with the distance between the primaries and no longer a fraction of the latter. In particular, for Figure 6.16 the assumption is no longer valid for $A_x= 2$ instead for Figure 6.17, the validity range increase rises and begins to be worse for $A_x= 4$, and so on for Figure 6.18 for $A_x= 7$.

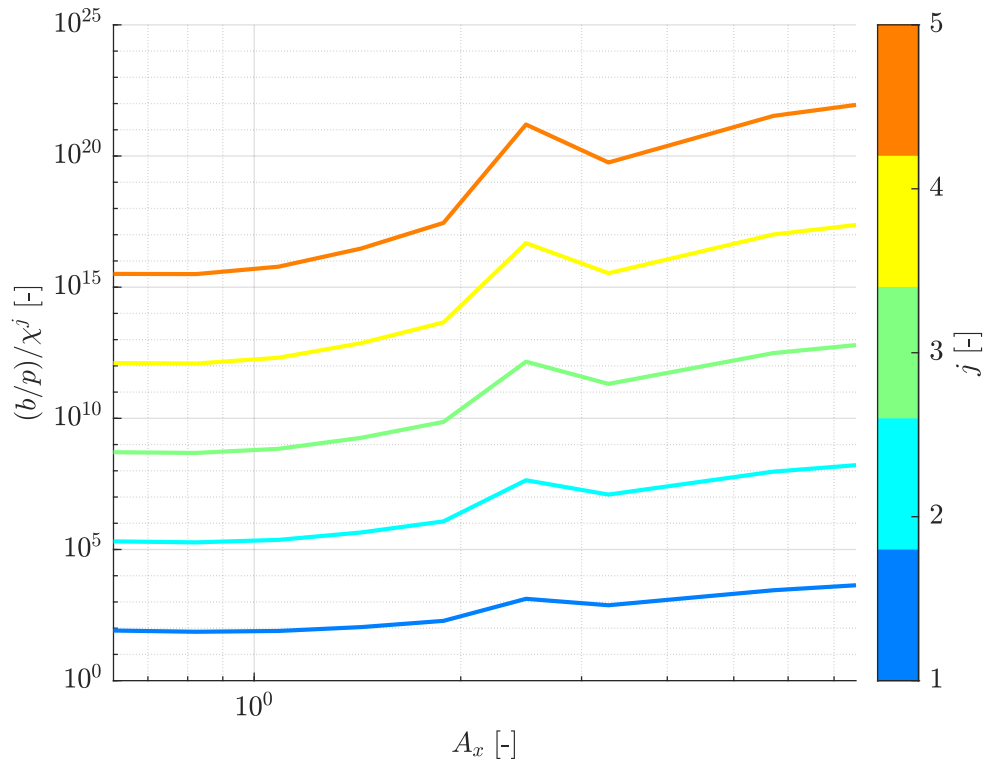


Figure 6.16: Trend of the assumption $b/p = \mathcal{O}[\chi^j]$ for Sun-(Earth-Moon) system as the size of the orbit increases (A_x).

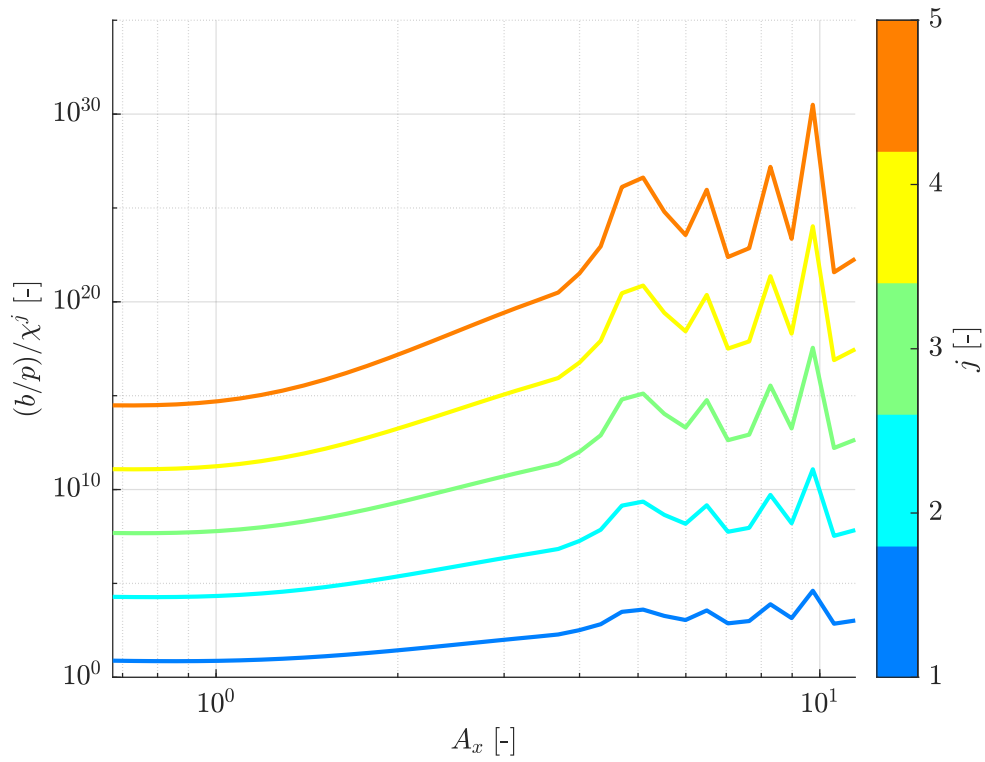


Figure 6.17: Trend of the assumption $b/p = \mathcal{O}[\chi^j]$ for Mars-Deimos system as the size of the orbit increases (A_x).

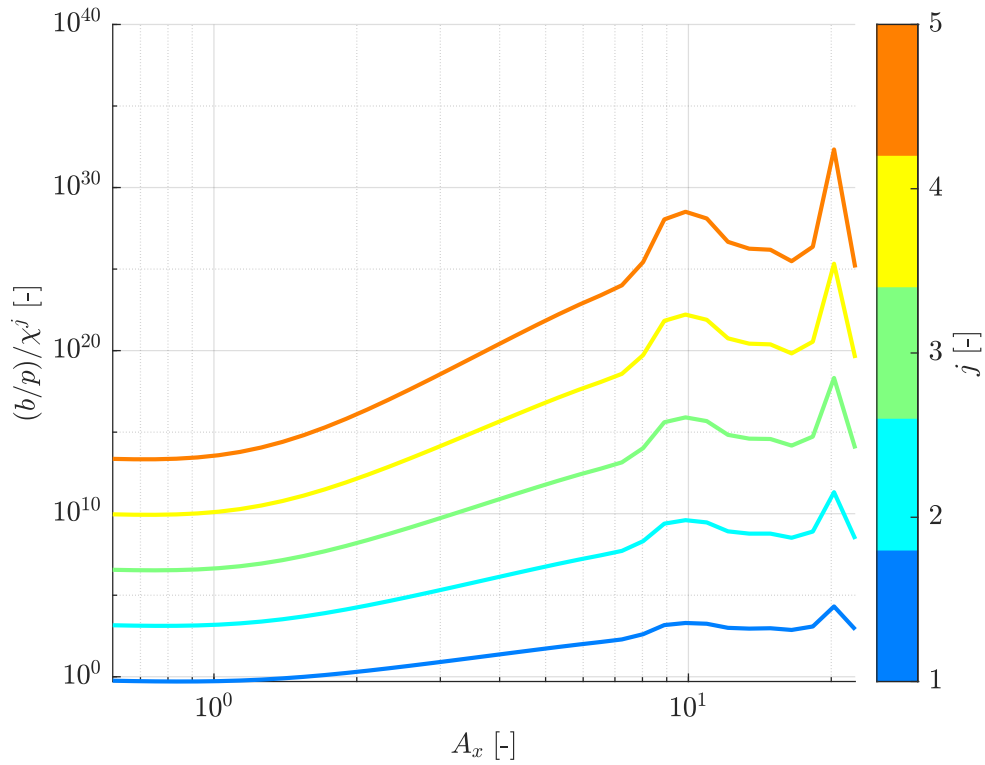


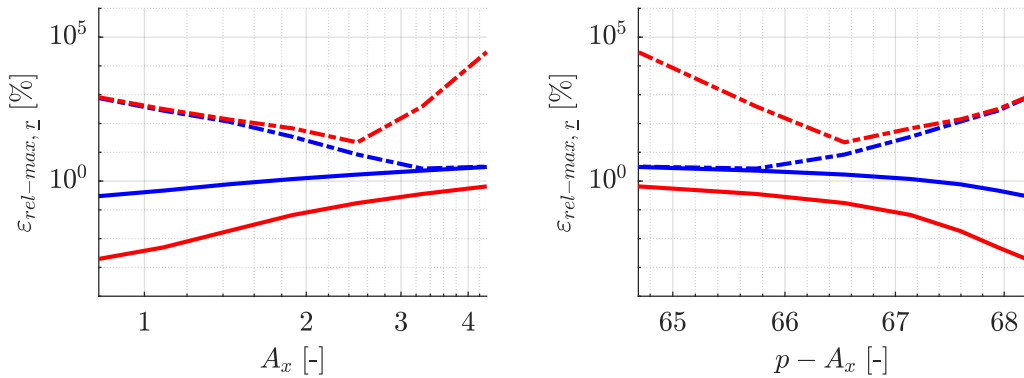
Figure 6.18: Trend of the assumption $b/p = \mathcal{O}[\chi^j]$ for Sun-Alauda system as the size of the orbit (A_x) increases.

6.4.1 Results for the model with assumption $\mathcal{O}[\chi^5]$

The model, associated with assumption $b/p = \mathcal{O}[\chi^5]$, represents a first attempt at resolution. It can be explained by the fact that the CR3BP-1₁₃ model is similar to the Hill model, to which some terms of the potential of the primary have been added. This fact allows us to better describe the behaviour of the third body (e.g. S/C). This fact, initially, led us to think that the dynamics was mainly governed by the Hill problem and that the addition of some terms was assumable at a perturbation. However, this assumption turned out to be untrue, as can be seen from the Figures 6.16 to 6.18. This can be explained by the fact that the DROs, which are part of the family f of Hénon, are at a high distance from the secondary attractor and therefore they are more influenced by the gravity of the primary. As we can also see from the Figures 6.19 to 6.21, where these plots show the trend of the maximum error along an orbital period. In particular the blue lines represent the error that the Hill model has with respect to CR3BP, instead the red ones the error that the CR3BP-1₁₃ model has, always, to the CR3BP model. In These figures, the maximum error, along an orbital period, of the analytical CR3BP-1₁₃ solution (dash-dot red line) is always greater than the Hill model. This is due to the fact that, although the Lie series has been completed up to the 9th order, with the assumption $b/p = \mathcal{O}[\chi^5]$, only the first 5 terms, of Equation (5.5), are considered. Consequently, with the increase of A_x the influence of the primary is predominant, even for low mass ratios. In Figure 6.19 dash dot red line (analytical solution of CR3BP-1₁₃) reaches a minimum error of about 50 for $A_x = 2.5$ in the first part (on the left) the red line, for the analytical solution, remains above the blue line and then the red line increases again. For Figure 6.20, instead the error has a zone between $A_x = 2.5$ and $A_x = 6.5$ where it remains constant at about 1 and then increases again. In Figure 6.21 the error for the analytical solution (red line), reaches a minimum of about 0.1 to $A_x = 4.5$. To better understanding the error plots, in the Figures 6.22 to 6.24, we can see the behaviour, that the various models, numerical and analytical, predict, for different size orbits.

Legend

—	$nHill$
- - -	$aHill$ 5 SPC
—	$nCR3BP - 1_{13}$
- . - .	$aCR3BP - 1_{13}$ 5 SPC



(a) Respect to the secondary attractor.

(b) Respect to the primary attractor.

Figure 6.19: Trend of the maximum error as the size of the orbit in the Sun-(Earth-Moon) system increases with the assumption $b/p = \mathcal{O}[\chi^5]$.

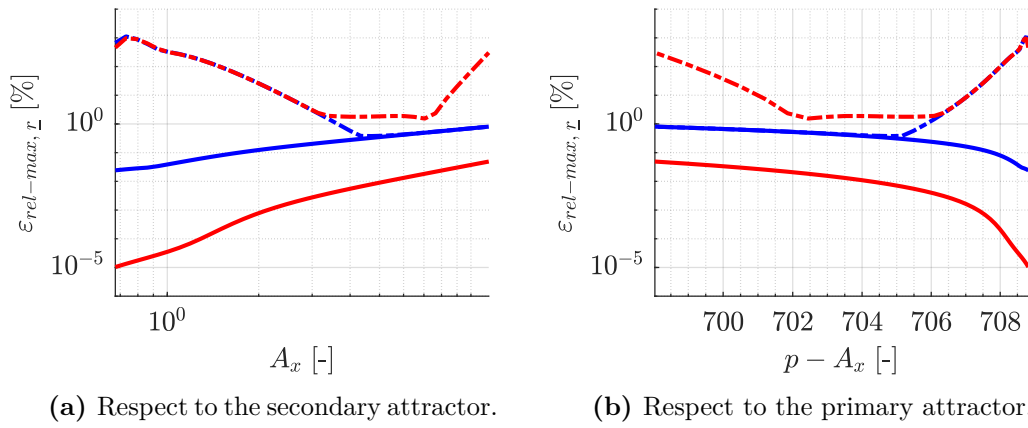


Figure 6.20: Trend of the maximum error as the size of the orbit in the Mars-Deimos system increases with the assumption $b/p = \mathcal{O}[\chi^5]$.

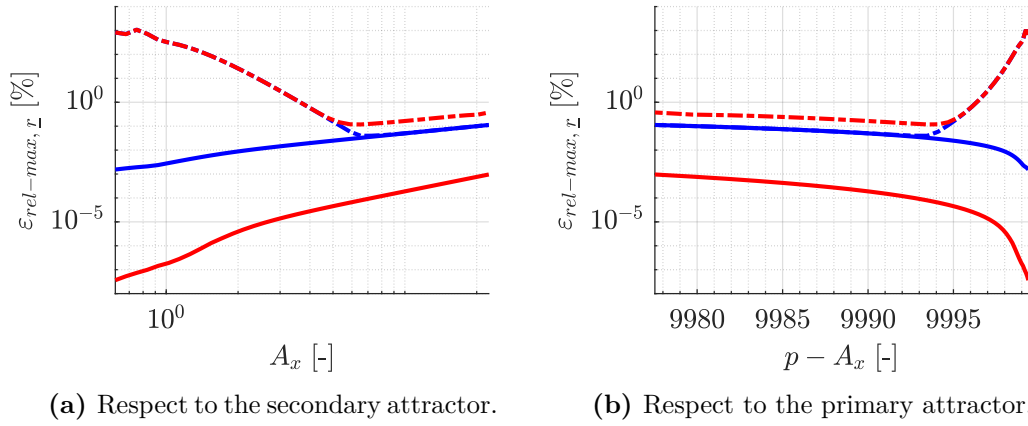


Figure 6.21: Trend of the maximum error as the size of the orbit for Sun-Alauda system increases with the assumption $b/p = \mathcal{O}[\chi^5]$.

Legend

—	$nCR3BP$
- - -	$nCR3BP - 1_{13}$
- - -	$nHill$
- - -	$nHill\ 9; SPC$
- - -	$nCR3BP - 1_{13}; SPC$

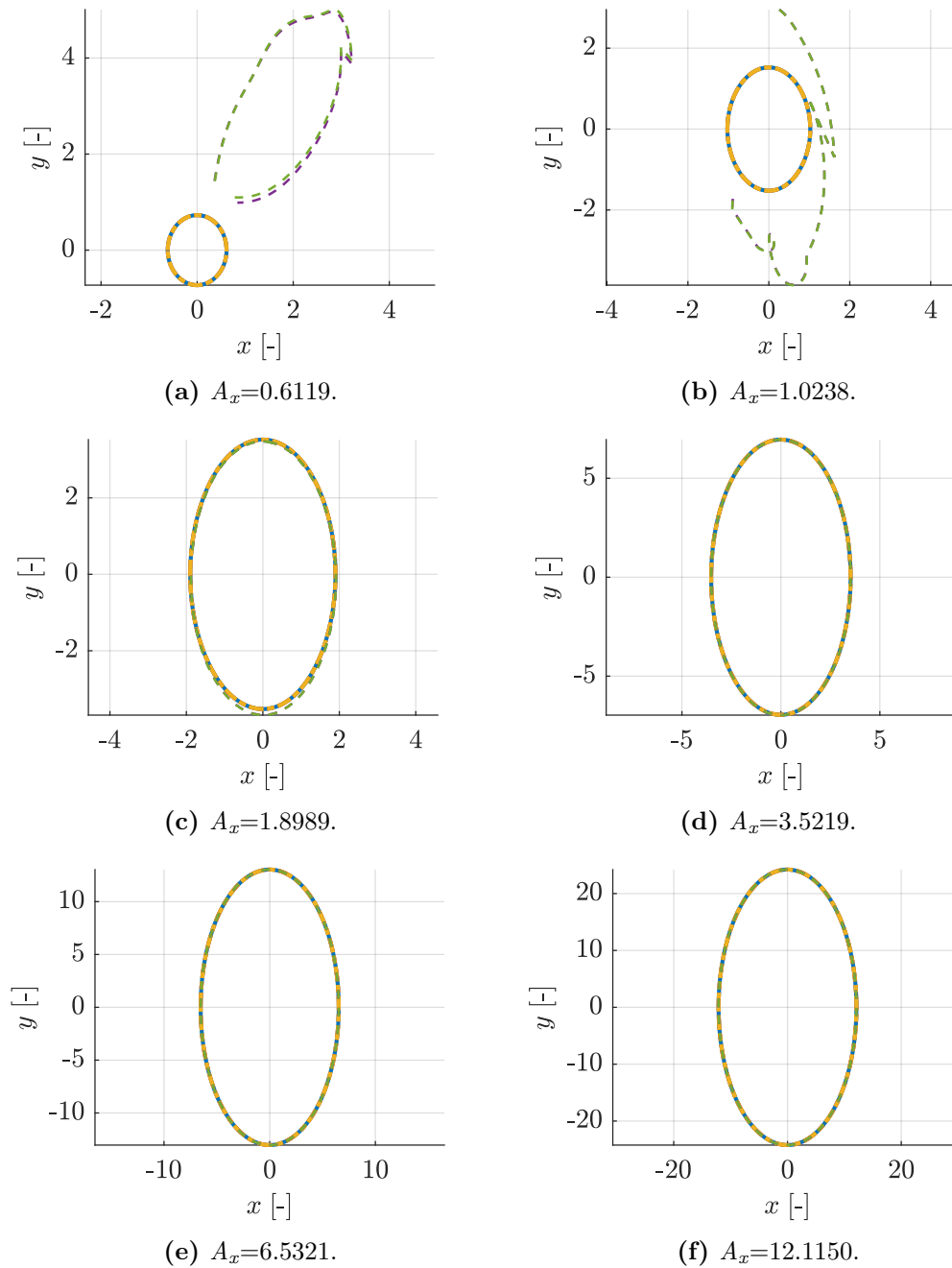


Figure 6.22: Behaviour of the various numerical and analytical models to vary the size of the orbit for Sun-Alauda system, with analytical model under the hypothesis $b/p = \mathcal{O}[\chi^5]$.

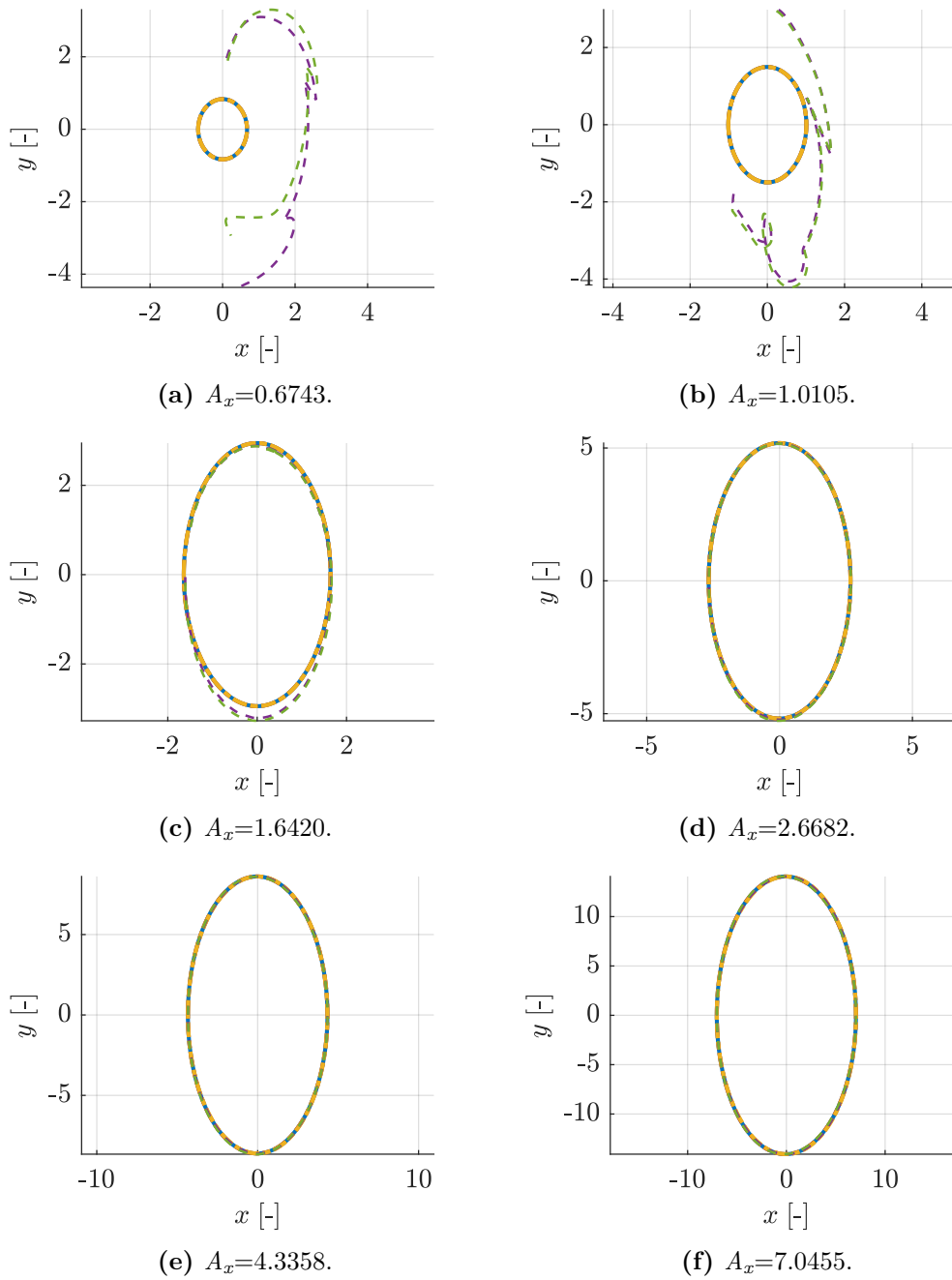


Figure 6.23: Behaviour of the various numerical and analytical models to vary the size of the orbit for a Mars-Deimos system, with analytical model under the hypothesis $b/p = \mathcal{O}[\chi^5]$.

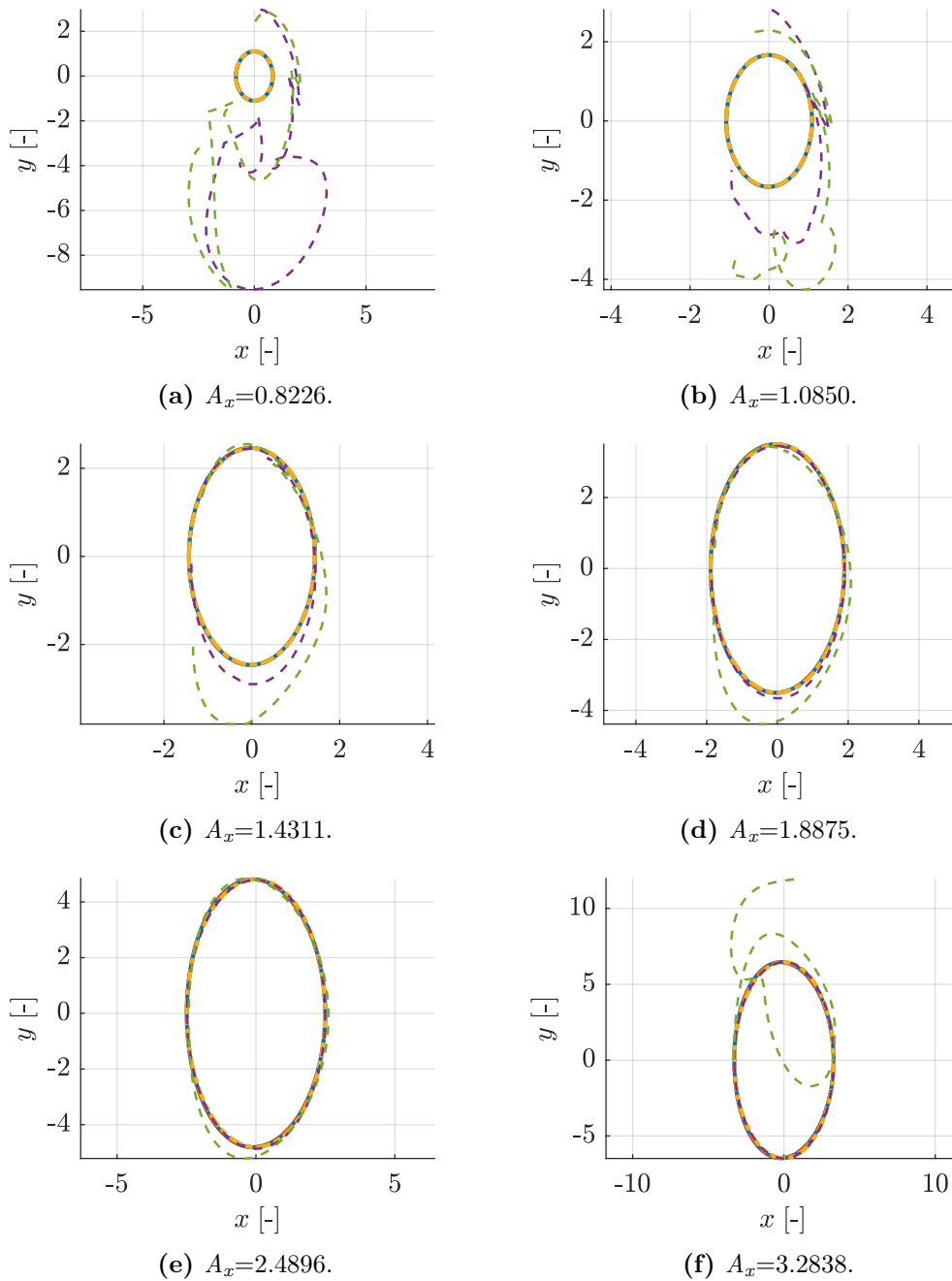


Figure 6.24: Behaviour of the various numerical and analytical models to vary the size of the orbit for a Sun-(Earth-Moon) system, with analytical model under the hypothesis $b/p = \mathcal{O}[\chi^5]$.

6.4.2 Results for the model with assumption $\mathcal{O}[\chi^3]$

This case represents a first improvement compared to the one seen before. In fact, assumption $b/p = \mathcal{O}[\chi^3]$, as can be seen from Figures 6.16 to 6.18, represents a considerable improvement, of various order of magnitude, compared to the case with $b/p = \mathcal{O}[\chi^5]$. This derives from the fact that, the assumption of \mathcal{O} is not referred to the fact that the Hill problem determines the most important dynamics but on the contrary the dynamics depends on the distance that the third body (e.g. S/C) has with respect to the two main attractors. This leads to the fact that the oscillation of the centre of the orbit increases the closer one gets to the primary attractor. Consequently, in order for this assumption to be verified in a range of major orbits, the assumption $b/p = \mathcal{O}[\chi^j]$ must necessarily have values of $j < 4$. Having said that, it is more understandable, how the course of the maximum errors, on one orbital period, Figures 6.25 to 6.27 are better than the previous case. These plots show the trend of the maximum error along one orbital period. In particular the blue lines represent the error that the Hill model has with respect to CR3BP, instead the red ones the error that the CR3BP-1₁₃ model has, always, to the CR3BP model. In particular, the dash-dot represent the analytical solution. We want to point out in particular as the maximum error, in the case Sun-Alauda system, is lowered considerably for larger orbits. In Figure 6.25 the analytical solution (red line) reaches a minimum error of about 50 for $A_x = 2$ in the first part (on the left) the red line remains above the blue line, (Lara solution) and then the red line increases again. For Figure 6.26, instead the error has a zone between $A_x = 3$ and $A_x = 6.5$ where it remains constant at about 1 and then increases again, in the first part (on the left) the red line, for the analytical solution, remain equal to the blu one. In Figure 6.27 the error for the analytical solution (red Line) reaches a minimum of about 0.05 to $A_x = 6$ and remains roughly equal to the dash-dot blue one up to $A_x = 20$. In a similar way to what has been proposed before, in Figures 6.28 to 6.30, some orbits are proposed. They show how the various numerical and analytical solutions and models predict behaviour at the same conditions. That allow to better understand how the analytical models behave at the vary the dimensions of the orbit and the mass parameter. In a similar way to before, when the mass parameter decreases the analytical model behaves gets better.

Legend

—	<i>nHill</i>
- - -	<i>aHill 5 SPC</i>
—	<i>nCR3BP - 1₁₃</i>
- - -	<i>aCR3BP - 1₁₃ 5 SPC</i>

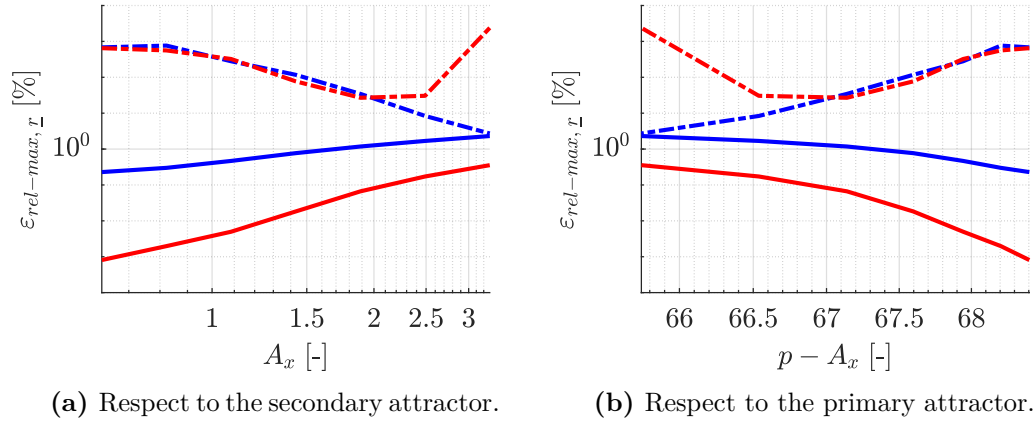


Figure 6.25: Trend of the maximum error as the size of the orbit in the Sun-(Earth-Moon) system increases with the assumption $b/p = \mathcal{O}[\chi^3]$.

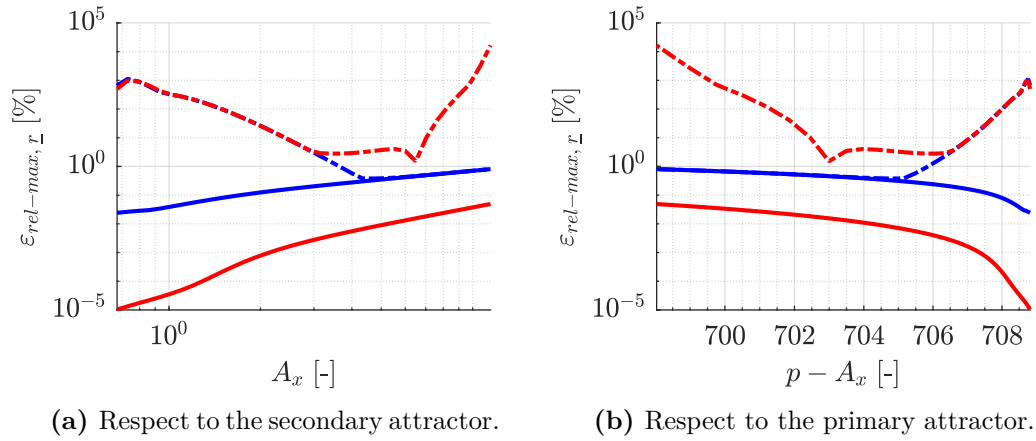


Figure 6.26: Trend of the maximum error as the size of the orbit in the Mars-Deimos system increases with the assumption $b/p = \mathcal{O}[\chi^3]$.

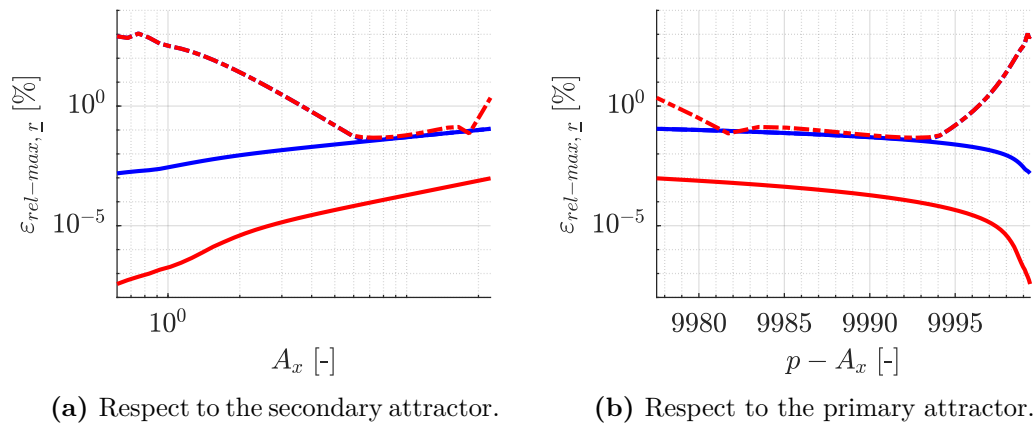


Figure 6.27: Trend of the maximum error as the size of the orbit for Sun-Alauda system increases with the assumption $b/p = \mathcal{O}[\chi^3]$.

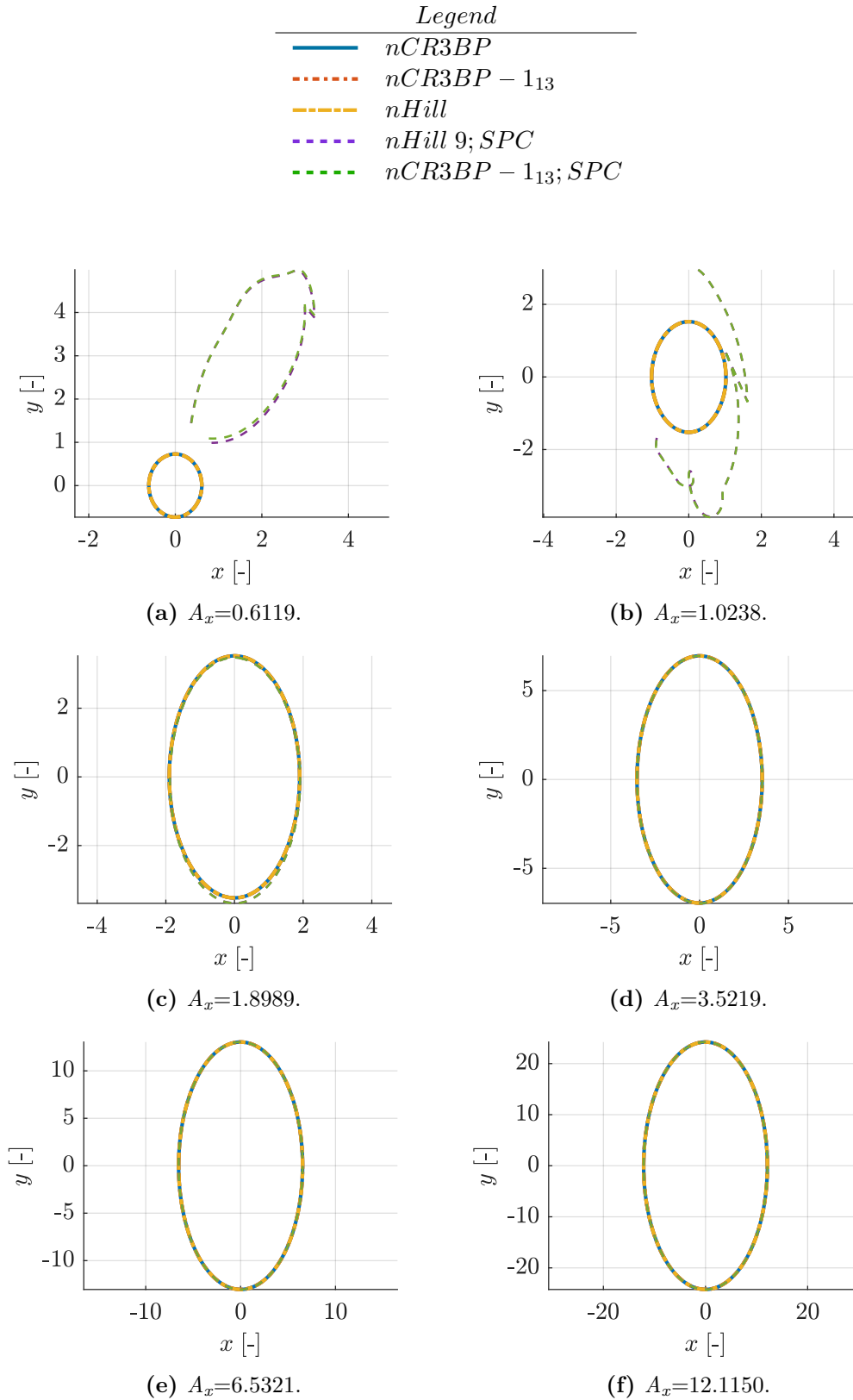


Figure 6.28: Behaviour of the various numerical and analytical models to vary the size of the orbit for Sun-Alauda system, with analytical model under the hypothesis $b/p = \mathcal{O}[\chi^3]$.

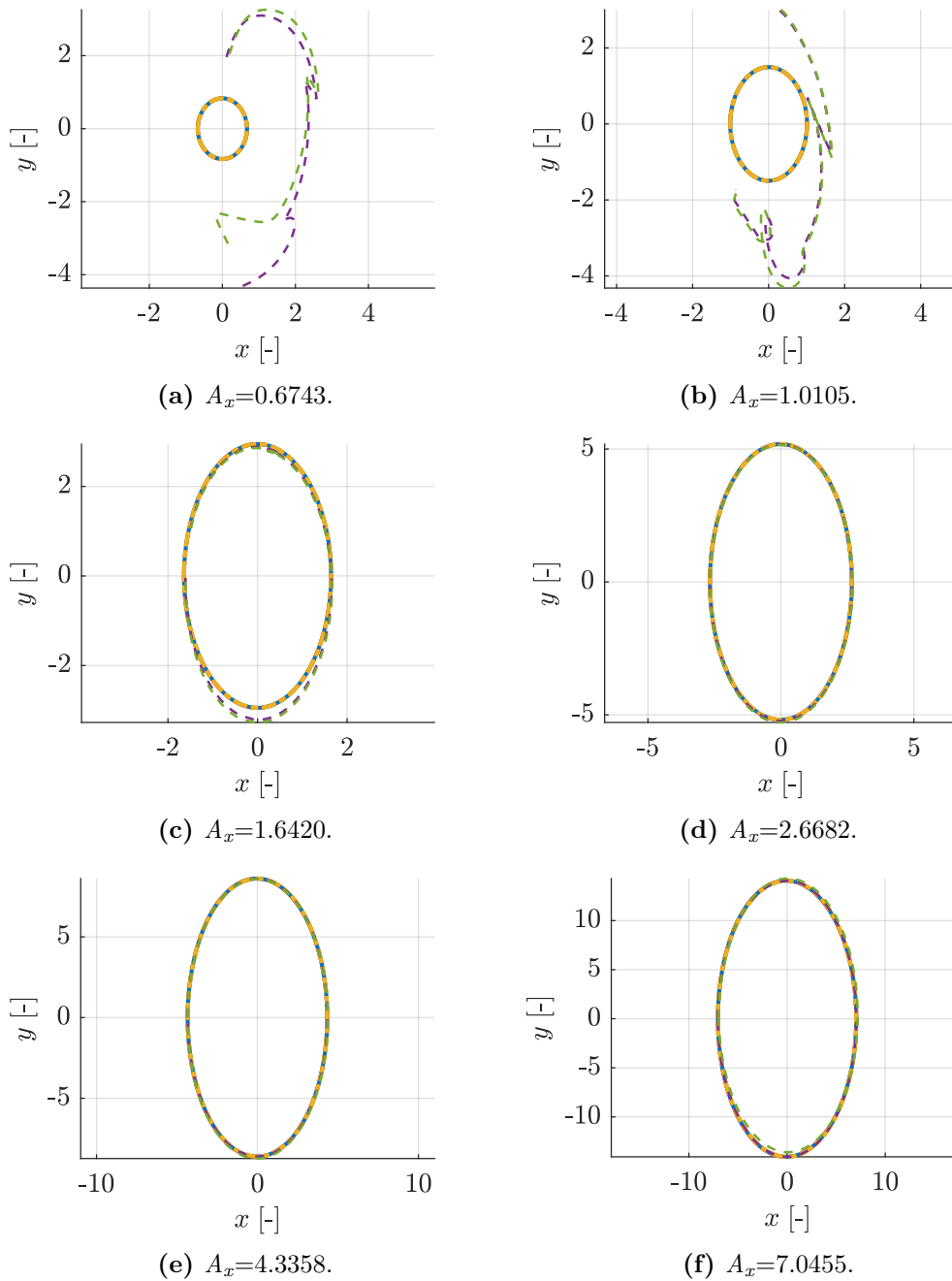


Figure 6.29: Behaviour of the various numerical and analytical models to vary the size of the orbit for a Mars-Deimos system, with analytical model under the hypothesis $b/p = \mathcal{O}[\chi^3]$.

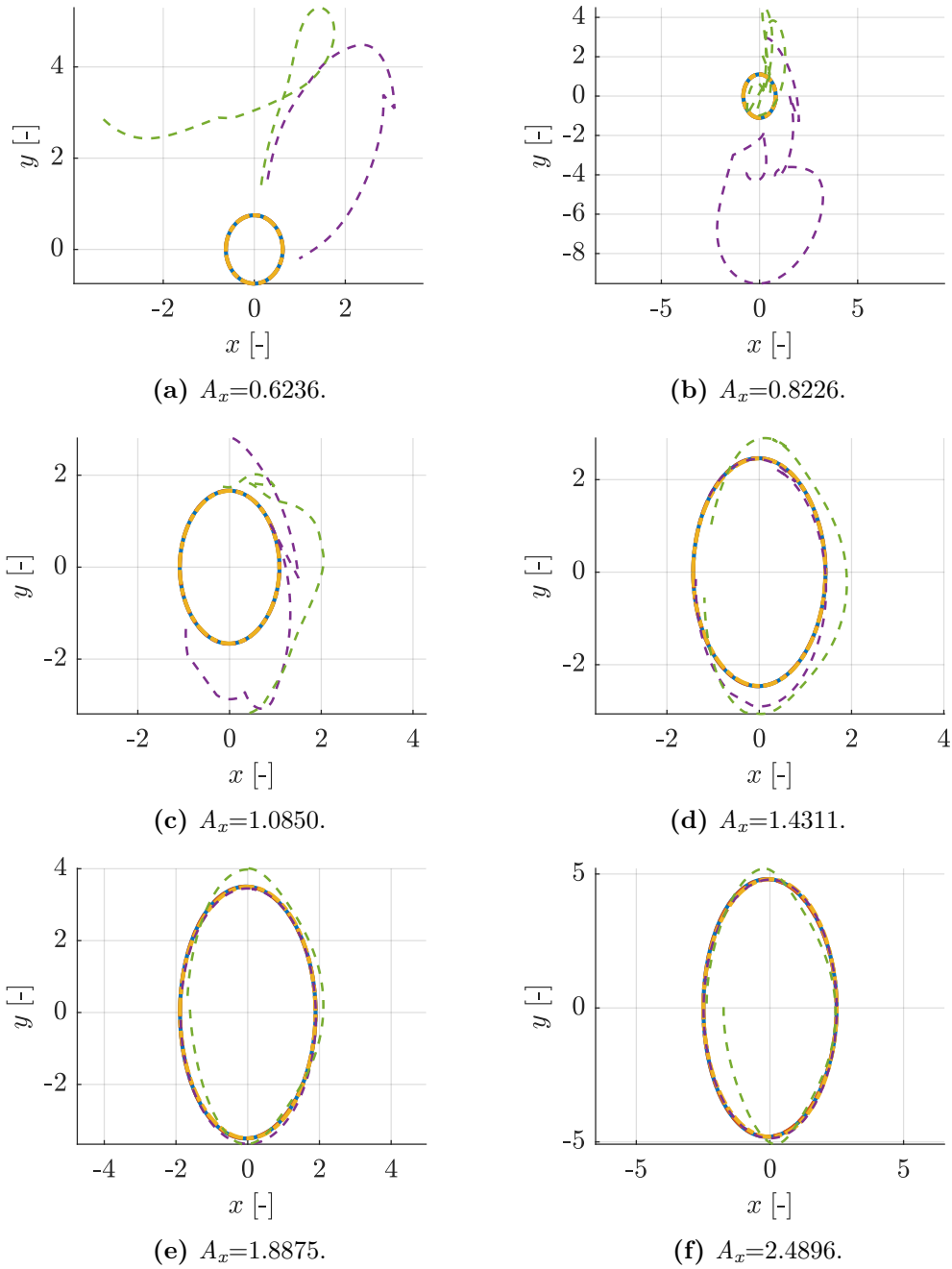


Figure 6.30: Behaviour of the various numerical and analytical models to vary the size of the orbit for a Sun-(Earth-Moon) system, with analytical model under the hypothesis $b/p = \mathcal{O}[\chi^3]$.

6.4.3 Results for the model with assumption $\mathcal{O}[\chi^2]$

This case represents the solution proposed in the previous chapter associated with the assumption $b/p = \mathcal{O}[\chi^2]$. This assumption guarantees a good trade off between the accuracy of the solution and the fact that it allows to develop a lot of terms of the Lie series without encountering particular problems in the analytical integration, e.g. to determine the mean Hamiltonian or the generating function. The Figures 6.31 to 6.33 represent the trend of the maximum error along one orbital period. In particular the blue lines represent the error that the Hill model has with respect to CR3BP, instead the red ones the error that the CR3BP-1₁₃ model has, always, to the CR3BP model. In particular, the dash-dot represent the analytical solution. From Figures 6.31 to 6.33, we can see that as the mass parameter decreases, the validity range of the assumptions and consequently of the model increases. In particular, the model is less reliable as the size of the orbit increases. As already seen in the Figures 6.16 to 6.18, the deviation of the centre of the orbit increases, tending to be comparable with the distance between the two attractors and no longer a fraction. Consequently the model is particularly reliable and usable for low mass ratio systems, so that for further decreasing μ the maximum error related to the CR3BP-1₁₃ model (dash-dotted line) is lower than that of Hill (dash-dot blue line). To better understand the error plots we will show the behaviour of some orbits in the various systems and for various dimensions. In the Figures 6.34 to 6.36, it is clearer how, at the same initial conditions (found with a suitable differential correction, proposed in the Appendix B) the various models (numerical and analytical) are reliable in the respective areas identified in the Figures 6.31 to 6.33. then, we want to point out, how the model obtained in Chapter 5 follow the one in Chapter 4 until the assumption concerning b/p remains sufficiently valid. In Figure 6.31 the analytical solution (red line) reaches a minimum error of about 80 for $A_x = 2$ in the first part (on the left) the red line, for the analytical solution, remains above the dash-dot blue line and then the red line increases again. For Figure 6.32, instead the error has a zone between $A_x = 3.5$ and $A_x = 6.5$ where it remains constant at about 1 and then increases again, in the first part (on the left) the red line, for the analytical solution, remain equal to the blue one. In Figure 6.33 the error reaches a minimum of about 0.003 to $A_x = 7$ and is less than the blue line then the red line remains roughly equal to the blue one up to $A_x = 20$.

Legend

—	<i>nHill</i>
- - -	<i>aHill 5 SPC</i>
—	<i>nCR3BP - 1₁₃</i>
- - -	<i>aCR3BP - 1₁₃ 5 SPC</i>

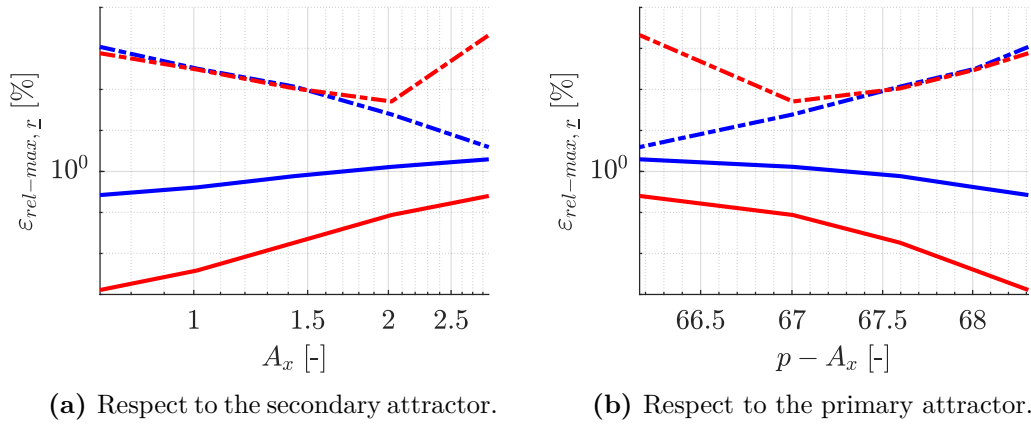


Figure 6.31: Trend of the maximum error as the size of the orbit in the Sun-(Earth-Moon) system increases with the assumption $b/p = \mathcal{O}[\chi^2]$.

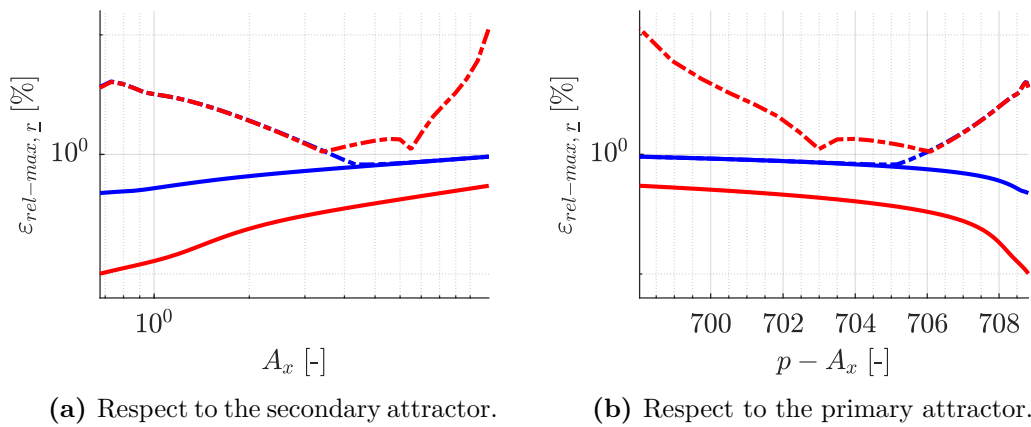


Figure 6.32: Trend of the maximum error as the size of the orbit in the Mars-Deimos system increases with the assumption $b/p = \mathcal{O}[\chi^2]$.

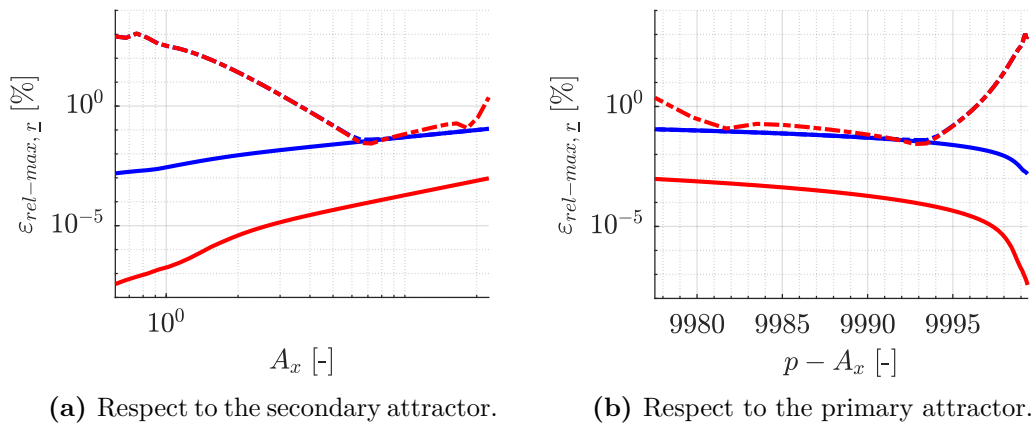


Figure 6.33: Trend of the maximum error as the size of the orbit for Sun-Alauda system increases with the assumption $b/p = \mathcal{O}[\chi^2]$.

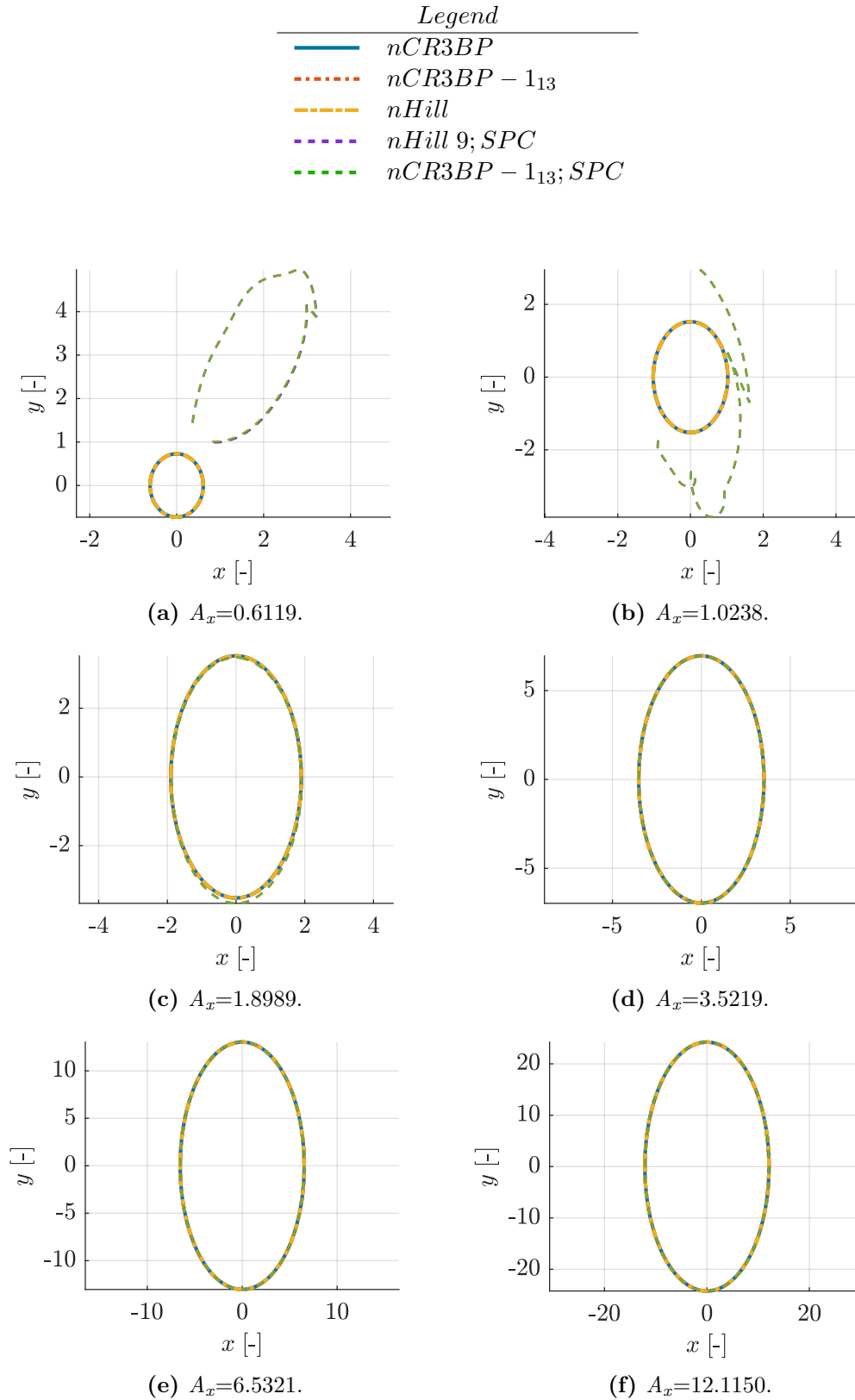


Figure 6.34: Behaviour of the various numerical and analytical models to vary the size of the orbit for Sun-Alauda system, with analytical model under the hypothesis $b/p = \mathcal{O}[\chi^2]$.

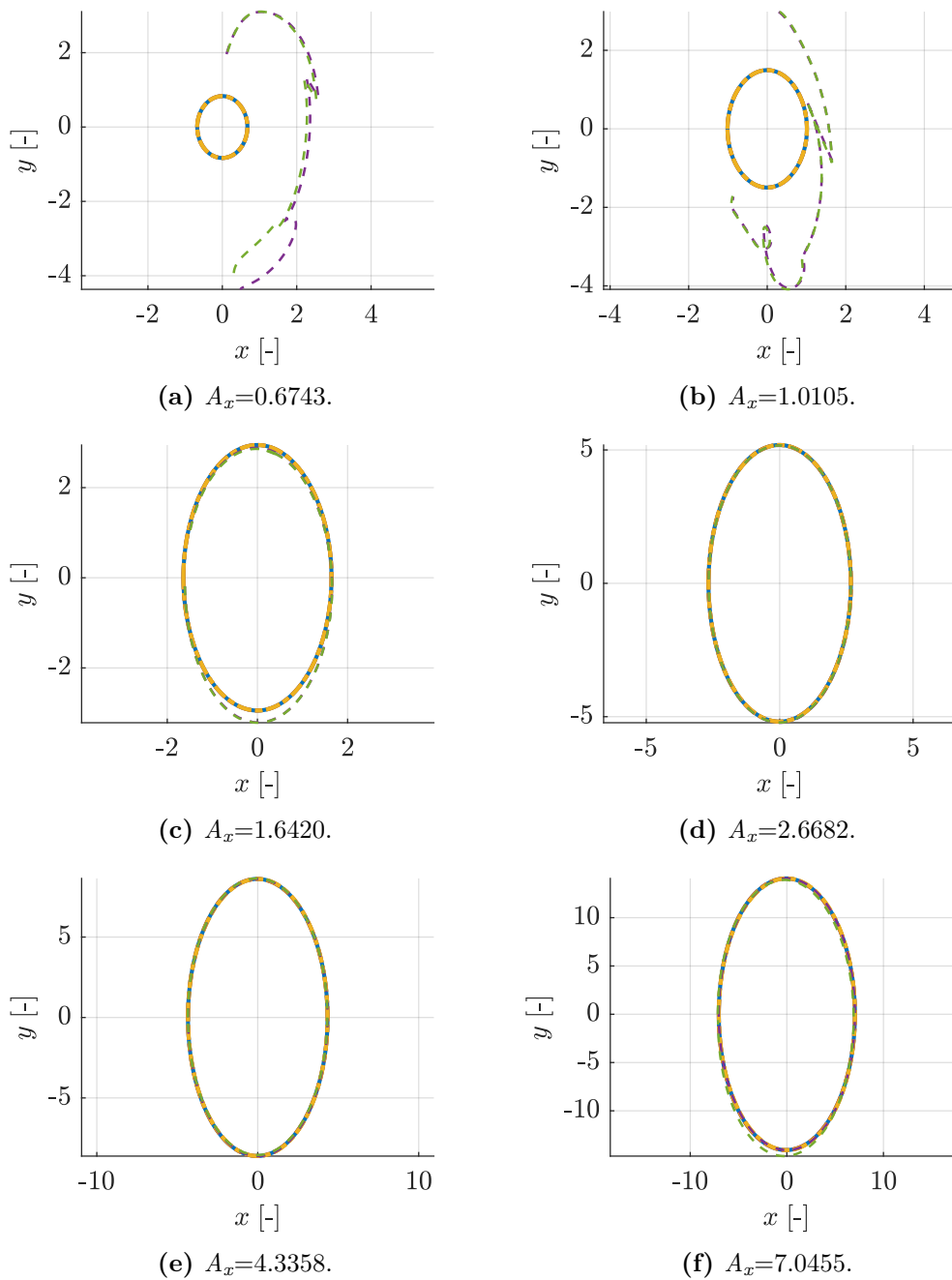


Figure 6.35: Behaviour of the various numerical and analytical models to vary the size of the orbit for a Mars-Deimos system, with analytical model under the hypothesis $b/p = \mathcal{O}[\chi^2]$.

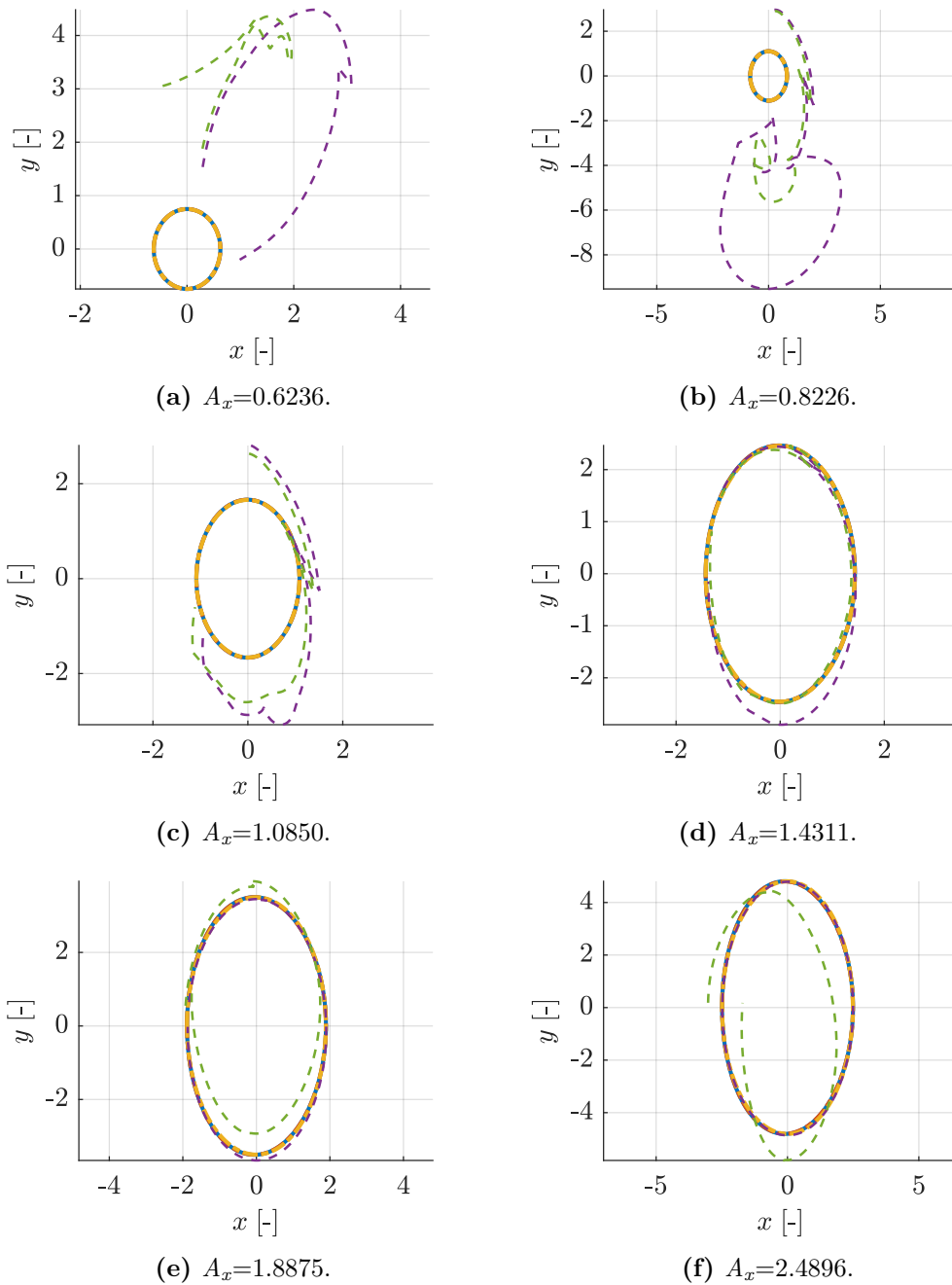


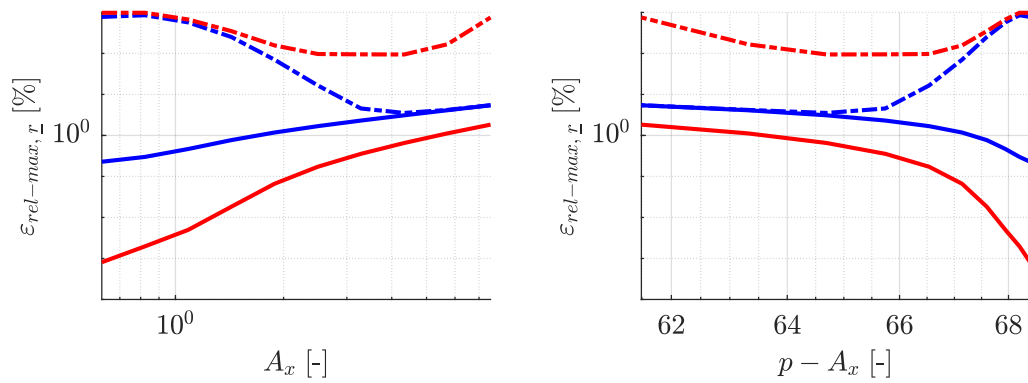
Figure 6.36: Behaviour of the various numerical and analytical models to vary the size of the orbit for a Sun-(Earth-Moon) system, with analytical model under the hypothesis $b/p = \mathcal{O}[\chi^2]$.

6.4.4 Results for the model with assumption $\mathcal{O}[\chi^1]$

During the thesis work and in particular observing the Figures 6.16 to 6.18, we tried to further improve the results obtained with the model presented in Chapter 5. The Figures 6.16 to 6.18, show how the assumption $b/p = \mathcal{O}[\chi^2]$ is not much more valid when A_x increases, i.e. when the orbit is closer to the primary attractor. In this sense, we work was started to produce a model under $b/p = \mathcal{O}[\chi^1]$ assumption. However, the model obtained came to a halt in the order 5 of the Lie series, while in the works proposed in Chapters 4 and 5 we reached order 8/9. This is mainly due to the coupling between the terms obtained from the potential of the secondary (Equations (4.67f) to (4.67k)) and the new terms of the potential of the primary (Equations (5.5a) to (5.5f)), which lead to the analytic integration of incomplete elliptical integrals of the first and second type. For completeness of the results the same graphs of Section 6.4.3 will be re-proposed as regards the maximum error trend over a single orbital period, when size of the orbit increases and for the same mass ratios as before, Figures 6.37 to 6.39. These plots represent the trend of the maximum error along one orbital period. In particular the blue lines represent the error that the Hill model has with respect to CR3BP, instead the red ones the error that the CR3BP-1₁₃ model has, always, to the CR3BP model. In particular, the dash-dot represent the analytical solution. Also in this case, the error tends to improve for smaller mass parameters and for larger orbits. However, due to the fact that fewer orders were considered during the Lie series, both the effect of the primary and the secondary are approximated with less precision. In Figure 6.37 the red line, for the analytical solution, reaches a minimum error of about 100 for $A_x = 3.5$ in the first part (on the left) the red line, for the analytical solution, remains above the blue line and then the red line increases again. For Figure 6.38, instead he red line, for the analytical solution, reaches a minimum error of about 5 for $A_x = 4$. In Figure 6.39 the error of red line reaches a minimum of about 0.05 to $A_x = 8$ then the red line increase again. Similarly to how it was done before, in the Figures 6.40 to 6.42, we report the behaviours that the various models and analytical and numerical solutions predict, with equal initial conditions, to better understand the error charts.

Legend

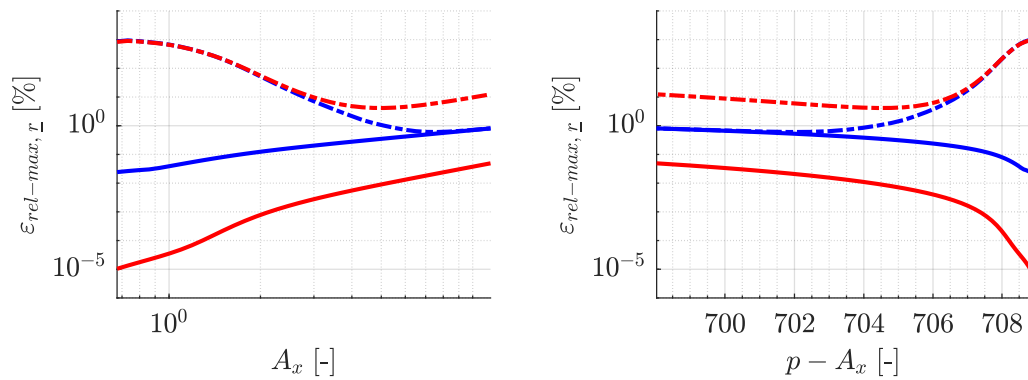
—	<i>nHill</i>
- - - -	<i>aHill 5 SPC</i>
—	<i>nCR3BP - 1₁₃</i>
- - - -	<i>aCR3BP - 1₁₃ 5 SPC</i>



(a) Respect to the secondary attractor.

(b) Respect to the primary attractor.

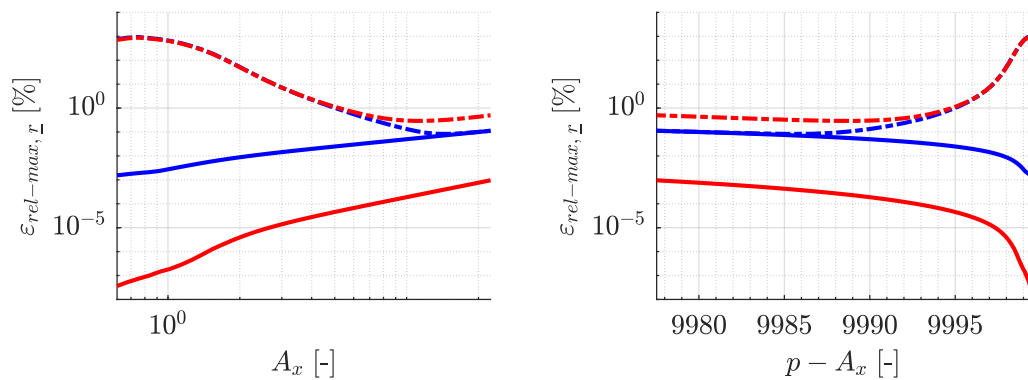
Figure 6.37: Trend of the maximum error as the size of the orbit in the Sun-(Earth-Moon) system increases with the assumption $b/p = \mathcal{O}[\chi^1]$.



(a) Respect to the secondary attractor.

(b) Respect to the primary attractor.

Figure 6.38: Trend of the maximum error as the size of the orbit in the Earth-Moon system increases with the assumption $b/p = \mathcal{O}[\chi^1]$.



(a) Respect to the secondary attractor.

(b) Respect to the primary attractor.

Figure 6.39: Trend of the maximum error as the size of the orbit for Sun-Alauda system increases with the assumption $b/p = \mathcal{O}[\chi^1]$.

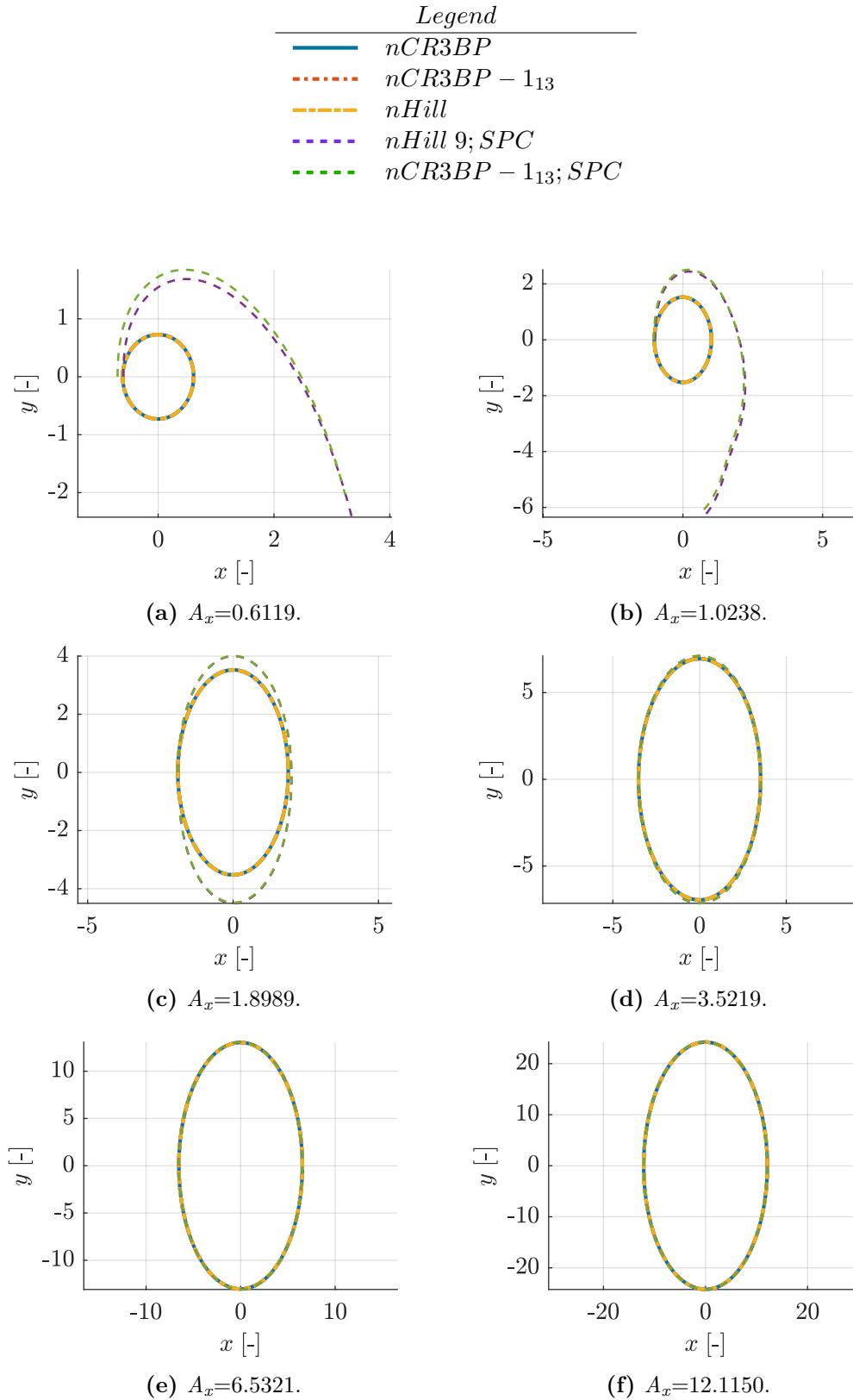


Figure 6.40: Behaviour of the various numerical and analytical models to vary the size of the orbit for Sun-Alauda system, with analytical model under the hypothesis $b/p = \mathcal{O}[\chi^1]$.

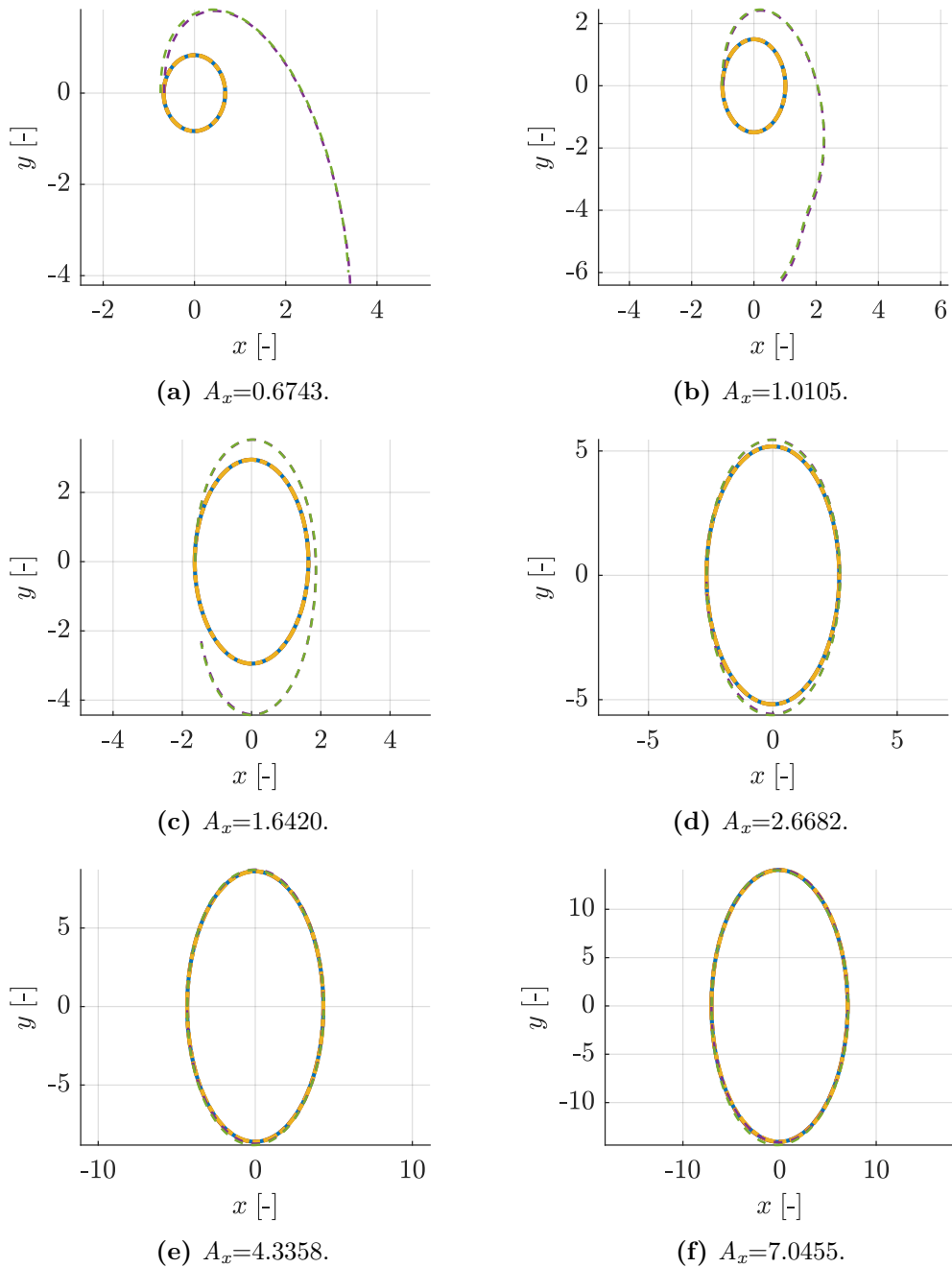


Figure 6.41: Behaviour of the various numerical and analytical models to vary the size of the orbit for a Mars-Deimos system, with analytical model under the hypothesis $b/p = \mathcal{O}[\chi^1]$.

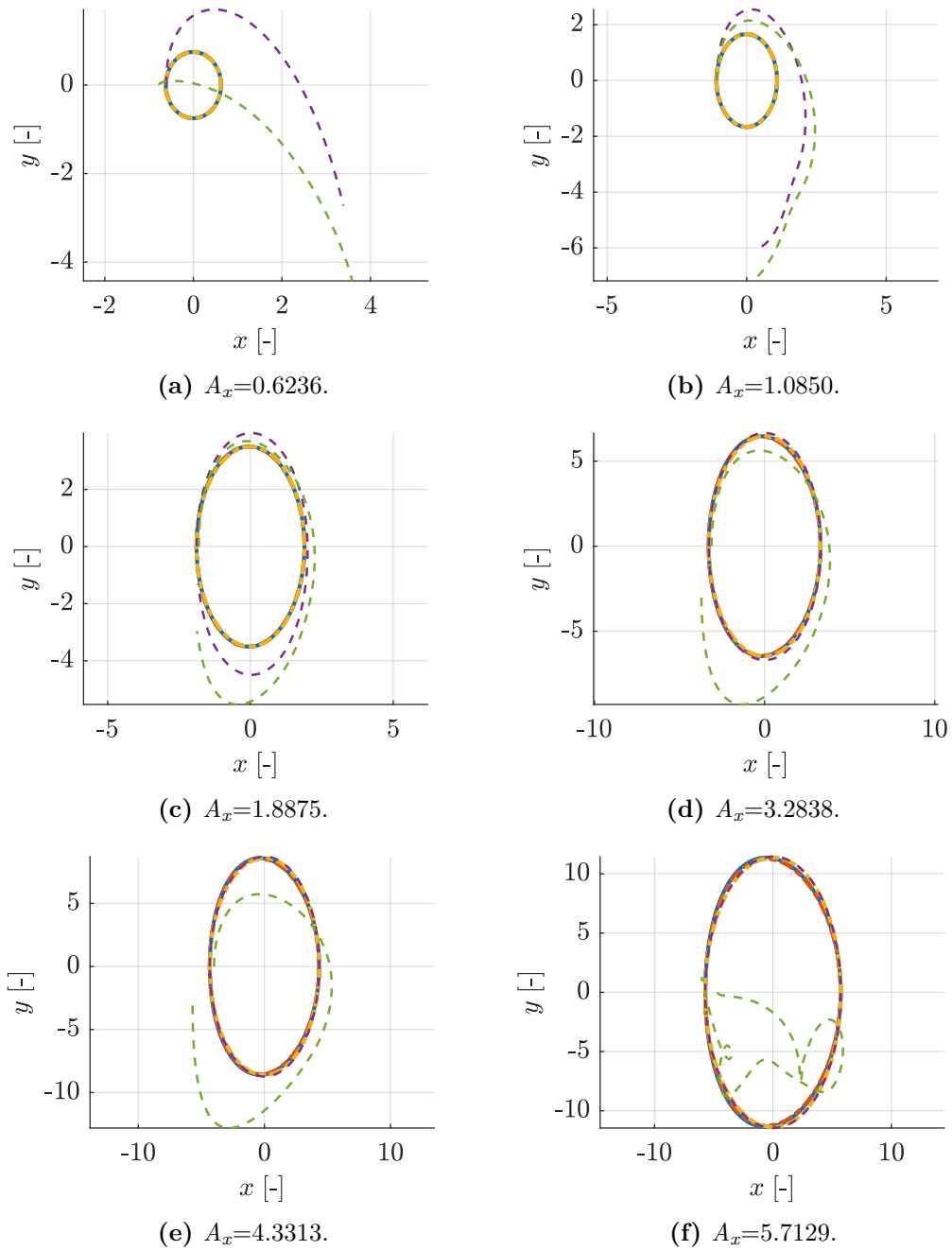


Figure 6.42: Behaviour of the various numerical and analytical models to vary the size of the orbit for a Sun-(Earth-Moon) system, with analytical model under the hypothesis $b/p = \mathcal{O}[\chi^1]$.

Chapter 7

Conclusion

The main purpose of this thesis is to produce a first approximate analytical solution for the orbits DRO starting from the solution that Lara [38, 39] found for the Hill model. The mathematical model used here, is the planar CR3BP in a simplified version; in fact, the method proposed by Szebehely is used to obtain the immediately following approximation of the Hill model. This new model, little discussed in the literature, is very interesting as it allows to improve the Hill problem and can be exploit even in regions closer to primary attractor. Summarising, the thesis work produced a series of analytical solutions for the first term of the CR3BP using various assumptions. In particular, the assumption that results in a considerable improvement is the one involving the $b/p = \mathcal{O}[\chi^2]$, because, in this way, the different orders of the theory have been obtained with a more accurate assumption. However, the analytical solution of the Hill model with respect to the CR3BP-1₁₃ is the same in the vicinity of the secondary attractor, because it can be considered as a perturbation in the framework of the canonical perturbation theory. On the other hand, in the Hill model the contribution of the primary attractor is solved correctly, this is not true in the analytical solution of the CR3BP-1₁₃, where the additional terms are considered perturbations. Therefore, the closer the spacecraft is to the primary attractor the lesser those terms can be considered as perturbations. The assumptions made are valid for DROs and do not seem to be applicable to other situations; since the DROs have an elliptical shape centred in the secondary attractor. As previously said, the most important and restrictive assumption is the one on b/p ; its application involves several couplings that make the use of Lie transformation complicated, even at low order of the theory. In addition, a strong limitation is due to the initial conditions, which must be appropriately obtained to have a periodic dynamic.

The most interesting feature of DROs is the great distance they can reach from the second body, simultaneously remaining periodic around the secondary and presenting a great stability on long period. This leads to a considerable number of possible applications, in fact, as indicated in the thesis, numerous studies on these orbits have been carried out: from the prevention of impacts on our planet to the study of moons in systems such as the Martian or Jovian system, to missions on Mars where they could be exploited for supplies or refuelling. During the thesis work the software Wolfram Mathematica was used for the analytical part and later Matlab for the simulation part. The model is decidedly advantageous from the point of view of computational times, however it is slowed down by the calculation of the elliptical integrals, in particular the incomplete ones. In any case, the errors that the analytical model produces are acceptable with respect to the numerical one.

7.1 Prospective works and improvements

There are various possibilities for future developments and improvements. First, it would be interesting try to continuing the development of the model with the assumption $b/p = \mathcal{O}[\chi^1]$ at least until the 7th order, in order to retain the terms of the most important primary potential. Secondly, it would be useful also considering more Hamiltonian terms of CR3BP-1 model without stopping only at CR3BP-1₁₃, so that it is possible to simulate even better the dynamics of the CR3BP. Another important aspect would be finding an algorithm for the calculation of the incomplete elliptic integrals more efficiently and faster, since most of the slowness derives precisely from this aspect. In fact, for the sake of simplicity, the functions already implemented by Matlab were exploited. A further aspect of progress could be to create an analytical algorithm for predicting the initial conditions, instead, in this work they were obtain by means of and iterative process, briefly reported in the Appendix B. It would also be interesting to apply the Lagrange planetary equations to the Hamiltonian of the CR3BP-1₁₃ or CR3BP-1 model to see if the variations of the orbital elements with respect to the secondary attractor are good in predictive terms for the Keplerian Map, [1]. Finally, this thesis required a lot of work in the development of the analytical model. A possible follow-up of this work is the exploitation of the formulas presented in this thesis, for applications to preliminary missions design and optimisation of DROs, where many initial conditions need to be investigated and therefore computational time and understanding of the problem are of paramount importance. Moreover, the present analytical algorithm, could be implemented on-board a spacecraft for orbit determination and control.

Appendix A

Coordinate frame transformations

Trajectories are often propagated under the equations of motion of the Circular Restricted Three-Body Problem. The reference frame for the CR3BP is a rotating, or synodic, frame centered about the barycenter. It is often useful to view trajectories in an inertial frame.

A.1 Rotating to inertial transformation

Consider the state in the rotating system:

$$\underline{X}_R = [x_R \ y_R \ z_R \ \dot{x}_R \ \dot{y}_R \ \dot{z}_R]^T \quad (\text{A.1})$$

The general equations that are necessary to rotate from a synodic frame to an inertial frame may be expressed as follows:

$$\underline{\underline{R}}_{R2I} = \begin{bmatrix} \underline{R}_R^I & \underline{0} \\ \underline{\dot{R}}_R^I & \underline{\underline{R}}_R^I \end{bmatrix} \quad (\text{A.2})$$

$$\underline{X}_I = \underline{\underline{R}}_{R2I} \underline{X}_R \quad (\text{A.3})$$

where \underline{R}_R^I is a transformation matrix from the rotating frame to the inertial one. At the time of the coordinate transformation, the synodic frame is rotated in the counterclockwise direction by an angle $\vartheta = nt + \vartheta_0$ with respect to the inertial frame. Now, \underline{R}_R^I and $\underline{\dot{R}}_R^I$ may be defined as follows:

$$\underline{R}_R^I = \begin{bmatrix} \cos(nt + \vartheta_0) & -\sin(nt + \vartheta_0) & 0 \\ \sin(nt + \vartheta_0) & \cos(nt + \vartheta_0) & 0 \\ 0 & 0 & 1 \end{bmatrix} \quad (\text{A.4})$$

$$\underline{\dot{R}}_R^I = \begin{bmatrix} -n \sin(nt + \vartheta_0) & -n \cos(nt + \vartheta_0) & 0 \\ n \cos(nt + \vartheta_0) & -n \sin(nt + \vartheta_0) & 0 \\ 0 & 0 & 0 \end{bmatrix} \quad (\text{A.5})$$

A.2 Inertial to rotating transformation

The conversion of the inertial frame to the rotating one is performed in an analogous manner. The rotating matrix from the inertial frame to the rotating one is the inverse

of the rotating matrix from the rotating to the inertial frame:

$$\underline{\underline{R}}_I^R = [\underline{\underline{R}}_R^I]^T \quad (\text{A.6})$$

Therefore:

$$\underline{\underline{R}}_I^R = \begin{bmatrix} \cos(nt + \vartheta_0) & \sin(nt + \vartheta_0) & 0 \\ -\sin(nt + \vartheta_0) & \cos(nt + \vartheta_0) & 0 \\ 0 & 0 & 1 \end{bmatrix} \quad (\text{A.7})$$

$$\dot{\underline{\underline{R}}}_I^R = \begin{bmatrix} -n \sin(nt + \vartheta_0) & n \cos(nt + \vartheta_0) & 0 \\ -n \cos(nt + \vartheta_0) & -n \sin(nt + \vartheta_0) & 0 \\ 0 & 0 & 0 \end{bmatrix} \quad (\text{A.8})$$

The equations to transform from the inertial to the rotating frame are:

$$\underline{\underline{R}}_{I2R} = \begin{bmatrix} \underline{\underline{R}}_I^R & \underline{\underline{0}} \\ \dot{\underline{\underline{R}}}_I^R & \underline{\underline{R}}_I^R \end{bmatrix} \quad (\text{A.9})$$

$$\underline{\underline{X}}_R = \underline{\underline{R}}_{I2R} \underline{\underline{X}}_I \quad (\text{A.10})$$

Appendix B

Differential corrections and family continuation

B.1 Dynamical sensitivities

The closed-form analytical solutions are not available when the dynamical influences of more than two bodies are considered simultaneously.

Numerical methods are necessary, not only to propagate the differential equations of motion, but also to manipulate, or correct, a trajectory arch to meet some desired set of objectives and potentially generate a particular solution to the differential equations of motion. Accomplishment of such goals is facilitated by exploring the dynamical sensitivities and numerical strategies to exploit the information for the computation of solutions. Consequently, numerical differential correction schemes are an essential tool for designing trajectories in multi-body.

B.1.1 Obtaining a baseline solution

To produce a trajectory with some set of desired characteristics, the initial propagation of a baseline arc is essential. For this analysis, all archs are generated by numerically integrating the equations of motion, regardless of the dynamical system. For the computation of trajectories the second-order equations of motion are rewritten as a series of first-order differential equations in the form:

$$\dot{\underline{X}} = \underline{f}(t, \underline{X}) \quad (\text{B.1})$$

where \underline{X} is the state vector:

$$\underline{X} = [x \ y \ z \ \dot{x} \ \dot{y} \ \dot{z}]^T \quad (\text{B.2})$$

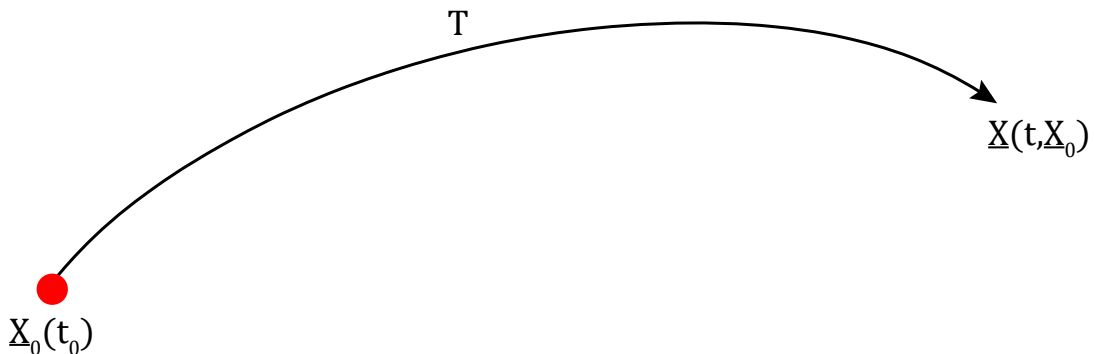


Figure B.1: Baseline Arch.

B.1.2 State transition matrix

The state transition matrix, $\underline{\Psi}(t, t_0)$, has widespread use in the field of astrodynamics, and is particularly useful in analyzing libration point orbits. The STM maps deviations in the state vector from one time to another. For the CR3BP, the state \underline{X} (Equation (B.2)). Let $\delta\underline{x}$ be a small deviation from the nominal trajectory. The nonlinear function $\underline{f}(t, \underline{X} + \delta\underline{x})$ may be approximated using a Taylor series expansion to expand the function about \underline{X} :

$$\dot{\underline{X}} + \delta\dot{\underline{x}} = \underline{f}(t, \underline{X}) + \frac{\partial \underline{f}(t, \underline{X})}{\partial \underline{X}} \delta\underline{x} + \mathcal{O}[(\delta x)^2] + \dots \quad (\text{B.3})$$

If the terms higher than the first order are neglected, the equation simplifies to the following:

$$\delta\dot{\underline{x}} = \frac{\partial \underline{f}(t, \underline{X})}{\partial \underline{X}} \delta\underline{x} \quad (\text{B.4})$$

The solution to Equation (B.4) has the form:

$$\delta\underline{x} = \underline{\Psi}(t, t_0) \delta\underline{x}_0 \quad (\text{B.5})$$

The STM, $\underline{\Psi}(t, t_0)$, is a matrix composed of the partial derivatives of the state:

$$\underline{\Psi}(t, t_0) = \frac{\partial \underline{X}}{\partial \underline{X}_0} \quad (\text{B.6})$$

with the initial conditions:

$$\underline{\Psi}(t_0, t_0) = \underline{I} \quad (\text{B.7})$$

A matrix of partial derivatives, \underline{A} , is used to propagate the :

$$\underline{A} = \frac{\partial \dot{\underline{X}}}{\partial \underline{X}} \quad (\text{B.8})$$

$$\dot{\underline{\Psi}}(t, t_0) = \underline{A}\underline{\Psi}(t, t_0) \quad (\text{B.9})$$

If the matrix \underline{A} is constant, the state transition matrix may be determined analytically, but for most applications, numerical integration is generally required. In the CR3BP, the matrix \underline{A} is given by:

$$\underline{A} = \begin{bmatrix} 0 & \underline{I} \\ \underline{G}_R & \underline{G}_V \end{bmatrix} \quad (\text{B.10})$$

where \underline{G}_R and \underline{G}_V are matrices composed of the partial derivatives of the vector $\underline{f}(t, \underline{X})$, with respect to position and velocity, respectively:

$$\underline{G}_R = \begin{bmatrix} \Omega_{xx} & \Omega_{xy} & \Omega_{xz} \\ \Omega_{yx} & \Omega_{yy} & \Omega_{yz} \\ \Omega_{zx} & \Omega_{zy} & \Omega_{zz} \end{bmatrix} \quad (\text{B.11})$$

$$\underline{G}_V = \begin{bmatrix} 0 & 2n & 0 \\ -2n & 0 & 0 \\ 0 & 0 & 0 \end{bmatrix} \quad (\text{B.12})$$

where Ω is given in Equation (2.19).

Monodromy matrix

The Monodromy matrix, \underline{M} , is a useful application of the state transition matrix in the study and analysis of periodic orbits. It is computed by propagating the STM for one full orbital period, such that

$$\underline{M} = \underline{\Psi}(t_{2\pi}, t_0) \quad (\text{B.13})$$

B.2 Single shooting differential corrector

There are countless families of periodic and quasi-periodic orbits that exist about the libration points. The single-shooting method to construct three-dimensional periodic orbits is described here in detail.

To construct a periodic orbit in the CR3BP, one needs to find a set of initial conditions that will return to the same state when propagated through time. When a periodic orbit crosses the $x-z$ plane, it will have position components in the x and z -directions, and a velocity only in the y -direction:

$$\underline{X}_0 = [x_0 \ 0 \ z_0 \ 0 \ \dot{y}_0 \ 0]^T \quad (\text{B.14})$$

For this initial condition, the orbit will be periodic if, after some integration time, another perpendicular $x-z$ crossing may be found. At the second $x-z$ crossing, the state will be:

$$\underline{X}(t_{2\pi}/2) = [x \ 0 \ z \ 0 \ \dot{y} \ 0]^T \quad (\text{B.15})$$

An orbit will be considered periodic if at time $t_{2\pi}/2$, $|\dot{x}|$ and $|\dot{z}| < \text{Toll}$. Hence, $\delta\dot{x} = 0 - \dot{x}$ and $\delta\dot{z} = 0 - \dot{z}$ are desired. However, unless the initial conditions were selected perfectly, when the trajectory is integrated to the point $y = 0$, there will be some velocity components in the x and z -directions. These values can be decreased by updating the states of two of the three initial conditions and integrating again, taking advantage of the STM.

The corrections to the initial conditions are defined as:

$$\delta\underline{X}_0 = [\delta x_0, 0, \delta z_0, 0, \delta \dot{y}_0, 0]^T \quad (\text{B.16})$$

The adjustments can be computed using the STM, which is used to relate the final state and initial one:

$$\delta\underline{X} = \underline{\Psi} \cdot \delta\underline{X}_0 + \dot{\underline{X}}\delta(t_{2\pi}/2) \quad (\text{B.17})$$

Thus, the corrections can be computed from the following:

$$\delta\underline{X} \cong \underline{\Psi}(t_{2\pi}/2, t_0) \cdot \delta\underline{X}_0 + \frac{\partial \underline{X}}{\partial t} \delta(t_{2\pi}/2) \quad (\text{B.18})$$

Given Equation (B.17), and knowing that $\delta y_0 = 0$, the change in y may be found:

$$\delta y = 0 = \Psi_{2,1}\delta x_0 + \Psi_{2,3}\delta z_0 + \Psi_{2,5}\delta \dot{y}_0 + \dot{y}\delta(t_{2\pi}/2) \quad (\text{B.19})$$

To change the components of z_0 and y_0 and leave x_0 fixed, the following equation is used:

$$\begin{bmatrix} \delta\dot{x} \\ \delta\dot{z} \end{bmatrix} = \left[\begin{pmatrix} \Psi_{4,3} & \Psi_{4,5} \\ \Psi_{6,3} & \Psi_{6,5} \end{pmatrix} - \frac{1}{\dot{y}} \begin{bmatrix} \ddot{x} \\ \ddot{z} \end{bmatrix} \right] \begin{pmatrix} \Psi_{2,3} & \Psi_{2,5} \end{pmatrix} \begin{pmatrix} \delta z_0 \\ \delta \dot{y}_0 \end{pmatrix} \quad (\text{B.20})$$

Alternatively, to change x_0 and y_0 and keep z_0 fixed, use:

$$\begin{bmatrix} \delta \dot{x} \\ \delta \dot{z} \end{bmatrix} = \begin{bmatrix} (\Psi_{4,1} & \Psi_{4,5}) \\ (\Psi_{6,1} & \Psi_{6,5}) \end{bmatrix} - \frac{1}{\dot{y}} \begin{bmatrix} \ddot{x} \\ \ddot{z} \end{bmatrix} (\Psi_{2,1} & \Psi_{2,5}) \begin{bmatrix} \delta x_0 \\ \delta \dot{y}_0 \end{bmatrix} \quad (\text{B.21})$$

Since the system was linearized in this procedure, the adjustments will not correct the unwanted motion perfectly. The process will need to be iterated until it converges on an orbit.

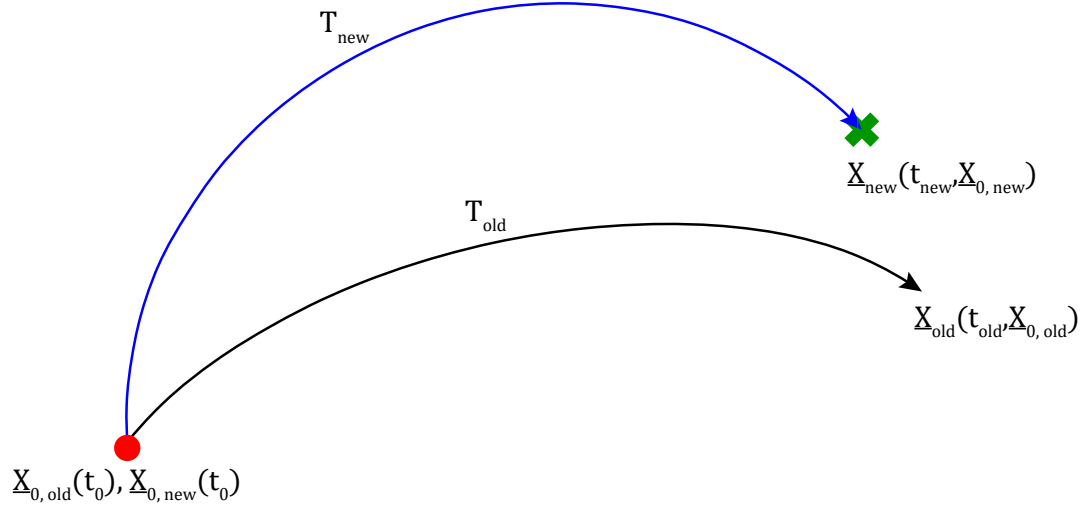


Figure B.2: Variable-Time Single Shooting Differential Corrector.

B.3 Family continuation

In this section we will study the evolution of Hénon's orbit families in the CR3BP dynamics. Starting from the initial conditions, we can calculate the new initial state vector that characterizes each periodic orbit. Using the differential correction method Appendix B.2 coupled with a continuation method, it is possible to calculate the new complete map of the periodic orbits. The numerical algorithm used in the differential correction method typically converges in some iterations if the initial guess conditions are close to the short ones. For our work it was necessary to calculate periodic orbits of great arbitrary amplitude. So, we have to use the numerical continuation to generate a family of periodic orbits.

We proceeded as follows. Suppose we have a first initial condition already correct, as:

$$\underline{X}_{0-old} = [x_0 \ y_0 \ z_0 \ \dot{x}_0 \ \dot{y}_0 \ \dot{z}_0]^T \quad (\text{B.22})$$

At this point we apply a small perturbation in the desired direction (to enlarge or reduce the orbit). For example, for the families of Hénon along the x axis vice versa for Halo along z. The perturbation is at least 2 orders of magnitude lower to the variable itself.

$$\underline{X}_{0-guess} = \begin{bmatrix} x_0 \\ y_0 \\ z_0 \\ \dot{x}_0 \\ \dot{y}_0 \\ \dot{z}_0 \end{bmatrix} + \begin{bmatrix} \delta x \\ 0 \\ 0 \\ 0 \\ 0 \\ 0 \end{bmatrix} \quad (\text{B.23})$$

Subsequently we applied the correction method, illustrated above, to obtain the new correct conditions. This procedure is iterated until the dimensions of the orbit are desired.

$$\underline{X}_{0-new} = [-A_x \ y_0 \ z_0 \ \dot{x}_0 \ \dot{y}_0 \ \dot{z}_0]^T \quad (\text{B.24})$$

An example of the continuation proposed in the Figure B.3.

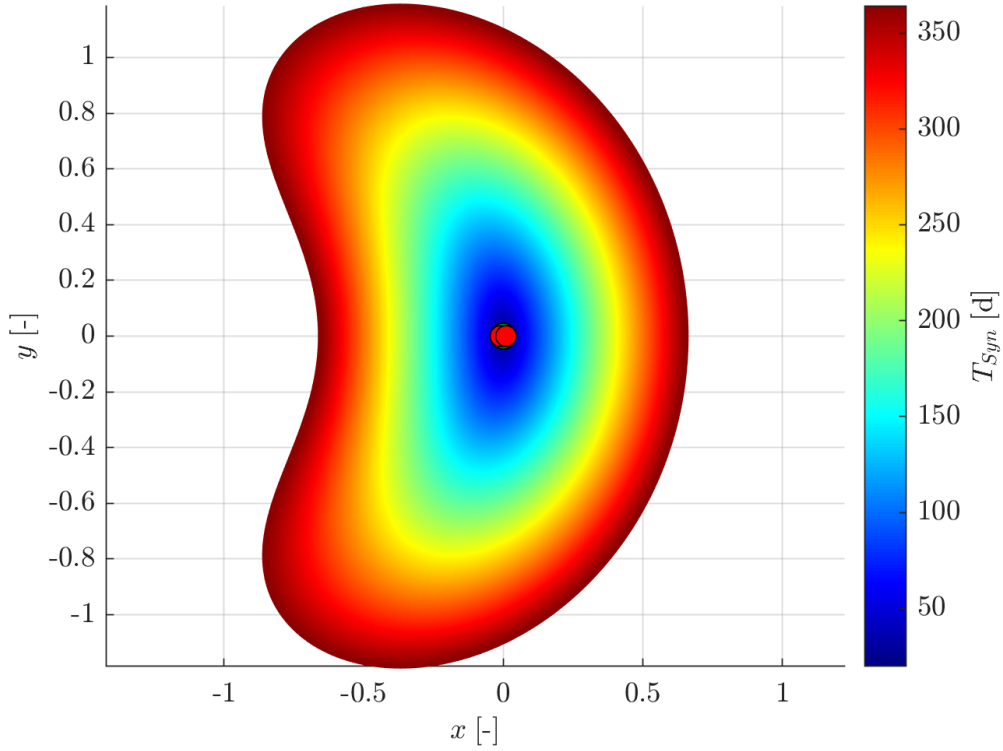


Figure B.3: Hénon family- f orbit continuation in Sun-(Earth-Moon) synodic system.

References Cited

- [1] Elisa Maria Alessi and Joan Pau Sánchez. “Semi-Analytical Approach for Distant Encounters in the Spatial Circular Restricted Three-Body Problem”. In: *J. Guid. Control. Dyn.* 39.2 (2016), pp. 351–359. ISSN: 0731-5090. DOI: 10.2514/1.G001237. URL: <http://arc.aiaa.org/doi/10.2514/1.G001237>.
- [2] Antonio Giorgilli. “Sistemi Hamiltoniani e teoria delle perturbazioni”. Milan. URL: <http://www.mat.unimi.it/users/antonio/hamsys/hamsys.html>.
- [3] Vladimir I gorevic Arnold, Valery Kozlov, and Anatoly I. Neishtadt. *Mathematical Aspects of Classical and Celestial Mechanics*. Third Edit. Springer, 2010, p. 526. ISBN: 9783540282464. DOI: 10.1007/978-3-540-48926-9. arXiv: 0402023 [hep-th]. URL: <http://books.google.com.hk/books?id=PROuMQEACAAJ>.
- [4] Richard H. Battin. *An Introduction to the Mathematics and Methods of Astrodynamics*. American Institute of Aeronautics and Astronautics, 1999, p. 840. ISBN: 9781563473425. DOI: 10.2514/4.861543. URL: <http://books.google.com.hk/books?id=0jH7aVhiGdcC>.
- [5] G Benettin, L Galgani, and A Giorgilli. “2. Meccanica Newtoniana”. 1991. URL: <http://www.mat.unimi.it/users/penati/didattica/FISMAT1/vmec2.pdf>.
- [6] Giancarlo Benettin, Jacques Henrard, and Sergei Kuksin. *Hamiltonian Dynamics: Theory and Applications*. Ed. by Antonio Giorgilli. Springer, 2005. ISBN: 9783642122446. DOI: 10.1007/b104338. URL: <file:///Users/Brian/Caudle/Documents/Papers/2005/Benettin/2005Benettin.pdf>.
- [7] Collin Bezrouk and Jeffrey S. Parker. “Ballistic capture into distant retrograde orbits around Phobos: an approach to entering orbit around Phobos without a critical maneuver near the moon”. In: *Celest. Mech. Dyn. Astron.* 130.2 (2018), p. 10. ISSN: 0923-2958. DOI: 10.1007/s10569-017-9798-0. URL: <http://link.springer.com/10.1007/s10569-017-9798-0>.
- [8] Collin Bezrouk and Jeffrey S. Parker. “Long term evolution of distant retrograde orbits in the Earth-Moon system”. In: *Astrophys. Space Sci.* 362.9 (2017), p. 176. ISSN: 0004-640X. DOI: 10.1007/s10509-017-3158-0. URL: <http://link.springer.com/10.1007/s10509-017-3158-0>.
- [9] Collin J. Bezrouk and Jeffery Parker. “Long Duration Stability of Distant Retrograde Orbits”. In: *AIAA/AAS Astrodyn. Spec. Conf.* August (2014), pp. 1–9. DOI: 10.2514/6.2014-4424. URL: <http://arc.aiaa.org/doi/10.2514/6.2014-4424>.
- [10] Dino Boccaletti and Giuseppe Pucacco. *Theory of Orbits : Volume 1: Integrable Systems and Non-perturbative Methods*. Springer Berlin Heidelberg, 1996, p. 393. ISBN: 9783642082108. DOI: 10.1007/978-3-662-03319-7.
- [11] Dino Boccaletti and Giuseppe Pucacco. *Theory of orbits : Volume 2 : Perturbative and geometrical methods*. Second Edi. Springer, 1998. ISBN: 978-3-642-08222-1. URL: <http://adsabs.harvard.edu/abs/1998thor.conf.....B>.

- [12] John R. Brophy and Brian Muirhead. “Near-Earth Asteroid Retrieval Mission (ARM) Study”. In: *33rd Int. Electr. Propuls. Conf.* IEPC Paper 2013-082 (2013), pp. 1–16.
- [13] Silva Pais Cabral. “On the Stability of Quasi-Satellite Orbits in the Elliptic Restricted Three-Body Problem”. PhD thesis. 2011.
- [14] Lucía Capdevila, Davide Guzzetti, and Kathleen C. Howell. “Various transfer options from Earth into Distant Retrograde Orbits in the vicinity of the Moon”. In: *Adv. Astronaut. Sci.* 152.1 (2014), pp. 3659–3678. ISSN: 00653438.
- [15] John R. Cary. “Lie transform perturbation theory for Hamiltonian systems”. In: *Phys. Rep.* 79.2 (1981), pp. 129–159. ISSN: 0370-1573. DOI: 10.1016/0370-1573(81)90175-7. URL: <https://www.sciencedirect.com/science/article/pii/0370157381901757>.
- [16] John R. Cary. “Lie Transforms and Their Use in Hamiltonian Perturbation Theory”. In: January 1979 (1978), p. 66.
- [17] Camilla Colombo, Giorgio Mingotti, Franco Bernelli-Zazzera, and Colin R. McInnes. “Multiple spacecraft transfers to Sun-Earth distant retrograde orbits for Asteroid detection missions”. In: (2014). URL: <http://eprints.gla.ac.uk/98908/>.
- [18] Davide Conte and David B. Spencer. “Mission analysis for Earth to Mars-Phobos distant Retrograde Orbits”. In: *Acta Astronaut.* 151 (2018), pp. 761–771. ISSN: 00945765. DOI: 10.1016/j.actaastro.2018.06.049. URL: <https://linkinghub.elsevier.com/retrieve/pii/S0094576518303801>.
- [19] Davide Conte, Marilena Di Carlo, Koki Ho, David B. Spencer, and Massimiliano Vasile. “Earth-Mars transfers through Moon Distant Retrograde Orbits”. In: *Acta Astronaut.* 143 (2018), pp. 372–379. ISSN: 0094-5765. DOI: 10.1016/J.ACTAASTRO.2017.12.007. URL: <https://www.sciencedirect.com/science/article/pii/S0094576517309736?via=ihub>.
- [20] Jacob Demeyer and Pini Gurfil. “Transfer to Distant Retrograde Orbits Using Manifold Theory”. In: *J. Guid. Control. Dyn.* 30.5 (2007), pp. 1261–1267. ISSN: 0731-5090. DOI: 10.2514/1.24960. URL: <http://arc.aiaa.org/doi/10.2514/1.24960>.
- [21] André Deprit. “Canonical transformations depending on a small parameter”. In: *Celest. Mech.* 1.1 (1969), pp. 12–30. ISSN: 0008-8714. DOI: 10.1007/BF01230629. URL: <http://link.springer.com/10.1007/BF01230629>.
- [22] André Deprit. “The elimination of the parallax in satellite theory”. In: *Celest. Mech.* 24.2 (1981), pp. 111–153. DOI: 10.1007/BF01229192. URL: <http://link.springer.com/10.1007/BF01229192>.
- [23] Paulo J.S. Gil and Julia Schwartz. “Simulations of Quasi-Satellite Orbits Around Phobos”. In: *J. Guid. Control. Dyn.* 33.3 (2010), pp. 901–914. ISSN: 0731-5090. DOI: 10.2514/1.44434. URL: <http://arc.aiaa.org/doi/10.2514/1.44434>.
- [24] Pini Gurfil and N. Jeremy Kasdin. “Canonical modelling of coorbital motion in Hill’s problem using epicyclic orbital elements”. In: *Astron. Astrophys.* 409.3 (2003), pp. 1135–1140. ISSN: 0004-6361. DOI: 10.1051/0004-6361:20031162. URL: <http://www.aanda.org/10.1051/0004-6361:20031162>.
- [25] Pini Gurfil, N. Jeremy Kasdin, and Egemen Kolemen. “Hamilton-Jacobi modelling of stellar dynamics”. In: *Adv. Sp. Res.* 36.6 (2005), pp. 1143–1150. ISSN: 02731177. DOI: 10.1016/j.asr.2005.06.041.

- [26] Massimiliano Guzzo. “Qualche appunto aggiuntivo sulle lezioni di Meccanica Hamiltoniana”. In: (2014), pp. 1–32.
- [27] Michel Hénon. “Exploration numérique du problème restreint. I. Masses égales ; orbites périodiques”. In: *Ann. d’Astrophysique* 28 (1965), pp. 499–511. URL: <http://adsabs.harvard.edu/abs/1965AnAp...28..499H>.
- [28] Michel Hénon. “Exploration numérique du problème restreint. II. Masses égales, stabilité des orbites périodiques”. In: *Ann. d’Astrophysique* 28 (1969), pp. 992–1007. URL: <http://adsabs.harvard.edu/abs/1965AnAp...28..992H>.
- [29] Michel Hénon. *Generating families in the restricted three-body problem*. Springer-Verlag, 1997. ISBN: 9783540696506.
- [30] Michel Hénon. “Numerical Exploration of the Restricted Problem. V.” In: *Astron. Astrophys.* 1 (1968), pp. 223–238.
- [31] Michel Hénon. “Numerical Exploration of the Restricted Problem. VI. Hill’s Case: Non-Periodic Orbit”. In: *Astron. Astrophys.* 9 (1970), pp. 24–36. ISSN: 1098-6596. DOI: 10.1017/CB09781107415324.004. arXiv: arXiv:1011.1669v3. URL: <http://adsabs.harvard.edu/abs/1970A&A...9...24H%5Cnhttp://adsabs.harvard.edu/cgi-bin/nph-data%5Fquery?bibcode=1970A&A...9...24H%5Cnlink%5Ftype=ARTICLE>.
- [32] Michel Hénon. “Vertical Stability of Periodic Orbits in the Restricted Problem. I. Equal Masses”. In: *Astron. Astrophys.* 28 (1973), pp. 415–426. URL: <http://adsabs.harvard.edu/abs/1973A&A...28..415H>.
- [33] Michel Hénon. “Vertical Stability of Periodic Orbits in the Restricted Problem. II. Hill’s Case”. In: *Astron. Astrophys.* 30 (1974), pp. 317–321. URL: <http://adsabs.harvard.edu/abs/1974A&A...30..317H>.
- [34] Michel Hénon and Jean-Marc Petit. “Series expansions for encounter-type solutions of Hill’s problem”. In: *Celest. Mech.* 38.1 (1986), pp. 67–100. ISSN: 0008-8174. DOI: 10.1007/BF01234287. URL: <http://link.springer.com/10.1007/BF01234287>.
- [35] George William Hill. “Researches in the Lunar Theory”. In: *Am. J. Math.* 1.1 (1878), pp. 245–261. ISSN: 00029327. DOI: 10.2307/2369430. URL: <https://www.jstor.org/stable/2369430?origin=crossref>.
- [36] George William Hill. “Researches in the Lunar Theory”. In: *Am. J. Math.* 1.1 (1878), pp. 5–26. ISSN: 00029327. DOI: 10.2307/2369430. URL: <https://www.jstor.org/stable/2369430?origin=crossref>.
- [37] Try Lam and Gregory J Whiffen. “Exploration of Distant Retrograde Orbits Around Europa”. In: *AAS/AIAA Sp. Flight Mech. Meet. Copp. Mt. Color.* (2005), pp. 1–19.
- [38] Martin Lara. *Higher order analytical solution to the Distant Retrograde orbits problem*. 2018. URL: <https://iafastro.directory/iac/paper/id/42642/summary/> (visited on 11/05/2018).
- [39] Martin Lara. “Nonlinear librations of distant retrograde orbits: a perturbative approach—the Hill problem case”. In: *Nonlinear Dyn* (2018), p. 22. DOI: 10.1007/s11071-018-4304-0.

- [40] Martín Lara, Jesús F. Palacián, and Ryan P. Russell. “Mission design through averaging of perturbed Keplerian systems: The paradigm of an Enceladus orbiter”. In: *Celest. Mech. Dyn. Astron.* 108.1 (2010), pp. 1–22. ISSN: 09232958. DOI: 10.1007/s10569-010-9286-2. URL: <http://link.springer.com/10.1007/s10569-010-9286-2>.
- [41] Martín Lara, Ryan Russell, and Benjamin F. Villac. “Classification of the Distant Stability Regions at Europa”. In: *J. Guid. Control. Dyn.* 30.2 (2007), pp. 409–418. ISSN: 0731-5090. DOI: 10.2514/1.22372. URL: <http://arc.aiaa.org/doi/10.2514/1.22372>.
- [42] M. L. Lidov and M. A. Vashkov’yak. “Perturbation theory and analysis of the evolution of quasi-satellite orbits in the restricted three-body problem.” In: *Cosm. Res.* 31 (1993), pp. 187–207. URL: <http://adsabs.harvard.edu/abs/1993CosRe..31..187L>.
- [43] M.L. Lidov and M.A. Vashkov’yak. “On quasi-satellite orbits for experiments on refinement of the gravitation constant”. In: *Astron. Lett.* 20.2 (1994).
- [44] M. A. Lidov, M. L.; Vashkov’yak. “On quasi-satellite orbits in a restricted elliptic three-body problem”. In: *Astron. Lett.* 20 (1994), pp. 676–690. URL: <http://adsabs.harvard.edu/abs/1994AstL...20..676L>.
- [45] Xu Ming and Xu Shijie. “Exploration of distant retrograde orbits around Moon”. In: *Acta Astronaut.* 65.5-6 (2009), pp. 853–860. ISSN: 0094-5765. DOI: 10.1016/J.ACTAASTRO.2009.03.026. URL: <https://www.sciencedirect.com/science/article/pii/S0094576509001404>.
- [46] G. Mingotti, F. Topputo, and F. Bernelli-Zazzera. “Transfers to distant periodic orbits around the Moon via their invariant manifolds”. In: *Acta Astronaut.* 79 (2012), pp. 20–32. ISSN: 00945765. DOI: 10.1016/j.actaastro.2012.04.022.
- [47] Naomi Murakami and Koji Yamanaka. “Trajectory design for rendezvous in lunar Distant Retrograde Orbit”. In: *IEEE Aerosp. Conf. IEEE*, 2015, pp. 1–13. ISBN: 978-1-4799-5379-0. DOI: 10.1109/AERO.2015.7119023. URL: <http://ieeexplore.ieee.org/document/7119023/>.
- [48] Fathi Namouni. “Secular Interactions of Coorbiting Objects”. In: *Icarus* 137.2 (1999), pp. 293–314. ISSN: 00191035. DOI: 10.1006/icar.1998.6032.
- [49] J Oberst, K Willner, and K Wickhusen. “DePhine-The Deimos and Phobos Interior Explorer-A Proposal to ESA’s Cosmic Vision Program”. In: 11 (2017). URL: <https://core.ac.uk/download/pdf/86640168.pdf>.
- [50] Yusuke Oki and Junichiro Kawaguchi. “Escape Trajectories from Sun-Earth Distant Retrograde Orbits”. In: *Trans. JAPAN Soc. Aeronaut. Sp. Sci. Aerosp. Technol. JAPAN* 14.ists30 (2016), Pd_167–Pd_175. ISSN: 1884-0485. DOI: 10.2322/tastj.14.Pd_167. URL: https://www.jstage.jst.go.jp/article/tastj/14/ists30/14{_}Pd{_}167/{_}article.
- [51] R. L. Ticker P. A. Abell, D. D. Mazanek, D. M. Reeves, P. W. Chodas, M. M. Gates, L. N. Johnson. “NASA’s Asteroid Redirect Mission (ARM), in Lunar and Planetary Science Conference”. In: 25143 (2017), p. 2652.
- [52] Ettore Perozzi, Marta Ceccaroni, Giovanni B. Valsecchi, and Alessandro Rossi. “Distant retrograde orbits and the asteroid hazard”. In: *Eur. Phys. J. Plus* 132.8 (2017), p. 367. ISSN: 2190-5444. DOI: 10.1140/epjp/i2017-11644-0. URL: <http://link.springer.com/10.1140/epjp/i2017-11644-0>.

- [53] Javier Roa and Casey J. Handmer. “Quantifying hazards: asteroid disruption in lunar distant retrograde orbits”. In: (2015). arXiv: 1505.03800. URL: <http://arxiv.org/abs/1505.03800>.
- [54] Hanspeter Schaub and John L. Junkins. *Analytical Mechanics Of Space Systems*. Reston ,VA: American Institute of Aeronautics and Astronautics, 2012. ISBN: 978-1-56347-563-4. DOI: 10.2514/4.861550. URL: <http://arc.aiaa.org/doi/book/10.2514/4.861550>.
- [55] Michele Stramacchia, Camilla Colombo, and Franco Bernelli-Zazzera. “Distant Retrograde Orbits for space-based Near Earth Objects detection”. In: *Adv. Sp. Res.* 58.6 (2016), pp. 967–988. ISSN: 02731177. DOI: 10.1016/j.asr.2016.05.053. URL: <http://linkinghub.elsevier.com/retrieve/pii/S0273117716302769>.
- [56] Victor Szebehely and William H. Jefferys. *Theory of Orbits: The Restricted Problem of Three Bodies*. Vol. 36. 4. 1968, pp. 375–375. ISBN: 978-0126806502. DOI: 10.1119/1.1974535. URL: <http://aapt.scitation.org/doi/10.1119/1.1974535>.
- [57] Mark Wallace, Jeffrey Parker, Nathan Strange, and Daniel Grebow. “Orbital Operations for Phobos and Deimos Exploration”. In: *AIAA/AAS Astrodyn. Spec. Conf.* (2012), pp. 1–10. DOI: 10.2514/6.2012-5067. URL: <http://arc.aiaa.org/doi/10.2514/6.2012-5067>.
- [58] Stephen D. Webb. “Canonical (and non-canonical) Transformations: A Differential Approach”. In: (2012). arXiv: 1205.2146. URL: <http://arxiv.org/abs/1205.2146>.
- [59] Chelsea M. Welch, Jeffrey S. Parker, and Caley Buxton. “Mission Considerations for Transfers to a Distant Retrograde Orbit”. In: *J. Astronaut. Sci.* 62.2 (2015), pp. 101–124. ISSN: 0021-9142. DOI: 10.1007/s40295-015-0039-z. URL: <http://link.springer.com/10.1007/s40295-015-0039-z>.

References No Cited

- [60] Alexander B. Batkhin and Natalia V. Batkhina. “Hénon’s generating solutions and the structure of periodic orbits families of the restricted three-body problem”. In: (2014), pp. 1–12. arXiv: 1411.4933. URL: <http://arxiv.org/abs/1411.4933>.
- [61] Daniel Benest. “Effects of Mass Ratio on the Existence of Retrograde Satellites in the Circular Plane Restricted Problem”. In: *Astron. Astrophys.* 32.1 (1974), pp. 39–46. ISSN: 1098-6596. DOI: 10.1017/CB09781107415324.004. arXiv: arXiv:1011.1669v3.
- [62] Daniel Benest. “Libration effect for retrograde satellite in the restricted three-body problem”. In: *Cel. Mech.* 13 (1974), pp. 203–215.
- [63] John V. Breakwell and John V. Brown. “The ‘Halo’ family of 3-dimensional periodic orbits in the Earth-Moon restricted 3-body problem”. In: *Celest. Mech.* 20.4 (1979), pp. 389–404. DOI: 10.1007/BF01230405. URL: <http://link.springer.com/10.1007/BF01230405>.
- [64] Rohitashwa Chattopadhyay, Tirth Shah, and Sagar Chakraborty. “Lie transform Hamiltonian perturbation theory for limit cycle systems”. In: (2016). arXiv: 1610.05218. URL: <http://arxiv.org/abs/1610.05218>.
- [65] O. E. Gerhard and P. Saha. “Recovering galactic orbits by perturbation theory”. In: *Mon. Not. R. Astron. Soc.* 251.3 (1991), pp. 449–467. ISSN: 0035-8711. DOI: 10.1093/mnras/251.3.449. URL: <https://academic.oup.com/mnras/article-lookup/doi/10.1093/mnras/251.3.449>.
- [66] S. Greenstreet, B. Gladman, H. Ngo, M. Granvik, and S. Larson. “Production of near-earth asteroids on retrograde orbits”. In: *Astrophys. J. Lett.* 749.2 (2012), pp. 2–6. ISSN: 20418205. DOI: 10.1088/2041-8205/749/2/L39.
- [67] Sarah Greenstreet, Henry Ngo, and Brett Gladman. “The orbital distribution of Near-Earth Objects inside Earth’s orbit”. In: *Icarus* 217.1 (2012), pp. 355–366. ISSN: 00191035. DOI: 10.1016/j.icarus.2011.11.010. URL: <http://dx.doi.org/10.1016/j.icarus.2011.11.010>.
- [68] Jeannette Heiligers, Sander Hiddink, Ron Noomen, and Colin R. McInnes. “Multiple spacecraft transfers to Sun-Earth distant retrograde orbits for Asteroid detection missions”. In: (2014). URL: <http://eprints.gla.ac.uk/98910/>.
- [69] Gen-Ichiro Hori. “Theory of general perturbation with unspecified canonical variables”. In: *Publ. Astron. Soc. Japan* 18.4 (1966), pp. 287–296. ISSN: 0004-6264. URL: <http://adsabs.harvard.edu/full/1966PASJ...18..287H7>.
- [70] Brian Kantsiper. “The Double Asteroid Redirection Test (DART) mission electric propulsion trade”. In: *2017 IEEE Aerosp. Conf. IEEE*, 2017, pp. 1–7. ISBN: 978-1-5090-1613-6. DOI: 10.1109/AERO.2017.7943736. URL: <http://ieeexplore.ieee.org/document/7943736/>.

- [71] Wang Sang Koon, Martin W. Lo, Jerrold E. Marsden, and Shane D. Ross. *Dynamical systems, the three-body problem and space mission design*. 2011, p. 312. ISBN: 978-0-615-24095-4.
- [72] M. Lara and J. Peláez. “On the numerical continuation of periodic orbits”. In: *Astron. Astrophys.* 389.2 (2002), pp. 692–701. ISSN: 0004-6361. DOI: 10.1051/0004-6361:20020598. URL: <http://www.aanda.org/10.1051/0004-6361:20020598>.
- [73] Leonid Mal'ys'kin and Scott Tremaine. “The keplerian map for the planar restricted three-body problem as a model of comet evolution”. In: *Icarus* 141.2 (1999), pp. 341–353. ISSN: 00191035. DOI: 10.1006/icar.1999.6174. arXiv: 9808172 [astro-ph].
- [74] Kenneth R. (Kenneth Ray) Meyer, Glen R. Hall, and Daniel C. (Daniel Clyde) Offin. *Introduction to Hamiltonian dynamical systems and the N-body problem*. Springer Science+Business Media, 2009, p. 399. ISBN: 9780387097244.
- [75] Ali Hasan Nayfeh and Wiley InterScience (Online service). *Perturbation methods*. John Wiley & Sons, 2000, p. 425. ISBN: 9780471399179. URL: <https://www.wiley.com/en-us/Perturbation+Methods-p-9780471399179>.
- [76] Cesar A. Ocampo and George W. Rosborough. *Transfer trajectories for distant retrograde orbiters of the Earth*. 1993. URL: <https://utexas.influent.utsystem.edu/en/publications/transfer-trajectories-for-distant-retrograde-orbiters-of-the-eart>.
- [77] Nathan L. Parrish, Jeffrey S. Parker, Steven P. Hughes, and Jeannette Heiligers. “Low-Thrust Transfers From Distant Retrograde Orbits To L2 Halo Orbits in the Earth-Moon System”. In: *Int. Conf. Astrodyn. Tools Tech.* 2 (2016), pp. 1–25.
- [78] Shane D. Ross and Daniel J. Scheeres. “Multiple Gravity Assists, Capture, and Escape in the Restricted Three-Body Problem”. In: *SIAM J. Appl. Dyn. Syst.* 6.3 (2007), pp. 576–596. ISSN: 1536-0040. DOI: 10.1137/060663374. URL: <http://epubs.siam.org/doi/10.1137/060663374>.
- [79] E. Baylis Shanks. “Higher order approximations of Runge-Kutta type”. In: September (1965).
- [80] Vladislav Sidorenko and Vladislav. “Distant retrograde orbits for the Moon’s exploration”. In: *40th COSPAR Sci. Assem. Held 2-10 August 2014, Moscow, Russ. Abstr. id.# B0.1-38-14*. 40 (2014). URL: <http://adsabs.harvard.edu/abs/2014cosp...40E3072S>.
- [81] C. Simó and T.J. Stuchi. “Central stable/unstable manifolds and the destruction of KAM tori in the planar Hill problem”. In: *Phys. D Nonlinear Phenom.* 140.1-2 (2000), pp. 1–32. ISSN: 0167-2789. DOI: 10.1016/S0167-2789(99)00211-0. URL: <https://www.sciencedirect.com/science/article/pii/S0167278999002110?via=ihub>.
- [82] B. A. Steves, A. J. Maciejewski, and M. Hendry. *Chaotic Worlds: from Order to Disorder in Gravitational N-Body Dynamical Systems (Nato Science Series II: (closed))*. Ed. by B. A. Steves, A. J. Maciejewski, and M. Hendry. Springer Netherlands, 2006. ISBN: 1402047053. DOI: 10.1007/978-1-4020-4706-0. URL: <http://www.amazon.com/exec/obidos/redirect?tag=citeulike07-20&path=ASIN/1402047053>.

- [83] Michele Stramacchia. “Distant periodic orbits for asteroid detection”. PhD thesis. 2013. URL: https://www.politesi.polimi.it/handle/10589/80709?mode=full{\&}submit{_}simple=Visualizza+tutti+i+metadati+del+documento.
- [84] N. N. Subbotina. “The method of characteristics for Hamilton—Jacobi equations and applications to dynamical optimization”. In: *J. Math. Sci.* 135.3 (2006), pp. 2955–3091. ISSN: 1072-3374. DOI: 10.1007/s10958-006-0146-2. URL: <http://link.springer.com/10.1007/s10958-006-0146-2>.
- [85] G. B. Valsecchi, E. Perozzi, and A. Rossi. “A space mission to detect imminent Earth impactors”. In: *Proc. Int. Astron. Union* 10.H16 (2012), pp. 488–489. ISSN: 1743-9213. DOI: 10.1017/S1743921314011909. URL: https://www.cambridge.org/core/product/identifier/S1743921314011909/type/journal{_}article.
- [86] Franco Bernelli Zazzera, Francesco Topputo, and Mauro Massari. “Assessment of mission design including utilization of libration points and weak stability boundaries”. In: *Ariadna Study, ESA* 31.0 (2003).
- [87] J.L. Zhou, Y.S. Sun, J.Q. Zheng, and M.J. Valtonen. *The transfer of comets from near-parabolic to short-period orbits: map approach*. Vol. 364. EDP Sciences [etc.], 2000, pp. 887–893. URL: <http://adsabs.harvard.edu/full/2000A{\%}26A...364..887Z>.

Index

A			
Angular Momentum			10
B			
Binomial Form			46
C			
Characteristic			
Mass			11
Time			12
Collinear Libration Points		14, 23	
Conjugate Moments	27, 29, 33–35		
Canonical			40
Coordinate			
Canocnial			41
Generalized			30
Original/Physical			43, 51
D			
Deprit			67
Method			46
Triangle			57, 58
Diffeomorphism			38
E			
Elliptic Integrals			
Complete			48
Incomplete			48
Energy			
Kinetic	27–29, 31, 32, 35		
Level			16
Potential	22, 27–29		
Epicyclic Variables			42, 46
Equation			
Hamilton			28, 38
Hamilton-Jacobi			39, 40
Lagrange	27, 28, 30–32		
F			
Function			
Generating	39, 40, 42, 46, 47, 58, 65, 68		
Hamiltonian	27–31, 33–35, 38–41, 65		
Canonical	38, 39, 41, 42, 45, 46, 50, 52, 66		
Lagrange			27
Lagrangian			27–32, 35
Potential	13, 20, 27, 31–33, 35		
		Centrifugal	13
G			
Gravitational Constant			9
non-dimensional			12
H			
Hénon			32
Hamiltonian	5–7, 38, 67, 68, 70, 112		
Hill	1, 2, 5, 7, 22, 23, 25, 31, 32, 68, 71, 78, 100		
Model	1–3, 5, 6, 9, 22, 25, 32, 33, 65, 73, 111		
Problem	2, 4–6, 20, 22, 23, 40–42, 47, 77		
Reference Frame			22
Regions			16
Surface			16
J			
Jacobi			15
Constant			16, 23, 30
K			
Kamel			67
Kepler			12
L			
Lagrangian Points			14
Libration Points			14
Collinear			14
Equilateral Triangle			14
Lie			38
Operator			46
Lindstedt-Poincaré			6, 53
M			
Maclaurin serie			22, 25, 47
Mean Motion			12
non-dimensional			12, 13
Monodromy Matrix			117
N			
Newton			9
P			
Parameter			
Mass			12
Time			12
Poisson Bracket			46

R

Reference Frame

Inertial 10, 13, 28, 113, 114

Rotating 10, 13, 29, 113, 114

S

State Transition Matrix 116, 117

T

Transformation

Canonical 39, 40, 42, 43, 51

Legendre 27, 28

Lie 46

Trasformation

Canonical 65